June 30, 2015
Faculty of Aerospace Engineering
Delft University of Technology

LOW EMISSION REGIONAL AIRLINER

FINAL DESIGN REPORT

AE3200: Design Synthesis Exercises

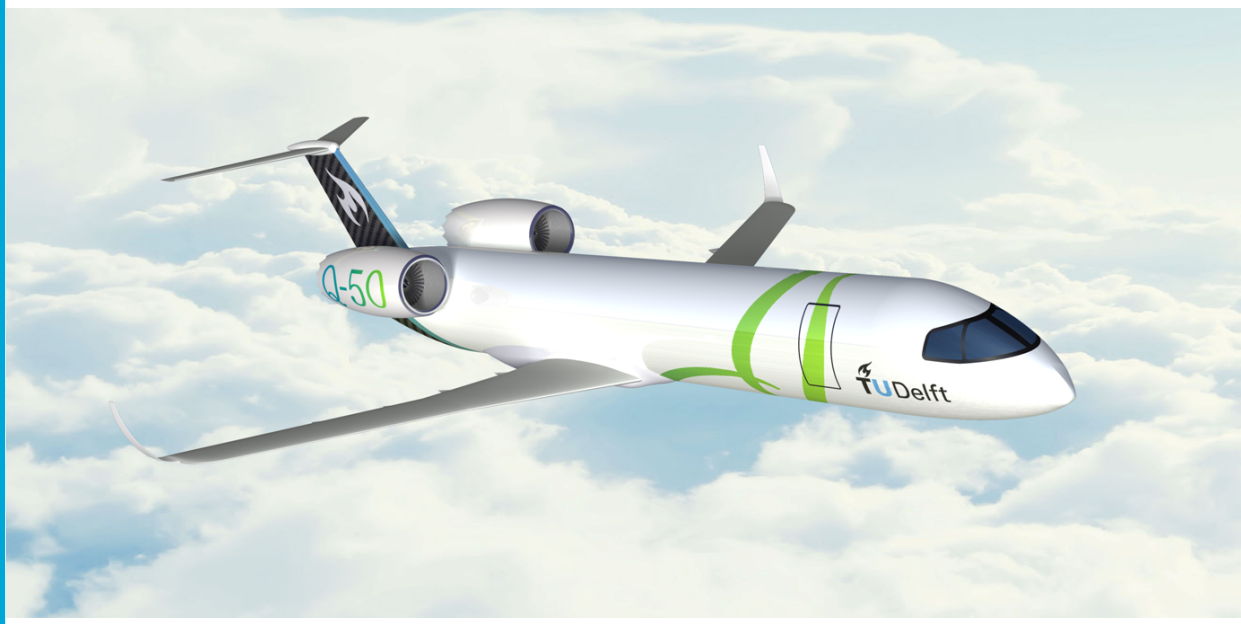

Authors:	D.K. Arnell	1176374	*Tutor*:	W. Verhagen
	T.E. Boogaart	4228642		
	S.C.D. Hellemans	1356631	*Coaches*:	G. Correale
	A. Ion	4201124		A. Cooperman
	R. Nederlof	4204271		
	N. Nuus	4163176		
	M.U. Oudkerk	4022815		
	G.N. Pappie	4133897		
	T.F. Spaan	4205472		

TUDelft

Preface

Delft, June 30, 2015

This is the final report of the Design Synthesis Exercise 2015, conducted at the faculty of Aerospace Engineering at Delft University of Technology. This project is the result of hard work of nine students over a period of eleven weeks from 20 April 2015 until 3 July 2015. It contains the design of a windowless low-emission regional aircraft to fit 50 passengers. To perform iterations on both weight and performance, MATLAB programs have been developed. The main focus lies on designing a high performance, lightweight aircraft, using efficient engines and innovative technologies to reduce both gaseous and acoustic emissions.

We would like to express our gratitude to our tutor dr. ir. W.J.C. Verhagen, our coaches dr. ir. A.M. Cooperman and ir. G. Correale for their guidance and advice, without which this project would not have been as successful. Additional thanks to the entire staff of the faculty of Aerospace Engineering at Delft University of Technology for their input and insights.

Summary

As air transportation gains in popularity, more aircraft are going to take to the skies. With sustainability becoming an important aspect of our lives, gaseous and acoustic emissions need to be continuously reduced. QLEAR Q-50 will be a revolutionary 50-seat low-emission regional jet, which will serve as a stepping stone towards sustainability, meeting the strict emission reduction requirements set by the European Commission for 2050. QLEAR Q-50 can be seen as an intermediate step between regional aircraft currently in service and future zero-emission aircraft. The CO_2 emissions and the NO_x emissions need to be reduced by 50% and 25%, respectively. Moreover, the perceived noise needs to be reduced by 50%. The regional airliner still needs to be able to fly at a minimum of Mach $= 0.75$ over a range of 2,000 km. Lastly, the low emission regional aircraft should not exceed a maximum take-off weight of 23,000 kg and have a maximum unit cost of USD 35 million. To fulfill these strict requirements, major questions regarding the technical feasibility of alternative propulsion modes, supporting infrastructure and achieved environmental impact are to be answered.

A market analysis was done to get better understanding of the competition and also to compare the design with the competition. A market share of 35% is expected. After the market analysis, a literature study into a sustainable design was conducted, from where a windowless fuselage is chosen. This choice to remove the windows and add Oled screens, results in a hourly reduction of the operating cost of USD 2.71. The biggest game changer in the weight reduction is achieved in the material selection. With the choice for carbon-reinforced polymers, the empty weight of Q-50 is greatly reduced. A lighter design, will result in a lower fuel used. The reduction of the weight together with the selection of the NACA 07-411 airfoil resulted in a wing with a surface area of 43 m^2 and a span of 19.9 m. Compared to similar aircraft, the reduced surface area of the wing contributed to a reduction in drag experienced by the aircraft.

The main load carrying structure will be a wingbox, using T-shaped stringers. Furthermore, the location of the ribs is linked with the design of the high-lift-devices, spoilers and ailerons. The wing will be equipped with full span leading edge slats, double slotted flaps, which span 70%, outboard ailerons and spoilers. The high lift devices give a $\Delta C_{L_{max}}$ of 1.45. The landing gear is sized to ensure maneuverability and ground stability, while the tail design ensures stability both in flight and during maneuvers. The surface areas of the horizontal and vertical tail are 8.35 m^2 and 6.78 m^2 respectively. Lastly, the fuselage is modeled and designed to withstand all the loads occurring during flight, such as the tensile stress from the pressurization, as well as the nose gear impact. The stringers will be head-shaped, to be able to take all the torsional stresses, as where the frames, which run circumferential, are shaped as I-stringers, to take the bending. The aerodynamic design of the aircraft ensures flight stability of the eigenmotions in both longitudinal as lateral direction.

The second major point of improvement in fuel consumption can be found in the propulsion system. Innovative turbofan engines, which are approximately 20% more efficient than current models, were specially designed for the Q-50. Their specific fuel consumption of 0.057 kg/Nhr is capable of reducing the overall aircraft fuel consumption while also reducing engine noise and offering a the high cruise speed required. The required maximum thrust during take-off will be around 55 kN. The improved aerodynamic characteristics and the reduced weight will result in smaller and lighter engines, translate to a maximum take-off weight of 17,425 kg. This value is 27% less than the competition. Together with the increased efficiency of the engines, a fuel consumption of 0.24 kg/s will be achieved. Since the CO_2 emission is coupled with the fuel consumption, the gaseous emissions will be reduced by 49% compared to the ERJ-145. A further 1% CO_2 emission reduction is achieved by using carbon-capturing material, which could be used on the manufacturing facilities. The required noise reduction of 50% is achieved by landing gear fairings, improved slats, lower engine jet velocity and a higher bypass ratio.

The aircraft will have a good performance in both take-off and landing. In the two situations, the required field length are 1267 m and 1456 m respectively. The maximum rate of climb will be 13 m/s, as where the maximum value for the climb gradient will be 19%. The optimum flight conditions are achieved at an altitude of 10,278 m and a airspeed of Mach $= 0.81$. A redundant fuel and fly-by-wire control system will be used, to ensure safe and stable manoeuvring in all conditions. The use of Required Navigation Performance will allow improved accuracy and and reduced missed approaches which will save fuel and improve safety. The power budget for the aircraft's control and utilities is estimated to be 189.5 kW.

The Q-50 will offer a minimum turn-around time of 22 minutes, on a minimum parking area of 30x25 m, which will maximize its utilization and increase revenues for its operators. Since sustainability is a key factor for all stages of the project, the production of the Q-50 will be executed using a Lean Manufacturing philosophy, where almost all parts are made and assembled in the same factory. This exceptionally sustainable aircraft will be available for the price of USD 28.2 million, far below the imposed maximum of USD 35 million.

As we step forward in the 21st century, advanced technologies and fresh perspectives from young engineers will revolutionize the aviation industry. This revolution will begin with the Quiet Low Emission Advanced Regional aircraft.

Table of Contents

List of Figures

List of Tables

Nomenclature

Symbol	Description	Unit
Greek Symbols:		
α	Angle of attack	[rad/°]
α_{0_l}	Local aerodynamic twist	[rad]
β	Prandtl compressibility correction factor	[-]
γ_{air}	Heat capacity ratio	[-]
ϵ	Downwash angle	[rad/°]
η	Tailplane effectiveness	[-]
η_p	Spanwise location; propeller efficiency	[-]
η_{th}	Thermal efficiency	[-]
Λ	Sweep angle	[rad/°]
λ	Taper ratio	[-]
ρ	Density	[kg/m^3]
σ	Density ratio	[-]
$\sigma_{t,y}$	Tensile yield strength	[MPa]
$\sigma_{c,y}$	Compressive yield strength	[MPa]
Roman Symbols:		
A	Aspect ratio	[-]
A_h	Aspect ratio horizontal tail	[-]
a	Speed of sound	[m/s]
b	Wing span	[m]
b_f	Maximum width of fuselage, Span of flaps	[m]
c	Local chord length	[m]
$\bar{c} = MAC$	Mean aerodynamic chord	[m]
c_g	Mean geometric chord	[m]
c_r	Root chord	[m]
c_t	Tip chord	[m]
c_T	Specific fuel consumption	[kg/Ns]
C_1	First Diederich factor	[-]
C_2	Second Diederich factor	[-]
C_3	Third Diederich factor	[-]
C_4	Fourth Diederich factor	[-]
C_{D_0}	Zero-lift drag coefficient	[-]
C_D	3D drag coefficient	[-]
C_d	2D drag coefficient	[-]
C_L	3D lift coefficient	[-]
C_l	2D lift coefficient	[-]
C_m	2D moment coefficient	[-]
C_p	Pressure coefficient	[-]
d_e	Jet engine diameter	[m]
e	Oswald factor	[-]
E	Jones's edge-velocity correction	[-]
E_t	Tensile modulus of elasticity	[GPa]
E_c	Compressive modulus of elasticity	[GPa]

Continued on next page

Continued from previous page

Symbol	Description	Unit
F	Fuel consumption	[kg/s]
g	Gravitational acceleration	[m/s^2]
h	Altitude	[m]
k	Take-off parameter	[Ns/m^3]
L/D	Lift over drag ratio	[-]
l_h	Tail length	[m]
$l_{fuselage}$	Length fuselage	[m]
M	Mach number	[-]
M_{crit}	Critical mach number	[-]
n_{max}	Maximum load factor	[-]
P_r	Power required	[W]
P_a	Power available	[W]
R	Gas constant	[J/kgK]
Re	Reynolds number	[-]
S	Wing surface area	[m^2]
S_h	Horizontal tail surface area	[m^2]
SFC	Specific fuel consumption propeller	[lbs/hr/hp]
t/c	Thickness over chord length	[-]
T	Engine thrust	[N]
T_a	Available engine thrust	[N]
T/W	Thrust loading	[-]
V	True airspeed	[m/s]
V_h/V	Horizontal tail - wing speed ratio	[-]
W	Weight	[N]
W/S	Wing loading	[N/m^2]
W/P	Weight to power ratio	[N/W]
x_{LEMAC}	Location leading edge of mean aerodynamic chord	[m]
$\bar{x_{ac}}$	Location of the aerodynamic center	[m]
$\bar{x_{cg}}$	Location of the centre of gravity	[m]

Introduction

As air transportation gains in popularity, more aircraft are going to take to the skies. With sustainability becoming an important aspect of our lives, gaseous and acoustic emissions need to be continuously reduced. Since aviation is solely responsible for 3% of the total greenhouse gas emissions in Europe, the design of a low-emission regional airliner is needed, which will serve as a stepping stone towards sustainability.

In the mid-term report [1], three concepts were analyzed and the most suitable one was selected for the design of the regional airliner. The high-wing turboprop design was scrapped due to large amounts of noise produced during operation and its relatively high operating cost. The hybrid design was not deemed feasible because of its high operational weight and the fact that the required technology might not be available by the time the airliner had to enter into service. In the end, the chosen configuration for QLEAR Q-50 was a conventional one, with a low main wing and T-tail configuration. In this final report, the detailed design of the Q-50 and the sizing of all its main systems are performed.

The steps taken in the design of QLEAR Q-50 and milestones achieved until the Final Report are summarized in Chapter 2. For a successful result, the project needs to be meticulously organized. This subject will be dealt with in Chapter 3. The basis for profitability of this project will analyzed in Chapter 4, where a market analysis is carried out and the main competitors are identified. As sustainability is a key element of the project, the sustainability strategies will be introduced in Chapter 5. The actual design process begins with Chapter 6 where the interface between all aircraft systems are identified with the aid of an N2 chart. Also, the iterative design process used in this report is described. With the iterations converging to a final wing surface area and maximum take-off weight, the weight and balance of Q-50 will be analyzed in Chapter 7. Following this, the wing planform will be sized in Chapter 8 and possible tail configurations will be evaluated. The process of choosing the optimum airfoil for Q-50 and the determination of the main aerodynamic characteristics of the aircraft will be done in Chapter 9. One of the ways to reduce the overall emissions is by having a lighter aircraft. The use of both current and future materials, such as CFRP will be treated in Chapter 10. Also, multiple load cases and the optimization of the structure will be dealt with in Chapter 11. Another source of noise and emission is the propulsion system. Multiple new technologies will be combined in Chapter 12 to designed the most appropriate engine for the Q-50. All design choices made up to this point will be tested in Chapter 13, where the stability of the aircraft will be analyzed. Afterwards, Chapter 14 will proceed with the detailed design of the wing, tailplane and landing gear. The performance of the aircraft during take-off, cruise and landing will be analyzed in Chapter 15. The layout of the fuel and hydraulic systems and the main components of the communication, navigation and avionics can be found in Chapter 16. The final budget break-down of the aircraft is performed in Chapter 17. To finalize the design process, a sensitivity analysis is carried out in Chapter 18, in order to investigate the impact of various design parameters on final aircraft design. The main issues encountered during the operational life of the aircraft are identified in Chapter 19. To increase the reliability of the Q-50, the main risks are established in Chapter 20 and mitigation strategies are formulated. Following with the sustainability approach, lean manufacturing techniques will be used in the production of the regional airliner. More information on that can be found in Chapter 21. The final unit cost of the Q-50 and estimations of the direct operating cost can be found in Chapter 22. Strategies used to mitigate acoustic and gaseous emissions are summarized in Chapter 23. A requirements compliance matrix is set up in Chapter 24 to determine whether all the project requirements have been met. Also, the steps that could be taken after the end of the DSE will be presented in Chapter 25.

From Baseline to Final

The design of the QLEAR Q-50 is the result of an elaborate process, consisting of many different phases. The first phase started with determining the stakeholders of the project and analyzing the basic requirements provided by the main customer. The aircraft should be able to fit 50 passengers, have a maximum range of 2500 km, fly at a Mach number of at least 0.75 at an altitude of 11,278 m and enter into service in 2035. The main goal of the assignment is to develop a low-emission aircraft, which results in requirements for a reduction in acoustic noise and CO_2 of 50% and a reduction of 25% of NO_x compared to the competition. Finally, the aircraft should not exceed a MTOW of 23,000 kg and have a maximum unit cost of USD 35 million, with a minimum return on investment of 5% in 5 years. Besides the basic requirements many other requirements based on the multiple stakeholders are set in Appendix D, regarding performance and operations of the aircraft. The second phase of the project was to perform a market analysis, in which it became clear that there is indeed a market for a 50-seat aircraft, however only when the range is reduced from 2500 km to 2000 km.

After the market analysis was conducted, a literature study was performed in the fields of structures, aerodynamics, materials, propulsion, fuselage design, fuels and emissions. The main goal of this literature study was to create a Design Option Tree (DOT) and start eliminating the options that are not suited for this assignment. Following the literature study, sixteen conceptual designs were created, using different options from the Design Option Tree. Since the main assignment is develop a quiet, low-emission aircraft, one of the most important parts of the project was to develop and continuously adapt a sustainability strategy. This was started during the Baseline, and has been extended and increased in detail up until the last day of the project. Finalizing the Baseline Report [2], a trade-off was performed to reduce the number of concepts from sixteen to three. The three final concepts can be seen in Figures 2.1 until 2.3.

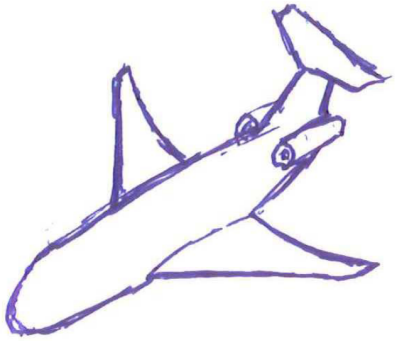

Figure 2.1: Concept 1: low-wing, turbofan

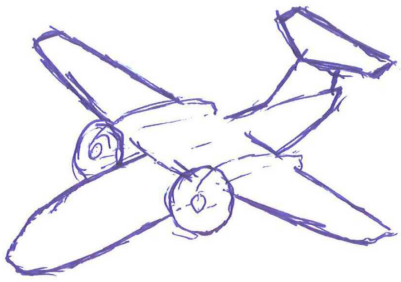

Figure 2.2: Concept 2: high-wing, propeller

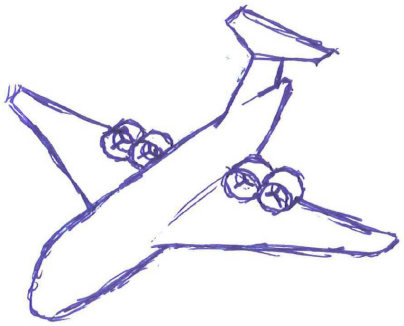

Figure 2.3: Concept 3: hybrid, distributed propulsion

The goal of the Midterm Report [1] was to compare the three concepts that have been selected from the first trade-off in performance, cost and operations. Furthermore, a final trade-off was performed in order to select the best design and develop this concept further. The first step was to identify the the interfaces between the different systems and to set up an iterative process to obtain a weight estimate for each concept. Weight was chosen as one of the most important parameters, since the weight of the aircraft is a good measure of the performance and therefore cost of the aircraft. The iterative process started with a Class I weight estimation, mostly based on references and including fudge factors for the more novel Concept 3. Based on the requirements an initial airfoil choice was made for all designs: NACA 63-510. Following the airfoil selection, the initial wing sizing was performed using Torenbeek [3], where the surface area was modelled as a reference trapezoidal area. After the initial sizing of the wing, the general fuselage and cabin layout was designed. Finally, the aircraft weight was estimated for all main components of the aircraft using Class II weight estimation, resulting in a more detailed OEW and MTOW of all concepts, scissor plots to determine the location of the wing and the optimal horizontal tail size. Finally the loading diagrams for each concept, showing the center of gravity ranges and critical phases with regards to stability during operations. The results of the Class II weight estimation finalized the interface iterations, however there are more aspects of designing an aircraft that will influence its performance and therefore the final trade-off. For this reason the performance of the concepts was analyzed (including payload range diagrams and V-n diagrams) and optimized for cruise, since this will take up the largest part of the mission. In order to see the difference between the three concepts operation-wise, the operations and maintenance, RAMS and risk of all concepts were analyzed, mostly focusing on the differences in propulsion system. Finally, the cost for each concept was estimated, divided into unit cost and operating cost. Again, the main focus lied in the differences between

the three concepts.

The final step after analysing the differences between all concepts for multiple aspects of the design was to perform the trade-off. The final trade-off and its results are shown in Table 2.1.

Table 2.1: Trade-off matrix

Parameter	**Concept 1**	**Concept 2**	**Concept 3**
Emissions (46.2%)			
CO_2 emissions (15.4%)	3	5	5
NO_x emissions (15.4%)	4	7	8
Noise emissions (15.4%)	6	2	8
Cost (27.4%)			
Production cost (21.92%)	9	4	5
Operating cost (5.48%)	9	1	5
Performance (17.8%)			
Weight (12.46%)	7	6	1
Speed (1.78%)	9	5	5
Specific Fuel Consumption (3.56%)	6	7	6
Risk (8.6%)			
Technology Readiness Level (6.88%)	9	9	4
Bird strike (0.86%)	5	3	5
One Engine Inoperative (0.86%)	7	6	8
TOTAL	6.4364	4.87	5.4182

From Table 2.1 it becomes clear that the final concept is Concept 1, a conventional, low-wing configuration with turbofan engines mounted on the fuselage. The choice of this design, finalizes the Midterm report. The next step is to go into more detail to design and develop the aircraft, which will be conducted in this Final Report.

Project Organization and Planning

Designing an aircraft in a limited amount of time requires a lot of planning. In this chapter, the project objectives (Section 3.1) and organization of the project and its team members is described as well as the planning and scheduling of the final phase. Section 3.2 describes the organizational structure including tasks, the persons responsible and the hierarchy. The required work is planned and scheduled in Section 3.3 and all design steps and processes necessary for the project are identified.

3.1 Project Objectives

With the new emission requirements given by the international aviation organizations the demand for a low emission airliner arises. The DSE Group 16 has challenged themselves with designing a low emission regional airliner under the company name QLEAR (Quiet, Low-Emission, Advanced, Regional). The QLEAR aircraft is to perform better than the current regional jets on the market as well as comply with the emission requirements. This leads to a full requirement list given in Appendix D.

For the DSE design group, this project allows for practise in the full design cycle of an aircraft. Not only the technical aspect of a design process, such as weight estimations, airfoil analysis, planform design etcetera, but also more in dept research in the commercial side, for instance market response to the product, is covered.

The market analysis lead to a change in requirements which resulted a meeting with the customer to discuss the changes, as costumers do not always have realistic expectations and therefore it is the engineers job to find a balance between the wishes of the customer and what is actually possible. Because meetings with the customer and creating the right overview of the design requirements is very important in the first phases, communication should be of high standards, both internally and externally. Another reason for efficient external communication is the fact that in order to come to the best result possible, a lot of expertise from faculty members has to be brought in.

The project allows for a more in-depth look at new technologies as well as new software in the design process. The project therefore allows for self-enrichment for the students to get a better understanding of current technologies and trends. Also to see where the true interests of individual people lie and what their strengths and weaknesses are. Not only in the matter but also in group cohesion and organizational tasks within the group.

3.2 Organisational Structure

As discussed in the Project Plan [4], the team will hold meetings twice a day conducted by the chairman, to discuss the plan and progress of the day. To help this process an Organizational Breakdown Structure (OBS) is made, to define the main managerial tasks each group member is responsible for and to provide hierarchical structure. The organizational tasks are described in Table 3.1 and the hierarchy is shown in Figure 3.1.

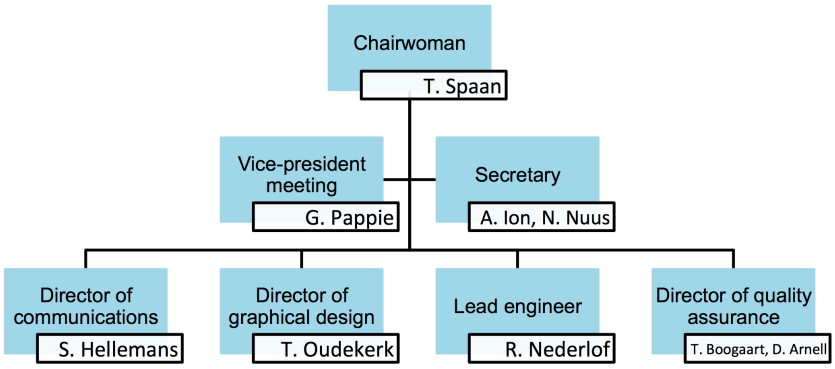

Figure 3.1: Structure of managerial tasks

Table 3.1: Description of organizational tasks

Organizational task	Responsibilities & Functions	Person(s) assigned
Chairman	Lead the group, keep track of all activities done/coming up, conduct daily meetings	T.F. Spaan
Vice-president meeting	Assist chairman and secretary by taking the lead in the meetings with tutor and coaches	G.N. Pappie
Secretary	Take notes during meetings, document notes/questions/problems/answers	A. Ion, N. Nuus
Director of communications	Arrange and keep track of all external communication, send reports to tutor+coaches	S.C.D. Hellemans
Director of graphical design	Create configuration drawings with CATIA, manage layout of presentations	M.U. Oudkerk
Lead engineer	Keep track of all technical content and assist in different fields when needed	R. Nederlof
Director of quality assurance	Manage reporting, perform spelling/layout checks	T.E. Boogaart, D.K. Arnell

Finally, every team member is in charge of a certain technical aspect of the project. This division can be seen in Figure 3.2. Also, the lead engineer will keep track of what happens in the other departments, monitored by the chairman, such that a concurrent engineering approach is enforced, where all departments work together in order to obtain the final design.

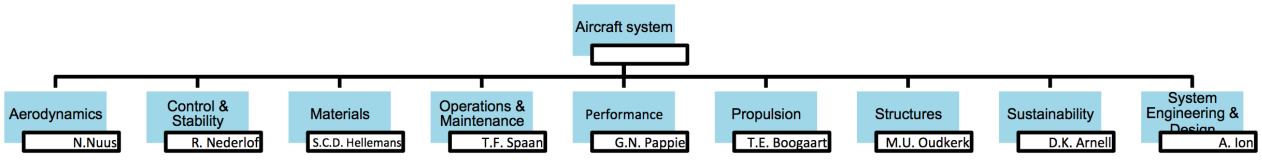

Figure 3.2: Division structure of the technical aspects of the project

3.3 Work-flow Diagrams and Work-flow Breakdown Structure

The design of this low-emission regional airliner will take eleven weeks and involve many different steps and processes. For this reason the first report [4] was dedicated to the planning of the entire project, and more specifically this chapter to the work flow. In other words: what do we need to do in order to come up with a good design?

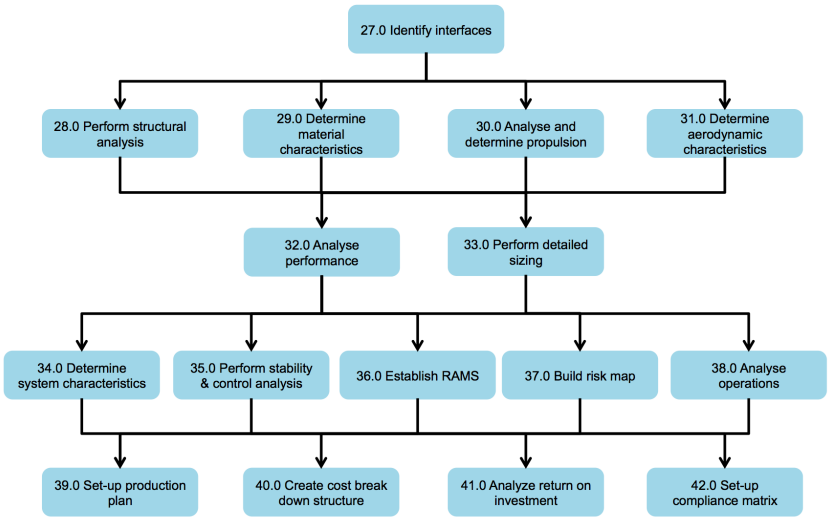

Figure 3.3: Work flow diagram final design

Using the work break down structure and work-flow diagrams from [4], the updated versions for the final review can be seen in Figure 3.3. The work break down structure for the final review can be seen in Figure 3.4.

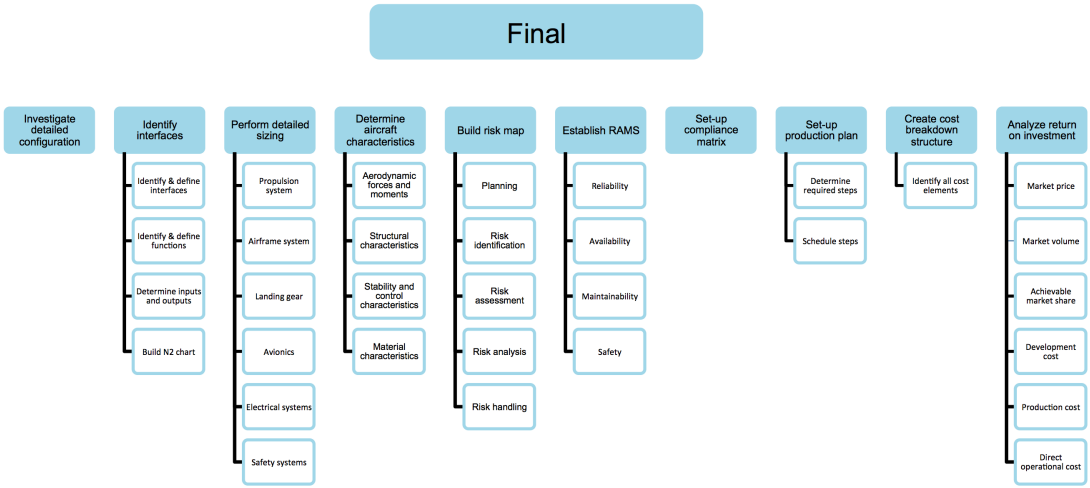

Figure 3.4: Work break down structure final design

Market Analysis

Every product development requires a market analysis. This analysis is essential to establish a basis for profitability. Some questions to be answered are: Who are the customers? Who are the competitors? What is the size of the market? How will the market change over time? This chapter provides answers to these questions by analyzing multiple aspects of the market. It starts with an analysis of global development in the years to come and its implications on aviation in Section 4.1. Subsequently, potential competitors for the QLEAR Q-50 are identified in Section 4.2. The market capture envisioned for the Q-50 is discussed in Section 4.3. Finally, the main factors which will make the Q-50 a successful regional aircraft are presented in Section 4.4.

4.1 Current Economic Context and Impact on Aviation

According to the World Bank, a United Nations (UN) international financial institution, the global Gross Domestic Product (GDP) is expected to rise 3.2% annually over the next 20 years. The fastest-growing regions are identified as South Asia with a GDP increase of 6.8%; Africa, 5.1%; the Middle East, 3.5%; and Latin America, 3.3%. For North America and Europe the growth is estimated to be around 2.5% and 1.9% annually, respectively.[1]

A 2009 UN survey shows that more than half of the world's population lives in urban areas.[2] Moreover, it is expected that half of the people in China and the Asia-Pacific region will live in urban areas by 2020. Half of all Africans will live in urban cities by 2035 [5]. Urbanization will further boost global demand for transportation. While today's market concentrates on connecting large cities, for the upcoming years the low and mid-density markets will experience a boom. This will boost the connectivity with non-trunk routes, making regional aircraft an essential element for the future of air transportation industry [5].

In recent years air transport growth has been directly linked to low cost carrier (LCC) expansion. Close to 30% of current worldwide capacity generated by flights up to 3000 km are offered by LCCs, which is twice the value of the year 2000 [5]. In Europe 40% of air travel capacity is supplied by LCCs, according to IATA.[3] In the hub-and-spoke system, regional airlines have been essential in feeding the main hubs, required for global connectivity. However, network carriers are restructuring their businesses to compete with the LCCs which means that LCCs need to start considering new strategies to access lower-density markets in order to sustain their growth. Thus, a new generation of fuel-efficient regional aircraft with a low operating cost will bring great benefits to legacy airlines as well.

4.2 Main Competitors for QLEAR Q-50

With the help of Figure 4.1, the main competitors for Q-50 can be identified. This figure shows all regional aircraft (up to 130 seats) that are currently in service and includes the maximum number of passengers and range. It can be seen that there is a big cluster of airliners in the 70 - 90 seat market, while for the 50-seat market the main competitors would be CRJ-200, ERJ-145 and ATR-42. With the CRJ-200 no longer in production, there is indeed a niche in the 50-seat market.
To better understand the competition, the fuel consumption was also considered. Figure 4.2 shows the fuel consumption in gallons per seat hour for a number of regional aircraft. As a general observation, the fuel consumption tends to go down when the number of seats increases. In the 50-seat market, the ERJ-145 and CRJ-200 use around 7 gallons per seat hour. The advance engine design presented in Chapter 12 enabled the QLEAR Q-50 to reach a fuel consumption of 0.24 kg/s in cruise. This means 3.5 gallons per seat hour, thus offering a 50% reduction compared to its main competitors.

4.3 Market Capture of QLEAR Q-50

After analyzing the current market outlook for 2014-2033 of both Embraer [5] and Bombardier [6], the two main players in the regional market segment, Table 4.1 was created. This table summarizes the expected number of 50-70 seat airliners around the globe by 2033. From Table 4.1, it can be seen that the largest number of deliveries is expected to take place in North America. Also a significant number of regional airliners are expected to be delivered to airlines within Europe, China, Latin America and the Asia-Pacific region.

[1] http://www.worldbank.org/en/publication/global-economic-prospects/data [cited 1-5-2015]
[2] http://www.un.org/en/development/desa/population/publications/urbanization/urban-rural.shtml [cited 1-5-2015]
[3] http://www.iata.org/whatwedo/documents/economics/airline_cost_performance.pdf [cited 1-5-2015]

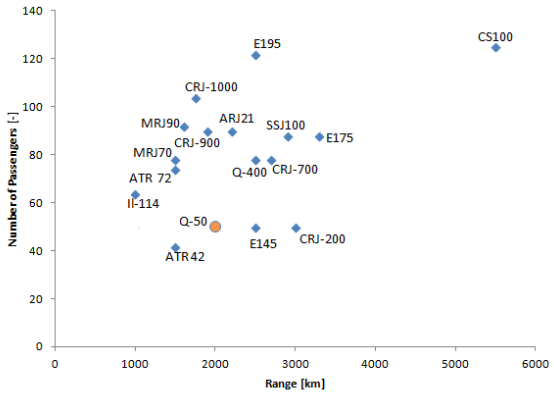

Figure 4.1: Number of seats versus range for current regional aircraft

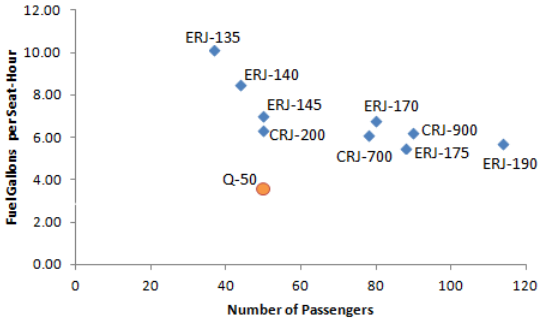

Figure 4.2: Fuel consumption of current regional aircraft

Table 4.1: Expected number of deliveries per region by 2033

Region	Replacement	Growth	Total
Africa	99	131	230
Asia-Pacific	161	359	520
China	133	887	1020
CIS	201	179	380
Europe	616	524	1140
Latin America	259	441	700
Middle East	100	150	250
North America	1950	60	2010
Total	3519	2731	6250

The versatility of the aircraft can be seen in Figure 4.3. In this figure, one can see that the Q-50 can operate short haul routes, such as Amsterdam - London and even medium haul routes, such as Amsterdam - Reykjavik, making it a perfect choice for airlines operating a vast network.

Figure 4.3: QLEAR Q-50 range map from Amsterdam airport

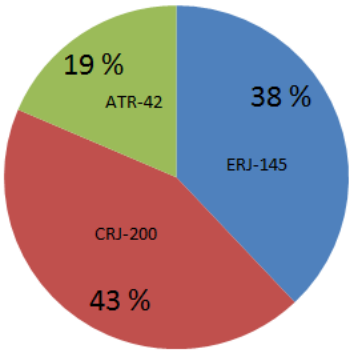

Figure 4.4: Current estimated market share in the 50-seater segment

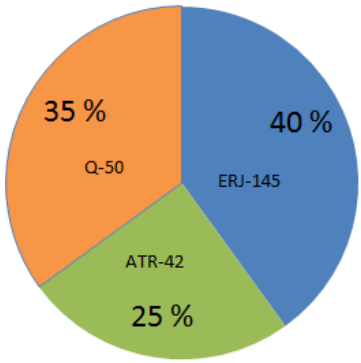

Figure 4.5: Expected market share in the 50-seater segment in 2035

During the Maintenance, Repair & Overhaul Conference on April 14 - 16, in Miami, Florida, Embraer announced that based on the current number of deliveries their company holds a 62% share in the regional market segment. [4] However, this figure takes into account all regional aircraft with a capacity of up to 130 passengers. To get a more realistic view on the 50-seater market segment, the pie chart in Figure 4.4 was created by taking into account the number of units built until now for the main players: ERJ-145, CRJ-200, ATR-42. A similar pie chart is created for the year 2035. This can be seen in Figure 4.5. Since the CRJ-200 will no longer be produced, there will be a big gap in the market that needs to be filled. The Mitsubishi Regional Jet which is scheduled to enter into service in 2017 was not included in this analysis because it

[4] http://centreforaviation.com/members/direct-news/embraer-promotes-commercial-aviation-customer-support-at-mro-americas-2187 cited 15-06-2015

will accommodate between 70 and 90 passengers. The QLEAR Q-50 is estimated to capture 35% of the entire 50-seater market share. This accounts for a slightly growth of the market share for both ATR-42 and ERJ-145. However, as soon as the Q-50 enters into service and airlines are convinced that it can actually deliver lower levels of noise and emissions and a reduced operating cost compared to other airliners in their fleet, it is most likely that the market share will increase in the years following its inaugural flight. With the assumed 35% market share and the expected number of 2300 regional airliners with a capacity of up to 70 seats (36% of the total number given in Table 4.1 according to [5]) to be delivered by 2035, a number of 805 Q-50 units are expected to be built. This accounts for both traffic growth and aircraft replacement in all regions around the globe.

4.4 Key Success Factors for QLEAR Q-50

Airlines looking to purchase a regional jet should choose the QLEAR Q-50 because:

- Q-50 offers a 50% lower fuel consumption compared to its main competitors (CRJ-200 and ERJ-145). This was achieved by a combination of advanced propulsion systems and the optimization of the aerodynamic characteristics of the aircraft during cruise.
- Q-50 generates less noise compared to similar regional aircraft. This will enable aircraft operators to fly to airports with strict noise regulations. Also, airport charges will be lower for airports where landing fees are related to the noise produced by the aircraft on approach.
- Q-50 produces less CO_2 and NO_x emissions compared to its competition. According to the European Commission [5], 3% of the EU's total greenhouse gas emissions stem from the aviation sector. Thus, opting for an airliner with lower emission will minimize the impact of air travel on the environment.
- Q-50 features screens on both sides of the cabin. Besides all the features that are addressed in Chapter 5.1.1 extra revenue could be produced by showing advertisements on the screens. Passengers could also pay an extra fee to ensure they do not get advertisements during their flight. The screens could also show the amount of produced CO_2 compared to other aircraft, that way passenger would feel better flying the Q-50.
- The fuselage design of the Q-50 allows for the development of a family of aircraft which could accommodate more passengers. In the future, QLEAR Q80 and Q100 could be developed, with a capacity of 80 and 100 passengers, respectively. This is advantageous for an airline because the same crew would be able to operate the entire QLEAR fleet, thanks to the similar cockpit design which will be implemented.

[5] http://ec.europa.eu/clima/policies/transport/aviation/index_en.htm, cited 16-06-2015

Sustainable Development Strategy

Sustainability is more important now than ever. The impact of burning fossil fuels is becoming very noticeable and humanity is keeping an eye out for the protection of our environment. Even marketing strategies are starting to use sustainability as a selling point. That is why it is very important to make sure that the preservation of nature has a high priority during all design phases. One can distinguish four stages in the aircraft life where sustainability can be considered: design (Section 5.1), production (Section 5.2), operation (Section 5.3) and end-of-life (Section 5.4).

5.1 Design Phase

The Design Synthesis Exercise can basically be interpreted as the design phase of the aircraft so this chapter describes what has been done to make the aircraft sustainable. Luckily the evolution in aviation helped since newly developed technologies are often more sustainable than its older counterpart. The engine and materials are perfect examples since the specific fuel consumption goes down with every new generation of engines and the introduction of lighter materials results in lower thrust requirements thus lower fuel consumption. These are beneficial for sustainability and for the operating cost of the Q-50.

One of the killer requirements of the project was to have a 50% reduction in CO_2 which would basically translate into a 50% reduction in fuel consumption if the aircraft was the only variable. To achieve this a lot of research and work has been done to make sure the engines are at the optimum of efficiency, which is explained in detail in Chapter 12. Ways to reduce the noise of the engine and other ways of noise abatement are treated in Chapter 23.

Design choices made on other parts of the aircraft decreased either drag or weight resulting in a reduction of required thrust. For instance winglets have been added to the design of the wing. This reduces drag and increases the effective aspect ratio resulting in less fuel consumption. It furthermore reduces the noise usually created by the wingtips. A bold move has been made by going windowless as will be explained in Section 5.1.1. Material selection also contributed (Chapter 10) by offering lighter and stronger materials than are being used by the competition.

NO_x emissions had to be reduced by 25%, another requirement that was met by careful engine design (Chapter 12). QLEAR's facilities will also be contributing to the active reduction of NO_x concentrations in the ambient air using technology explained in Section 5.2.

5.1.1 Windowless Fuselage

In an effort to reduce the operational empty weight even more, and thus reducing the fuel consumption, the use of a windowless fuselage has been considered. Torenbeek [3] provides an equation to estimate the weight reduction when removing all the windows in the cabin as shown in Equation 5.1.

$$W_S = 23.9 A_{ap} \sqrt{b_f} \tag{5.1}$$

The equation results in a 4 kg weight saving per window, or 104 kg for the entire aircraft. To assure certain amount of travel comfort an alternative must be provided so screens will be added. These screens can show the surroundings of the aircraft, or any other scenery for that matter, although the former would be preferred as a means to avoid motion sickness. Flight information could be shown on the screens as well as landmarks and other points of interest like the ISS as shown in Figure 5.1.

What is important for the design of the Q-50 is whether the fuel savings due to the removal of the windows outweigh the fuel needed to carry and power the screens. Since QLEAR wants to provide the passengers with an in depth experience using 9 seamlessly connected 55" OLED screens per side, the system would consume around 1,800 W[1] in total thus burning 150 grams of jet fuel per hour. Furthermore would the screens require regular overhauls, due to the short lifespan of the blue OLED's, which would cost around USD 45,000[2].

Toshiba Matsushita Display Technology has developed an OLED panel with a lifespan of 60,000 hours which is a substantial increase and would result in an overhaul every 15 years (depending on the use of the aircraft). The OLED association believes an OLED TV may achieve lifetimes in excess of 100,000 hours [7]. The prices of OLED screens are quite high at the moment since it is a very new technology but are bound to go down as is the trend with all new technologies. When looking at the trend line of the price of LED technology (shown in Figure 5.2) it can be seen that its price dropped by almost 95% between 2005 and 2013 even though its performance increased.

[1] http://www.displaymate.com/LG_OLED_TV_ShootOut_1.htm
[2] http://www.lg.com/us/tvs/lg-55EC9300-oled-tv

Figure 5.1: Artistic rendering of the inside of a windowless aircraft

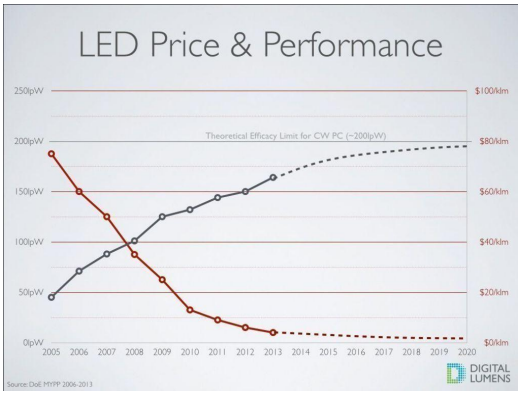

Figure 5.2: Evolution in price and performance of LED technology

This trend line can be extrapolated if the date of introduction of OLED technology is taken into account. This would mean an 80% decrease in price would be more fitting. Considering this it can be assumed that by 2035 an operator would have to overhaul the screens every 100,000 hours which would cost USD 9,000.

The weight of the screens themselves obviously play an important role. OLED screens have been chosen because they consume little power, provide crisp images, have a high contrast ratio, a high viewing angle, are thin, can be bent to fit to the curvature of the fuselage and most of all because they are light. The weight of the lightest OLED TV at the moment[3] will be used, which is 1.9 kg, since it is doubtful that screens will become much lighter. The aircraft boasts 18 screens so the total added weight will be 34.2 kg for the screens alone. Power will be supplied via one of the many power cables running along the aircraft although some cables for the video-input must be added. The screens must also be attached to the inner fuselage which should be fairly easy due to the low weight. Attachment rails can be moulded in the skin of the fuselage without any noticeable weight gain and the attachment hooks for the screens themselves will not weigh more than 100 g resulting in 2 kg per screen. The system will require around 92 m of high quality HDMI cables which will weigh in around 7 kg in total[4] and 2m of power-cable is added per screen as to connect to the nearest power-line running along the aircraft. We assumed 1.5 mm^2 cores for the power cables which is probably too thick but this will result in conservative weight estimations. These power-cables weigh about 0.3 kg/m [5] so a total of 11 kg will be added due to the 3 6m of power-cables. Finally this means that the implementation of the screens would add around 54 kg to the Q-50, reducing the total weight reduction obtained by removing the windows to a marginal 50 kg.

However, even the smallest weight reduction is beneficial so now it is important to calculate whether the money needed to overhaul the airplane after 100,000 hours does not nullify (or worse) the money saved by consuming less fuel. This tiny weight reduction of 50 kg results in a reduction in fuel consumption of 14 kg per mission where a mission is defined as flying the maximum range of 2,000 km. At full speed this would require a little under 2 hours and 30 minutes but taking into account acceleration and deceleration at the beginning and the end of the mission, the mission time is rounded up to 3 hours. This results in an hourly reduction in fuel consumption of 4.67 kg or 4.52 kg per hour when the power consumption of the screens is taken into account. The density of jet fuel is 0.81 kg/l and at the moment of writing the price of jet fuel is USD 0.486 per litre. This results in an hourly reduction in operating cost of USD 2.8.

$$\frac{4.52 \cdot 0.486}{0.81} = \$2.712 \tag{5.2}$$

Assuming the screens will be turned on during the entire flight, the total amount of money saved is simply the result of equation 5.2 multiplied by 100,000 hours of service resulting in USD 280,200. Deduce the cost of replacing the screens (USD 9,000) and the end result is an hourly saving of USD 2.62. Appendix B) shows two tables of aircraft from Delta Air Lines and US Airways containing flight data gathered for both the CRJ-200 and the ERJ-145. These are just 2 of the 10 tables that were made to calculate the average daily flight time which was found to be 9 hours and 8 minutes, which would mean the screens would have to be replaced after 31 years. One can imagine that this is a cost that will not be made. In case the aircraft will be used to the fullest of its potential yet restricted by obligated maintenance intervals and curfews imposed by airports,

[3] http://www.oled-info.com/lg-display-demonstrates-097-mm-thick-55-flat-oled-tv-panel

[4] http://www.homedepot.com/p/CE-TECH-50-ft-Deluxe-High-Speed-HDMI-Cable-with-Ethernet-MC8202A0122010/203705950

[5] http://www.nexans.nl/eservice/Netherlands-nl_NL/navigateproduct_540149238/VO_YMvKas_mb_3_x_1_5_1_5_mm_100m_.html#characteristics

it will have 20 operational hours. If the screens are turned on during turnaround the replacement interval is approximately 14 years. In case the screens are shut down during turnaround the interval is increased to approximately 19 years.

5.2 Production Phase

A lot of emissions are produced during production since an entire plant has to be powered. Next to reducing the amount of energy that is required one could also make sure that the required electricity is generated in a sustainable way. The roof of all QLEAR facilities should contain solar panels and the rest of the required electricity can be bought from so called 'Green Electricity Providers'. Another way to minimize the damage on the environment is by using the required materials and resources responsibly. An optimized production line will save a lot on energy consumption and a way to optimize it is by using lean manufacturing which has been discussed extensively in the mid-term report [1].

A lot of carbon fibre will be used to build a single aircraft. To produce one kilogram of high strength carbon fibre one would need to carbonize a little over 2 kilograms of polyacrylonitrile (PAN) [8, 9] in multiple furnaces, a process that requires a lot of energy. Carbon fibre also has a pretty big environmental footprint due to the fact that polyacrylonitrile is a fossil-resource-based polymer. Using recycled carbon fibres in as many parts as possible is a good way to keep the power consumption down since it would require almost 20 times less energy as is shown in Table 5.1 [10] and would also mean it is not necessary to process new PAN. At the moment a recycling process is being researched where reclaimed carbon fibres retain 97% of their original strength and experience no change in modulus so the problem of severely weakened recycled fibres will no longer exist by 2035 [10]. Furthermore is there a lot of research underway that is aimed towards developing renewable carbon fibre where fossil-resource-based PAN is no longer a requirement. One of which is the development of carbon fibre using lignin (a class of complex organic polymers important in the formation of cell walls in wood) as a precursor instead of PAN [11]. Obtaining lignin will not be a problem since it is a by-product from the production of bio-fuel and paper.

Table 5.1: Comparison of virgin and recycled carbon fibre

	Materials ($/lb)	Energy (kWh/lb)
Virgin carbon fiber	15-30	25-75
Recycled carbon fiber	8-12	1.3-4.5

A lot less metal alloys will be used compared to the competition but by using recycled metals a lot of energy could be saved and emissions reduced drastically. For example, recycled aluminum uses only 5% of the energy and produces only 5 percent of CO_2 emissions when compared to the production of virgin metal[6]. Since the aluminium in the Q-50 does not have dead set requirements its properties are allowed to vary slightly.

All QLEAR facilities will be coated with materials like polyethylenimine (PEI) and titaniumdioxide (TiO_2) to reduce the CO_2 and NO_x concentrations in the air. PEI adsorbs CO_2 when it's coated on zeolites [12] and TiO_2 can synthesize harmless nitrate ions (NO_3^-) out of NO_x-molecules [13].

If a zeolite is coated with PEI it is able to adsorb CO_2 out of the surrounding air and thus lower the local CO_2 concentrations which will contribute to the reduction of CO_2 of the entire program. At the moment results of the amount of CO_2 that is successfully being captured vary greatly but one can assume 4.5 wt% as the current achievable value for MCM-41-PEI-75 at sea level (288 K, 100 kPa). So for every kilogram of coated zeolite 45 g of CO_2 will be adsorbed every hour. The downside is that after an hour the zeolite will have reached maximum capacity and needs to be purged (by heating it up to 100°C) to be able to be used again. It is safe to assume that this technology will mature a lot by 2035 resulting in higher capacities and higher adsorb percentages.

TiO_2 can be coated on every concrete surface but is sensitive to wear. It has been empirically shown that it lowers the NO_x concentrations in the surrounding air by an average of 19%. At the moment the coating remains effective for about 11 months on actively used surfaces such as pavement and would then need to be replaced, but the durability is expected to increase substantially by 2035 although regular recoating will still be necessary. If the coating is applied to concrete surfaces that don't encounter a lot of traffic (like concrete walls) the coating will remain effective for a much longer time. Here it can be assumed that the durability will increase by 2035.

5.3 Operational Phase

The operational phase is where the product has to perform as was intended otherwise the proposed reductions will not be achieved. During the design phase it has been analytically estimated how much the aircraft would

[6] http://www.benefits-of-recycling.com/recyclingmetals/

emit but only now will this be actually measurable. If designed correctly the aircraft, its operator and the entire world benefits and this for an extended period of time since the aircraft will fly for about two decades. Other ways to make the flights even more sustainable are SESAR and CDA (among other things) which will be explained in Chapter 19.1.

To make aviation more sustainable a lot of attention is being paid to alternative fuels. This is something that is not specific to the Q-50 and thus does not add to the reduction of CO_2 emissions compared to the competition. At the moment biofuels produced from algae, also known as third generation biofuels, seem like the best option. An other possibility are fourth generation biofuels which are made from specially engineered plants or trees which have higher energy yields and can be grown on non-agricultural land or bodies of water. They would actually go well with the production of lignin-based carbon fibres since lignin would be a byproduct. That way the flora will provide the Q-50 with lignin for its sustainable carbon fibre and it will provide biomass for the production of biofuel. Biofuel has a lower density and less aromatics and thus still needs to be mixed with traditional jet fuel to be usable. Since the production of biofuel produces 84.38% less CO_2 [2] and the Q-50 will be using a 50:50 mix, one can claim that 42.19% less CO_2 will be emitted during the production of the fuel that will be used.

When the aircraft is not airborne it would be interesting to use pushback tractors to do as much of the ground manoeuvres as possible. They can be powered by alternative fuels or electricity but would move at a slower pace than the aircraft would on its own reducing the capacity of the airport, so careful planning is required. The previously mentioned compounds (PEI and TiO_2) that are applied to all facilities would also do their job during the operational phase making them a very interesting investment.

5.4 End of Life Phase

There are three options when an aircraft has reached the end of its life: recycle, repurpose or dump. Dumping is obviously not sustainable and thus not a possibility. Both recycling and repurposing provide a range of possibilities but ultimately the goal is to reduce the amount of materials that end up on landfills to an absolute minimum.

Recycle

Recycling metallic parts is a well known procedure since this has been done on a large scale in other industries so this should not pose a big challenge. The implementation of composites has increased drastically over the past decade and only now are companies starting to think about how to handle the inevitable increase of outdated composite parts. Some companies have sprung up that specialise solely in recycling composite materials and thus far the benefits of recycling seem very promising as was previously shown in chapter 5.2. A few years ago about 50% of an aircraft was recycled, a shockingly small number compared to the current 80%. The Aircraft Fleet Recycling Association[7] is aiming to increase this number to 90% by the end of 2016. It is estimated that the Q-50 will be fully recyclable if recycling technology keeps up. The recycling of LEDs for instance is not optimized yet but is expected to be by 2035 due to global pressure.

Repurpose

Parts of the cockpit are often still usable and can be taken out and reused in other, still operable aircraft. This already is common practice with line replaceable units in older aircraft but they have become unwieldy with the rise of glass cockpits which does not imply that the screens in glass cockpits cannot be used again on other airplanes or for entire different purposes. The interior of the aircraft can be used again as well and are often very sought after by aircraft enthusiasts. It is also a possibility to repurpose entire parts of the aircraft for entirely different applications. There are examples all over the world of airplane parts being used as furniture and parts of houses.

[7] http://www.afraassociation.org/

Interface Identification and Iterations

This chapter describes the interface identification for the QLEAR Q-50 airliner in Section 6.1, followed by the iterative process set up by using the N2 chart, as can be seen in Figure 6.1. The N2 chart is set up to visualize the interactive process followed when designing the aircraft. The iterative process is performed through different functions and their corresponding interfaces.The main functions during operation of the aircraft are set on the diagonal elements. More elaborated information about all the function can be seen in the functional flow diagram in Chapter 19.1.1. The basics behind the iteration process is to do the Class I weight estimation based on reference data. The outputs of the Class I estimation are then used to size the subsystems. Afterwards the, more detailed, Class II weight estimation is performed. The subsystems will be sized again according to the output of the Class II weight estimation. Next the performance parameters are estimated and used as an input for the Class I. The above mentioned process is repeated again until the offset between the two weight estimations is within a desired margin.

6.1 N^2-Chart

The chart is compiled using the functions as defined in the functional breakdown structure in Section 19.1.1. The main functions are shown on the diagonal elements of the chart and it works in the counter-clockwise direction. Starting at a certain diagonal element, the vertical column indicates the output of that block. Then following this output horizontally, so left or right, it gives the input to another diagonal element. The other way around, starting from a diagonal element going horizontally indicates the requirement of this block which is needed for another diagonal element. An example can be given for the two explanations. For the first explanation: one of the outputs (vertically) of the function 'Provide ground manoeuvring capabilities' is 'Provide thrust during ground roll' which is the input (horizontally) for the function 'Provide power'. By the use of the second explanation: starting from 'Provide thrust', this function (going horizontally) should 'Provide thrust during ground roll' for (going vertically) function 'Provide ground manoeuvring capabilities'. The N2 chart for the QLEAR Q-50 can be seen in Figure 6.1. The N2 chart is useful for establishing the relation between the functions dictating a design. As can be seen in the chart, almost every aspect of an aircraft's design is connected to every other aspect. Therefore it is useful to list all these connections in a graph, so as to keep track of them more easily during the design process. This diminishes the risk of accidentally forgetting how a single change in a component's design influences the other aspects of the project.

6.2 Optimizing Take-off Weight, Wing and Horizontal Tail Surface Areas

Chapter 10 explains how the use of composite materials results in a significant weight savings, compared to the results of the class II weight estimation presented in the mid-term report [1]. This is because the method of Torenbeek, explained in detail in [3], assumes that the aircraft is build out of aluminum. To account for the use of composite material, the following reduction factors were applied to the output of the class II weight estimation: fuselage - 51%, wing - 40%, horizontal wing - 40%, vertical stabilizer - 40%. Because the weight reduction is significant, there is a need to adjust the weight of all the main components, such that the wing, landing gear and all further systems are sized for the appropriate weight and the final design of the aircraft is optimized for a value close to the actual take-off weight of the aircraft. The iteration process followed in this chapter is summarized in Figure 6.3. The first step is to establish an estimate for the OEW, and MTOW using the class I method. This method takes into account the mission profile, thus the FW (Fuel Weight) can also be estimated. For the first iteration, the initial values are based on statistics and were derived in the mid-term report. For subsequent iterations, the following procedure will be followed:

- The ratio of the operational empty and maximum take-off weights obtained at the previous step (class II weight estimation) is computed $k = \frac{OEW}{MTOW}$, from which the operational empty weight can be written as $OEW = k \cdot MTOW$;
- The fuel weight is calculated with $W_{fuel} = 0.1523 \cdot MTOW$ based on the fuel fractions and the mission profile [1];

Provide accessibility for maintenance & inspection	Maintain and inspect fuel system	Maintain and inspect internal fuselage	Maintain and inspect passengers doors	Inspect and maintain cargo doors	Inspect and maintain emergency exits	Maintain and inspect landing gear	Maintain and inspect communication/navigation system	Maintain and inspect information system	Maintain and inspect aerodynamic surfaces	Maintain and inspect structure (spars, skin, etc.	Maintain and inspect engines	Maintain and inspect power system	Maintain and inspect aerodynamic surfaces	Maintain and inspect safety equipment	Maintain and inspect landing gear brakes
Provide accessible fuelling valves	Provide fuel	Provide separation of fuel and passengers compartments	Provide clearance to perform actions simultaneously	Provide clearance to perform actions simultaneously		Fuel used for unassisted ground manoeuvring		Provide proper indications to pilots	Fuel storage in an aerodynamic fashion	Minimise fuel tank size	Have a proper and redundant fuel line system to engines	Feed fuel to APU to ensure owner on the ground	Balance fuel and shut valves in case of OEI		
Provide easy accusable fuselage parts	Provide separation of fuel and passengers compartments	Provide passenger, crew & cargo accommodation	Provide cabin layout such that passengers don't block aisles	Provide separation of cabin and cargo compartments	Ensure that fuselage design helps with emergency	Provide storages for landing gear			Ensure minimal frontal area	Minimise cut-outs and drilling in structural components	Provide proper engine attachment location	Provide space for electrical and other power systems	Provide proper distance and shielding from engines	Provide fuselage design where safety equipment can be installed	
Provide accusable doors	Provide clearance to perform actions simultaneously	Provide doors that are not interfering with fuselage design	Provide loading/unloading passengers capabilities	Provide clearance to perform actions simultaneously	Ensure passengers don't block emergency exits	Ensure ground control is not influenced by loading	Ensure loading does not influences the calibration	Ensure loading does not influences the calibration	Ensure doors close completely	Ensure limited door size	Ensure no damage of the engines while loading and unloading			Ensure no damage of the aircraft while loading and unloading	
Provide accusable and easy usable cargo doors	Provide clearance to perform actions simultaneously	Provide separation of cabin and cargo compartments	Provide clearance to perform actions simultaneously	Provide loading/unloading cargo capabilities	Emergency unloading should be fast and efficient	Ensure ground control is not influenced by loading	Ensure loading does not influences the calibration	Ensure loading does not influences the calibration	Ensure doors close completely	Ensure limited door size	Ensure no damage of the engines while loading and unloading			Ensure no damage of the aircraft while loading and unloading	
Provide accusable and easy usable emergency equipment	Shut down fuel flow in case of emergency	Provide comfort for passengers and cargo	Ensure safe slides and emergency exits	Ensure cargo is protected during emergency	Provide emergency capabilities	Ensure landing gear is not damaged during an emergency		Ensure emergency does not influence the instrumentation	Ensure emergency exits are closed completely	Ensure limited emergency exits and equipment size	Ensure engines are not influenced by emergency exits	Ensure power system is not damaged during emergency		Safety equipment should be used during an emergency	Ensure proper braking during emergency
Easy access to landing gear fairings	Ensure fuel flow is not interrupted by ground manoeuvring	Provide comfort for passengers and cargo	Ensure doors are closed when taxiing	Provide clearance for cargo doors	Ensure ground control is maintained during emergency	Provide ground manoeuvring capabilities	Ensure communication is maintained during taxiing	Ensure taxing does not influences the calibration	Provide aerodynamic shaped landing gear (retractable)	Ensure small landing gear				Ensure safety during taxiing	Provide braking during ground roll
Provide accusable and easy usable communication/navigation units					Communication systems must be operative in an emergency	Provide communication with the tower during taxi	Provide communication/navigation		Provide optimal flight profile	Provide small and light system		The system should use minimal power	Ensure proper navigation during engine failure(s)		
Provide accusable and easy usable sensor units	The system should be controlled properly by the instrumentations	Ensure pressurisation is done correctly		Ensure doors are closed completely	Ensure sensors and instruments work properly	Ensure steering during taxiing	Provide instrumentation for the navigation and communication	Provide instrumentation/sensors	Provide proper aerodynamic data	Provide small and light system	Provide proper engine instrumentation and censoring	The system should use minimal power	The system should be able to inform an engine failure		Provide adequate braking controls
	Ensure distribution of the fuel tanks and fuel level	Provide comfort for passengers and cargo	Ensure doors are of suitable shape	Ensure doors are of suitable shape	Ensure stability for emergency configurations	Ensure clearance of landing gear			Provide aerodynamic performance	Minimise structural loads	Ensure proper inflow		Ensure smooth shape to reduce of ineffective airflow	Stay within the flight envelope	Provide proper spoilers
Provide maintenance hatches	Ensure that fuel system is strong enough to withstand loads	Provide comfort for passengers and cargo	Ensure doors are of suitable dimensions	Ensure doors are of suitable dimensions	Provide clearance between surfaces and emergency exits	Ensure structure can handle loads imposed during ground roll	Ensure proper casing and sealing of system	Ensure proper casing and sealing of system	Provide a structure capable of withstand the aerodynamic loads	Provide structural integrity	Provide a structure capable of withstand all loads from the engine	Provide a structure capable of withstand all loads from the APU	Ensure engine(s) stay attached during failures	Provide safe structures	Provide a structure capable of withstand all loads during braking
Provide easy attachable and cleared engines	Have a low fuel consumption	Try to minimise engine noise and emission	Provide clearance between door and engine for safe loading/ unloading	Provide clearance between door and engine for safe loading/ unloading	Ensure thrust during emergency	Provide thrust during ground roll			Minimise wake interference	No structural damage during operation of engines	Provide thrust	Provide powering by the engines	Provide fuel cut off in case of engine fire/ failure	Ensure safe and reliable operation of engines	Provide thrust reversing system
Provide accessible and clear separated electrical system	Provide clearance between external power plug and fuelling system	Provide power for cabin systems (screens, lights, etc.)	Ensure proper lighting of the cabin	Ensure automatic closure of cargo doors	Ensure power during emergency	Provide power during ground roll	Provide power to the system	Provide power to the system	Provide power for control surfaces		Ensure engine start-up	Provide power	Ensure (try) engine start-up	Provide power for safety equipment	Provide powered braking assist
	Provide safety by shutting down fuel flow to prevent fire	Provide proper distance and shielding from engines			Ensure emergency is possible during OEI	Ensure ground roll during OEI	Ensure system stays online during engine failure(s)	Ensure system stays online during engine failure(s)	Minimise induced drag due to OEI	Ensure structure's high temperature properties and provide fail-safe structure	Ensure enough thrust is generated during OEI		Provide engine(s) inoperative capability		
Provide accessible and easy safety equipment	Ensure safe handling and storage of fuel	Ensure that the cabin is equipped with proper safety equipment	(Un)loading should go in a fast and safe manner	Ensure cargo bay is equipped with safety equipment	Safety equipment should be used during an emergency	Safety equipment should be available during taxiing	Ensure back-up system	Ensure back-up system	Provide proper de-icing	Report defects	Prevent FOD	Ensure safe power generation and conduction of electricity		Safety capabilities	Provide redundant braking system (manual)
Provide accessible and easy landing gear brakes		Provide comfort for passengers and cargo			Ensure proper braking during emergency	Provide braking during ground roll			Provide fairings	Minimise structural loads			Ensure proper breaking while OEI	Ensure safe braking (heating)	Provide braking capabilities

Figure 6.1: N^2-chart

- The weight of the trapped fuel and oil is assumed to be equal to 1% of the take-off weight [14];
- Having expressed all the weights in terms of the take-off weight, a new estimation for the MTOW can be obtained with $MTOW = \frac{W_{payload}}{1-(k+0.1523+0.01)}$;
- New estimates for the OEW and FW can be computed with the previously obtained value of the take-off weight.

Having new values for the weights, the second step is to look back at the preliminary sizing performed in the mid-term report. The result of this initial sizing can be summarized in Figure 6.2. This figure shows the design point of the aircraft after considering the performance of the aircraft during take-off, climb and landing and analyzing the effect of various stall speeds and load factors. A detailed explanation on how this graph was obtained and the governing equations behind each curve can be found in [1]. The two ratios corresponding to the design point shown in Figure 6.2 with green are the wing loading (W/S = 4000 N/m^2) and the thrust loading (T/W = 0.32).

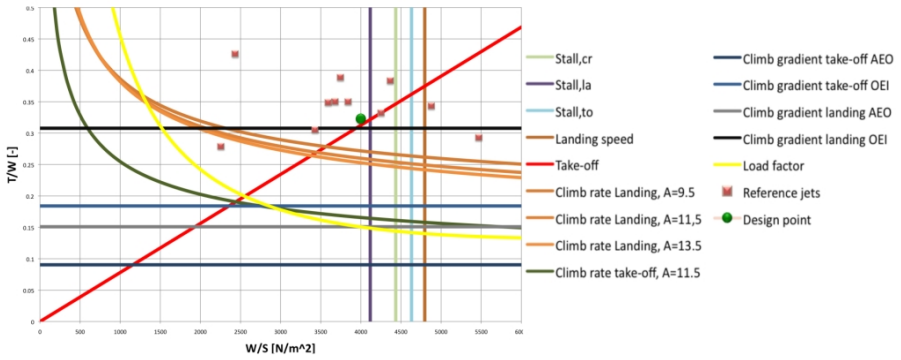

Figure 6.2: Results of the initial sizing of the aircraft

Because a new take-off weight was determined, a new wing surface area and engine thrust is required for an optimal design. The new values for these two parameters are computed using the ratios above and new estimate for MTOW. However, a new thrust means that the weight of the engine also changes. The estimation of the new engine weight represents the third step. In order to understand the relationship between the required take-off thrust and the weight of the engine, Figure 6.4 was created, where the weight of engines currently in service versus their thrust are displayed. A trend-line can be obtained, such that the engine weight can be computed with $W_{engine} = 0.1761 \cdot T_{take-off} + 199.6$, where the take-off thrust is expressed in Newton.

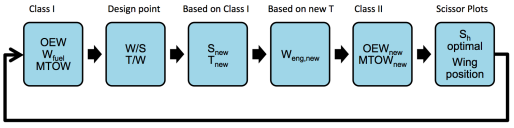

Figure 6.3: Iteration loop

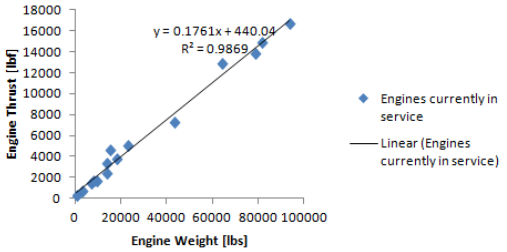

Figure 6.4: Engine weight - Thrust relationship

Having new estimates for OEW, MTOW, FW and W$_{engine}$, the fourth step of the iteration can now begin. For this step, the new inputs will be fed to the class II weight estimation script that was developed and introduced in the mid-term report. As explained in [1], the script is based on the Torenbeek method and estimates the weight of the main aircraft systems, taking into account geometric aspects such as aspect ratio, sweep angle, wing surface area, fuselage diameter, chord length and taper ratio. The script was adapted since the mid-term report, such that it takes into account the reduction factors obtained by using composite materials, which were mentioned before. The optimum surface area of the horizontal wing and the position of the main wing with respect to the fuselage will be adjusted based on the outputs of the scissor plot. Summing up the individual weights new values for the OEW and MTOW are obtained. This new values will be used in the class I weight estimation (step 1), closing thus the loop of the iteration cycle.

Table 6.1: Verification results - sizing and iterations

Item	Analytic	Numerical	Diff. [%]
OEW_it.1 [kg]	10156	10156	0.0
FW_it.1 [kg]	2726	2726	0.0
MTOW_it.1 [kg]	19181	19181	0.0
S_it.1 [m^2]	43.9	43.9	0.0
OEW_it.3 [kg]	9915.3	9913.6	0.017
FW_it.3 [kg]	2682	2682	0.0
MTOW_it.3 [kg]	17599	17596	0.017
S_it.3 [m^2]	43.2	43.2	0.0
OEW_it.5 [kg]	9915.3	9912.7	0.026
FW_it.5 [kg]	2682	2682	0.0
MTOW_it.5 [kg]	17595	17595	0.026
S_it.5 [m^2]	43.2	43.2	0.0

Table 6.2: Inputs and outputs of iterations

Item	Input	Output	Difference %
OEW [kg]	12955	9755	- 24.7
MTOW [kg]	20860	17425	- 16.5
S_{wing} [m^2]	47.0	43.0	- 8.5
$T_{take-off}$ [kN]	64.0	55.1	- 13.9
$W_{eng.}$ [kg]	775	700	- 9.7
S_h [m^2]	9.4	8.35	- 11.2
x_{lemac}/l_{fus} [-]	0.5160	0.4960	- 3.9

6.3 Verification of MATLAB Script

Since the whole iteration process is highly repetitive, it was decided to build a MATLAB script. This would speed up the process and eliminate unwanted calculation errors. However, one should not trust blindly such a script and the results produced by it. Therefore, the script needs to be thoroughly verified and the results validated prior to its use for the project. The verification and validation steps that were taken for the iteration script have been recorded and are presented in detail in Table 6.1.

When looking at the differences between the analytic and numerical results for the iterations, it can be seen that for the first iteration the difference is zero. For the third and fifth iteration however, the differences become slightly larger which is due to the fact that the round-off errors accumulate during each iteration. Since the program converges quite rapidly, the differences will remain relatively small. Therefore it can be concluded, also for this script, that the program provides accurate results.

6.4 Iteration Results

The final results of the iterations are presented in this section. The input and output parameters can be found in Table 6.2. Figures 6.5 and 6.6 show the impact on the operation empty and take-off weights and wing surface area as the number of iterations increases.

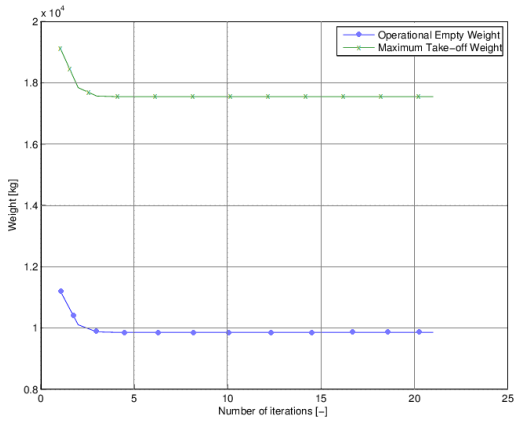

Figure 6.5: Iterated weight values

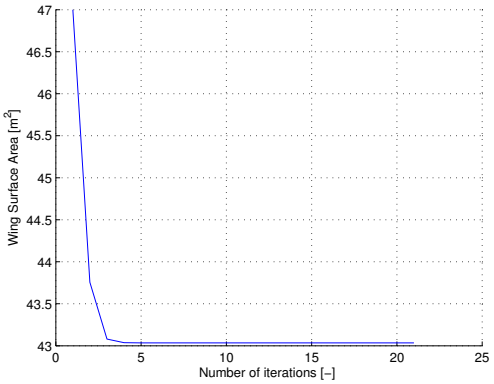

Figure 6.6: Iterated wing surface area values

As seen from the two figures, because of the reduction factors applied to the fuselage, wings and tail, there is a negative trend in all these plots. The curves are steep at the beginning, because the reduction factors greatly reduced the weight of the main aircraft components, which in turn required a smaller wing surface area, less take-off thrust and thus, lighter engines. Also, considering the stability and controllability aspects, the horizontal wing surface area and wing position were adjusted. These will be expanded in Chapter 7.

Weight and Balance

Now that the preliminary sizing and wing design are finished, the weight and balance of the aircraft can be analyzed. The verification and validation of the script used in this chapter is done in Section 7.1. The component weight estimation is done in Section 7.3 and the center of gravity of each component and the entire aircraft are estimated in Section 7.3.1. Using the stability and controllability curves the scissor plot will be created which will be used in Section 7.4 to size the horizontal and vertical tails. In this chapter the method of Torenbeek [3] is used for the component weight estimation and for the determination of the OEW center of gravity location.

7.1 Verification and Validation of Class II Script

In order to perform the Class II weight estimation, a MATLAB program is developed. As a verification procedure, first the program is initialised by making sure all entered parameters are in SI-units. After this, the code is verified by debugging the software. The verification results are shown in Section 7.1.1 and the discrepancies and iterations performed are discussed in Section 7.1.2.

7.1.1 Verification Results

For the calculation verification, several unit tests are performed on the different blocks of the MATLAB program, from which some results can be seen in Table 7.1. For the analytical approach the equations from Torenbeek [3] were used and computations were performed by hand. For the numerical approach, the formulas were put into a MATLAB script. There was no difference in assumptions for both methods, except for the assumptions stated by Torenbeek itself. The only difference occurs in the accumulation of results. When performed by hand fewer significant digits are used as when computed by MATLAB. It should be noted that for the verification of the Class II weight estimation, data from the Fokker 100 is used.

Table 7.1: Verification results block 1 (Class II weight estimation)

Parameter	Analytical	Numerical	Difference
W_{wing} [kg]	3260.82	3259.68	0.030%
W_h [kg]	515.97	515.83	0.027%
W_v [kg]	310.54	311.16	0.200%
W_{pg} [kg]	4112.35	4111.71	0.015%
W_{air} [kg]	697.51	697.51	0.0%
W_{el} [kg]	1060.90	1060.89	0.0%

Table 7.2: Verification results of the system tests (Class II weight estimation)

Parameter	Analytical	Numerical	Difference
W_{fg} [kg]	18703.2	18696.0	0.03%
W_{wg} [kg]	5520.8	5516.0	0.07%
OEW [kg]	24247.5	24212.0	0.14%
c.g.$_{fg}$ [% LEMAC]	33.5	33.4	0.30%
c.g.$_{wg}$ [% LEMAC]	46.8	45.9	1.96%
c.g.$_{total}$ [% LEMAC]	36.5	36.4	0.27%

After performing unit tests on the separate blocks of the program, system tests are performed to check if the different modules work well together to provide the correct results. In this case, for the Class II weight estimation, this was done by comparing the weight and centre of gravity location of the fuselage, wing and tail group and the total OEW. The results can be seen in Table 7.2.

7.1.2 Discrepancies and Iterations

As can be seen in the tables above, the differences between the analytic and numerical results are small. The main reason for the differences can be attributed to round-off errors in the analytical solution. For the determination of the location of centre of gravity, the moment arms are determined manually for both the analytic and numerical solution. Therefore again the differences between the numerical and analytic solutions are very small. Besides that, the difference between the analytic and numerical results for the c.g. location of the wing is relatively large compared the other differences. The reason for this is that a slightly different formula is used to obtain the numerical results. Since the discrepancies are small in general, and the larges ones can be accounted for, it can therefore be concluded that the simulation tool works well and provides results without any errors. It has to be noted that the results presented in Tables 6.1 and 7.2 are the final results.

7.2 Validation of Results

This section discusses the validation process used to assure that the simulation tool is computing the right thing. In order to validate the Class II simulation model and the iteration model that is based on it, the operational empty weight and tail volume coefficients of similar aircraft is plotted and it is checked if the computed OEW and tail volume coefficients are reasonably close to the reference values. The validation results are shown in Section 7.2.1and the discrepancies and iterations performed are discussed in Section 7.2.2.

7.2.1 Validation Results

The main goal of the Class II weight estimation is to come up with a more accurate estimation of the operational empty weight. Therefore one way to validate the MATLAB program is to compare the output obtained by the program with reference aircraft that have similar passenger numbers, propulsion system, range and configuration. The results can be seen in Figure 7.1. From this it can be seen that the OEW of the Fokker 100 (red dot) is close to the OEW of reference aircraft. Moreover, Table 7.3 shows the real OEW and tail surface area of the Fokker 100 [1].

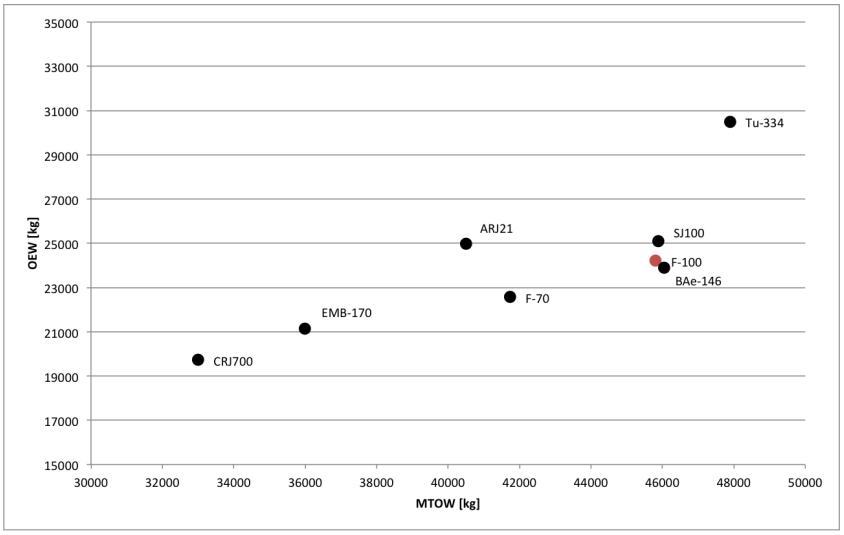

Figure 7.1: Maximum Take-off Weight versus Operational Empty Weight for reference aircraft and the Fokker 100

Table 7.3: Difference in manufacturer data and numerical results for the Fokker 100

Parameter	Manufacturer Data	Numerical Result	Difference [%]
OEW	24594 kg	24212 kg	1.57
Horizontal tail surface area	21.3 m^2	20.1 m^2	5.97
Vertical tail surface area	12.3 m^2	11.8 m^2	4.23

7.2.2 Discrepancies and Iterations

As to be expected there are some discrepancies in the validation data. When looking at Figure 7.1, the Fokker 100 data point is relatively close to other reference aircraft, however since the OEW and MTOW depend on many characteristics of the aircraft, it is impossible to obtain equal results. As can be seen in Table 7.3, the differences between the manufacturer data and the obtained numerical results are relatively small. The discrepancies that are present are mostly due to round-off errors and small items and coefficients that were estimated during the Class II weight estimation, since there was not enough detailed information available.

7.3 Component Weight Estimation

This section estimates the weight of the main aircraft components. But before proceeding to the actual results, the common assumptions and parameters used throughout the weight estimation process are presented in Table 7.4 given below.

[1] `http://www.flyfokker.com/fokker_100`, [cited 13-05-2015]

Table 7.4: Assumptions on Class II weight estimation

	Parameter	Assumed Value
Passengers and Crew	Number of passengers	50
	Weight of passenger	85 kg [15]
	Weight of luggage	15 kg [15]
	Number of crew members	3
	Weight of crew members + luggage	100 kg
Performance	Range	2000 km
	Ultimate load factor	2.5
Fuselage	Height	2.6 m
	Width	2.6 m
	Length	25 m
	Cabin length	14 m
Operational Items	Number of toilets	1
	Weight of toilet	136 kg [3]
	Number of galleys	1
	Weight of galley	114 kg [3]
	Weight of seat	10 kg [2]
	Weight of emergency equipment	100 kg [3]

The reduction factors discussed in Chapter 10 due to the use of composite materials were applied, compared to the values obtained in the mid-term report. The results presented in this section are those corresponding to the final aircraft design, thus after all the iterations carried out in Chapter 6. Reduction factors of 51%, 40% and 40% were applied to the weights of the fuselage, wing and tails (vertical stabilizer and horizontal tail), as obtained from the weight estimation formulas provided by Torenbeek in [3]. The final results are shown in Table 7.5 (fuselage group) and Table 7.6 (wing group), where the weight of each component can be seen, both in kilograms and as percentage of the maximum take-off weight.

Table 7.5: Fuselage group component weight

Aircraft Component	Weight [kg]	% of MTOW
Horizontal tail	190	1.1
Vertical tail	100	0.6
Fuselage	1925	11.1
Nose landing gear	140	0.8
Nacelle	150	0.9
Propulsion Group	1920	11.0
APU	180	1.0
Avionics	385	2.2
Hydraulics	290	1.7
Electrics	870	5.0
Furnishing	850	4.9
Air-Conditioning	410	2.4
Miscellaneous	100	0.6
Operational items	530	3.0
Total fuselage group	8040	46.2

Table 7.6: Wing group component weight

Aircraft Component	Weight [kg]	% of MTOW
Wing	740	4.2
Main landing gear	600	3.4
Surface Controls	375	2.2
Total wing group	1715	9.9

Summing up all the values in the previous two tables, the OEW is found to be 9755 kg. The payload which accounts for 5000 kg (28.6% of MTOW) and the fuel weight of 2670 kg (15.3% of MTOW) were not included in these tables. Adding these two values, the MTOW is equal to 17425 kg. Compared to the value obtained in the mid-term report (for Design 1), the operational empty weight is roughly 33% lower. Also, the take-off weight is 20% below of that obtained in the mid-term report, where all the calculations were based on aluminum materials. This value coincides with the percentage obtained by Boeing when they designed the 787-Dreamliner. According to the brochure "Boeing 787 from the Ground Up" [16], the use of an airframe consisting nearly half of carbon fiber composites, reduced the weight by 20 percent when compared to the more conventional aluminum design.

7.3.1 Center of Gravity Position Estimation

The location of the center of gravity of the operational empty aircraft will be determined from the component weight estimations made is Section 7.3 and shown in Tables 7.5 and 7.6. Equation 7.1 was used, where the sum of the weight of each component multiplied with its center of gravity location with respect to the aircraft nose was divided by the sum of weights of all components. Tables 7.7 and 7.8 summarizes individual c.g.

locations and the final results obtained for the wing and fuselage groups. The final center of gravity location for the empty aircraft is found to be at 12.7 m from the aircraft nose, or at 0.51· x_{cg}/l_{fus}.

$$x_{c.g.} = \frac{\Sigma_1^n W_i \cdot x_{cg_i}}{\Sigma_1^n W_i} \tag{7.1}$$

Table 7.7: Fuselage group c.g. locations

Component	c.g. [m]	Assumption made
Horizontal tail	25.0	Scaling of the CRJ-200 [17]
Vertical tail	22.5	Scaling of the CRJ-200 [17]
Fuselage	11.8	At 47% of fuselage length [3]
Nose landing gear	3.4	Scaling of the CRJ-200 [17]
Nacelle	18.4	Scaling of the CRJ-200 [17]
Propulsion Group	18.4	Scaling of the CRJ-200 [17]
APU	23.8	At 95% of fuselage length [3]
Avionics	1.5	Between bulkhead and nose gear [3]
Hydraulics	12.5	At 50% of fuselage length [3]
Electrics	12.5	At 50% of fuselage length [3]
Furnishing	7.0	At 50% of cabin length [3]
Air-Conditioning	7.0	At 50% of cabin length [3]
Miscellaneous	7.0	At 50% of cabin length [3]
Operational items	7.0	At 50% of cabin length [3]
Fuselage group	12.5	

Table 7.8: Wing group c.g. locations

Aircraft Component	c.g. [m]	Assumption made on c.g. location
Wing	12.4	At 16% MAC behind LEMAC, following procedure outlined in [3]
Main landing gear	13.0	Based on scaling of the CRJ-200 blueprints [17]
Surface Controls	13.0	At 100% MAC behind LEMAC [3]
Total wing group	13.4	

7.4 Tail Design

As mentioned in the Baseline Report [2], the choice was made to use a T-tail configuration, mostly since the tail will not be in the wake of the main wing and will therefore encounter clean air, which is beneficial and more efficient. Since a T-tail configuration is used, the assumption was made that the down wash due to the main wing can be neglected. However, after researching the different possibilities with regard to the mobility of the horizontal tail, it was decided to go for a fixed tail. The main reason for this is that this will significantly decrease the weight, complexity, manufacturability and risk of failure of the horizontal tailplane. The design approach that is taken for both the horizontal as well as the vertical tail is shown in Figure 7.2. Since many values are taken from reference or computed using basic formulas, only the airfoil selection process is described in the following sections, together with the stability considerations. The final values are shown in Table 14.19.

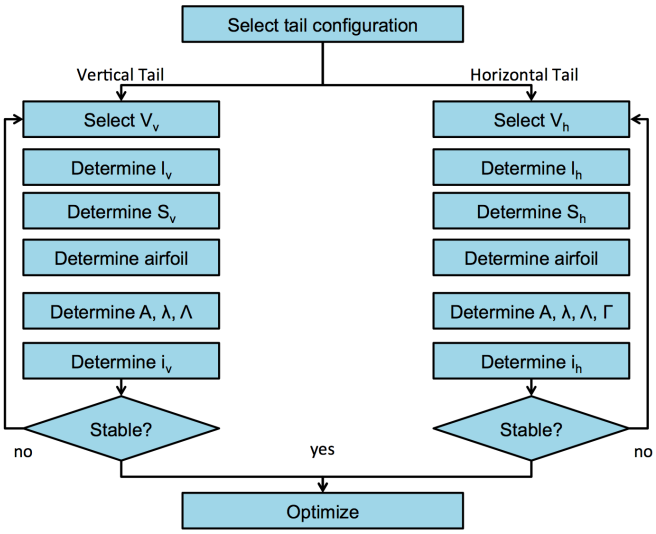

Figure 7.2: Flowchart of the sequential steps taken during the design of the tail

Now that the center of gravity location of the aircraft was determined, the loading diagram of the aircraft can be created. This loading diagram shows how the center of gravity of the aircraft varies during ground operations. The result can be seen in Figure 7.4, where the 2-2 seat configuration was used, with a pitch of 31 inches and the first row located 5.9 m behind the nose of the aircraft. The fuel was assumed to be located 30% MAC behind the LEMAC. The loading diagram was obtained in the following manner:

- with blue, from bottom to top: all bags are placed in the front cargo bay → all bags are placed in the rear cargo bay → passengers with aisle seats board from the front of the cabin towards the rear → passengers with window seats board from the front of the cabin towards the rear → aircraft fuel is added
- with green, from bottom to top: all bags are placed in rear cargo bay → all bags are placed in front cargo bay → passengers with aisle seats board from the rear of the cabin towards the front → passengers with window seats board from the rear of the cabin towards the front → aircraft fuel is added

The minimum and maximum location of c.g. is measured and a 2% margin is added to account for in-flight variations. Then, the wing is moved forward by decreasing the ratio of $x_{LEMAC}/l_{fuselage}$ by 10% and backwards by increasing the $x_{LEMAC}/l_{fuselage}$ ratio by 10%. Again, the loading diagrams are created. They are shown in Figures 7.5 and 7.6. With the minimum and maximum values of c.g. (also including the 2% margin), the following c.g. range diagram in Figure 7.3 can be constructed, which will be used in the scissor plot. The most aft c.g. position is limited by static longitudinal stability (stick fixed, flaps retracted, cruise speed). The most forward c.g. position is limited by the aircraft controllability at minimum speed during approach with flaps fully extended. From the loading diagram, one can see that the c.g. position for the aircraft at MTOW is located at 12.3 m from the nose.

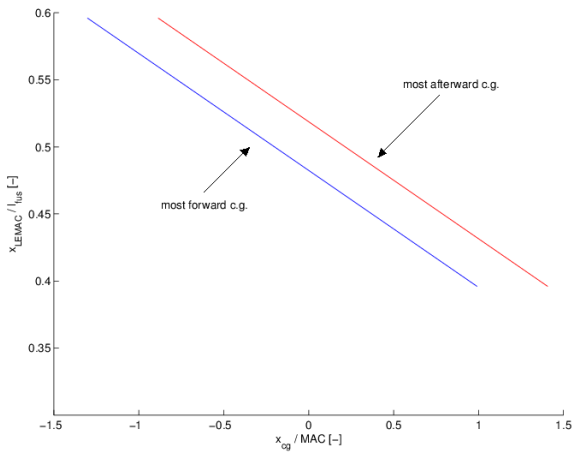

Figure 7.3: Center of gravity range

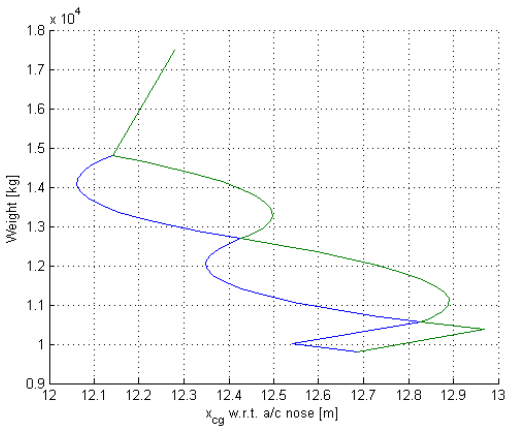

Figure 7.4: Aircraft loading diagram

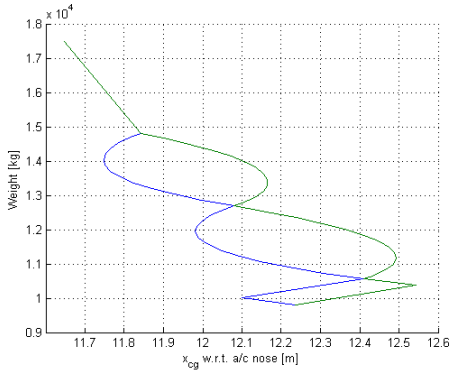

Figure 7.5: Loading diagram with wing moved forward, $(x_{lemac}/l_{fus}) = 9.9$ m

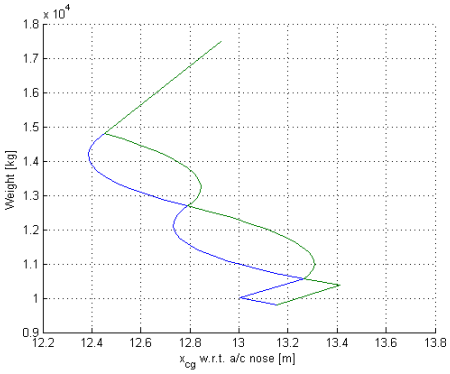

Figure 7.6: Loading diagram with wing moved backward, $(x_{lemac}/l_{fus}) = 14.9$ m

Using the aerodynamic characteristics of the airfoil and the wing, the scissor plot will be created for the next step. This plot comprises of the two lines, the stability and controllability curves. These are used to determine the admissible c.g. range such that the aircraft is stable during ground operations and also during flight, while it is still able for the crew to control it. The x_{cg} are normalized by MAC and plotted in terms of S_h/S. For the neutral stability curve a stick-fixed static margin of 0.05 is used [18]. Equations 7.3 and (7.2) were used for the stability and controllability, respectively. The derivation of all required parameters for these equations was explained in detail in the mid-term report [1].

$$\bar{x}_{cg} = \bar{x}_{ac} - \frac{C_{m_{ac}}}{C_{L_{A-h}}} + \frac{C_{L_h}}{C_{L_{A-h}}} \frac{S_h l_h}{S\bar{c}} \left(\frac{V_h}{V}\right)^2 \tag{7.2}$$

$$\bar{x}_{cg} = \bar{x}_{ac} + \frac{C_{L_{\alpha_h}}}{C_{L_\alpha}} \left(1 - \frac{d\varepsilon}{d\alpha}\right) \frac{S_h l_h}{S\bar{c}} \left(\frac{V_h}{V}\right)^2 - 0.05 \tag{7.3}$$

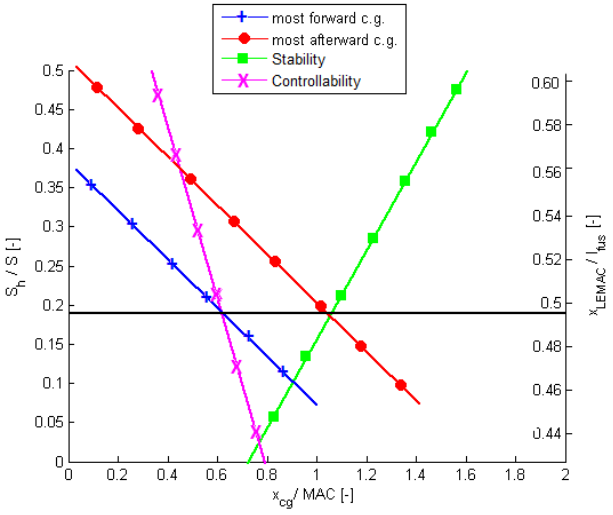

Figure 7.7: Scissor plot

The plots presented here are the result of the iteration process conducted in Chapter 6. As can be seen from Figure 7.7, the optimal surface area of the horizontal tail is found to be 8.35 m^2, with the wing leading edge of the mean aerodynamic center positioned at 12.4 m from the nose of the aircraft. Section 14.2.2 will treat the design of the tail planes in detail.

Initial Sizing

Having determined the weight and the balance of the aircraft, it is now time to perform the initial sizing of the Q-50. Firstly, the preliminary design of the wing planform as conducted in the Midterm Report [1] is finalized in Section 8.1. This is followed by the design of the fuselage and cabin in Section 8.2 and finally the initial tail configuration in Section 14.2.

8.1 Wing Sizing

To determine the shape of the wing, the planform in particular, we use the method by Diederich mentioned in Torenbeek [3] to determine an optimal elliptic lift distribution. The book distinguishes 2 non-dimensional components that add up to the theoretical lift distribution along the span of the wing, namely the basic lift distribution (L_b) and the additional lift distribution (L_a), both of which can be calculated as shown in Equations 8.1 and 8.2.

$$L_a = C_1 \frac{c}{c_g} + \frac{4C_2}{\pi}\sqrt{1-n^2} + C_3 f \tag{8.1}$$

$$L_b = L_a C_4 \cos\Lambda \left(\frac{\epsilon}{\epsilon_t} + \alpha_{0_l}\right) E\sqrt{1-M_\infty^2} \tag{8.2}$$

In these equations, the variables c and c_g are the local chord length and the geometric chord length respectively. The variable n is the spanwise location. Λ is the quarter chord sweep, ϵ and ϵ_t are the local twist and the wingtip twist respectively, E is Jone's edge velocity factor which is equal to the ratio of the semi-perimeter of the wing and its span [19] and M_∞ is the free stream Mach number. The constants C_1, C_2, C_3, C_4 and f can be read from Figure 8.1 and Figure 8.2.

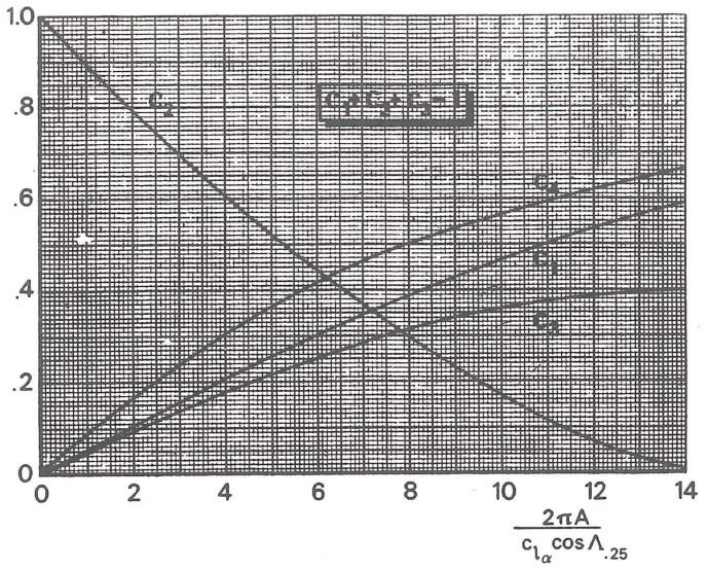

Figure 8.1: The curves to determine Diederich's constants

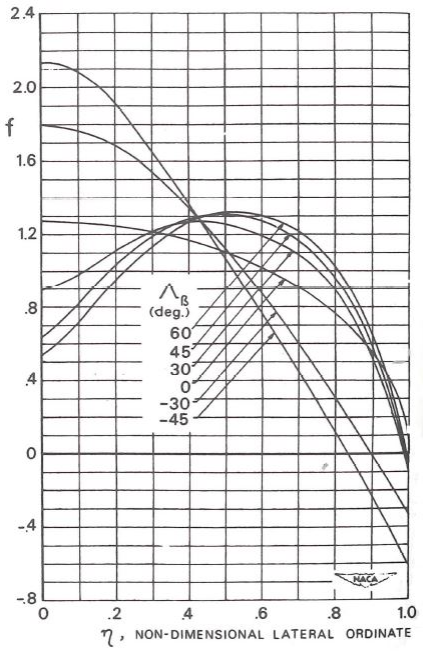

Figure 8.2: The lift distribution function

When changing the sweep, the constants C_1, C_2, C_3, C_4 and f change as well, as does the sweep variable in Equation 8.2 obviously. When changing the taper, the local chord length changes, thus changing the values for Equation 8.1. If we plot graphs of the sum of L_a and L_b where we change the taper and the sweep, we get a visual interpretation of where a certain planform is most beneficial. These graphs can be seen in Figures 8.3 and 8.4.

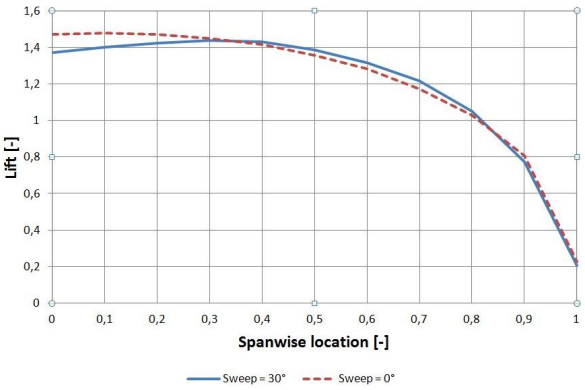

Figure 8.3: The lift distribution for different sweep angles

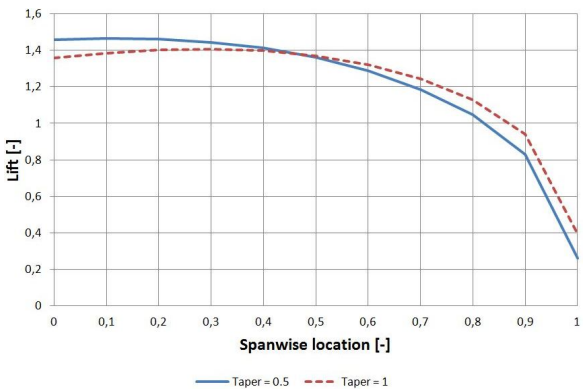

Figure 8.4: The lift distribution for different taper ratios

It can be seen that to obtain an optimal lift distribution one needs to have a change in sweep at 35% of the span where the inboard part has a lower sweep (preferably close to 0°) and a change in taper at 45% of the span where the inboard part has a higher taper. These relations should be kept in mind as well as the desired surface area while making the planform. It is preferable to have a simple shape because that would simplify the manufacturing process. That is why the planform has a quasi-straight leading edge and the trailing edge varies in a way that conforms to the previously found relations. Furthermore is it preferred to have the inboard part of the trailing edge orthogonal to the airstream for multiple reasons:

- Increased efficiency for rolling maneuvers
- Stiffening of the wing
- More space for landing gear systems
- Increased surface area at a low cost
- A relative smaller thickness ratio contributing to
  - a delayed sonic wave on a large part of the wing
  - onset of stall before the wingtip

When implementing the wingbox within the wing, these parameters were taken into account as to obtain a optimized wing.

8.2 Cabin and Fuselage Sizing

Not only the external configuration of the aircraft needs to be designed and developed, which is done in the previous chapters, but also the internal configuration is of importance for the performance of the aircraft. The fuselage layout has an influence on the component weight and thus the final weight of the aircraft. Moreover, the fuselage and cabin design should be flexible, in order for the possible expansion due to an increase in seats when looking at a family of aircraft. This chapter deals with the sizing of the fuselage and the cabin, including the fuselage length, diameter and seating configuration.

Seating Arrangement

The sizing of the fuselage is based on the layout of the cabin. This in turn is based on the number of passengers. Statistics has shown a relationship between number of passengers and abreast seat count [20].

$$n_{sa} = 0.45 * \sqrt{n_{pax}} \tag{8.3}$$

This number is between three and four for a 50 seat regional aircraft. When taking into account the possible future stretch to accommodate a family of low emission aircraft, this number tends more towards four seats abreast. Other cabin parameters are shown in Tables 8.1 & 8.2. All these parameters are chosen to match the competition.

Fuselage Diameter

The cabin wall thickness, the distance between inner wall and outer skin, requires an estimation for the sizing of the fuselage. It is assumed to be 125 millimeters, on the lower end of the range of 100 to 200 millimeters

Table 8.1: Cabin sizing parameters

Parameter	Inches	Meters
Seat Pitch	31	0.787
Seat Width	17	0.432
Aisle Width	19	0.483
Aisle Height	73	1.854
Head Room	57	1.450

Table 8.2: Initial fuselage sizing

Parameter	Meters
Fuselage Outer Diameter	2.625
Fuselage Length	24
Cockpit Section Length	3
Cabin Section Length	13
Tail Section Length	9
Cabin Wall Thickness	0.1

mentioned in [21]. Using this wall thickness and the values mentioned in Table 8.2, a value for the outer fuselage is determined. The outer fuselage diameter is 2.625 m. This is a reduction 65 millimeters from the CRJ-200 outer diameter which has the same seating configuration. This reduction in fuselage diameter can be attributed to a slight reduction in aisle width and a reduction in cabin wall thickness.

Fuselage Length

The fuselage length is not directly related to the cabin requirements. The complete cabin including lavatory, galley and wardrobe, is 13 meters in length. The cockpit section including radome is set at three meters, which is small but manageable. The cockpit section of a Boeing 737 is of similar dimensions. The CRJ-200 has a total length of 27 meters. The ATR-42 has a length of approximately 22.5 meters. An intermediate initial estimation is therefor set in between at 24 meters of total fuselage length.

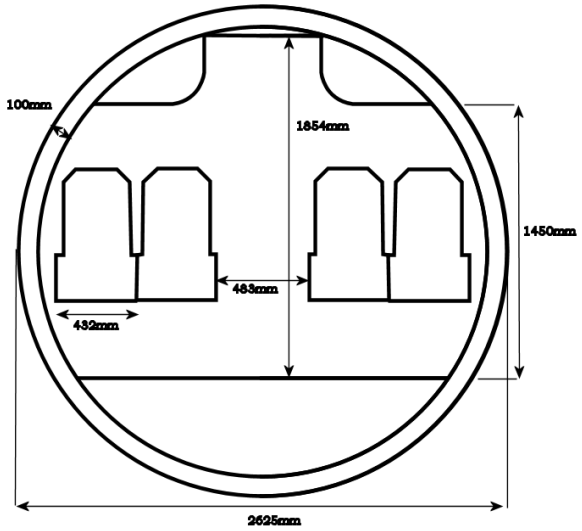

Figure 8.5: Fuselage cross section

Aerodynamic Performance

This chapter is dedicated to the aerodynamics of the aircraft. An explanation on the airfoil selection for the main wing is given. Furthermore, the drag, lift and moment graphs are presented and it is explained how they were obtained. The aerodynamic characteristics were optimized for minimum drag, and thus minimum fuel consumption, to help lowering the emissions.

9.1 Airfoil Selection

The first step in the wing design is the selection of the airfoil. The process of the airfoil selection is explained in this section. Besides, the main wing, the tail surfaces also need an airfoil. The selection process for the vertical and horizontal tail surfaces will be explained briefly in this section. Furthermore, a sensitivity analysis is performed.

The airfoil is selected based on its performance during the most fuel intensive mission leg, the cruise phase. During cruise, the aircraft weight needs to equal the total lift: $L_{tot} = W_{cruise}$. The lift that needs to be generated by the wing can be approximated by: $L = 1.1\ L_{tot}$. The 10% margin is introduced in order to compensate for negative lift contribution generated by the tail in order to trim the aircraft. The required wing lift coefficient is calculated with $C_L = 1.1\frac{1}{q}\frac{W}{S}$. However, due to fuel consumption the aircraft weight changes during the flight. When q is assumed to be constant during cruise, C_L will vary over time. The aircraft needs to be trimmed at these different values of C_L. To determine the wing design lift coefficient, $C_{L_{design}}$, the average of C_L values during the cruise phase is considered, so $\frac{W}{S} = \frac{1}{2}(\frac{W}{S}_{begincruise} + \frac{W}{S}_{endcruise})$. When it comes to airfoil selection, it is assumed that the required lift can be generated by an airfoil of lift coefficient C_l, with the following relation:

$$L = qSC_{L_{design}} = q_{eff}SC_l \tag{9.1}$$

Where $q_{eff} = \frac{1}{2}\rho V_{eff}^2 = \frac{1}{2}\rho(V_\infty cos\Lambda)^2$. Leading to $C_{l_{design}} = \frac{C_{L_{design}}}{cos^2\Lambda}$. The design lift coefficient for the wing and the design lift coefficient of the airfoil is related by the wing sweep angle, Λ. During the midterm design, a certain sweep angle was chosen. This value is used in order to compute $C_{l_{design}}$. Later on in the wing design process, this value might be changed. The values that are used in order to calculate $C_{l_{design}}$ are listed in Table 9.1.

Table 9.1: Input values in order to compute $C_{l_{design}}$

Parameter	V_{cruise} [m/s]	S [m^2]	$W_{end-cruise}$ [N]	$W_{end-cruise}$ [N]	ρ [kg/m^3]	Λ [degrees]
Value	241.5	43	$1.6769 \cdot 10^5$	$1.5830 \cdot 10^5$	0.4	23

After computing a $C_{l_{design}} = 0.42$ is found. The airfoil should be able to fly at this C_l during cruise having a minimum amount of drag. Another important property is that the airfoil should have a high critical Mach number in order to prevent shockwave formation, which increases the drag drastically. A high $C_{l_{max}}$ value is also desired. Furthermore, the airfoil should have a sufficient thickness in order to store enough fuel in the wings. The next step is to select an appropriate airfoil.

9.1.1 Selecting Different Airfoils for the Trade-off

The two types of parameters that influence the performance of the airfoil are the flow parameters and the geometric airfoil parameters. At this stage of the design, the flow parameters are fixed. The aircraft flies at an altitude of $h = 10278$ m, at a Mach number of M = 0.81. The Reynolds number is computed using Equation 9.2.

$$Re = \frac{\rho V c}{\mu} \tag{9.2}$$

Using a reference chord length of $c = 2.15$ m and a viscosity coefficient of μ=1.45 $\cdot$ 10^{-5} Pa·s an Reynolds number of $R_e = 1.5 \cdot 10^7$ is obtained. What can be changed are the geometric parameters of the airfoil. The following parameters can easily be adjusted:

- Thickness
- Thickness location
- Camber
- Camber location
- Leading edge radius

For the different airfoils, certain geometric parameters are changed and the influence of these changes are monitored. For the airfoil that is chosen after the trade-off, the effect of these changes are shown. Using the JAVAFOIL [1] program different airfoils are selected. Some airfoils where already selected for the midterm report. The chosen airfoils are shown in Table 9.3. The next step is to perform a trade-off in order to select the best airfoil.

9.1.2 Trade-off

Since new requirements have been defined, a new trade-off approach has to be used, as other things may become more important (compared to airfoil trade-off method the last report). First of all, the list of airfoil types that are being examined has been altered and extended. Second, a more analytical method to determine the weights of the criteria has been used and last, the grading is corrected since the linear approach does not yield the most fair results anymore. It is first explained how the criteria weights were determined.

Determining the Criteria Weights

The analytical hierarchy process (AHP) was used to determine the criteria weights (M_{crit}, L/D, $C_{l,max}$, C_m). When determining the weights, the following reasonings were the most influential:

- M_{crit} is the most important criterium, as the aircraft is required to fly rather fast (M = 0.81) and shocks should be avoided as those will increase the drag drastically
- L/D is interesting in so far that whenever the creation of shocks on the airfoil is minimized, L/D should be maximized. In this case all values for L/D were quite average, with four high outliers, however their M_{crit} behaviour was worse and they therefore scored lower in total
- $C_{l,max}$ and C_m are not driving requirements, it would just be better if they are higher and smaller respectively
- The thickness was not included as a separate criterium, because from structural analysis and fuel tank dimensioning it was concluded that the minimum thickness should be 10% of the chord and thus only airfoils with a thickness of 10% were examined

Applying the AHP method and the rationale described above yields the weights presented in Table 9.2.

Table 9.2: Trade-off criteria weights (main wing airfoil)

Criterion	M_{crit}	L/D	$C_{l_{max}}$	C_m
Weight	53.28	27.80	11.35	7.56

Grading Approach

In this section it will be explained how the airfoils are graded for the criteria that were presented above. In Table 9.3 the airfoils examined and their properties are presented. The values in this table will be discussed and a grading method is set-up in order to translate the numbers to a certain grade.

Table 9.3: Airfoil performance

Type	L/D	$C_{l,max}$	M_{crit}	C_m
NACA 2410	51.22	1.31	0.67	-0.052
NACA 4410	52.60	1.52	0.68	-0.099
NACA 3510	51.77	1.41	0.70	-0.089
NACA 38010	50.98	1.16	0.60	-0.020
NACA 38008	53.71	1.01	0.58	-0.019
NACA 36010	51.41	1.38	0.65	-0.037
NACA 63410	138.07	1.22	0.70	-0.091
NACA 64412	100.28	1.36	0.68	-0.093
NACA 64410	140.80	1.21	0.70	-0.092
NACA 65410	142.49	1.17	0.70	-0.093
NACA 07-410	56.16	1.23	0.72	-0.102
NACA 07-411	69.95	1.29	0.71	-0.102
NACA 07-412	69.35	1.35	0.70	-0.103
NACA 07-408	61.16	1.11	0.74	-0.100
EQ 1030/3070	55.13	1.24	0.73	-0.140

Keeping in mind the trade-off reasoning, the following grading schemes were setup: Table 9.4 applies to $C_{l,max}$, M_{crit}, C_m and Table 9.5 to L/D. A linear relation was used in the first case, because the values are

[1] http://www.mh-aerotools.de/airfoils/jf_applet.htm

relatively close to each other. In the values for L/D, there are some high outliers, even though this should not dictate the outcome of the trade-off since the other L/D values are just fine and because M_{crit} is more important. Therefore a non-linear grading approach is taken. The grading is distributed such that airfoils with the very high L/D do not come out of the trade-off only due to their high L/D, since an L/D of around 50 is sufficient. Beneath 30 however is decided to be undesirable and therefore it immediately would get a grade 1.

Table 9.4: Grading scheme for $M_{crit}, C_{l,max}, C_m$

Grade	Reason
11	best of the series
⋮	linear distribution
6	average of the series
⋮	linear distribution
1	worst of the series

Table 9.5: Grading scheme for L/D

Grade	When L/D is
9	>150
8	70-150
7	60-70
6	55-60
5	50-55
4	40-50
3	30-40
1	<30

Grading the airfoils and multiplying them by the weights, in the way that was explained before, the outcome is as follows:

Table 9.6: Airfoil trade off

Type:	L/D grade	Clmax grade	Mcrit grade	Cm grade	Total grade
NACA 2410	5	6.7	7.0	8.3	6.52
NACA 4410	5	11.0	7.1	4.4	6.78
NACA 3510	5	8.7	8.5	5.2	7.31
NACA 38010	5	4.0	2.4	10.9	3.93
NACA 38008	5	1.0	1.0	11.0	2.87
NACA 36010	5	8.1	5.1	9.5	5.76
NACA 63410	8	5.1	8.6	5.0	7.76
NACA 64412	8	7.7	7.3	4.9	7.35
NACA 64410	8	4.9	8.5	5.0	7.66
NACA 65410	8	4.1	8.8	4.9	7.74
NACA 07-410	6	5.2	10.0	4.1	7.88
NACA 07-411	7	6.4	9.4	4.1	7.98
NACA 07-412	7	7.6	8.8	4.1	7.83
EQ 1030/3070	6	5.5	10.6	1.0	8.02

From Table 9.6 it becomes clear that the EQ 1030/3070 is the most suitable airfoil, because of its relatively high critical Mach number. However, due to limited time and due to the complicated architecture of this airfoil which leads to a complicated structural analysis, it was decided to go for the second best option which is the NACA 07-411 airfoil. This has a fairly straight layout in which a simple wing box can easily be fitted and therefore the structural analysis is highly simplified. The only parameter that is compromised in this situation is M_{crit}, however only by a small amount such that it is still ensured that there is not a huge drag increase over the wing during cruise.

9.1.3 Sensitivity Analysis of the Trade-off

To check if the trade-off method is not extremely sensitive to minor changes, a sensitivity analysis is performed. Since the critical Mach number is such a very important criterion it is considered not appropriate to lower its weight, however it is shown in the table, to demonstrate this fact. All weight criteria are increased and decreased one by one with 6%, where the other criteria are decreased or increased respectively by 2% to make a total of 100% again. The results of the sensitivity analysis are shown in Table 9.7. It must be noted that the EQ airfoil is not included in this analysis. It can be conlcuded that this trade-off method is solid, and not highly sensitive to minor changes. Only if the $C_{l,max}$ criterion is decreased the NACA 07-411 and 410 score equally because the 411 has a higher $C_{l,max}$ which then weighs less, and if the M_{crit} criterion weighs higher then the 410 airfoil wins because of its slightly higher critical Mach number.

Table 9.7: Sensitivity analysis of airfoil trade-off method

Weights of L/D, Clmax, Mcrit, Cm respectively	**Winning airfoil**
27.8, 11.3, 53.3, 7.6	NACA 07-411
21.8, 13.3, 55.3, 9.6	NACA 07-411
29.8, 5.3, 55.3, 9.6	NACA 07-411/410
29.8, 13.3, 47.3, 9.6	NACA 07-411
29.8, 13.3, 55.3, 1.6	NACA 07-411
33.8, 9.3, 51.3, 5.6	NACA 07-411
25.8, 17.3, 51.3, 5.6	NACA 07-411
25.8, 9.3, 59.3, 5.6	NACA 07-410
25.8, 9.3, 51.3, 13.6	NACA 07-411

9.1.4 Analysis of the Chosen Airfoil

The airfoil selected is the NACA 07-411 (Figure 9.1. In this subsection the properties and aerodynamic characteristics are presented.

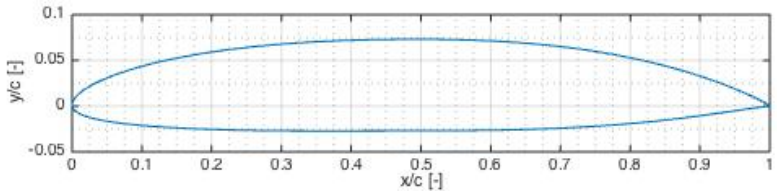

Figure 9.1: Geometry of the NACA 07-411 airfoil

JAVA-foil can compute and graph the C_l, C_d, C_m and C_p values at different angle of attack. However, it is not able perform these calculations accurately at Mach numbers higher than $M = 0.5$ - 0.6. To obtain the right values and curves at the Mach number of $M = 0.81$, the following approach is used. With the use of JAVA-foil the aerodynamic parameters are computed at $M = 0$. Using the Karmen-Tsien rule [22] the values are corrected for $M = 0.81$. Equation 9.3 shows the Karmen-Tsien relation applied to the C_l values ($C_{l,0}$ is the C_l value at $M = 0$) This rule can also be applied to the C_d and C_m values.

$$C_l = \frac{C_{l,0}}{\sqrt{1 - M_\infty^2} + [M_\infty^2/(1 + \sqrt{1 - M_\infty^2})]C_{l,0}/2} \tag{9.3}$$

Figure 9.2 shows the $C_l - \alpha$ curve at the theoretical value $M = 0$ and the corrected value $M = 0.81$. As can be seen from the graphs, the $C_l - \alpha$ curves shifts upwards at higher Mach numbers. At $M = 0.81$, C_{l-max} = 1.47.

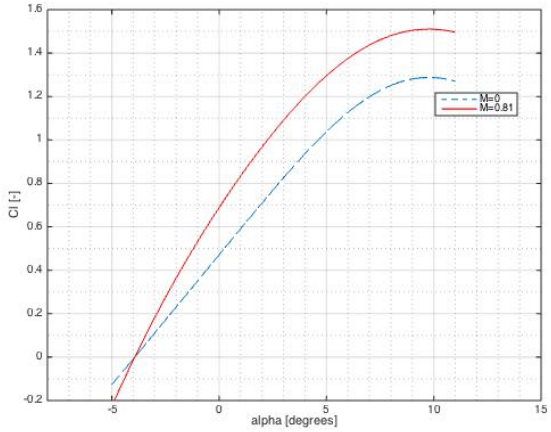

Figure 9.2: $C_l - \alpha$ curve for $M = 0$ and $M = 0.81$ at $R_e = 1.86 \cdot 10^7$

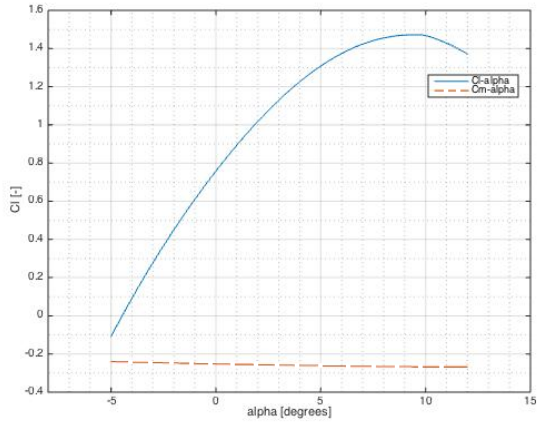

Figure 9.3: $C_l - \alpha$ and $C_m - \alpha$ curve at $M = 0.81$, $R_e = 1.86 \cdot 10^7$

To reach a C_l = 0.42 during cruise, the aircraft needs to fly at an angle of attack of α = -0.8. The corresponding critical mach number is, M_{crit} = 0.73. It is important that $M_{cruise}cos\Lambda \leq M_{critical}$. In order to meet this condition the minimum sweep angle of the wing needs to be at least $\Lambda = 25°$.

9.2 Aerodynamic Characteristics of the Main Wing

Now that the aerodynamic characteristics of the wing profile are known, it is time to translate this to the entire wing and examine what the aerodynamic characteristics of the main wing are. $\frac{dC_{L,w}}{d\alpha}$, $C_{L,max}$ and α_{stall} were determined and with those parameters known, the lift curve was assembled [18]. To generate the corresponding $C_L - C_D$ curve, the following relation was used:

$$C_{D,w} = C_{D_{0,w}} + \frac{C_{L,w}^2}{\pi Ae} \tag{9.4}$$

Where $C_{L,w}$ is obtained from the lift curve. The zero-lift drag coefficient for the main wing is calculated with the following relation [23]:

$$C_{D_{0,w}} = C_{f_w} f_{tc_w} f_M \frac{S_{wet_w}}{S} (\frac{C_{d_{min,w}}}{0.004})^{0.4} \tag{9.5}$$

9.2.1 Going from 2D to 3D Lift

As was explained in this chapter, an airfoil was selected based on the performance requirements of the Q50, for which lift and drag curves were obtained by the use of Javafoil. In this section it is explained how this translates to the entire 3D wing. First the lift curve is examined, since the drag depends on the lift [18]. It should be noted that C_l, C_d, C_m indicate the aerodynamic coefficients of the airfoil and C_L, C_D, C_M are the aerodynamic coefficients of the entire 3D wing. In this section the lift produced by the main wing during cruise is examined. The first step in going from 2D to 3D is constructing the slope of the 3D curve. For this purpose the following equation is used (DATCOM method):

$$\frac{dC_L}{d\alpha} = C_{L_\alpha} = \frac{2\pi A}{2 + \sqrt{4 + (\frac{A(1-M_{cr}^2)}{\eta})^2 (1 + \frac{tan(\Lambda_{0.5c})^2}{(1-M_{cr}^2)^2})}} \tag{9.6}$$

The inputs are shown in Table 9.8.

Table 9.8: Inputs for 3D lift slope calculation

Parameter	Value	Description
A	8.5 [-]	Wing aspect ratio
M_{cr}	0.81 [-]	Cruise Mach number
η	0.95 [-]	Airfoil efficiency
$\Lambda_{0.5c}$	22.98°	Half chord sweep angle

Table 9.9: Inputs for the calculation of $C_{L_{max}}$

Parameter	Value [unit]	Description
$C_{l_{max}}$	1.47 [-]	Maximum lift coefficient of the wing, corrected for compressibility
$\Lambda_{0.25c}$	25.78 [°]	Quarter chord sweep angle

These inputs yield a slope of $C_L - \alpha$ curve = 6.08. The next step is to determine the zero lift angle of attack, $C_{L_{max}}$ and the stall angle. The zero lift angle of attack of the wing is equal to that of the airfoil, α_{0L} = -3.9°. For the maximum lift coefficient the following formula is used:

$$C_{L_{max}} = 0.9 C_{l_{max}} \cdot \cos \Lambda_{0.25c} \tag{9.7}$$

The inputs for this equation are shown in Table 9.9, yielding $C_{L_{max}} = 1.19$. To determine the stall angle the following formula is used:

$$\alpha_s = \frac{C_{L_{max}}}{C_{L_\alpha}} + \alpha_{0L} + \Delta\alpha_{C_{L_{max}}} \tag{9.8}$$

Where all inputs were determined in this section, except for $\Delta\alpha_{C_{L_{max}}}$ which accounts for the non-linear effects of LE vortices, which was determined to have a value of 3.2° according to the DATCOM method [18]. It should be noted that the method used is appropriate for $0.2 < M < 0.6$ thus the cruise Mach number for the Q50 falls outside this range, however it is used to get an approximation and it will be corrected by hand if necessary. For exact aerodynamic data for the 3D case, wind tunnel experiments should be done. Input values used for the DATCOM method are presented in Table 9.10.

Table 9.10: Inputs for the calculation of $\Delta\alpha_{C_{L_{max}}}$

Parameter	Value [unit]	Description
Δ_y	3.2 [-]	Leading edge sharpness parameter, computed with CATIA
Λ_{LE}	30 [°]	Leading edge sweep angle

Now all parameters necessary to construct the $C_L - \alpha$ graph for the 3D wing in cruise condition are known. The result is shown in Figure 9.4 and compared with the 2D case.

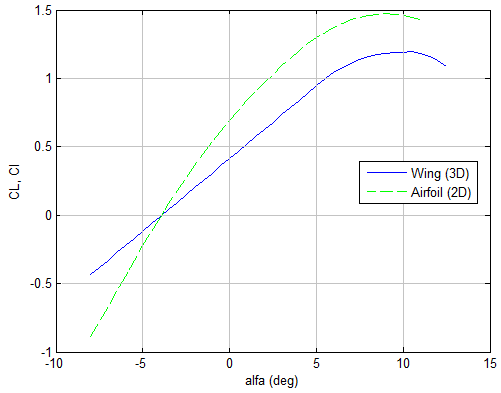

Figure 9.4: Lift curves of wing and airfoil at $M = 0.81$

9.2.2 Going from 2D to 3D Drag

In this section the drag produced by the entire wing will be discussed, where the most important relationship for this matter is Equation 9.5. Where $C_{L,w}$ is obtained from the lift curve. The zero-lift drag coefficient for the main wing is calculated with the following relation [23]:

$$C_{D_{0,w}} = C_{f_w} f_{tc_w} f_M \frac{S_{wet_w}}{S} \left(\frac{C_{d_{min,w}}}{0.004}\right)^{0.4} \tag{9.9}$$

For the specific input values, see Appendix A. Analysis of this relation yields curves for $C_L - C_D$ and $L/D - C_L$ of the main wing during cruise, as presented in Figures 9.5 and 9.6.

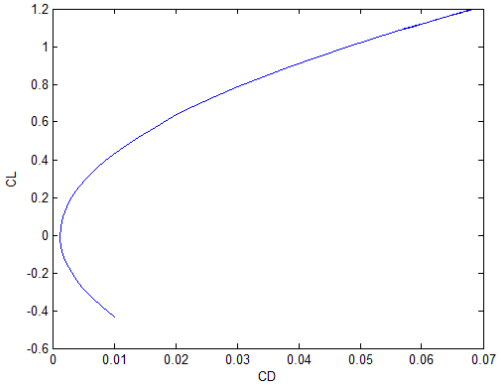

Figure 9.5: C_L vs. C_D of the main wing during cruise

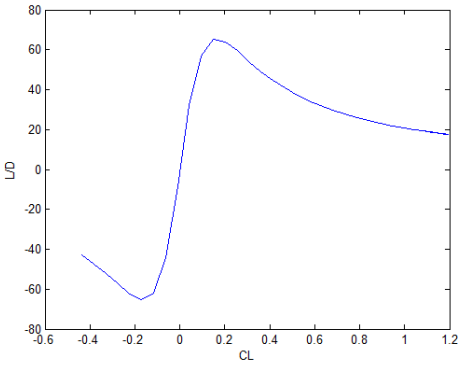

Figure 9.6: L/D vs. C_L of the main wing during cruise

From these graphs some important parameters can extracted, they are shown in Table 9.11.

Table 9.11: Outcome of drag analysis of main wing during cruise

Parameter	$C_{L_{design}}$	L/D_{design}	$C_{D_{design}}$	$C_{D_{min}}$	$C_{D_{0w}}$
Value	0.36	49	0.00735	0.00125	0.0015

Material Selection

The optimized airfoil of the wing contributes to a high lift production. This will create high stresses through our wing, the wingbox and surrounding structures. It is important to determine the right materials for a specific job and keep aiming for the lightest option available. The introduction of composite materials will set us apart from the competition and will be readily accepted despite its higher cost because it will end up saving the operator money and will ultimately have a smaller environmental impact to boot.

10.1 Advanced Composite Materials (ACM)

Advanced Composite Materials are becoming more common (and noticeable) all around the world. And for good reason, because they are light and strong and can have more specific properties depending on the type of composite. About 50% of the Boeing 787 Dreamliner is made of advanced composite materials [24, 25]. ACMs usually consist of remarkably high strength fibers with high stiffness bound together by weaker matrices. The number of different advanced composites is staggering because the specifications depend on the combination of fibers and matrices and there are numerous variations of each of them. The three basic fiber types are aramid (10.1.1), glass (10.1.2) and carbon fiber (10.1.3) which can be present in the ACM in the form of tows, yarns, rovings, chopped strands and woven fabric mats. The commonly used matrices are either thermosets like epoxy or polyester, or thermoplastics like nylon or polyethylene. An exception to all this are ceramic matrix composites (10.1.4) which consist of ceramic fibers embedded in a ceramic matrix.

The matrix that will be used is epoxy because of its high specific strength, stiffness and relatively low density. Nylon is stronger stiffer and lighter but is a thermoplast which means that it becomes plastically deformable at around 80°C which means that the composite would melt when a fire breaks out which is unacceptable. That is why an epoxy will be used as a matrix. A mesh will be integrated in the skin sections to conduct electricity through the aircraft in case of lightning strike. All composite parts will be outfitted with a smart sensing system to aid in the early detection of failures.

The challenge with advanced composites is that they have directional strength properties which means that fibers must be placed in such a way that stresses are properly transferred. If the fibers are not oriented in the same direction as the forces propagating through the part, a thicker cross section will be required or they will fail. For parts subjected to simple load cases, such as a beam under pure bending, it is easy to determine the required orientation of the fibers. The more complicated a load case gets, the harder it is to find optimal fiber orientation. It is possible to lay fibers in multiple directions to make your part able to carry loads in multiple directions, but the strength of the entire laminate will go down. So if fibers are oriented in the right direction successfully, the weight benefit could be substantial.

For example, when looking at the amount of skin and stringers in a fuselage with bonded frames with contoured flange based on NASA Contractor Report 4418 [26], one can conclude that 50 w% of the fuselage is skin and 20 w% are stringers. If the weight of the fuselage is assumed to be 2000 kg, 1400 kg would consist out of skin and stringers. When making the skin and stringers out of composites and using conservative numbers for its strength and thickness, a quick calculation shows that the thickness of skin and stringers could be lowered by 43.7% (based on the knocked down average of the ten strongest composites researched compared to the strongest aluminum researched) resulting in a new total weight of skin and stringers of 787 kg. When taking into account that composites have about half of the density of aluminum the weight is reduced even more to 393.5 kg. Frames, splices and miscellaneous parts of the fuselage add up to 30 w% which account for 600 kg of the reference weight. So the new total weight would become 993.5 kg which is a 50.3% reduction of the total fuselage weight. Again, this is only a reference calculation with conservative values.

Another problem when using fiber reinforced plastics is the fact that very little is known about its fatigue life. A lot of research is under way on fatigue life prediction of fiber reinforced polymers but a definable fatigue endurance limit is still lacking. Engineers often design in large safety margins to ensure suitable reliability at the expense of potential weight reduction. However; a relatively simple fatigue model has been determined [27] which can serve as a guideline to determine fatigue life of composites subjected to a certain stress. Based on this model it can be extrapolated that the stress applied to the composite laminate should not exceed 80% of that laminates ultimate strength.

Damage to the laminate is often hard to detect but could potentially lead to catastrophic failure. A way to mitigate this is by using self-healing composites where the matrix is filled with micro-capsules or even vascular networks that contain a liquid healing agent. When cracks appear the healing agent will fill the crack and return the strength of the composite close to normal. If a dye is added to this healing agent (that is not visible to the naked human eye) maintenance crew could easily detect cracks in the structure and perform the necessary repairs.[28, 29]

For all advanced composites a knockdown factor needs to be applied. It is a safety margin to account for barely visible impact damage, material scatter and environmental factors (even though our composites will have a coating to protect it from ultraviolet radiation and moisture). Eventually the strength and modulus of the composites will go down with 58.4%.

10.1.1 Aramid Fiber Reinforced Plastic (AFRP)

Aramid fibers distinguish themselves from other more well-known fibers due to their ability to cope with high temperatures and their tolerance to damage. The fibers are already being used for fire protective clothing for that specific reason. A composite made from these fibers and a temperature resistant matrix would be ideal for application in the hotter regions of the engine. The aramid fibers are known to deteriorate when reaching temperatures above 500°C, beyond this point ceramic matrix composites could be considered as an alternative to the traditional metal alloys. AFRPs are currently being used for turbine containment belts to protect the passenger compartment in case of engine failure [30]. We will do the same thing by using Kevlar 29 for the engine cowlings. If the technology is matured by 2035 (which is expected) and the price difference is marginal we could use poly p-phenylene-2,6-benzobisoxazole or PBO in short (such as Zylon) instead of aramid fibers. Its strength and modulus are almost double that of aramid and its decomposition temperature is about 100°C higher.

10.1.2 Glass Fiber Reinforced Plastic (GFRP)

GFRPs are pretty common and can be found all around. Their range of applications is exceptionally broad from storage tanks, surfboards, tentpoles and circuit boards to bicycles, auto body parts, helmets and water slides. Their popularity can be due to the fact that they are less brittle and a lot cheaper, although not as strong and stiff as CFRPs. E- and S-glass are the two major types of GFRPs where S-glass is a lot stronger and primarily used in high demanding industries. The structurally essential parts of the Q-50 will be made by CFRP or more traditional materials. GFRP will be used for internal non-essential structures such as the cockpit panel, the overhead storage bins, the lavatory and inner walls of the fuselage. They can also be used in acoustic panels incorporated into nacelles [30] helping to reduce the acoustic emissions of the aircraft. A GFRP with a polyester (PET) matrix and 50% E-glass fibers, PET-50%E will be used.

10.1.3 Carbon fiber Reinforced Plastic (CFRP)

These composites are well known for their immense strength and are applied in high-demanding industries for that exact reason. They traditionally consist of carbonized polymer fibers but since graphene and carbon nanotubes are also carbon-based, they will be discussed as well in sub-chapters. The biggest downside is that they are very expensive resulting in everlasting trade offs whether CFRPs are absolutely necessary for a specific part. But when a high strength-to-weight ratio and rigidity are required CFRPs are usually a very good option. We will be making extensive use of these composites because the high strength-to-weight ratio allows us to design a very light aircraft which results in less fuel consumption. We will be having a full CFRP skin on the fuselage, wings and control surfaces as well as CFRP stringers, frames and ribs if the budget allows this. Since CFRP are an-isotropic we could have chosen two different prepregs, one for parts under sheer compression (Hexcel M76) and one for all other load cases (Hexcel M91), but since the specific compressive strength of M91 doesn't differ all that much from M76, parts that are only under compression are pretty rare and with easy manufacturability in mind we have chosen to use Hexcel M91. Table 10.1 clearly shows the properties.

Graphene Reinforced Plastic (GrRP)

Graphene is a 2D layer of carbon atoms in a hexagonal lattice which shows extraordinary optical and electronic properties but especially the mechanical properties are of interest to us. Thus far it has only been created in laboratory conditions and a lot of the numbers are based on theoretical prospects using graphene that is unflawed containing no imperfections. This will not be the case once graphene hits the market and will be mass produced, but at least it shows the potential of this amazing material.

The ultimate strength of graphene is an extraordinary 130,000 MPa, which is about 20 times higher than carbon fiber (depending on manufacturing process), yet weighs only 0.77 mg/m^2. Composites made with graphene sheets instead of carbon fiber would be substantially stronger and a lot lighter. Unfortunately there are no graphene composites in production just yet but considering that usually 60% of a laminate consists of reinforcements and graphene is 20 times stronger than carbon fiber, one could deduce that GrRP will be around 12 times stronger than CFRP.

Carbon Nanotube Reinforced Plastics (CNRP) and Metal Matrix Composites (CNT-MMC)

These composites are sure to gain ground in the (far) future although they are still in the research phase. CNRPs have the lead though since they have already been successfully implemented in Lockheed Martins F-35 [31], albeit as a non-load bearing airframe component for the reduction of specification requirements. CNRPs still use carbon fiber as reinforcement but the binding matrix is a carbon nanotube filled epoxy. This epoxy has also been commercialized as an adhesive to tightly bond composites to wood, metal and other composites [32]. So it can be stated with fair certainty that CNRPs and the adhesive developed by Zyvex can be used on the Q-50.

The idea with CNT-MMCs is to take advantage of the immense tensile strength of carbon nanotubes but the synthetic techniques to produce these are still not very economical, able to guarantee homogeneous dispersion of nanotubes or guarantee strong interfacial adhesion between the metallic matrix and the carbon nanotubes. Theoretical (and some experimental) tensile strengths are already known but since it is still in the research phase little is known about the price of this emerging material. Furthermore is it unclear how mature this material will be by the time our aircraft should go in production. These uncertainties makes it unable to choose CNT-MMC as a viable material in the design.

10.1.4 Ceramic Matrix Composites (CMC)

CMCs can be built up out of any ceramic fiber embedded in any ceramic material. They are weak and heavy compared to other composites but overcome the major disadvantages of conventional technical ceramics, such as brittle failure and low fracture toughness and have extreme thermal shock resistance. Therefore, their applications are in fields requiring reliability at high-temperatures and resistance to corrosion and wear such as the combustion chamber and turbine blades of an engine. Silicon Carbide CMCs (SiC/SiC) can withstand temperatures greater than 1316°C yet are a third of the weight of nickel-based super-alloys which are the conventional metal alloys used for these parts [1]. Some Carbon Silicon Carbide CMCs show even better properties which is why we will be using those for the parts in the engine that are subjected to the highest temperatures.

10.2 Metal Alloys

Metal alloys are still the dominant material in aerospace structures at the moment although they are being caught up by composites as was mentioned earlier. However their manufacturability and low price still make it a competitive material for some specific tasks. We will be focusing on aluminum (10.2.1), titanium (10.2.2), nickel (10.2.3) and steel alloys (10.2.4).

10.2.1 Aluminium Alloys

Aluminum alloys are the most common metal alloys used in aerospace by a landslide. They are cheap, easy to manufacture, lightweight and can have a pretty high strength to weight ratio if they are processed right and have the right composition. The yield strength of the aluminum alloys in Table G.2 range from 89.6 MPa up to 503 MPa with only a little bit of difference in density. This way one can choose a specific alloy that is suited best for the task at hand. In our case we will be using a ductile aluminum alloy for the leading edges of our wings, stabilizers and nacelles. If the leading edges would have been made of CFRPs then impacts would have resulted in inner delamination which could be missed during inspections. Therefore we wish to use a material that clearly shows impact damage. Since our wing will be bending quite a lot we choose Al 2124-T851 since it is strong, has a relatively low Young's modulus and a high percentage of elongation at break.

10.2.2 Titanium Alloys

These alloys are primarily used when high strength and temperature resistance is needed at a low weight. Titanium alloys are often used in temperature up to 550°C. The biggest problem with titanium alloys is that they require up to three Vacuum Arc Remelting (VAR) processes to be produced. This VAR process ensures elevated chemical and mechanical homogeneity resulting in stronger materials, but it is also time consuming and most of all very expensive. So titanium alloys are only used if other materials are not a possibility. This is the case for a lot of parts inside the engines although AFRCs and CMCs could be better alternatives by 2035. For the parts that cannot be made by AFRCs or CMCs (due to material properties or price) we will be using Ti-6Al-4V.

[1] http://www.compositesworld.com/articles/ceramic-matrix-composites-heat-up

10.2.3 Nickel Alloys

Nickel alloys are the material of choice for the hottest parts of engines. They have an excellent resistance to high temperatures and some alloys, such as Ni-alloy 718, are perfectly capable of handling temperatures of 650°C and then start weakening until failure at around 900°C. On the downside they are very heavy, about twice as heavy as titanium alloys and are not even all that cheaper. So it stands to reason that these alloys will be used when absolutely necessary and maybe AFRCs and CMCs will become the better alternatives by 2035, like with titanium alloys. For the parts that cannot be made by AFRCs or CMCs (due to material properties or price) we will be using NiCr 80:20.

10.2.4 Steel Alloys

Steel is an alloy in itself so the name steel alloy may sound strange. But since certain elements are being added to steel to obtain better mechanical properties the name steel alloy is justified. These alloys are not dominantly represented in the bill of materials of an aircraft due to its high density and relatively low strength. However; its strength could almost triple if it has the right composition and has gone through the right production process. The alloys , 300M and HY-TUF are examples of such steels, the last two are shown in Table G.2 with the precursor FeC (steel is the alloy of iron and carbon, thus Fe and C). It is notable that these steel alloys are all High Strength, Low Alloy Steels (HSLA) and have undergone VAR which explains their increased strength. Unfortunately it also increases its price although it still remains pretty cheap. 300M has the same additives as 4340M and HY-TUF making them stronger and resistant to environmental factors (corrosion) but contains a very small amount of Vanadium as well, making it even stronger and the material of choice for Boeing [23]. We will be taking the same road as Boeing and will be using 300M for our landing gear.

10.3 Honeycomb Structures

Honeycomb structures are usually made by forming thin plates in a hexagonal lattice, much like graphene. They provide a structure with relative high out-of-plane compression and shear properties with minimal density. Honeycomb structural materials are commonly made by putting a honeycomb material between two thin layers. These layers of skin provide strength in tension whilst the honeycomb structure provides spacing between the two plates, increasing the moment of inertia and increasing its stiffness. We will be using honeycomb structures for our control surfaces.

Table 10.1: Used materials on the Q50 (including knockdown factors for composites)

Material	$\sigma_{t,y}$ [MPa]	$\sigma_{c,y}$ [MPa]	E_t [GPa]	E_c [GPa]	ρ [kg/m^3]	Application [-]
Kevlar 29	582.40	97.76	31.62	23.3	1440	Engine cowling
PET-50%E	86.11	86.11	2.29	7.16	1800	Internal non-essential structures, acoustic lining
Hexcel M91	1464.32	782.08	73.22	46.3	1617	Stringers, frames, spars, ribs and skin
CMC C/SiC	158.08	291.20	41.60	-	2200	Ultra high temperature parts (combustion chamber, turbine vanes)
Al 2124-T851	430	430	71	72	2780	Leading edges
Ti-6Al-4V	880	880	114	116	4430	Engine spike, intermediate temperature parts (CMC preferred)
NiCr 80:20	800	800	210	214	8400	High temperature parts (CMC preferred)
FeC 300M	1731	1731	205	209	7870	Landing gear
FeC 17-7	1275	1275	196.5	200	7806	Guiding rails, internal attachment points

[2] http://www.boeing.com/commercial/aeromagazine/aero_22/alloy_story.html#top
[3] http://www.herculesht.com/steel-heat-treating.html

Structural Design

Once the material is chosen, the logical step to take is to continue with the design of the structural components of the aircraft. The structural analysis of the aircraft is very important, since the aircraft has to withstand all different loads. In this chapter, a division is made to analyze different components separately. In Section 11.2, the wing is taken into detail and the main wingbox is designed. After that in Section 11.3, the design of the tail is done. As last, the design of the fuselage is explained in Section 11.4.

11.1 Load Factor

The driving factor for the structural design of the aircraft is the flight envelope, which is depicted in a loading diagram in figure 11.1. The aircraft has to be able to encounter the maxima of the flight envelope without breaking apart. These maxima are multiplied by a factor of 1.5 to determine the ultimate load factor. Figure 11.1 shows a manoeuvre load factor of 2.5 and a gust load factor of 3.5. The structural design of the aircraft is done according to the manoeuvre load factor, except for the tail structure which is subjected to the gust loads more than than any other part of the aircraft. So, for the tail an ultimate load factor of 5.25 is used and for the rest of the aircraft an ultimate load factor of 3.75 is used.

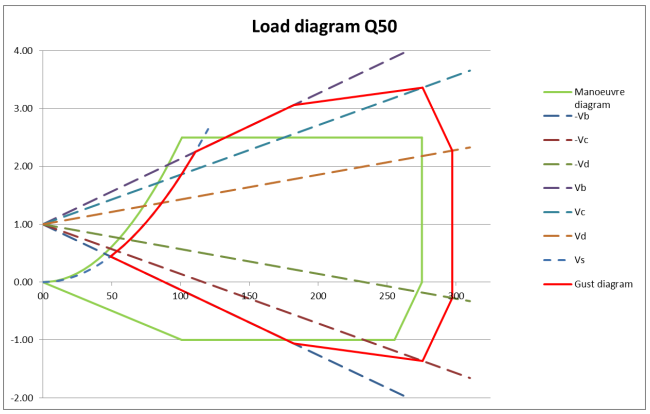

Figure 11.1: Flight envelope of the Q-50

11.2 Wingbox

A wingbox is a structural element, which supports and gives rigidity to the wing. Its main function, apart from keeping the wings in place, is to absorb the forces exerted on the wings. This means it has to be able to withstand shear- and normal stresses. Without the structure, the wings would just be attached to the fuselage without prevention of bending upwards due to the lift forces (or downwards due to gravity while taxiing). Beside these functions, it also has to be able to withstand and absorb impacts on the wings such as turbulence. In Subsection 11.2.1, the general assumptions for the wingbox design are stated. In Subsection 11.2.3 & 11.2.4, the geometry and the reference frames are discussed respectively. In Subsection 11.2.5, the input parameters for the design are stated. The governing equations are explained in Appendix F.

11.2.1 General Assumptions

This subsection will discuss several assumptions that are used to simplify the wingbox design. Based on their effect on the solution they have been divided into primary assumptions, which have major implications on the results, and secondary assumptions, which have minor implications on the results, but can not be neglected.

Primary Assumptions

- The wingbox is being modelled as a tapered hollow square beam. The camber of the wing will only give a better structural performance.
- The mass of the wingbox is neglected, which means that there is less force counteracting the lift, which is why the wingbox will be slightly over-designed. Currently only the fuel weight counteracts the lift. Thus the number of loads that need to be taken into account are reduced, which simplifies the calculations.

- The resultant force distribution due to lift acts at 0.25 chord. The front spar is located at the 0.25 chord to carry the loads.
- The wingbox is the only load carrying structure, which means that the airfoil and the other components of the wing are irrelevant for the structural analysis. Since in reality, the entire wing structure carries a part of the load (however small), the beam model will be over-designed.
- Aerodynamic effects (aside from lift) are neglected. This means that drag and tip vortices effects are not considered. The effects of this assumption are: ignoring tip vortices leads to a lower stress being detected at the tip (a linear decrease until 0 from root to tip instead of a small rise close to the tip); drag would influence the bending moment as well as the torsional contribution - as such, since it is discounted and because of the squaring of the stress in the von Mises equation, the stress distribution produced by the analytical/numerical solution will be lower in magnitude than in reality.

Secondary Assumptions

- It is assumed that the structure is thin walled, which means that higher order terms of thicknesses can be neglected in the calculations.
- Thicknesses of each small structural element do not vary span-wise within a segment. In this way, the thicknesses for each wingbox element are assumed to be constant and the average of the span-wise element chosen.
- The shear flow is constant throughout each element in the thickness direction, which is a result of the assumption that the thicknesses of each wingbox element are assumed to be constant together with the thin walled assumption.
- The aircraft is flying parallel with respect to the earth reference frame, in which the earth is assumed to be flat. This way, the weight of the fuel is acting downwards, parallel to the vertical body axis of the wing, and the lift acts upwards, parallel to the vertical body axis of the wing. The aircraft angle of attack and pitch angle is 0°, meaning the weight acts downwards, parallel to the y-axis.
- Plane stress is assumed, thus the stress vector along a certain surface is assumed to be zero, which complies with the previous assumption of a thin-walled structure, that is acted upon only by load forces that are parallel to them. This means that instead of a 3-dimensional matrix, a 2-dimensional matrix can be used to calculate the stress distribution.

11.2.2 Load Case

The design criterion used for the wing is aircraft at MTOW in cruise condition. The aircraft with maximum payload with zero fuel is also a design option, but the wingbox of the Q-50 encounters more stresses at MTOW in cruise. For the lift, a combination between an elliptical and a linear distribution is used. This is the so-called Schrenk distribution [33], which is modeled as an average of the above mentioned distributions. See Appendix F for the governing equations that define the forces. The shear force distribution span-wise can be seen in Figure 11.2.

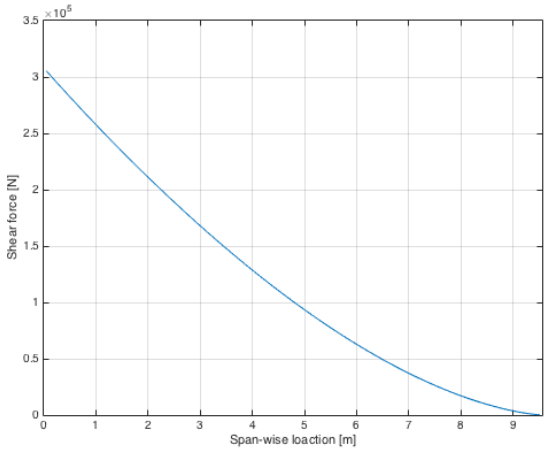

Figure 11.2: Shear force distribution on the wingbox

11.2.3 Wingbox Geometry

In this subsection, the geometry of the wingbox is explained in more detail. As shown in Figure 11.4, the wingbox is located between 25% and 65% of the chord, to be able to keep a square cross section. It was

chosen to keep a straight and non-tapered wingbox section inside the fuselage and to have a tapered and sweeped section outside the fuselage. These two different sections are indicated in Figure 11.3 with $L1$ and $L2$ respectively. During this chapter, the right wing will taken into consideration separately, since the left wing will be the same but then mirrored.

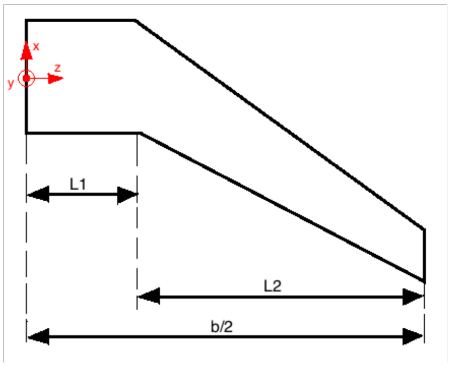

Figure 11.3: Schematic top view of the wingbox with all dimensions, including the main reference frame (right wing)

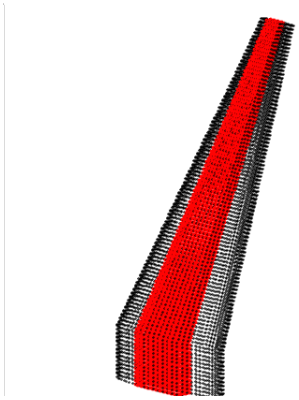

Figure 11.4: View of the wingbox inside the wing (right wing)

In Figure 11.4, an initial view of the wingbox inside of the wing can be seen. In this view, it was assumed that the wing part outside of the fuselage had one fixed sweep and taper to reduce complexity, since the wingbox was defined as being in between two percentages of the chord length. It was decided to keep the wingbox shape the same, even if an additional taper would be introduced in the wing. This was done to avoid kinks in the wingbox, which would result in stress concentration.

11.2.4 Reference Frame Used

In order to be consistent in the calculations a convenient reference frame has to be chosen. The main reference is chosen to be in the middle of the cross section, which is located at the root, as can bee seen in Figure 11.5. In Figure 11.6 the local reference system of each cross section is shown.

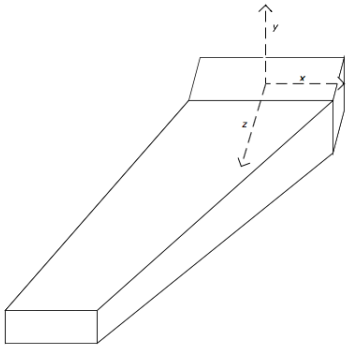

Figure 11.5: Side view of wingbox with the main reference system

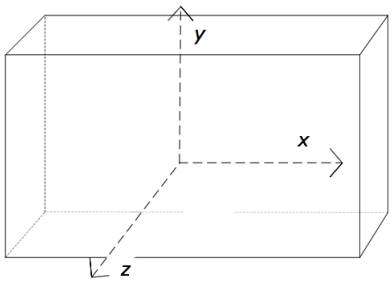

Figure 11.6: Cut of the wingbox with the local reference system

All the governing equation are given in Appendix F. The equations in this section all come from [34] or are derived from them. The governing equations are the basis for the analytic and numerical models, which can be used to verify the method used.

11.2.5 Input and Approach

The input data for the wingbox calculation can be seen in Table 11.1. With the use of the these parameters, all the stresses can be calculated. These data are used for the numerical and analytical approach. The numerical approach performs better at solving non-linear models, which will be used after the current design phase of the wingbox. The analytical approach is used to validate the data. The further design phase which is referred to is not discussed in this report.

Table 11.1: Input parameters for the wingbox design of one wing

Parameter	Meaning	Value
A	Aspect ratio	8.5
S	Surface area	43.2 m^2
$\Lambda_{0.25c}$	Sweep angle at quarter chord	25 °
$b/2$	Half span	9.58 m
C_r	Root chord	3.20 m
C_t	Tip chord	0.96 m
L_1	Inner wingbox length	1.3 m
L_2	Outer wingbox length	8.28 m
$MTOW$	Maximum Take-Off Weight	17, 425 kg
n_{max}	Ultimate load factor	3.75

Numerical Approach

For the numerical approach, the wingbox is segmented into n sections. It is important to note that for each small sampling section the average is taken to be in the middle of the section. Thus, for a small section we assume a constant mean cross section. This procedure is shown in Figure 11.7.

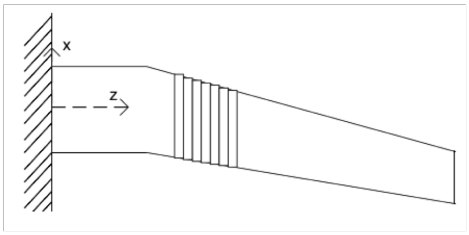

Figure 11.7: Discretisation of the wing into elements (top view)

Figure 11.8: Discretisation of the cross section of the wingbox

The outline of the numerical program is as follows:

1. Calculation of the wingbox dimensions and 2^{nd} moment of inertia as function of distance to the tip in the n elements.
2. Calculation lift based on the Schrenk distribution as a function of the n elements.
3. Calculation of the moment and torsion in every plate of the wingbox element as function of distance to the tip.
4. Calculation of the shear and shear flow in every plate of the wingbox element as function of distance to the tip.
5. Calculation of the maximum shear and normal stresses due to bending, shear and torsion in every plate of the wingbox element.

Analytic Approach

The internal forces and stresses are calculated with the different analytical expressions for their corresponding forces. The internal shear force is determined by setting an equilibrium between the resulting lift force and the internal shear. Equation 11.1 gives the expression for the internal shear force *V*.

$$V = -\int_0^x q(x)\ \mathrm{d}x \qquad (11.1) \qquad\qquad M = -\frac{3x(4+\pi)}{9\pi}\int_0^x q(x)\ \mathrm{d}x \qquad (11.2)$$

Here, *q(x)* is the lift distribution. The internal bending moment is determined by setting equilibrium between the moment of the resultant of the lift distribution to the section and the internal moment. Equation 11.2 shows the expression for the internal bending moment in the wing modelled as a beam, it runs from the tip of the wing to the root. The internal normal stresses and shear flow are determined by Equation F.11 and F.12. The subsection for validation and verification shows the comparison between the analytical and the numerical calculations.

11.2.6 Stiffening

The wingbox is further optimized by adding stringers and ribs to the structure. The stringers resist bending and axial loads, they divide the skin into small panels and thereby increase its ability to resist buckling stresses.

Table 11.2: Input values to determine stringer spacing

Parameter	value
k	4
b	1 m
σ_{comp}	206.1 MPa
E	46.3 GPa
ν	0.3

Table 11.3: Values to determine rib spacing

Parameter	value
P_{cr}	24.7 kN
E	46.3 GPa
I	1.22 $\cdot 10^{-8}$ m^4
L	0.47 m

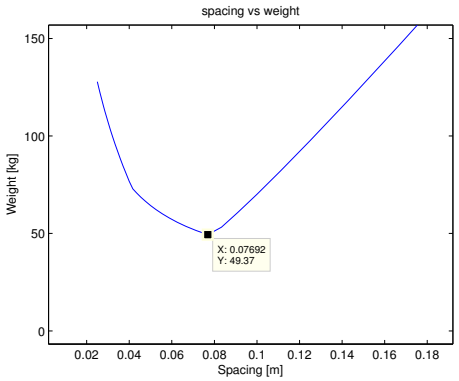

Figure 11.9: Weight of stiffened panel as function of stringer spacing

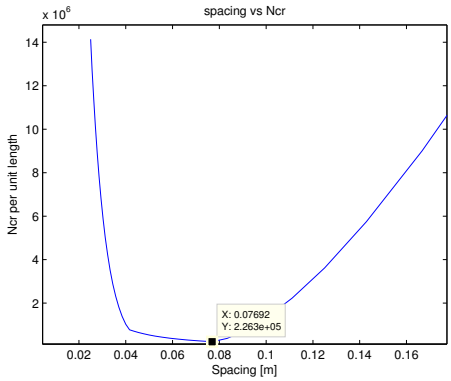

Figure 11.10: Axial buckling load per unit length as function of stringer spacing

The ribs maintain the cross-sectional shape, they establish the column length of the stringers to increase their column buckling stress.

Stringers

According to Howe [35], CFRP plates fail in compression as it is dependend on the resin and fiber. When in tension, CFRP is mainly dependend on the fiber. The stringers on the top plate of the wingbox are chosen to have a T-profile as they have a good ability to carry axial loading and compression stresses since the flange of the T-section serves as a compression member. T-stringers are also easy to manufacture since they are nothing more than two L-profiles attached to each other. The profile thickness is assumed to be equal to the minimal skin thickness of 2 mm. The stringer spacing is determined by the plate buckling theory. The expressions used are derived from the analysis of potential energy theory of plates [34]. These equations are described in Equations 11.3 and 11.4.

$$N_{x,cr} = \frac{k\pi^2 D}{b^2} \qquad (11.3)$$

$$D = \frac{Et^3}{12(1-\nu^2)} \qquad (11.4)$$

Where k is the plate buckling coefficient, b is the width of the loaded end of the plate, $N_{x,cr}$ is the critical buckling load per unit length, t is the plate thickness, ν is the poisson's ratio. The buckling coefficient k is set to the minimum value of 4 [34]. $N_{x,cr}$ is determined by multiplying the maximum compression normal stress in the swept part of the wing with the width of the panel. The optimal stringer spacing is determined by looking for the combination of skin thickness and amount of stringers that will be able to carry the compression stresses while being as light as possible. The input values are stated in Table 11.2 and Figures 11.9 and 11.10 show the results for the optimal stringer spacing.

Figure 11.10 shows that the minimum value of $N_{x,cr}$ is also reached at the minimum stringer spacing. It is desired for $N_{x,cr}$ to be as small as possible to such that the potential energy of the buckled plate would be minimal [34]. From Figure 11.9 it can be concluded that the optimal stringer spacing for the top panel is 7.7 cm. The panel will buckle if the spacing is larger than 7.7 cm.

At this design phase the bottom plate is stiffened identically to the top plate. Since the bottom plate is in tension during cruise, it is not expected to fail due to the tensile stresses [35]. This implies that the bottom plate is not accordingly designed.

Wing Ribs

The rib spacing is determined by analyzing the stringers separately for column buckling. The axial force on the stringers due to the maximum normal stress for the ultimate loading case is set as the critical buckling load. The minimum length L at which a stringer will buckle is determined from Equation 11.5.

$$P_{cr} = \frac{\pi^2 EI}{L^2} \tag{11.5}$$

Where the critical buckling load P_{cr}, the Young's modulus E of the material and the moment of inertia I of the stringer are used as input variables. The critical buckling load of a stringer is determined by taking the product of the maximum compression normal stress and the stringer area. Table 11.3 shows the input values and the resulted buckling length for the stringers. This L is set as the maximum spacing between the ribs as they serve as panel breakers. In practice the spacing between the ribs is strategically determined by the location of the hinge positions for control surfaces and the ends of the wing fuel tanks. The ribs are placed perpendicular to the spars to allow a lighter wingbox structure [36]. Figure 11.11 shows the layout of the wingbox stiffeners.

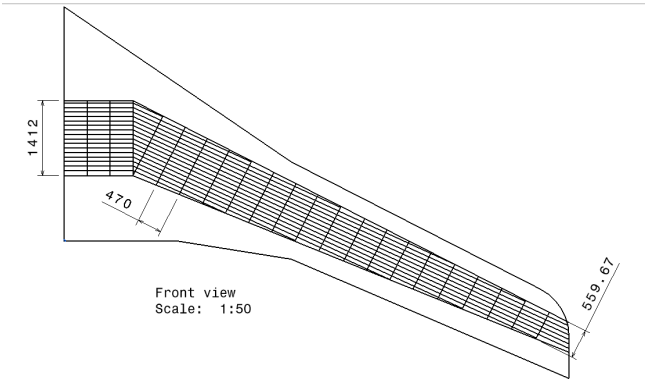

Figure 11.11: Lay out of wingbox including stiffeners

Wing Spar Design

The spars resist bending and shear stresses from the lift distribution. They are modeled as tapered I-beams for analysis because of their ability to resist bending and shear. It is assumed that the flanges take the normal forces due to bending and the web takes the shear stress due to shear and torsion. The taper ratio of the beam is fixed to the taper ratio of the wingbox in general. To size the front and rear spars, the internal shear force at the beginning of the swept part of the wingbox is used as the design load. First the shear stresses in the spar webs are determined from boxed beam analysis, afterwards the spar is analyzed separately to size the flanges. Table 11.4 shows the input values used to determine the stresses in the spars.

Table 11.4: Input values to calculate to design the tapered wing spar

Parameter	value
V	$2.48{\cdot}10^5$ N
M	$7.9{\cdot}10^5$ Nm
h	0.34 m
t_{web}	2 mm
$\frac{\partial y}{\partial z}$	0.014
τ_{all}	105 Mpa
$\sigma_{all,comp}$	514 MPa
$\sigma_{all,tens}$	925 MPa

Table 11.5: Calculated properties for the design of the wing spars

Parameter	value
P	$2.32{\cdot}10^3$ kN
$\tau_{max,front}$	91.2 Mpa
$\tau_{max,rear}$	91.2 Mpa
Minimum top flange area	$4.9{\cdot}10^3$ mm^4
Minimum bottom flange area	$2.7{\cdot}10^3$ mm^4

The internal bending moment translates to a force couple in the flanges of the spars. As mentioned already, the flanges will take the normal stresses. Table 11.5 shows the input values and the resulting flange area for the wing spars at the fuselage location. It can also be noted that the spar web does not fail in shear under the given load. The flange area will gradually get smaller along the span as the wingbox is tapered. Since the wingbox section is symmetrical, the front and rear spar will be identical.

11.2.7 Verification

For the verification of the wingbox structure design method, the MATLAB code that is used to determine the internal forces and stresses and hence the sizing is debugged and checked for syntax errors. After the software is debugged, the numerical output is compared with the analytic output. Table 11.6 shows the comparison

of the internal moment and torque between the numerical and the analytic solution and also the bending and shear stress. For the shear stress value, the maximum value on the upper plate is taken, as where the bending stress is constant over the top plate. The differences are given in absolute values. The discrepancies between the two solutions are due to the assumptions that are mentioned at the beginning of the chapter.

Table 11.6: Verification for the wingbox structural analysis

Location (spanwise)	**Shear [kN]**	**Moment [Nm]**	**Torque [Nm]**	**Bending stress [Pa]**	**Shear stress [Pa]**
z = 0 m					
Analytic	$3.2182 \cdot 10^5$	$-1.1654 \cdot 10^6$	$-1.6729 \cdot 10^5$	$-1.6389 \cdot 10^8$	$-2.6275 \cdot 10^7$
Numerical	$3.2180 \cdot 10^5$	$-1.1503 \cdot 10^6$	$-1.6845 \cdot 10^5$	$-1.6176 \cdot 10^8$	$-2.8379 \cdot 10^7$
|Difference|	0.0055%	4.7168%	0.6914%	1.3168%	7.4148%
z = 1.3 m					
Analytic	$2.5324 \cdot 10^5$	$-7.9235 \cdot 10^5$	$-2.1193 \cdot 10^5$	$-1.1142 \cdot 10^8$	$-2.6943 \cdot 10^7$
Numerical	$2.5614 \cdot 10^5$	$-7.9488 \cdot 10^5$	$-2.1036 \cdot 10^5$	$-1.1159 \cdot 10^8$	$-2.8407 \cdot 10^7$
|Difference|	1.1354%	0.9893%	0.7454%	0.1488%	5.1533%
z = 8.0 m					
Analytic	$1.6686 \cdot 10^4$	$-1.0017 \cdot 10^4$	62.1363	$-1.7440 \cdot 10^7$	$-4.3529 \cdot 10^6$
Numerical	$1.7854 \cdot 10^4$	$-1.0340 \cdot 10^4$	61.0017	$-1.7554 \cdot 10^7$	$-4.4550 \cdot 10^6$
|Difference|	6.5428%	1.8091%	1.1860%	0.6481%	2.2919%

11.2.8 Results

Table 11.7 shows the dimensional properties for the wingbox.

Table 11.7: Properties of the wingbox

C_r	4.1 m
C_t	0.52 m
Thickness	8%
Stringer spacing	0.8 m
Rib spacing	0.65 m
Spar web thickness	2 mm
Spar flange surface	191.2 mm^2

Table 11.8: Properties of the horizontal tail box

C_r	1.0 m
C_t	0.5 m
Thickness	8%
Amount of stringers	7
Stringer spacing	0.15 m
Amount of ribs	3
Rib spacing	1.6 m
Spar web thickness	2 mm
Spar flange surface	$4.2 \cdot 10^3$ mm^2

Table 11.9: Properties of the vertical tail box

C_r	1.48 m
C_t	1.0 m
Thickness	9%
Stringer spacing	0.15 m
Maximum rib spacing	1.6 m
Spar web thickness	2 mm

11.3 Tail

The parts of the tail section is analyzed in the same analogy as the wing. The only difference between the shape of the horizontal tail box and the wingbox is that the tail box has no straight torsion box in the middle. The horizontal tail takes bending and torsion in both vertical directions. The design lift force for the tail is 13.3 kN. See Table 14.14. The stringers for the vertical tail are also T-stringers but the flange is 2 cm wide and the web is 1 cm in height. The thickness is still 2mm. Table 11.9 shows the results for the vertical tail. The vertical tail is designed to resist the extra loads from yaw manoeuvre plus a gust of 20 m/s which translates to a 1 kN force. Table 11.8 shows the results for the horizontal tail.

11.4 Fuselage

The fuselage makes up the largest part of the aircraft by volume. It is the payload carrying structure and requires adequate stiffening to perform its task. The fuselage is modelled as a line containing all properties such as stiffness in order to simplify the analysis. The most extreme load case for the fuselage is determined and set as the design point. The amount of stringers and the skin thickness are determined based on the extreme load case.

Primary Assumptions

- The fuselage analysis is based on the straight sections of fuselage that are attached to the wing section. The wing-fuselage integration is not included in this analysis. Its structural properties will be investigated in the future.

- The fuselage is modelled as a hollow circular beam with booms representing the stringers, as can be seen in Figure 11.12.
- The cut-outs required by the main doors and emergency exit are not part of the analysis and its required reinforcements will be determined in the future.
- The section to be analyzed is modelled as a cantilevered beam loaded by a distributed force along its length, and a force and moment at its tip, as can be seen in Figure 11.13.
- The fuselage is designed using the "Black Metal" approach, implying an isotropic material. The skin thickness increment is therefore defined as four times the thickness of a single ply.

Secondary Assumptions

- Thin walled assumptions hold for the fuselage skin as its thickness is a small fraction of the fuselage radius.
- All loads are assumed to act along the center line of the fuselage.
- The floor is assumed not to carry any loads.
- The weight and payload of the fuselage including frames, seats, passengers and luggage are assumed to be evenly distributed.
- The stringers are modelled as booms. The moment of inertia contribution of its shape is assumed negligible compared to the contribution of its area.

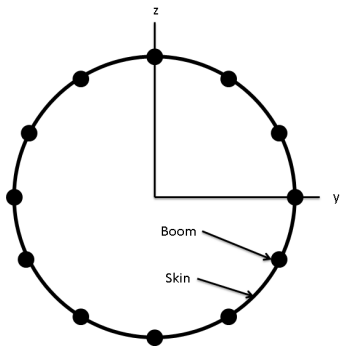

Figure 11.12: Fuselage model cross section

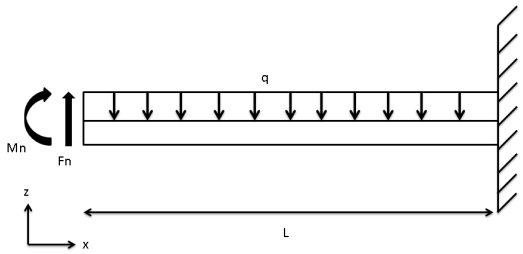

Figure 11.13: Side view of fuselage modelled as a cantilevered beam

11.4.1 Load Case

In order to determine the design point of the fuselage, the most critical load case is determined. This is found to be an overload of the nose gear in landing conditions resulting in five times the nominal landing gear load. Beyond this load, the nose attachment should fail, causing the fuselage to further absorb the impact energy. This load case requires an analysis of the front straight fuselage section protruding from the wing fuselage integration. In order to analyse this situation, three parameters, as mentioned in Figure 11.13, have to be applied to the model:

- Nose force (Fn). This force consists of the weights of the cockpit section frame, the avionics, the crew and operational items. The most important contribution however is provided by the nose gear force.
- Nose moment (Mn). This moment is induced by the offset application of weights mentioned above.
- Distributed load (q). This distributed load consists of the weights of the airframe, the passengers, luggage, and seats. These weights are assumed to be evenly distributed along its length.

11.4.2 Stiffening

The fuselage is designed as a semi monocoque circular tube, implying a loaded skin with support structure. The circular cross section is structurally very efficient when pressurized. The properties of the circular fuselage cross section are constant along its circumference, easing manufacturing. The support structure for this fuselage consists of stringers in longitudinal direction to provide bending stiffness, and fuselage frames to provide structural stability and circumferential bending stiffness. The necessity of the stringers is emphasized by the required skin thickness calculated to be more than 5 cm without the stringers. The frame pitch is heuristically determined at 50 cm, which is a typical value for commercial aircraft. The cross-sectional profile of the the frame is chosen to be an I-profile. The profile selected for the stringers in a "hat" profile. This profile is very suitable for composites and adds torsional rigidity due to its closed cross section. Stringers and skins are joined by means of co-curing.

11.4.3 Model Inputs

The values used as the input for the nose force and nose moment are presented in Table 11.10. The values used as input for the distributed load is presented in Table 11.11. The final cumulative inputs to the fuselage model are presented in Table 11.12.

Table 11.10: Nose force and nose moment

Origin	Force [N]	Moment arm [m]	Moment [Nm]	Comment
Avionics	-3730	1.5	-5595	Assuming all avionics to be located in the nose section. Chapter 7
Frame	-1890	1.5	-2835	Assuming 10% of the airframe weight. Chapter 7
Crew	-1960	1.5	-2940	Assuming 100kg per pilot, including luggage. Chapter 7
Operational items	-490	1.5	-735	Including items such as charts and manuals. Chapter 7
Nose gear	118950	0	0	Assuming five times the maximum load mentioned in Table 14.24

Table 11.11: Distributed load on full 14 m straight fuselage section

Origin	Force [N]	Comments
Passengers and luggage	-42690	Chapter 7
Frame	-13220	Assuming 70% of airframe weight. Chapter 7
Seats	-2450	Chapter 7

Table 11.12: Cumulative input value for fuselage model

	Fn [N]	Mn [Nm]	q [N/m]
Input value	110880	-12105	-4170

11.4.4 Tests

The following tests are performed on the fuselage design. All tests are passed.

- **Skin Buckling Test** In the skin buckling test, the maximum compressive stress is compared to the critical stress found in Equation 11.3.
- **Upper Fuselage Test** The ultimate stress encountered by the upper fuselage is compared to the equivalent ultimate stress of the material.
- **Lower Fuselage Test** This test is the same as the one mentioned above, but applies to the lower fuselage.
- **Pressure Test** The pressure test compares the hoop stresses due to pressure differential to the ultimate tensile strength of the material.
- **Stringer Buckling Test** The stringer buckling test compares the maximum compressive stress to the value from the column buckling equation (Equation 11.5). The stringer is assumed to be simply supported, which is a conservative assumption.
- **Shear Buckling Test** The shear buckling test compares the maximum shear stress with the critical shear buckling load.

Table 11.13 shows the results of the tests.

11.4.5 Results

Each increment in skin thickness requires a corresponding amount of stringers to pass all the tests. An optimum can be found in Figure 11.14. The minimum required skin thickness for water absorption is higher than the optimum. The next increment of skin thickness complying with the minimum required skin thickness for water absorption is therefore selected. A summary of the design can be found in Table 11.14

Table 11.14: Fuselage design summary

Skin thickness	Stringer amount	Mass
2.2 mm	84	622 kg

Condition	σ	σ_{all}
Skin buckling	-55.1 MPa	-84.7 MPa
Upper fuselage structure	-55.1 MPa	-514 MPa
	55.1 MPa	925 MPa
Lower fuselage structure	-55.1 MPa	-514 MPa
	55.1 MPa	925 MPa
Stringer buckling	-55.1 MPa	-1.26·10^3 MPa
Shear buckling	-6.05 MPa	-105 MPa

Table 11.13: Results of fuselage structure stress test

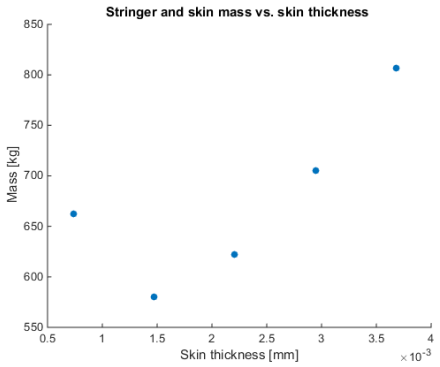

Figure 11.14: Skin and stringer mass vs. skin thickness

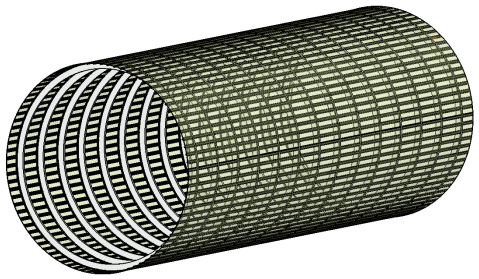

Figure 11.15: Fuselage structural visualization

11.4.6 Required Further Analysis

The fuselage structural design presented in this chapter provides an initial estimate of the skin and stringer arrangement of the fuselage skin and stringers. Many aspects of a full fuselage structural design remain to be determined. The following main aspects of the fuselage design are the most important factors that have yet to be determined.

- **Fuselage Frames** The fuselage frames provide important structural stability to the skin stiffener arrangement. The frame's main functions are to provide circumferential bending stiffness and to provide an even load introduction. The fuselage frames are of great importance to crash worthiness. Important load introduction points, such as nose gear, should coincide with frames to provide an efficient load propagation.
- **Door Cut-out Reinforcements** The cut-out locations for the main doors and the emergency exits weaken the fuselage structure and require adequate reinforcements to counter the stress concentrations caused by such cutouts.
- **Wing-Fuselage Integration** This is a very important area of the fuselage due to the load introduction of the wing. The fuselage requires a cut-out where the wingbox passes through the lower fuselage. The reduction in bending stiffness caused by this cutout is countered by the keel beam. Load introduction into the skin is done by means of fuselage frames as mentioned above. The skin around the cut-out also requires reinforcements to prevent stress concentrations.

Propulsion System Design

Despite having a conventional looking aircraft, all the internals will be changed in order to comply with the emission requirements. One of the major improvements is the engine of the aircraft. In order to reach the proposed specific fuel consumption multiple new technologies are combined in a newly designed engine. First of all, the bypass ratio will be increased with respect to older generation aircraft. Furthermore, the fan will be connected to a gearbox and an intercooler will be added after the first compressor. This chapter describes the engine layout and its components, as well as the reasons for choosing the specified components. After that, the estimates on the performance of the engine will be given.

12.1 Engine Layout

The chosen concept uses a turbofan engine. Current generation aircraft, like the CRJ-200 and the ERJ-145, have turbofan engines as well. Foremost to reach the desired speed and therefore altitude, while still being able to provide sufficient thrust.

12.1.1 Inlet

The main goal for the intake is to ensure an uniform flow with uniform pressure and velocity distribution, all while keeping the pressure loss at a minimum [37]. Another task of the intake is to slow down the flow for better compressor performance. Because the aircraft operates at high Mach numbers during cruise the airflow through the engine can reach Mach 1. When designing the inlet for slowing down the airflow, one must keep the friction losses to a minimum [37, 38].

Part of the inlet is the cowling, which houses the fan. During a fan blade failure, this cowling must be able to stop a lose blade. By using composite materials for the fan casing, General electric has saved 160 kg.[1] The fan on the GE engine is 2.8 m, which is double the size of this design. It is assumed that the area of a thin walled circular cross section is $2\pi rt$. Therefore the weight reduction from the fan casing is expected to be around 80 kg, when keeping the same length and thickness.

12.1.2 Geared Fan

In modern turbofans engines the fan on the front is directly connected with the low pressure compressor, or LPC. The fan limits the speed of the LPC, because when the fan, which has a large diameter, runs at large speeds the tips of the fan blades go supersonic. However, running the compressor at higher speeds allows for higher pressure ratios. One of the options would be by using a separate axle for the fan. This would require a separate turbine to power the fan, and more importantly, a triple axle set up, which is mechanically very difficult. A two axle system is already pushing the limit. A better solution is by using a gearbox between the LPC and fan.

A gearbox will still use the same axle used by the LPC however changes the speed of the output axle to the fan. Using this method the LPC can be run at higher speeds increasing the pressure ratio while the fan can be operated at lower speeds preventing the tips of the fan blades going supersonic. Basically the gearbox allows both components to be run at their optimal speeds. The cost of the gearbox is a weight increase as well as an increase in complexity, more parts that need maintenance, and lastly a larger mechanical loss or lower mechanical efficiency. With the improved fan and LPC performance this loss can be compensated.

12.1.3 Intercooler

The basic idea behind an intercooler is cooling the air that flows into the compressor so less work has to be applied by the turbine to reach the same pressure ratio. However, due to the definition of thermal efficiency (η_{th}) for the Brayton cycle, the thermal efficiency goes down when adding an intercooler [39]. However, this can be easily explained due to the constant pressure ratio. As a result of the intercooler, less work is required by the turbine so reach the same pressure ratio over the HPC. If the work were to be kept the same with and without an intercooler, the pressure ratio for the HPC will be larger in the case when the intercooler is present.

Normally an intercooler uses a special medium, such as cooling fluid, for the heat transfer. These intercooler systems add quite some weight to the engine in the form of fluid, pumps, and reservoirs. Therefore, in the proposed design, the heat exchange will take place between the bypass airflow and the LPC airflow. Both a specially deigned heat exchanger as well as counter flowing airflows have to make the required heat

[1] http://www.geaviation.com/press/genx/genx_20041214.html

transfer possible. Using metal 3D printing methods, the required complex structures can be produced. The counter flow and the intercooler itself does introduce pressure losses in the flow, both for the bypass airflow and the compressor airflow. In Section 12.2 more concrete values are given for the losses as well as the gains.

An additional benefit of the intercooler is, that the bypass air is heated, which means a better mixture of the exhaust gasses, which in turn offer better noise performance. The state of flow after the intercooler in complex, hence it is not clear whether the flow contains many vortices, which would mean a worse performance in noise. The research in this phenomenon would require further CFD simulations, which is not part of the preliminary design.

12.1.4 Combustion Chamber

The combustor determines the emissions and the inlet temperature for the turbine. The temperate determines what kind of material has to be used for the turbine blades. The temperature in the combustion chamber determines the NOx emissions. Generally speaking, the lower the combustion temperature, the lower the NOx emissions. However, not only the temperature is important, the fuel to air ratio and the way the flame front behaves, are important for the combustor efficiency. These last aspects, however, are very difficult to predict and are heavily dependant on empirical data [38]. Therefore, this engine was only designed for combustion temperature and estimates on the emission values were made.

12.2 Engine Performance

In order to predict the engine performance, GSP 11 by NLR has been used [40]. GSP allows for the creation of gas turbine model with various components. One of the big advantages of this program is its capability of predicting emissions. The emissions are determined from statistical data gathered by NLR. A relation between fuel consumption, thrust, and combustion temperature results in an emission value for various gasses [40]. For this project, only CO_2 and NO_x are considered. In order to validate the intercooler effectiveness, a model with equal pressure ratios and losses without the intercooler is made. This allows for a comparison between the two engines.

12.2.1 Assumptions

- The polytropic efficiencies for the inlet, fan, compressor, combustor, and turbines are chosen from reference data from the AE2230-II power & propulsion course, the GSP default engine models and the books [37, 38, 39, 41].
- The bleed airflow fraction is obtained from [37]. The fraction gives the ratio of the air mass flow of the intake which is used for bleed air.
- The intercooler uses two inputs: a heat flux in kW, which determines how much energy is transferred from one flow to the other. The heat flux is chosen to be 400 kW, which results in a temperature change of 24 K in the compressor flow. The values follow from [42, 43, 44]. The intercooler pressure loss is chosen a little less than twice the pressure loss in the ducts before the exhausts. The pressure loss will be significant in a counter flow intercooler, however, if the pressure loss it too large the positive effect of the intercooler will be lost. Because the engine is set to go into service in 2035, it is assumed that the intercooler technology will have matured enough so that these pressure losses are reasonable.
- Duct pressure losses are assumed to be 0.028, which follows from the example engines provided by NLR in the program.

12.2.2 Design Method

The model created can be seen in Figure 12.1 and it shows the various components. The input values for the various efficiencies are given in Table 12.1.

With the model set up, the engine parameters can be changed. The design point is chosen at cruise altitude with a Mach number of 0.81. The reason to fly at this speed is explained in Chapter 15. Although the range for this aircraft is not very large for further expansion in an aircraft family, a strong performing engine in cruise in beneficial. The performance at sea level must still be sufficient for take-off. The iterations were started with reference data for the intake mass flow, bypass ratio, compressor pressure ratios, combustion temperature and all efficiencies. These give a value for thrust and specific fuel consumption.

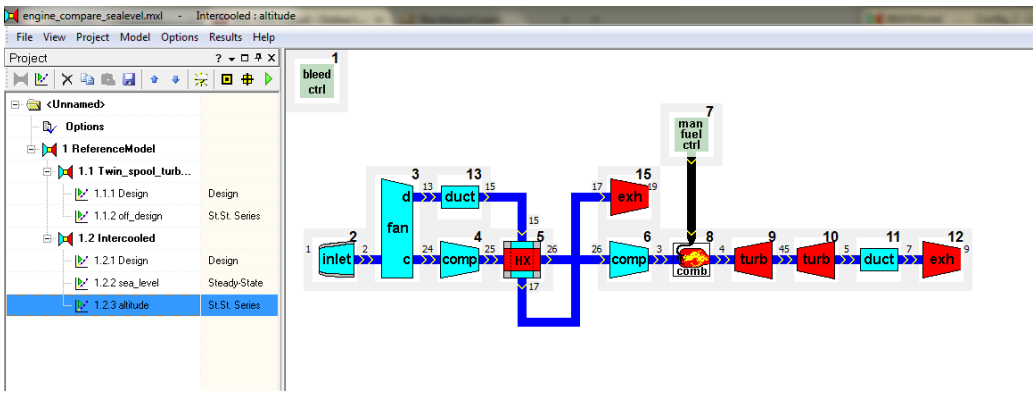

Figure 12.1: The GSP model with the various components and GSP interface

The next step is to change the pressure ratios to achieve the required thrust. Following the pressure ratios the efficiencies are improved if necessary. The efficiencies are changed with percentages of reference values, assuming in 20 years there are better compressors and turbines. After this first iteration, the exit velocities and exit area are checked. If the values are not as required, the mass flow in the inlet is changed as well as bypass ratios, after which the pressure ratios are changed again. When changing the values, one must keep in mind if the required pressure ratios are feasible on these smaller engines, as well the bypass ratio. A larger bypass ratio means a better SFC, however, if the bypass ratio were to become too large, the 'actual' core engine would be very small, which is not possible to produce. The engine was first designed without the heat exchanger, after which a version with the heat exchanger was designed. The reason for this is, is that there is very little known about a heat exchanger or intercooler. Therefore a normal engine was used for a baseline.

Another strong feature of this program is the fact that it allows for bleed airflow from the compressor and extra work losses from the turbine. For this model, only a bleed flow for high pressure turbine cooling is used. The values for the bleed airflow are a fraction of the main mass airflow and follows from [37]. The turbine work is determined by the power required from the aircraft power system. For all electronics as well as air-conditioning. This aircraft is not using any other bleed air systems apart from the turbine cooling and therefore has a larger power required from the turbine. The torque is assumed to be 200 Nm per engine, multiplied by two and multiplied with the mechanical efficiency of the generator, it gives the available torque for the aircraft subsystems [37, 38].

12.2.3 Results

The final engine uses the input parameters given in Table 12.1, which are obtained after several iterations. As stated in the assumptions, the duct pressure losses were taken from example engines, provided by the program.

Table 12.1: Input data for the engine model

Intake mass flow	110	[kg/s]	HPC PR	11.5	[-]
Intake Pressure ratio	1.0	[-]	HPC efficiency	0.890	[-]
			HPC bleed fraction	0.02	[-]
Bypass ratio	5.8	[-]			
Core side PR	1.65	[-]	Combustor Fuel flow	0.24	[kg/s]
Duct side PR	1.7	[-]	Combustor efficiency	0.995	[-]
Core side efficiency	0.930	[-]	Combustor pressure loss	0.04	[-]
Duct side efficiency	0.930	[-]			
			HPT efficiency	0.920	[-]
LPC PR	2.5	[-]	Mechanical efficiency	0.990	[-]
LPC efficiency	0.950	[-]	Spool inertia	0.35	[kgm^2]
Heat flux	400	[kW]	LPT efficiency	0.880	[-]
Core flow pressure loss	0.03	[-]	Mechanical efficiency	0.990	[-]
Duct flow pressure loss	0.04	[-]	Spool inertia	0.40	[kgm^2]
			External torque	200	[Nm]

Using the input data in Table 12.1, the thrust and thrust specific fuel consumption are given in Table 12.2. Furthermore, the table contains emission values given as a mass percentage of the mass flow in the engine.

Table 12.2: Final results for the engine at cruise altitude and cruise speed

	Altitude [m]	TT4 [K]	[CO2]4 [m%]	[CO]4 [m%]	[NO]4 [m%]	V9 [m/s]	V19 [m/s]	FN [kN]	WF [kg/s]	Aexit [m^2]	TSFC [kg/Nhr]
With inter-cooler	10278	1321	4.99	4.27E-7	0.04	451.2	316.6	14.9	0.245	0.87	0.059
	0	1528	6.08	1.08E-5	0.12	383.7	284.6	33.0	0.300	0.36	0.033
Without intercooler	10278	1364	4.99	9.46E-7	0.05	459.4	314.3	15.6	0.245	0.84	0.056
	0	1569	6.08	1.90E-5	0.14	403.4	294.3	34.2	0.300	0.35	0.032

The table shows that the emissions with the intercooler in place are lower, as well as the exit velocities of the two nozzles. The lower nozzle exit speeds mean a lower noise pressure, combining this with the fact that the bypass air is slightly warmer due to the heat exchange and the chevrons, the hot and cold gas mixing will be improved significantly.

12.3 Validation & Sensitivity

Because the program used is not self made, validation of the program is very important. It is assumed that the verification of the software is done. Despite this, a sensitivity analysis is performed to check whether changing a certain input value, for example the fuel flow, gives the expected effect. For the validation, aircraft engine data from the engine data set in Civil Jet Aircraft Design by Jenkinson [45]. The engines are chosen to be roughly the same size as the engine for this design, however, sometimes information was lacking, so in order to get a good number of reference data, other larger engines were looked at as well. The results for this analysis is given in Table 12.3.

Table 12.3: Validation data for the engine simulation

Engine	**Aircraft**		**Referance data**	**Computed value**	**Difference**
Honeywell LF507	Avro RJ85	Thrust [kN]	31.0	36.2	16.77%
		SFC [lb/lbf h]	0.41	0.40	2.44%
Rolls Royce Tay 620-5	Fokker F100	Thrust [kN]	61.6	65.0	5.52%
		SFC [lb/lbf h]	0.43	0.43	0.00%
GE CF34-4	CRJ-200	Thrust [kN]	38.8	35.8	7.73%
		SFC [lb/lbf h]	0.35	0.35	0.00%
IAE V2500	A320	Thrust [kN]	146.8	137.7	6.20%
		SFC [lb/lbf h]	0.37	0.37	0.00%

When changing the parameters, it was found that the efficiencies of the heat exchanger had serious effect as is explained above. Furthermore, the effect of the duct side pressure ratio for the fan is very susceptible for change. Because of the rather large bypass ratio, pressure ratios for the duct have significant effects.

12.4 Recommendations for Further Design

The outcomes from this simulations are the required pressure ratios and required efficiencies for all the components. These are however, idealized values and they still have to be met. For example, the compressor requires a certain pressure ratio, but this pressure ratio is has to be realized by determining the compressor blade geometry and how many stages it requires. Equally, the fan is a very important part in the engine, especially because of the large bypass ratio the fan has to be designed very well, in order to get the required efficiency.

The combustion chamber is another specially important piece in the engine. Because the combustion temperature for this engine is so small compared to current generation engines, the combustor needs to be specially designed. Main reason is because of the lower temperatures, incomplete combustion will be more prevalent. This will increase the carbon monoxide and CO_2 emission. One of the ways to counter this is, is by improving the fuel to air ratio [37, 41]. Predicting the combustor performance is very difficult and moreover predicting the combustion. Designing the combustor and its components such as, fuel injectors, flame stabilizers and cooling requires extensive CFD calculations and in the end real life tests.

Another aspect for further investigation is the noise from the engines. Again, the interaction between the exit flow from the bypass exhaust and the core exhaust (hot and cold air mixing), is very difficult to predict because of vortices from the exhaust as well as the heat transfer between the flows.

Stability and Control

In this chapter, the stability of the QLEAR-50 will be presented. In Section 13.1, the stability derivatives are computed. Then, the equations of motion are introduced, first for the symmetrical case (Section 13.2) and then for the asymmetrical one (Section 13.3). Also in this chapter, the eigenvalues and eigenvectors are calculated and, if they prove to be unstable, adjustments to the aircraft design will be proposed.

13.1 Stability Derivatives

In this section the stability derivatives are calculated. The most accurate values can be obtained from in-flight measurements. However, since the Q-50 is still in a design phase, all stability derivatives will be estimated based on empirical formulas provided by Roskam [46] and the Flight Dynamics Reader [47]. The estimations are based on geometric and aerodynamic characteristics of the aircraft, which were treated in the previous chapters. The results are shown in Appendix C, together with the formula used to compute each parameter and the required sign, as indicated in [47]. The parameters that were considered for this analysis are summarized in the list below:

- **Derivatives with respect to airspeed (C_{X_u}, C_{Z_u} and C_{m_u})** are influenced by the Mach and Reynolds numbers and the variation of the aircraft's aeroelastic deformation with airspeed.
- **Derivatives with respect to angle of attack ($C_{X_\alpha}, C_{Z_\alpha}$ and C_{m_α})** determine how the aircraft behaves when the angle of attack is varied. In the case of C_{X_α} and C_{Z_α}, the dominant contribution is provided by the wing. For stability, C_{m_α} has to be negative, such that the aircraft can generate a negative moment when it experiences an increase in angle of attack. In other words, the center of gravity has to lie ahead of the aerodynamic center in the case there is no tail.
- **Derivatives with respect to the acceleration along the top axis ($C_{X_{\dot\alpha}}, C_{Z_{\dot\alpha}}$ and $C_{m_{\dot\alpha}}$)** are used to analyze the behaviour of the aircraft after a sudden increase in airspeed, before the pressure distribution over the entire body has adjusted to the new flow conditions.
- **Derivatives with respect to sideslip angle (C_{Y_β}, C_{l_β} and C_{n_β})** are mainly influenced by the fuselage, vertical tailplane and dihedral. Also, the wing-fuselage integration is of importance because it can induce a rolling moment, generated by the difference in angle of attack of the two wings.
- **Derivatives with respect to rate of angle of sideslip ($C_{Y_{\dot\beta}}, C_{l_{\dot\beta}}$ and $C_{n_{\dot\beta}}$)** are of less importance. The only significant contribution is attributed by the vertical tailplane.
- **Derivatives with respect to roll rate (C_{Y_p}, C_{l_p} and C_{n_p})** express the behaviour of the aircraft during a roll maneuver. C_{Y_p} is usually neglected, unless the wing has a high sweep or a large vertical tailplane is used. The roll damping is measured by C_{l_p} and is normally negative, such that the generated moment slows the rolling motion down. The Dutch roll eigenmotion is influenced significantly by the roll rate derivatives.
- **Derivatives with respect to yaw rate (C_{Y_r}, C_{l_r} and C_{n_r})** are influenced by the rudder deflection and generate a rolling moment. This moment is due to the increased lift force on one wing and the decreased lift on the other. These derivatives also have a significant influence on the Dutch roll characteristics.
- **Derivatives with respect to pitch rate (C_{X_q}, C_{Z_q} and C_{m_q})** express the effect of changing the pitch on the aerodynamic parameters of the aircraft. The most important derivative is C_{m_q}, with the largest contribution supplied by the horizontal tailplane.
- **Derivatives with respect to the aileron angle ($C_{Y_{\delta_a}}, C_{l_{\delta_a}}$ and $C_{n_{\delta_a}}$)** predict the variation in side force, rolling and yawing moment with aileron deflection. Normally the side force contribution can be neglected.
- **Derivatives with respect to the rudder angle ($C_{Y_{\delta_r}}, C_{l_{\delta_r}}$ and $C_{n_{\delta_r}}$)** predict the variation in side force, rolling and yawing moment with rudder deflection. The greatest contribution is given by the yawing moment $C_{n_{\delta_r}}$.
- **Derivatives with respect to the elevator angle ($C_{X_{\delta_e}}, C_{Z_{\delta_e}}$ and $C_{m_{\delta_e}}$)** are important because the total drag created by the elevator deflection cannot be neglected, especially at a high speed. $C_{m_{\delta_e}}$ has the biggest influence on the aircraft motion. The horizontal tailplane influences this parameter the most.

13.2 Symmetric Analysis

The linear model for symmetric aircraft motions, as described in [47] is given in equation 13.1.

$$\begin{bmatrix} C_{X_u} - 2\mu_c D_c & C_{X_\alpha} & C_{Z_0} & C_{X_q} \\ C_{Z_u} & C_{Z_\alpha} + (C_{Z_{\dot\alpha}} - 2\mu_c)D_c & -C_{X_0} & (C_{Z_q} + 2\mu_c) \\ 0 & 0 & -D_c & 1 \\ C_{m_u} & C_{m_\alpha} + C_{m_{\dot\alpha}} D_c & 0 & C_{m_q} - 2\mu_c K_Y^2 D_c \end{bmatrix} \begin{bmatrix} \hat{u} \\ \alpha \\ \theta \\ q\frac{\bar{c}}{V} \end{bmatrix} = \begin{bmatrix} -C_{X_{\delta_e}} \\ -C_{Z_{\delta_e}} \\ 0 \\ -C_{m_{\delta_e}} \end{bmatrix} \delta_e \tag{13.1}$$

In order to evaluate the eigenmodes of the aircraft, this matrix has to be rewritten in state space form. This is done in Equation 13.2, where the symbols in this equation can be found in Table 13.1.

$$\begin{bmatrix} \dot{\hat{u}} \\ \dot{\alpha} \\ \dot{\theta} \\ \dot{q}\frac{\bar{c}}{V} \end{bmatrix} = \begin{bmatrix} x_u & x_\alpha & x_\theta & 0 \\ z_u & z_\alpha & z_\theta & z_q \\ 0 & 0 & 0 & \frac{V}{\bar{c}} \\ m_u & m_\alpha & m_\theta & m_q \end{bmatrix} \begin{bmatrix} \hat{u} \\ \alpha \\ \theta \\ q\frac{\bar{c}}{V} \end{bmatrix} + \begin{bmatrix} x_{\delta_e} & x_{\delta_t} \\ z_{\delta_e} & z_{\delta_t} \\ 0 & 0 \\ m_{\delta_e} & m_{\delta_t} \end{bmatrix} \begin{bmatrix} \delta_e \\ \delta_t \end{bmatrix} \tag{13.2}$$

Table 13.1: Symbols appearing in the general state-space representation of Eq. 13.2

	$x\ldots$	$z\ldots$	$m\ldots$
u	$\frac{V}{\bar{c}}\frac{C_{X_u}}{2\mu_c}$	$\frac{V}{\bar{c}}\frac{C_{Z_u}}{2\mu_c - C_{Z_{\dot\alpha}}}$	$\frac{V}{\bar{c}}\frac{C_{m_u} + C_{Z_u}\frac{C_{m_{\dot\alpha}}}{2\mu_c - C_{Z_{\dot\alpha}}}}{2\mu_c K_Y^2}$
α	$\frac{V}{\bar{c}}\frac{C_{X_\alpha}}{2\mu_c}$	$\frac{V}{\bar{c}}\frac{C_{Z_\alpha}}{2\mu_c - C_{Z_{\dot\alpha}}}$	$\frac{V}{\bar{c}}\frac{C_{m_\alpha} + C_{Z_\alpha}\frac{C_{m_{\dot\alpha}}}{2\mu_c - C_{Z_{\dot\alpha}}}}{2\mu_c K_Y^2}$
θ	$\frac{V}{\bar{c}}\frac{C_{Z_0}}{2\mu_c}$	$\frac{V}{\bar{c}}\frac{C_{X_0}}{2\mu_c - C_{Z_{\dot\alpha}}}$	$-\frac{V}{\bar{c}}\frac{C_{X_0}\frac{C_{m_{\dot\alpha}}}{2\mu_c - C_{Z_{\dot\alpha}}}}{2\mu_c K_Y^2}$
q	$\frac{V}{\bar{c}}\frac{C_{X_q}}{2\mu_c}$	$\frac{V}{\bar{c}}\frac{2\mu_c + C_{Z_q}}{2\mu_c - C_{Z_{\dot\alpha}}}$	$\frac{V}{\bar{c}}\frac{C_{m_q} + C_{m_{\dot\alpha}}\frac{2\mu_c + C_{Z_q}}{2\mu_c - C_{Z_{\dot\alpha}}}}{2\mu_c K_Y^2}$
δ_e	$\frac{V}{\bar{c}}\frac{C_{X_{\delta_e}}}{2\mu_c}$	$\frac{V}{\bar{c}}\frac{C_{Z_{\delta_e}}}{2\mu_c - C_{Z_{\dot\alpha}}}$	$\frac{V}{\bar{c}}\frac{C_{m_{\delta_e}} + C_{Z_{\delta_e}}\frac{C_{m_{\dot\alpha}}}{2\mu_c - C_{Z_{\dot\alpha}}}}{2\mu_c K_Y^2}$
δ_t	$\frac{V}{\bar{c}}\frac{C_{X_{\delta_t}}}{2\mu_c}$	$\frac{V}{\bar{c}}\frac{C_{Z_{\delta_t}}}{2\mu_c - C_{Z_{\dot\alpha}}}$	$\frac{V}{\bar{c}}\frac{C_{m_{\delta_t}} + C_{Z_{\delta_t}}\frac{C_{m_{\dot\alpha}}}{2\mu_c - C_{Z_{\dot\alpha}}}}{2\mu_c K_Y^2}$

Using a MATLAB script and the stability derivatives from Appendix C, the eigenvalues found for the symmetric case are given in Equation 13.3. Because both pairs of eigenvalues have a negative real part, the aircraft will be stable in symmetric flight.

$$\begin{aligned} \lambda_{c_{1,2}} &= -0.5860 \pm 1.2121i \\ \lambda_{c_{3,4}} &= -0.0068 \pm 0.0427i \end{aligned} \tag{13.3}$$

By applying an impulse input of 2° on the elevator for 1 second, two modes can be distinguished: the phugoid and short period. These modes will be analyzed in the following sections.

13.2.1 Short Period Mode

The short period mode is represented by the $\lambda_{c_{1,2}}$ eingenvalues. The short period eigenmotion can be seen in Figure 13.1. The response of the the aircraft's vertical speed, angle of attack, pitch angle and pitch rate can be seen from top to bottom respectively in Figure 13.2.

Figure 13.1 shows the relative amplitude (begins at 1) of the eigenvalue over a time span of 20 seconds. From the simplified calculations of the short period and eigenmotion shown, it can be derived that:

- The period $P = 5.1249$ s
- The time to half amplitude $T_{\frac{1}{2}} = 1.0761$ s
- The damping ratio $\zeta = 0.4651$
- The undamped natural frequency $\omega_0 = 1.3849$ rad/s

As expected, the 'short period', is a periodic eigenmotions which has a very small period and is also heavily damped [47]. The two figures of the short period confirm this expected behaviour.

13.2.2 Phugoid Mode

The phugoid mode is represented by the $\lambda_{c_{3,4}}$ eigenvalues. The phugoid eigenmotion can be seen in Figure 13.3. The response of the the aircraft's vertical speed, angle of attack, pitch angle and pitch rate can be seen from top to bottom respectively in Figure 13.4.
Figure 13.3 shows the relative amplitude (begins at 1) of the eigenvalue over a time span of 200 seconds. From the simplified calculations of the phugoid and the eigenmotion shown, it can be derived that:

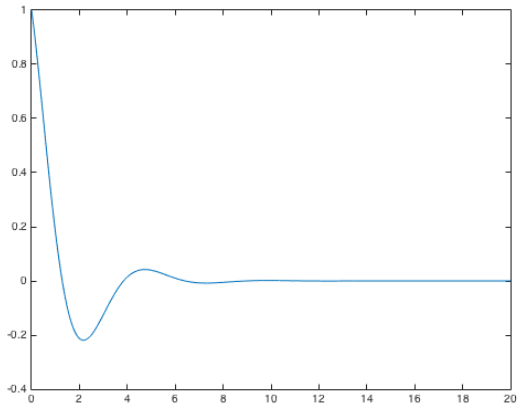

Figure 13.1: Short period eigenmotion

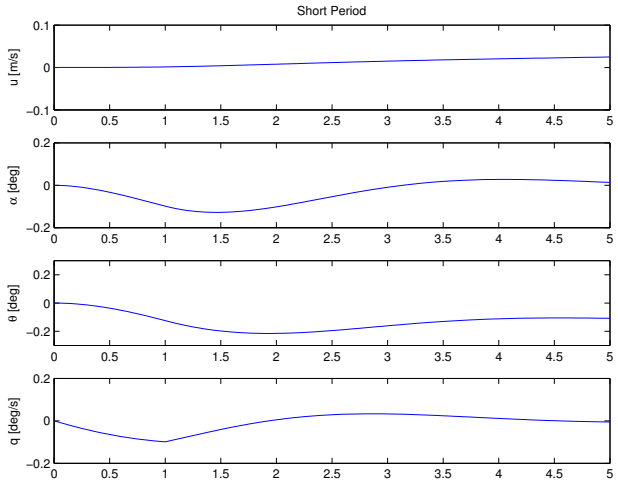

Figure 13.2: Short period mode

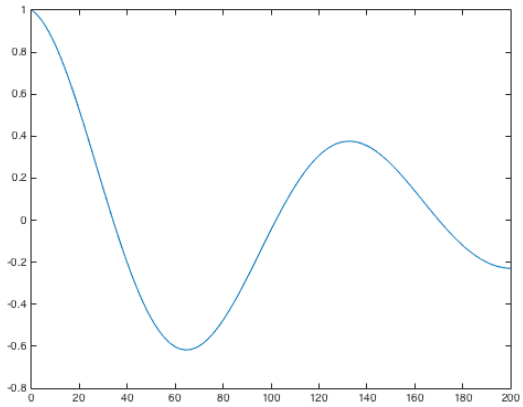

Figure 13.3: Phugoid eigenmotion

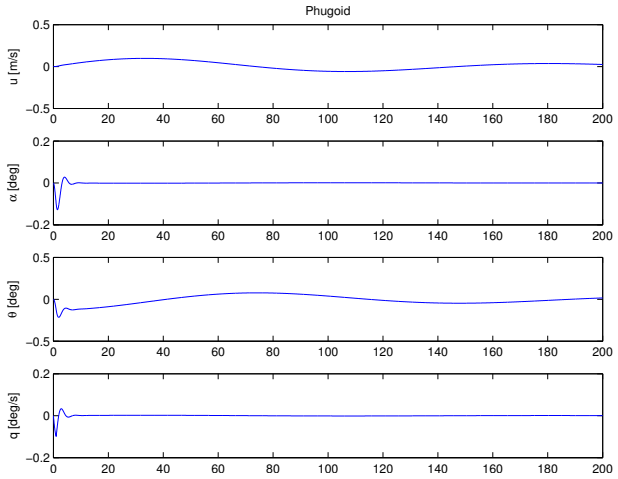

Figure 13.4: Phugoid mode

- The period $P = 136.0601$ s
- The time to half amplitude $T_{\frac{1}{2}} = 95.2050$ s
- The damping ratio $\zeta = 0.1557$
- The undamped natural frequency $\omega_0 = 0.0467$ rad/s

As expected from the pugoid, it is an eigenmotion with a (very) long period. As can be seen in the two figures of this eigenmotion, the pugoid is also lightly damped. The observed behaviour strikes with the expectations. Furthermore since both the phugoid and the short period are now confirmed, the conclusion can be drawn that the longitudinal stability derivatives are correct, hence the design will be stable in this direction [47].

13.3 Asymmetric Analysis

The equations of motion for the asymmetric case are found in [47] and given in 13.4.

$$\begin{bmatrix} C_{Y_\beta} + D_b(C_{Y_{\dot\beta}} - 2\mu_b) & C_L & C_{Y_p} & C_{Y_r} - 4\mu_b \\ 0 & (-1/2)D_b & 1 & 0 \\ C_{l_\beta} & 0 & C_{l_p} - 4\mu_b K_X^2 D_b & C_{l_r} + 4\mu_b K_{XZ} D_b \\ C_{n_\beta} + D_b(C_{n_{\dot\beta}}) & 0 & C_{n_p} + 4\mu_b K_{XZ} D_b & C_{n_r} - 4\mu_b K_Z^2 D_b \end{bmatrix} \begin{bmatrix} \beta \\ \varphi \\ \frac{pb}{2V} \\ \frac{rb}{2V} \end{bmatrix} = \underline{0} \qquad (13.4)$$

A similar approach to the symmetric case is used to write the aforementioned equation in a state-space form. The results is shown in Equation 13.5, where the terms can be found in Table 13.2.

$$\begin{bmatrix} \dot{\beta} \\ \dot{\varphi} \\ \frac{\dot{p}b}{2V} \\ \frac{\dot{r}b}{2V} \end{bmatrix} = \begin{bmatrix} y_\beta & y_\varphi & y_p & y_r \\ 0 & 0 & 2\frac{V}{b} & 0 \\ l_\beta & 0 & l_p & l_r \\ n_\beta & 0 & n_p & n_r \end{bmatrix} \begin{bmatrix} \beta \\ \varphi \\ \frac{pb}{2V} \\ \frac{rb}{2V} \end{bmatrix} + \begin{bmatrix} 0 & y_{\delta_r} \\ 0 & 0 \\ l_{\delta_a} & l_{\delta_r} \\ n_{\delta_a} & n_{\delta_r} \end{bmatrix} \begin{bmatrix} \delta_a \\ \delta_r \end{bmatrix} \tag{13.5}$$

Table 13.2: Symbols appearing in the general state-space representation of Eq. 13.5

	$y\ldots$	$l\ldots$	$n\ldots$
β	$\frac{V}{b}\frac{C_{Y_\beta}}{2\mu_b}$	$\frac{V}{b}\frac{C_{l_\beta}K_Z^2+C_{n_\beta}K_{XZ}}{4\mu_b(K_X^2K_Z^2-K_{XZ}^2)}$	$\frac{V}{b}\frac{C_{l_\beta}K_{XZ}+C_{n_\beta}K_X^2}{4\mu_b(K_X^2K_Z^2-K_{XZ}^2)}$
φ	$\frac{V}{b}\frac{C_L}{2\mu_b}$	0	0
p	$\frac{V}{b}\frac{C_{Y_p}}{2\mu_b}$	$\frac{V}{b}\frac{C_{l_p}K_Z^2+C_{n_p}K_{XZ}}{4\mu_b(K_X^2K_Z^2-K_{XZ}^2)}$	$\frac{V}{b}\frac{C_{l_p}K_{XZ}+C_{n_p}K_X^2}{4\mu_b(K_X^2K_Z^2-K_{XZ}^2)}$
r	$\frac{V}{b}\frac{C_{Y_r}-4\mu_b}{2\mu_b}$	$\frac{V}{b}\frac{C_{l_r}K_Z^2+C_{n_r}K_{XZ}}{4\mu_b(K_X^2K_Z^2-K_{XZ}^2)}$	$\frac{V}{b}\frac{C_{l_r}K_{XZ}+C_{n_r}K_X^2}{4\mu_b(K_X^2K_Z^2-K_{XZ}^2)}$
δ_a	$\frac{V}{b}\frac{C_{Y_{\delta_a}}}{2\mu_b}$	$\frac{V}{b}\frac{C_{l_{\delta_a}}K_Z^2+C_{n_{\delta_a}}K_{XZ}}{4\mu_b(K_X^2K_Z^2-K_{XZ}^2)}$	$\frac{V}{b}\frac{C_{l_{\delta_a}}K_{XZ}+C_{n_{\delta_a}}K_X^2}{4\mu_b(K_X^2K_Z^2-K_{XZ}^2)}$
δ_r	$\frac{V}{b}\frac{C_{Y_{\delta_r}}}{2\mu_b}$	$\frac{V}{b}\frac{C_{l_{\delta_r}}K_Z^2+C_{n_{\delta_r}}K_{XZ}}{4\mu_b(K_X^2K_Z^2-K_{XZ}^2)}$	$\frac{V}{b}\frac{C_{l_{\delta_r}}K_{XZ}+C_{n_{\delta_r}}K_X^2}{4\mu_b(K_X^2K_Z^2-K_{XZ}^2)}$

Again using a MATLAB script and the stability derivatives from Appendix C, the eigenvalues found for the asymmetric case are given in Equation 13.6. Because all eigenvalues have a negative real part, the aircraft will also be stable in asymmetric flight.

$$\begin{aligned} \lambda_{b_{1,2}} &= -0.3688 \pm 1.5667i \\ \lambda_{b_3} &= -4.9204 \\ \lambda_{b_4} &= -0.0090 \end{aligned} \tag{13.6}$$

Three modes can be distinguished: aperiodic roll, spiral and Dutch roll. These modes will be analyzed in the following sections.

13.3.1 Aperiodic Roll Mode

The aperiodic roll corresponds to the eigenvalue λ_{b_3}. For the simulation, a step input of 45° was given to the aileron and the initial roll angle ϕ was taken to be 15°. The aperiodic roll eigenmotion can be seen in Figure 13.5. The response of the the aircraft's sideslip angle, roll angle, roll rate and yaw rate can be seen from top to bottom respectively in Figure 13.6.
Figure 13.5 shows the relative amplitude (begins at 1) of the eigenvalue over a time span of 20 seconds. From the simplified calculations of the aperiodic roll and the eigenmotion shown, it can be derived that:

- The period $P =$ -
- The time to half amplitude $T_{\frac{1}{2}} =$ 0.1476 s
- The damping ratio $\zeta = 1$
- The undamped natural frequency $\omega_0 =$ 4.6959 rad/s

The expected behaviour of the aperiodic roll, is a highly damped (convergent), non-periodic motion, due to the fact that the eigenvalue is real and strongly negative. This expectation is confirmed by the observed behaviour shown in the figures of the aperiodic roll [47].

13.3.2 Spiral Mode

The spiral mode corresponds to λ_{b_4}. The response of the the aircraft's sideslip angle, roll angle, roll rate and yaw rate to the simulation can be seen from top to bottom respectively in Figure 13.8, where an initial roll angle $\phi = 15^\circ$ was taken. The eigenmotions can be seen in Figure 13.7.
The graph of the eigenmotion shows the relative amplitude (begins at 1) of the eigenvalue over a time span of 200 seconds. From the simplified calculations and eigenmotion shown, it can be derived that:

- The period $P =$ -
- The time to half amplitude $T_{\frac{1}{2}} =$ 75.0162 s
- The damping ratio $\zeta = 1$

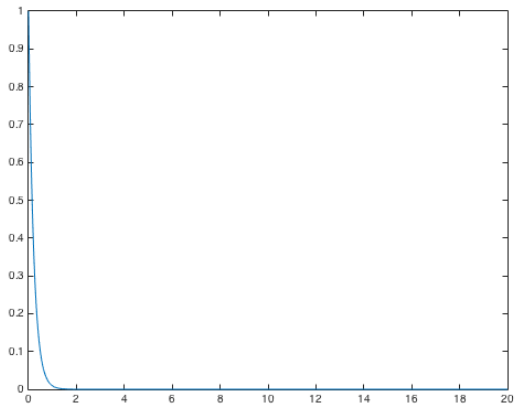

Figure 13.5: Aperiodic roll eigenmotion

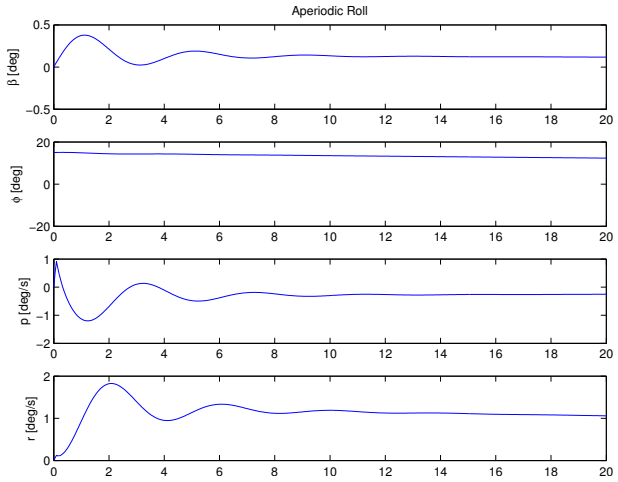

Figure 13.6: Aperiodic roll mode

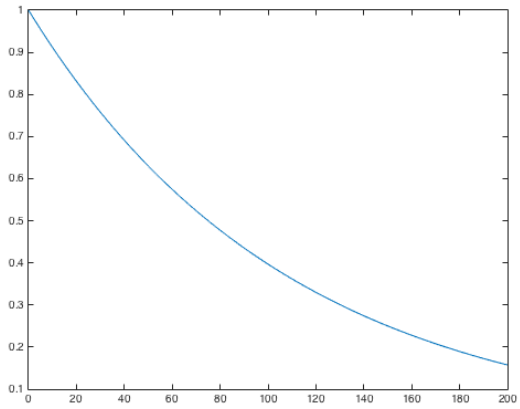

Figure 13.7: Spiral eigenmotion

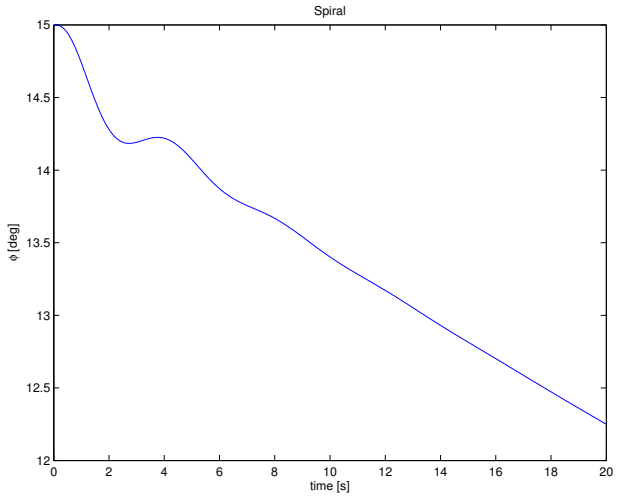

Figure 13.8: Spiral mode

- The undamped natural frequency $\omega_0 = 0.0092$ rad/s

The spiral is stable as can be seen in the two figures above. This can also be observed in the sign of the (real) eigenvalue. It is lightly damped though, but at least it is stable. Spiral instability however, is sometimes not a direct problem, because of the very small values of the eigenvalue, which determine the decay (or growth) of the motion [47].

13.3.3 Dutch Roll

The Dutch roll corresponds to the $\lambda_{b_{1,2}}$ eigenvalues. This was simulated by applying a 2° rudder deflection, with a step input of 1 second. The eigenmotion of the aircraft can be seen in Figure 13.9. The response of the the aircraft's sideslip angle, roll angle, roll rate and yaw rate can be seen from top to bottom respectively in Figure 13.10.
Figure 13.9 shows the relative amplitude (begins at 1) of the eigenvalue over a time span of 20 seconds. From the simplified calculations of the Dutch roll and the eigenmotion shown above, it can be derived that:

- The period $P = 2.9983$ s
- The time to half amplitude $T_{\frac{1}{2}} = 1.5434$ s
- The damping ratio ζ =0.0895
- The undamped natural frequency $\omega_0 = 2.1431$ rad/s

The Dutch roll motion is a stable, periodic motion in the case of the QLEAR-50, since the response of the eigenmotion is a damped sinusoidal over time, as can be seen in the above mentioned figures. However, although the period is quite small, the amplitude of the first couple of peaks is still significant. The Dutch

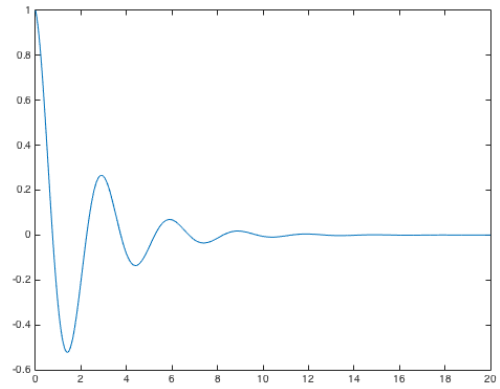

Figure 13.9: Dutch roll eigenmotion

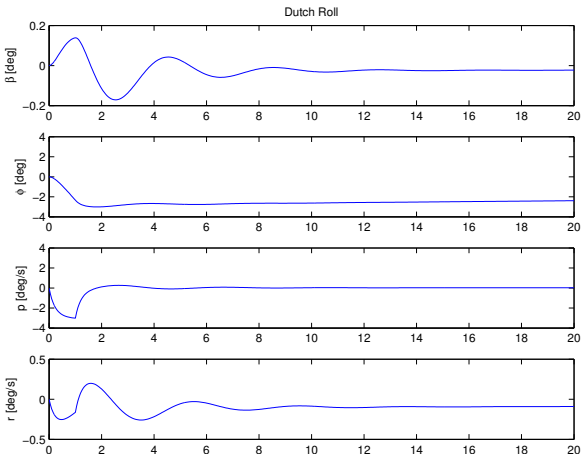

Figure 13.10: Dutch roll Mode

roll is a unwanted motion since it will cause very violent motions, far from the center of gravity. For that reason, the aircraft will be equipped with a so-called yaw-damper [47]. The QLEAR-50 is proven to be stable in all the eigenmotions! In the next section, the control forces on the tail will be briefly discussed.

13.4 Control Forces

In this section, an explanation of control forces on the tail is given. The normal force of the tail required to keep the aircraft in balance can be calculated by Equation 13.7. The required elevator deflection to create this force is given in Equation 13.8 [47].

$$N_h = \frac{1}{l_h}\left(C_{m_{ac}}\frac{1}{2}\rho V^2 S\bar{c} + W\left(x_{cg} - x_w\right)\right) \tag{13.7}$$

$$\delta_e = -\frac{1}{C_{m_{\delta_e}}}\left(C_{m_0} + \frac{C_{m_\alpha}}{C_{N_\alpha}}\frac{W}{\frac{1}{2}\rho V^2 S}\right) \tag{13.8}$$

The results of these equation can be seen in the figures below. In Figure 13.11, the tail normal force (N_h) with respect to the airspeed (V) is given. In Figure 13.12, the deflection of the elevator as function of the airspeed is given.

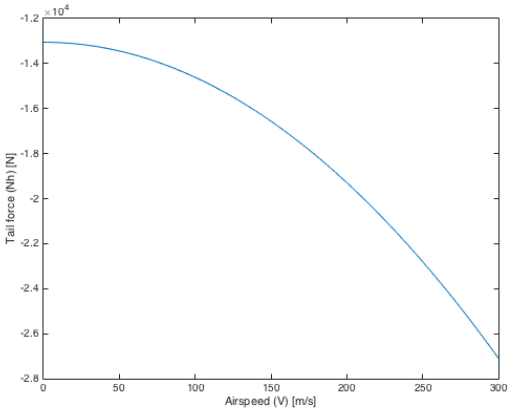

Figure 13.11: Normal force on the tail

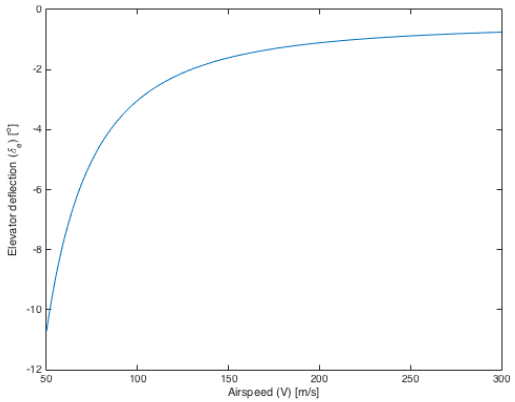

Figure 13.12: Elevator deflection

The results from this stability chapter, can be used in the sizing chapters to come up with the design and analysis of the tail.

Detailed Sizing

After performing analysis in all the main areas of aircraft design, such as aerodynamics, materials, structures, propulsion and stability, the next step is to perform detailed sizing of the aircraft. Section 14.1 contains the detailed design of the wing, followed by the detailed sizing of the tail in Section 14.2. Finally, the landing gear is designed in Section 14.3.

14.1 Detailed Wing Design

The most important function of the wing is to generate the lift required to fly. However, the lift requirements change during the mission phase and therefore important subsystems are located on the wing, that increase the performance and control of the aircraft, such as high lift devices, wingtips and control surfaces, to be able to fly as optimal as possible during the entire mission. In this section the high lift device design is treated after which an aerodynamic analysis follows.

14.1.1 High Lift Devices

In Chapter 9, the aerodynamic characteristics of the main wing were analyzed during cruise. However the aircraft also needs to be able to perform well during take-off and landing. Since the lift coefficient that is necessary to land is larger than for take-off, the high-lift devices are sized for landing. This is because the speed has to be lower, able to land. The first consideration when selecting an appropriate (set of) high lift device(s) is the increment in $C_{L_{max}}$ that is necessary to land, with respect to $C_{L_{max\_clean}}$. Through iterations it is known that:

$$C_{L_{max\_clean}} = 1.05 \qquad C_{L_{max\_landing}} = 2.5$$

Where $C_{L_{max\_clean}}$ was computed in the same way as $C_{L_{max\_cruise}}$, however at M = 0.2 instead of M = 0.81 because the aircraft will land at a speed of approximately M = 0.2, and $C_{L_{max\_landing}}$ computed using the stall speed [1]. This means therefore that the high lift devices need to be able to increase the lift coefficient by 1.45 in case of full flap deployment, which is generally in the range of 40° to 60° [18].

The second aspect that has to be considered is the part of the total wing span that the trailing edge HLD will occupy, because a part has to be reserved for installation of the ailerons. For this purpose the ratio of S_{wf}/S_{ref} is investigated: the span-wise portion of the reference wing area affected by the presence of the TE HLD. Typically the ailerons are installed between 50 and 90% of the wing span, and the high lift devices are installed in between the fuselage and the ailerons. This typically yields flapped area ratios (S_{wf}/S_{ref}) between 55-70% [1]. Using lecture material [18], the following relation was examined with Matlab:

$$\Delta C_{L_{max}} = 0.9 \Delta C_{l_{max}} (\frac{S_{wf}}{S_{ref}}) \cos \Lambda_{hinge\_line} \tag{14.1}$$

Where $\Delta C_{L_{max}} = 1.45$ as established before, $\Delta C_{l_{max}}$ depends on the type of HLD and the sweep angle at the hinge line depends on the position of the front or rear spar, which were determined during the wingbox design in Chapter 11. For more details on the inputs, see Appendix A. The results are presented in Table 14.1, here it is assumed that slats are used as leading edge device. It was also investigated what ratios would result when the leading edge device is a flap ("droop") which does not have the gap in between such that the drag and noise characteristics improve (however they produce less increment in lift), these can be found in Table 14.2.

It follows from Table 14.1 that the most suitable HLD type is the double slotted flaps, variable geometry because the flapped area is closest to 70% which was estimated to be the limit. This flap is a version of a slotted flap, where the flow separation over the flap is delayed by a movable vane placed in front of it. It reduces the drag and therefore improves take-off and climb performance, in comparison with less complex HLD types. It also increases the $C_{L_{max}}$ that can be reached [48]. Two drawbacks of this configuration are the complexity and its high weight. Another option (area ratio wise) would be the triple slotted flap however due to its complexity and high weight this option is discarded.

From Table 14.2 the flapped area ratios are high, and the question arises whether or not there will be enough space for the ailerons if this type is used. It is known from theory that the aileron takes up around 20-30 percent of the total wing span. Looking at one half of the wing, not including the fuselage part, this would mean that 1.9-2.9 m is occupied by an aileron section, leaving about 5.4-6.4 m of the span. Seen from the tip, 10% should be left free because of the high speed of the aircraft, causing twist and making the

[1] http://adg.stanford.edu/aa241/highlift/clmaxest.html

Table 14.1: Flapped area ratios for various types of TE HLD, with LE slats

HLD type (TE)	**Flapped area ratio (S_{wf}/S_{ref})**
Single slotted flap	1.04
Fowler flap: single slotted or double slotted with fixed vane	0.93
Double slotted flap with fixed vane	0.74
Double slotted flap with variable sections	0.71
Fowler flap: double and triple slotted, with flap extension	0.55

Table 14.2: Flapped area ratios for various types of TE HLD, with LE flaps

HLD type (TE)	**Flapped area ratio (S_{wf}/S_{ref})**
Single slotted flap	1.01
Fowler flap: single slotted or double slotted with fixed vane	0.94
Double slotted flap with fixed vane	0.80
Double slotted flap with variable sections	0.77
Fowler flap: double and triple slotted, with flap extension	0.60

ailerons ineffective. 10 percent translates to 1 meter, thus in the end leaving 4.4-5.4 m for the placement of TE HLD. Using CATIA, it was calculated that in case of $\frac{S_{wf}}{S_{ref}} = 0.71$, the HLD takes up 5 m of the span. This leaves 2.3 meter for the ailerons, of which the sizing method is explained in Section 14.1.5. During the sizing of the ailerons it was determined that 2.3 m is the minimum value for the span occupied by the ailerons and therefore $\frac{S_{wf}}{S_{ref}} = 0.71$ is maximum. Therefore it can be concluded that leading edge flaps are not an option (when triple slotted is discarded). To conclude, Table 14.3 presents the geometry parameters of the high lift devices.

Table 14.3: Geometry of high lift devices

Type:	S_{wf}/S_{ref}	S_{hld}	b_{HLD}	c_{HLD}/c	$\Delta C_{L_{max}}$
TE double slotted flaps	0.71	3.72 m^2	5 m	0.35	1.21
LE slats	0.98	2.65 m^2	8 m	0.15	0.24

Verification and Validation

To verify the Matlab script, a few flapped area ratios are calculated by hand and compared to the outcome of the program. To validate the program, statistical data and theory is compared to the outcome of the program. Three parts of the script were verified: the part of the trailing edge flapped area ratio, the part of the leading edge contribution to $\Delta C_{L_{max}}$, and the combination of those two. Table 14.4 shows the outcome of this verification process. It can be concluded that the script outcome is very close to the analytic outcome and thereby the script is verified. The differences that exist are due to rounding in the analytic process. Higher differences indicate more parameters that can be rounded are included.

Table 14.4: HLD verification process

Inputs	**Parameter calculated**	**Matlab**	**Analytical**	**Difference**
Single slotted, no LE devices, $\delta_f = 40°$	S_{wf}/S_{ref}	1.3424	1.3424	0.66%
Triple slotted, no LE devices, $\delta_f = 40°$	S_{wf}/S_{ref}	0.7182	0.7195	0.19%
LE flaps	$\Delta C_{L_{max}}$	0.2358	0.2358	0%
LE slats	$\Delta C_{L_{max}}$	0.3301	0.3302	0.03%
Single slotted, LE flaps, $\delta_f = 40°$	S_{wf}/S_{ref}	1.1241	1.1239	0.02%
Triple slotted, LE slats, $\delta_f = 40°$	S_{wf}/S_{ref}	0.5547	0.5553	0.11%

To validate the outcome of the program a comparison is made with the CRJ-200, see Figure 14.5. The values are obtained from a on-scale technical drawing and therefore minor errors are assumed to exist. Differences $< 10\%$ are assumed to be due to this drawing/measuring inaccuracies. The difference between flapped area ratio of the trailing edge devices are probably due to a smaller aileron of the CRJ-200. The largest difference can be seen in the chord ratio of the trailing edge devices, which is due to the fact that 0.35 was an assumed value which was presented in lectures, which might be off.

Table 14.5: Validation of the HLD design

Parameter	CRJ-200	Q-50	Difference
S_{wf}/S_{ref},trailing edge	0.81	0.71	12.34%
b_{HLD}, trailing edge	5.14 m	5 m	2.7%
c_{HLD}/c,trailing edge	0.24	0.35	45.8%
c_{HLD}/c, leading edge	0.16	0.15	6.3%
b_{HLD}, leading edge	8 m	8 m	0%

Table 14.6: Parameters to construct lift curves at landing(M = 0.2)

Parameter	Clean	TE	TE and LE
$\frac{dC_L}{d\alpha}$	4.5	5.1	5.1
$C_{L_{max}}$	1.01	2.1	2.5
α_{0L}	-3.9°	-18.9°	-18.9°
α_{stall}	12.1°	8.0°	11.7°

14.1.2 Effect of HLD on Aerodynamic Performance

The high lift devices have been sized with the purpose of enhancing the aircraft its aerodynamic performance during landing. To show the effect of flaps and slats on the aerodynamic characteristics this section is dedicated to the aerodynamic analysis of the main wing during landing. A distinction in made between the cruise and landing phase. It should be noted that take-off is not discussed since it is assumed that when the cruise and landing requirements are met, the take-off requirements are also met and that a 20 degree deflection of the flaps will be sufficient to achieve the required loads.

Lift During Landing Phase

In this section the lift characteristics of the main wing during the landing phase are examined. During the landing phase the high lift devices are deployed and their individual contributions are examined and shown in the form of $C_L - \alpha curves$. To be able to construct these curves the following information is needed:

- $\frac{dC_L}{d\alpha}$ for situations 1,2 and 3.
- $C_{L_{max}}$ for situations 1,2,3.
- α_{0L} for situations 1,2,3.
- α_{stall} for situations 1,2,3.

Where situation 1 is at M = 0.2 (landing speed) with clean configuration, situation 2 is at M = 0.2 with only trailing edge devices deployed and 3 with both TE and LE devices deployed. Following the same method as described for the cruise phase in Chapter 9 [18], the values presented in Table 14.6 were obtained. Compared to the cruise phase, the difference in inputs is mostly the lower Mach number in case of landing. For more detailed information about different inputs used consult [18]. Using this data, three curves were constructed and presented in Figure 14.1.

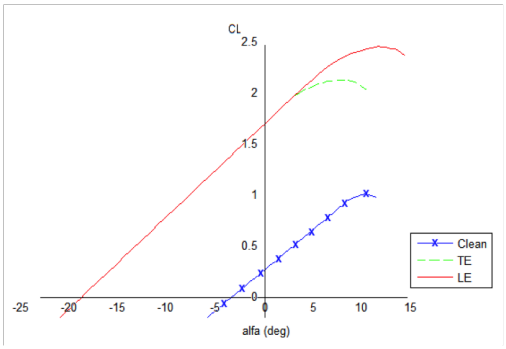

Figure 14.1: Lift curves for the main wing during landing, M = 0.2

14.1.3 Drag During Landing Phase

As one can imagine, extending the high lift devices heavily changes the aerodynamic characteristics. First of all the lift is increased, as that is what the high lift devices are designed for. Second of all, the extension of the flaps and all the gaps it creates drastically decreases the aerodynamic performance by an increase in drag. First of all the profile drag is increased (C_{D_0}), because of a larger wing surface. Second the lift induced drag is increased since the lift increases during landing. The increase in profile drag is determined with the following relation [3]:

$$\Delta C_{D_0} = C_{D_{0_{clean}}} \frac{S_{ws}}{S} \frac{c_s}{c} \cos \Lambda_{0.25c} \tag{14.2}$$

Which results in $C_{D_{0_{HLD}}} = 0.0017$ instead of 0.0015 in the clean configuration. To show the influence of the increased profile drag and increased lift after deployment of the high lift devices, the lift to drag ratios for the clean an fully extended flaps and slats are shown in Figure 14.2.

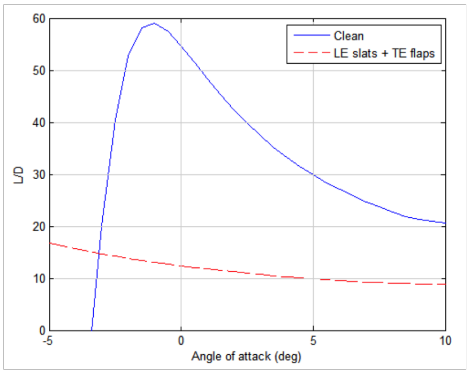

Figure 14.2: L/D for the main wing during landing, M = 0.2

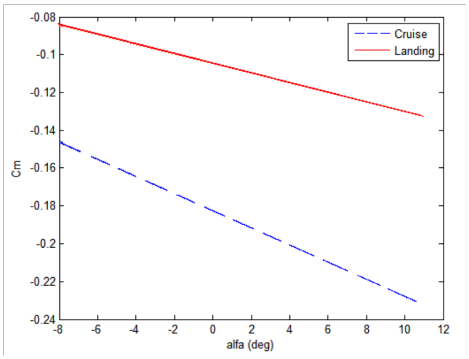

Figure 14.3: Moment produced by the airfoil during cruise (M = 0.81) and landing (M = 0.2)

14.1.4 Going from 2D to 3D Moment

The moment produced by the airfoil is known from Javafoil, and Figure 14.3 shows the moment versus the angle of attack for the cruise and landing phases. Note: the Karman-Tsien compressibility correction was applied to the incompressible outcome produced by Javafoil. It can be seen that when the speed increases, the forces on the airfoil become larger and therefore the moment experienced increases as well. The following question that arises is how does this moment around the airfoil translate to a moment around the complete wing? The answer is that it depends on the geometry of the wing. Also when along the span use is made of different airfoils this has an effect as well. Unfortunately there is no straight forward way to calculate this by hand. In case of further analysis of the design of the Q50, computational fluid dynamic (CFD) analysis techniques have to be consulted.

14.1.5 Wing Control Surfaces

The main control surfaces on the wing are the ailerons and spoilers, which will be designed in this section.

Spoilers Sizing and Positioning

Spoilers are used for multiple purposes:

- **Roll at high speed** By deploying one spoiler a roll motion can be initiated. However, since only one spoiler will be deflected and the spoilers are positioned more inboard than the aileron, the roll rate that can be accomplished will not be as large as when using an aileron. Still, at higher speeds, the forces will be much larger, which increases the moment.
- **Lift dumping** During landing the spoilers are used to increase drag and thus dump lift to decrease the landing distance.
- **Increase rate of descent** Spoilers increase the rate of descent without affecting the speed of the aircraft.

The most critical function of the spoilers is to dump lift and increase drag during landing. By doing so, the required landing of the aircraft is decreased. The spoilers will be designed in order to shorten the landing distance and to meet the landing distance requirement. The use of spoilers, and all other high lift devices should be reduced as much as possible, mostly to reduce the noise emissions of the aircraft. Since the most critical function for the spoilers is to dump lift during landing to decrease the landing distance, it will be designed for this purpose. The spoilers will be sized such that they will provide enough drag and reduce the lift during the landing. The first assumption made is that the spoilers will be able to deflect upward by 85°. Furthermore, the ratio spoilerspan over wingspan will be taken to be $\frac{b_s}{b} = 0.4$, which is a common value [49]. The difference in C_L due to the spoilers can be computed by Equation 14.3.

$$\Delta C_{L_s} = -C_{L_{wing-l}} \frac{b_s}{b} \tag{14.3}$$

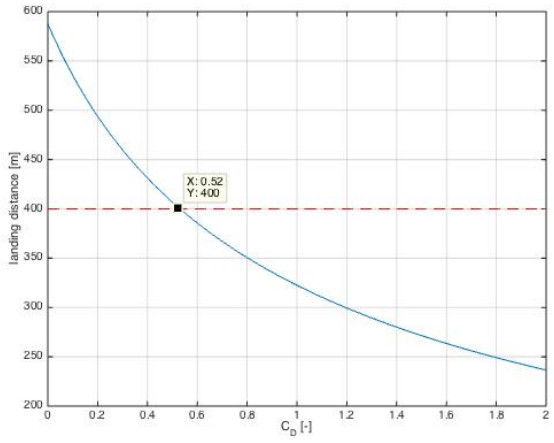

Figure 14.4: Landing distance for different C_D values

The total value of C_L during landing is calculated by Equation 14.4.

$$C_{L_l} = C_{L_{wing-l}} + \Delta C_{L_s} \tag{14.4}$$

The required C_D needed in order to meet the landing distance requirement is computed by Equation 14.5.

$$s_g = \frac{m}{\rho S(C_{D_l} - \mu_g C_{L_l})} ln[1 + \frac{\rho S(C_{D_l} - \mu_g C_{L_l}) V_{Landing}}{2(\mu_c + k\mu_c)mg}] \tag{14.5}$$

The values used are given in Table 14.7. μ_g and μ_b are the brake and the roll friction coefficient respectively. They are obtained from reference data. k is the break power. In Figure 14.4 the landing distance versus C_{D_l} is plotted. The required landing distance is plotted as well. At the intersection of the lines, the needed value for C_{D_l} is found. When knowing the total C_D value needed during landing, the value of C_D provided by the spoilers, C_{D_s}, can be easily computed.

Table 14.7: Input values of Equation 14.5

m_l [kg]	ρ [kg/m^3]	S [m^2]	μ_g [-]	μ_b [-]	k [-]	$V_{landing}$ [m/s]
15889	1.225	42.9	0.02	0.35	0.7	62.2

$$C_{D_s} = C_{D_l} - C_{D_w} \tag{14.6}$$

The required spoiler surface and required spoiler chord are computed by Equations 14.7 and 14.8.

$$S_s = \frac{C_{D_s} S}{1.9 sin(\delta_s)} \tag{14.7}$$

$$c_s = \frac{S_s}{b_s} \tag{14.8}$$

Finally, the position of the spoilers on the wing span, $\frac{b_{si}}{b}$ needs to be determined. As reference, its common to take as initial value the fuselage width over span ratio $\frac{D_f}{b}$. The final spoiler dimension and properties are presented in Table 14.8.

Table 14.8: Final spoiler values

$\frac{S_s}{S}$ [−]	$\frac{c_s}{c}$ [−]	$\frac{b_s}{b}$ [−]	$\frac{b_{s_i}}{b}$ [−]	C_{D_s} [−]	δ_s [°]
0.097	0.24	0.4	0.14	0.19	85

Ailerons Sizing and Positioning

The lateral control of the aircraft is assured using the ailerons. The rolling moment created by the ailerons depends on the aileron deflection (δ_a), the aileron size and its distance from the fuselage centre line. Out of the four possible options for ailerons (plain, differential, Frise and flaperons [2]), the choice is made to go for differential ailerons. They are effective and cheap to produce and reduce the adverse yaw significantly. Frise type ailerons are more effective against adverse yaw, however they increase the noise, which is why these are eliminated for this design. Since the Mach number at which the aircraft will fly is relatively high, deflecting the ailerons during cruise can cause wing twist, and therefore a higher torsion in the wing box and even

[2] http://www.faa.gov/regulations_policies/handbooks_manuals/aviation/pilot_handbook/media/PHAK20-20Chapter2005.pdf, Cited 10/06/2015

adverse roll. In order to avoid this, either an inboard aileron or spoilers are used. Inboard ailerons are usually placed on wings with a larger span and on a stiff place on the wing (engine pylon). Since this design has a relatively small wing span, fuselage mounted engines, and most importantly uses carbon composites which are stiffer than aluminum, the choice is made to use only outboard ailerons in combination with spoilers.

When sizing the ailerons, two aspects analyzed. Firstly the required surface area of the ailerons should be calculated and secondly it should be checked that the available surface area on the wing is sufficient to reach the required aileron surface area. In order to calculate the required aileron surface area, Equations 14.9 until 14.13 are used, where the input variables are stated in Table 14.9

Table 14.9: Final values for horizontal and vertical tail parameters

Parameter	Unit	Value	Comments
Span (b)	[m]	19.2	From wing geometry
Length (L)	[m]	25.0	From geometry
Maximum Take-off mass (m)	[kg]	17420	From Class II
Reference surface area (S_{ref})	[m^2]	32.0	From planform
R_x	[-]	0.22	From Raymer [20]
R_y	[-]	0.40	From Raymer [20]
R_z	[-]	0.45	From Raymer [20]
Required change in bank angle (θ)	[rad]	0.69	From [50]
Maximum time for change in bank angle (t)	[s]	8	From [50]
Moment arm (d)	[m]	7.44	From geometry based on reference [51]
Cruise speed (V)	[m/s]	241	From performance
Density at cruise altitude (ρ)	[kg/m^3]	0.36	From ISA
Maximum aileron deflection ($\delta_{a_{max}}$)	[°]	30	Assumed from [18]
$C_{l_{\delta_a}}$	[-]	0.0524	From stability and control

$$\theta = \frac{1}{2} \cdot \alpha \cdot t^2 \tag{14.9}$$

$$I_{xx} = \frac{b^2 \cdot M \cdot R_x^2}{4} \tag{14.10}$$

$$\Sigma M = I_{xx} \cdot \alpha = F \cdot d \tag{14.11}$$

$$\Delta C_l = C_{l_{\delta_a}} \cdot \Delta\delta_{a_{max}} \tag{14.12}$$

$$S_a = \frac{F}{0.5 \cdot \rho \cdot V^2 \cdot \Delta C_l} \tag{14.13}$$

Table 14.10: Final values for aileron design requirements

Parameter	Unit	Value	Comments
Mass moment of inertia (I_{xx})	[kg·m^2]	76092	From Eq. 14.10
Angular acceleration (α)	[rad/s^2]	0.0218	From Eq.14.9
Sum of moments (ΣM)	[Nm]	1659	From Eq. 14.11
Change in lift force required (ΔL)	[N]	223	From Eq. 14.13
Available change in lift coefficient (ΔC_l)	[-]	0.0262	From Eq. 14.12
Required aileron surface area per aileron ($S_{a_{req}}$)	[m^2]	0.8140	From Eq. 14.13
Required ratio of aileron surface area to total reference surface area (S_a/S_{ref})	[m^2]	0.0509	-

After determining the surface area required to generate a sufficiently large change in lift, the second step is to look at the geometry of the wing and the positioning of the ailerons. Figure 14.6 shows the geometry of the wing including the final position and size of the aileron.

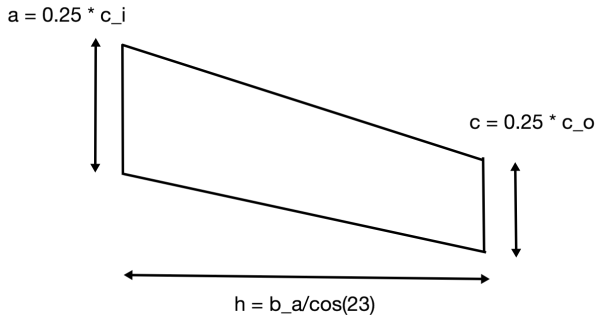

Figure 14.5: Sketch used to calculate the surface area of the aileron, elevator and rudder

From Sadraey [51], certain assumptions are made, which are iterated in order to get the right position and size. Both the initial values and the iterations are seen in Table 14.11. Where the input values as seen in the table are taken from [51] and [52] and the surface area of one aileron is calculated using the sketch in Figure 14.5 and Equation 14.14.

$$S = h \cdot \frac{a + c}{2} \tag{14.14}$$

Table 14.11: Final values for aileron sizing and positioning

Parameter	Initial	Iteration 1	Iteration 2
$\frac{b_i}{b}$	0.65	0.7	0.65
$\frac{b_o}{b}$	0.9	0.95	0.9
$\frac{b_a}{b}$	0.25	0.25	0.25
$\frac{c_a}{c}$	0.2	0.25	0.25
h	2.5	2.4	2.5
a	0.336	0.42	0.41
c	0.296	0.32	0.37
S_a	0.789	1.18	0.975
$\frac{S_a}{S_{ref}}$	0.0367	0.0453	**0.0609**

As can be seen in Table 14.11, the final surface area of one aileron is 0.975 m^2, and the ratio between the total aileron surface and the reference surface area is 0.0609. From [51], this ratio should be between 0.05 and 0.1, and therefore this requirement is met.

14.1.6 Wingtip Devices

At the wingtips, the air is able to flow from underneath the wing to the top of the wing. This airflow that occurs due to the pressure difference causes vortices at the wingtips. These vortexes are highly unfavourable, because they cause a large increase in drag and a local reduction in lift. A way to reduce the vortices at the wingtip is to make use of wingtip devices.

There are many advantages on using wingtip devices. They decrease the induced drag at take-off and cruise. Furthermore, the performance of the aircraft is improved. Less fuel is burned. Also, the aircraft makes less noise during take-off. The drawbacks of using wingtip devices are the increased cost and the increase in profile drag. So, an important aspect for the wingtip devices design, is to achieve a reduction in induced drag while keeping the increase in profile drag, due to the extra wetted surface of the winglets, as low as possible. Furthermore, the added weight needs to be minimum. More weights results in more drag. If a net reduction in total drag cannot be reached, it is useless to install winglets.

Winglet Design

There are many different wing tip devices [2]. For the regional aircraft, blended winglets are chosen. From Withcomb Classic Winglets Design, the winglet should have the following dimensions [53]:

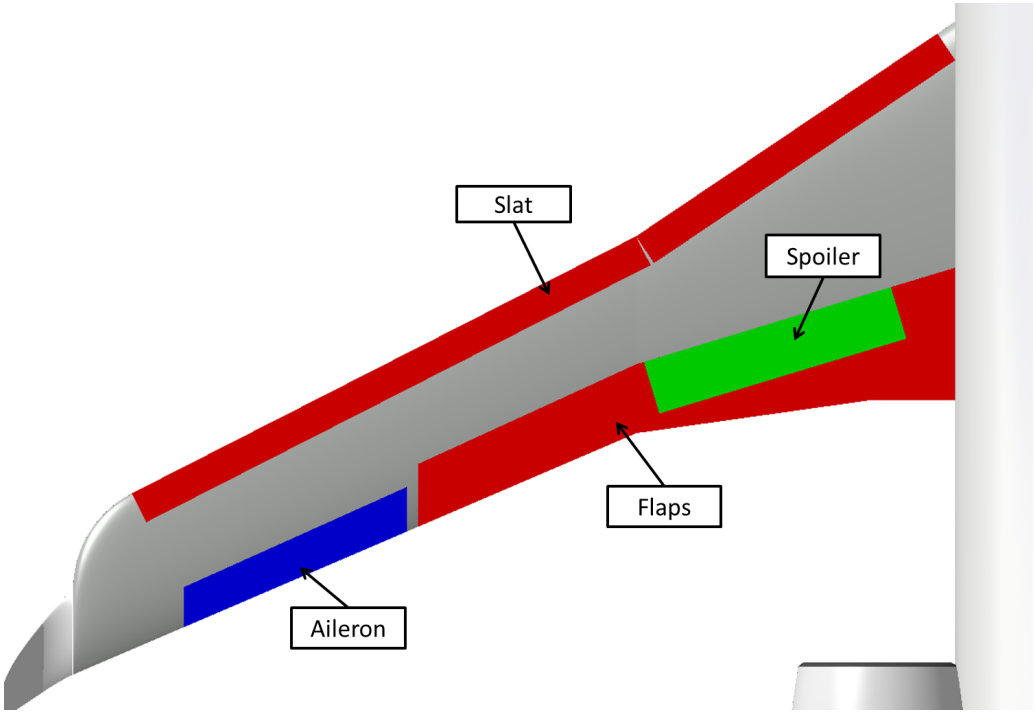

Figure 14.6: Final layout of the wing including ailerons and spoilers

- A height of 0.1-0.2 of the semi-span
- Taper ratio of $\lambda = 0.3$
- A t/c of 0.08 times the wingtip t/c

The winglet should have a large enough radius of inner curve to prevent interference drag. The airfoil used for the winglets is the NACA 0004. Using CATIA, the winglets are designed. Table 14.12 shows the dimensions of the winglet.

Table 14.12: Winglet dimensions

Winglet height [m]	Winglet taper [-]	Winglet thickness [%]
1.5	0.3	4

Effect on Performance

The effect of the winglets on the aircraft performance needs to be analyzed. Adding winglets will increase the weight. Not only because of the extra material used, but also because the structure at the wing tip needs to be enforced in order to carry the winglets. Equation 14.15 shows the calculation of the total drag which consist of the zero lift drag/ profile drag, D_0 and the induced drag, D_i. Increasing the weight will increase the induced drag. Adding winglets will also increase the profile drag because of the extra wetted area.

$$D = D_0 + D_i = C_{D0}\frac{1}{2}\rho V^2 S + \frac{W}{\pi A e \frac{1}{2}\rho V^2 S} \tag{14.15}$$

By adding winglets, the effective aspect ratio is increased. Increasing the aspect ration results in a lower induced drag. If the aspect ratio is increased by 15%, which some blended winglets had proven to do [3], the total drag decreases by 6%. Actual flight tests need to be performed in order to get an accurate value of the decrease in drag.

14.2 Detailed Tail Sizing

After designed the wing and its subsystems, the next step is to design the tail. It was already mentioned that a T-tail configuration will be used. The horizontal and vertical tail sizing will be treated separately in this section, including both the sizing of the actual tail surfaces, together with the design of the control surfaces. Finally, the verification and validation of the control surfaces MATLAB program is performed in Section 14.2.4.

[3] http://cms.education.gov.il/NR/rdonlyres/D9F6FC7B-A508-43C8-BB34-5C6D8AE0346D/178686/Understanding_Winglets_Technology.pdf

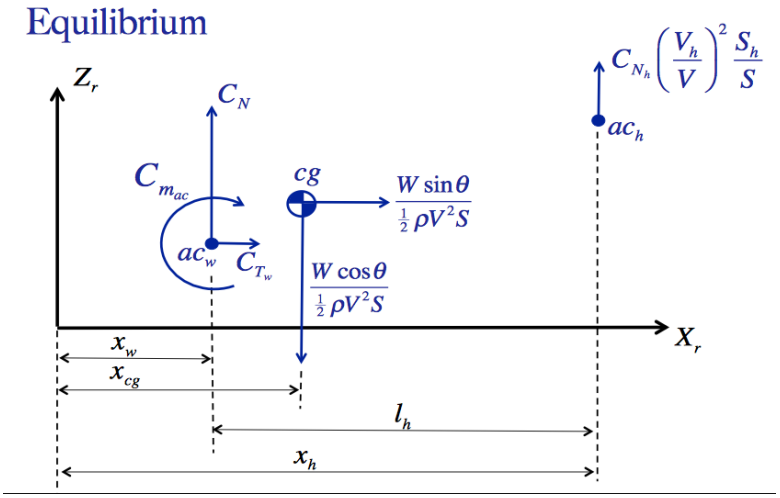

Figure 14.7: Free Body Diagram of the aircraft

14.2.1 Horizontal Tail

When looking at the airfoil of the horizontal tail, the most important aspect is that the main wing should stall before the horizontal tail stalls. The reason for this is that the aircraft should still be controllable after the wing has stalled. In order to achieve this, the thickness of the horizontal tail airfoil should be 1-2% smaller than that of the main wing and the sweep angle should be larger than the sweep angle of the main wing. Moreover, since the center of gravity shifts during the flight, the airfoil sometimes needs to generate positive and sometimes negative lift. Therefore the tailplane should behave similar during both a positive and negative angle of attack. This results in a symmetrical airfoil [51]. The tail should provide stability during the flight. Figure 14.7 shows a free body diagram of the aircraft. The forces that are drawn are made dimensionless. A few assumptions are made. The airfoil to be selected for the horizontal tail is a symmetrical one. Therefore, the tail does not as a moment around its aerodynamic center. For choosing the airfoil, the cruise phase is considered. The desired C_L and C_m values for take-off and landing are created by the control surfaces of the tail. The moment around the center of gravity is computed, using Equation 14.16.

$$C_m = C_{m_{ac}} + C_{N_w}\frac{x_{cg} - x_w}{c} - C_{N_h}\frac{S_h l_h}{Sc} \tag{14.16}$$

During cruise, the moment around the center of gravity needs to be zero, $C_m = 0$. The value of C_L needed in order to keep the aircraft stable can be computed. For small angles of attack, $C_N = C_L$. Equation 14.16 can be rewritten as:

$$C_{L_h} = (C_{m_{ac}} + C_{L_w}\frac{x_{cg} - x_w}{c})\frac{Sc}{S_h l} \tag{14.17}$$

The values used are obtained from the class 2 weight estimation and are presented in Section 7.3. During the flight, the center of gravity position of the aircraft changes. This is due to the fact that fuel is burned. The shift of the center of gravity has an effect on the overall stability of the aircraft. The lift force that the tail needs to provide in order to keep the aircraft stable changes. The tail needs to be trimmed at different C_{L_h} values. For the airfoil selection, it is important to see what the range of C_{L_h} values is that need to be covered during cruise. For the case of the most forward and the case of the most aft center of gravity position, the corresponding C_{L_h} values are computed. As explained before, a thin and symmetrical airfoil is desirable for the horizontal tail. The C_{L_h} range during cruise is used to examine the outcome of Javafoil, while examining symmetrical NACA airfoils, to check if the airfoil has a sufficient critical Mach number in that range such that the airfoil is optimized for cruise. Outside of the cruise range it is assumed that the elevator and trim tab will provide the camber necessary. As mentioned before, the airfoil thickness should be about 1-2% lower than the main wing airfoil thickness. It was therefore chosen to use the NACA 0008 as the horizontal tail profile, as the lower thickness allows for a higher Mach number and thus a smaller sweep angle which is beneficial in structural terms. The airfoil should not be too thin however, because the structure has to be able to carry the loads. Because a symmetrical airfoil is chosen, the critical Mach number of the airfoil is lower than that of the main wing airfoil and thus a higher sweep angle is necessary. It was decided that a sweep angle of 45° will be implemented such that the flow component perpendicular to the airfoil leading edge is M = 0.62. The NACA 0008 airfoil is capable of experiencing this speed without separation between $-2.2° < \alpha < 2.2°$ which is a sufficient range during cruise. Outside of the cruise phase the aircraft will fly slower and the elevator and trim tab are employed and therefore it is assumed that the airfoil will perform as

desired outside of the cruise phase as well, only it is optimized for the cruise phase as that is the largest part of the mission with the highest speed.

Elevator Sizing and Positioning

The longitudinal control of the aircraft is assured using the elevator on the horizontal tail surface. The pitch moment created by the elevator depends on the elevator deflection (δ_e), the elevator size and its distance from the fuselage centre line. In order to determine the size and position of the elevator, the same approach is used as for sizing and positioning the ailerons in Section 14.1.5. When sizing the elevators, again two aspects analyzed. Firstly the required surface area of the elevator should be calculated and secondly it should be checked that the available surface area on the horizontal tail is sufficient to reach the required elevator surface area. The input parameters and there values are shown in Table 14.13 for the Equations 14.18 until 14.21. It has to be noted that in order to size the elevator, the take-off is taken as the most critical phase, since during that phase, the horizontal stabilizer is required to provide enough negative lift to assure a certain rotation angle. From [51] it is taken that the stall speed should be taken as a minimum requirement, since this will increase the required surface area a bit, and therefore incorporates a safety factor.

Table 14.13: Input parameters for the elevator sizing

Parameter	Unit	Value	Comments
Angular acceleration (α)	[rad/s^2]	0.1047	From reference CS-25 [50]
Moment arm (d)	[m]	11.5	From geometry based on reference [51]
Stall speed (V)	[m/s]	61	From performance
Density at take-off (ρ)	[kg/m^3]	1.225	From ISA
Maximum elevator deflection up ($\delta_{e_{max}}$)	[°]	-25	Assumed from [51]
Maximum elevator deflection down ($\delta_{e_{max}}$)	[°]	20	Assumed from [51]
Lift coefficient slope horizontal tail ($C_{l_{\alpha_h}}$)	[1/rad]	3.73	From Class II
Change in horizontal tail angle of attack ($\Delta\alpha_h$)	[rad]	0.17	From [47]
$C_{l_{\delta_e}}$	[-]	0.43	From stability and control

$$I_{yy} = \frac{L^2 \cdot M \cdot R_y^2}{4} \qquad (14.18)$$

$$\Sigma M = I_{yy} \cdot \alpha = F \cdot d \qquad (14.19)$$

$$\Delta C_{l_h} = C_{l_{\alpha_h}} \cdot \Delta\alpha_h + C_{l_{h_{\delta_e}}} \cdot \Delta\delta_{e_{max}} \qquad (14.20)$$

$$S_e = \frac{F}{0.5 \cdot \rho \cdot V^2 \cdot \Delta C_{l_h}} \qquad (14.21)$$

Table 14.14: Final values for elevator design requirements

Parameter	Unit	Value	Comments
Mass moment of inertia (I_{yy})	[kg·m^2]	435500	From Eq. 14.18
Sum of moments (ΣM)	[Nm]	45597	From Eq. 14.19
Change in lift force required by horizontal tail (ΔL)	[N]	3965	From Eq. 14.21
Available change in lift coefficient horizontal tail (ΔC_{l_h})	[-]	1.468	From Eq. 14.20
Required elevator surface area ($S_{e_{req}}$)	[m^2]	1.19	From Eq. 14.21
Required ratio of aileron surface area to total reference surface area (S_e/S_h)	[m^2]	0.14	-

After determining the surface area required to generate a sufficiently large change in lift, the second step is to look at the geometry of the horizontal tail surface and the positioning of the elevator. Figure 14.8 shows the geometry of the horizontal tail including the final position and size of the elevator. The final values are seen in Table 14.15. Where the input values as seen in the table are taken from [51] and [52] and the surface area of half of the elevator is calculated using the sketch in Figure 14.5 and Equation 14.14.

Table 14.15: Final values for elevator sizing and positioning

Parameter	$\frac{b_i}{b}$	$\frac{b_o}{b}$	$\frac{b_e}{b}$	$\frac{c_e}{c}$	h	a	c	S_e total	$\frac{S_e}{S_h}$
Value	0.2	1.0	0.8	0.3	3.019	0.336	0.258	1.79	**0.2147**

As can be seen in Table 14.15, the final surface area of the elevator is 1.79 m^2, and the ratio between the total elevator surface and the horizontal tail surface area is 0.215. From [51] and [52], this ratio should be between 0.15 and 0.4, and therefore this requirement is met.

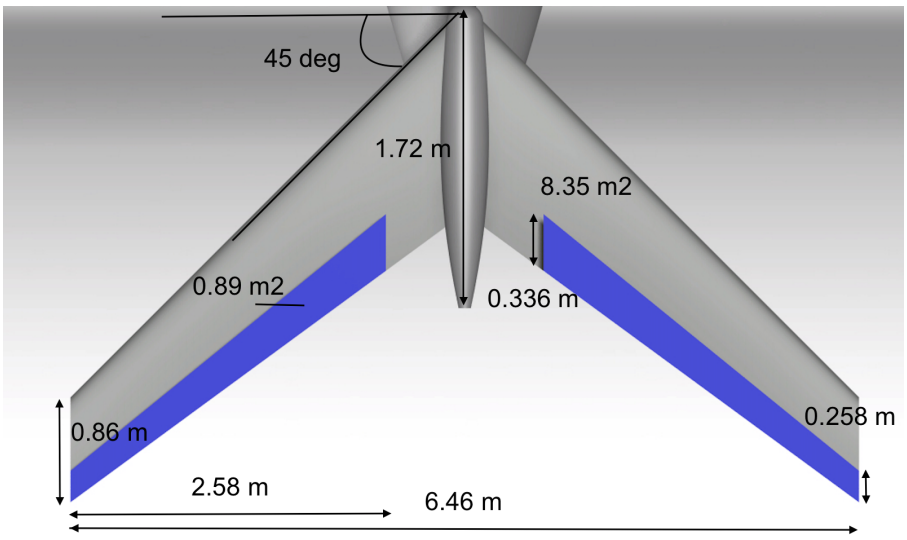

Figure 14.8: Final layout of the horizontal tail including elevator

14.2.2 Vertical Tail

For the airfoil of the vertical tail, the same rules apply as for the horizontal tail. The airfoil should be symmetrical due to the fact that the aircraft should be symmetric about the x-z plane, which also implies that the incidence angle should be zero. Also, the airfoil should be 1-2% thinner than the airfoil of the main wing, since the vertical tail should be cleared from compressibility. Finally, the chosen airfoil should have a high lift curve slope, since this will improve the static directional stability. Therefore a NACA 0008 or NACA 0009 profile will be chosen, where the final thickness depends on the outcome of the structural analysis. A thickness of 8% might be not enough to support the horizontal tail surface and deal with all the loads generated by the horizontal and vertical tail surface. Therefore a thickness of 9% is chosen to be able to carry more loads. A relatively high sweep angle of 40° is chosen [18]. The main reason for this is that a larger sweep angle decreases the wave drag at higher speeds, and the longitudinal stability is increased, since the moment arm for the horizontal tail is larger, therefore a smaller lift force is required to generate the same moment.

Rudder Sizing and Positioning

The directional control of the aircraft is assured using the rudder on the vertical tail surface. The yaw moment created by the rudder depends on the rudder deflection (δ_r), the rudder size and its distance from the fuselage centre line. In order to determine the size and position of the rudder, the same approach is used as for sizing and positioning the ailerons and elevator in Section 14.1.5 and 14.2.1.

Table 14.16: Input parameters for the rudder sizing

Parameter	Unit	Value	Comments
Angular acceleration (α)	[rad/s^2]	0.1047	From reference cs25 [50]
Moment arm (d)	[m]	9.04	From geometry based on reference [51]
Cruise speed (V)	[m/s]	241	From performance
Density at take-off (ρ)	[kg/m^3]	0.36	From ISA
Maximum rudder deflection ($\delta_{r_{max}}$)	[°]	25	Assumed from [51]
$C_{Y_{\delta_r}}$	[-]	0.182	From stability and control

When sizing the rudder, again two aspects analyzed. Firstly the required surface area of the rudder should be calculated and secondly it should be checked that the available surface area on the vertical tail is sufficient to reach the required rudder surface area. The input parameters and there values are shown in Table 14.16 for the Equations 14.22 until 14.25. It has to be noted that in order to size the rudder, the cruise phase is found to be the most critical phase, which is why the rudder is designed under the cruise conditions.

$$I_{zz} = \frac{L^2 \cdot M \cdot R_z^2}{4} \qquad (14.22)$$

$$\Sigma M = I_{yy} \cdot \alpha = F \cdot d \qquad (14.23)$$

$$\Delta C_{Y_r} = C_{Y_{\delta_r}} \cdot \Delta\delta_{r_{max}} \qquad (14.24)$$

$$S_r = \frac{F}{0.5 \cdot \rho \cdot V^2 \cdot \Delta C_{Y_r}} \qquad (14.25)$$

After determining the surface area required to generate a sufficiently large change in lift, the second step is to look at the geometry of the vertical tail surface and the positioning of the rudder. Figure 14.9 shows the

Table 14.17: Final values for rudder design requirements

Parameter	Unit	Value	Comments
Mass moment of inertia (I_{zz})	[kg·m^2]	23952	From Eq. 14.22
Sum of moments (ΣM)	[Nm]	1916	From Eq. 14.23
Change in side force required by vertical tail ΔY	[N]	211	From Eq. 14.25
Available change in side force coefficient vertical tail (ΔC_{Y_r})	[-]	0.0828	From Eq. 14.24
Required rudder surface area ($S_{r_{req}}$)	[m^2]	1.12	From Eq. 14.25
Required ratio of aileron surface area to total reference surface area (S_r/S_v)	[m^2]	0.166	-

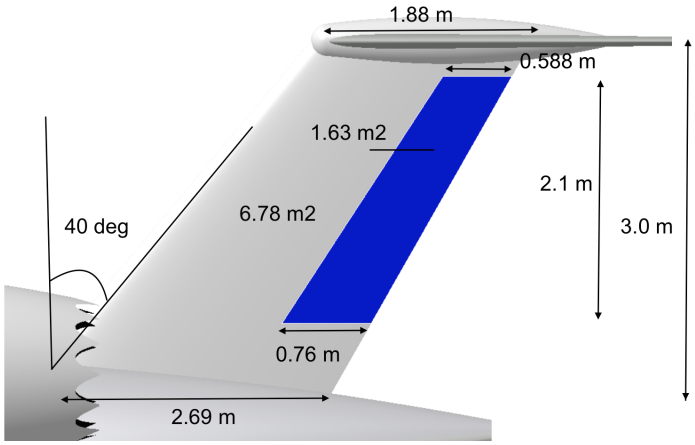

Figure 14.9: Final layout of the vertical tail including rudder

geometry of the vertical tail including the final position and size of the rudder. The final values are seen in Table 14.18. Where the input values as seen in the table are taken from [51] and [52] and the surface area of the rudder is calculated using the sketch in Figure 14.5 and Equation 14.14.

Table 14.18: Final values for rudder sizing and positioning

Parameter	Iteration 1	Iteration 2	Iteration 3
$\frac{b_{upper}}{b}$	0.85	1.00	0.9
$\frac{b_{lower}}{b}$	0.15	0.3	0.2
$\frac{b_r}{b}$	0.7	0.7	0.7
$\frac{c_r}{c}$	0.3	0.3	0.3
h	2.42	2.42	2.42
a	0.771	0.747	0.76
c	0.6	0.565	0.588
S_r total	1.66	1.59	1.63
$\frac{S_r}{S_v}$	0.2452	0.235	**0.241**

As can be seen in Table 14.18, the final surface area of the elevator is 1.63 m^2, and the ratio between the total rudder surface and the vertical tail surface area is 0.241. From [51] and [52], this ratio should be between 0.1 and 0.3, and therefore this requirement is met.

14.2.3 Final Tail Parameters

Table 14.19 shows all the final values of both the horizontal and vertical tail surfaces.

14.2.4 Verification and Validation

For the calculation and iterations of the size and positioning of the control surfaces, a MATLAB program is developed. This program needs to be checked for verification and validation, which is done in this section.

Verification of MATLAB script

In order to check that the MATLAB script is calculating the parameters in the correct way, verification is required. This is done by comparing the outcome of several equations both analytically and numerically, of which the results can be seen in Table 14.20.

Table 14.19: Final values for horizontal and vertical tail parameters

Parameter	Horizontal Tail	Vertical Tail	Comments
l [m]	12.6	10.14	Obtained from Class II
S [m2]	8.35	6.78	Result of iterations
V [-]	1.1	0.8	Calculated, and checked using reference [51] [54]
A [-]	5	1.3	Assumed from reference [18]
b [m]	6.46	3.0	Computed from A and S
Λ_{LE} [°]	45	40	Result of iterations
Λ_{TE} [°]	32	30	From geometry
λ [-]	0.5	0.7	From reference [18]
C_r [m]	1.72	2.69	Computed from b, A, S
C_t [m]	0.86	1.88	Computed from λ and C_r
α [°]	-0.02	0	Computed and assumed
i [°]	-1.0	0	Computed from α and assumed

Table 14.20: Verification results control surfaces

Parameter	Analytical	Numerical	Difference [%]
I_{xx} [kg·m^2]	76092	76092	0.0
I_{yy} [kg·m^2]	355000	355000	0.0
I_{zz} [kg·m^2]	23952	23952	0.0
ΔL [N]	223	223	0.0
ΔL_h [N]	36490	36490	0.0
ΔY [N]	211	211	0.0
S_{areq} [m^2]	0.813	0.814	0.123
S_{ereq} [m^2]	1.189	1.190	0.08
S_{rreq} [m^2]	1.119	1.121	0.178
$(\frac{S_a}{S})_req$ [-]	0.0508	0.0509	0.21
$(\frac{S_e}{S_h})_req$ [-]	0.139	0.14	0.198
$(\frac{S_r}{S_v})_req$ [-]	0.1658	0.166	0.248
$\frac{S_a}{S}$ [-]	0.0609	0.0609	0.0
$\frac{S_e}{S_h}$ [-]	0.2147	0.2147	0.0
$\frac{S_r}{S_v}$ [-]	0.241	0.241	0.0

Validation of MATLAB Script

After verifying the program, the next step is to validate the tool. This is done by comparing some outputs to the same parameters for a reference aircraft. The results can be seen in Table 14.21.

Table 14.21: Validation results control surfaces

Parameter	$\frac{c_a}{c}$ [-]	$\frac{b_i}{b}$ [-]	$\frac{b_o}{b}$ [-]	$\delta_{a_{max}}$ [°]	$\frac{b_e}{b}$ [-]	$\frac{c_e}{c_h}$ [-]	$\frac{S_e}{S_h}$ [-]	$\frac{c_r}{c_v}$ [-]	$\frac{S_r}{S_v}$ [-]	$\delta_{r_{max}}$ [°]
QLEAR Q-50	0.25	0.65	0.9	25	0.8	0.3	0.215	0.3	0.241	25
Cessna Citation III	0.3	0.56	0.89	12.5	1.0	0.37	0.37	0.27	0.26	25

Discrepancies

The differences that can be seen in Table 14.20 can be attributed to round-off errors in the area calculations. These differences accumulate in the required surface area and its ratio with respect to the reference surface area. Since the actual surface area is computed with a different approach and equation, the round-off errors are not accumulated in these values. When looking at the validation of the MATLAB script in Table 14.21, it can be seen that there are quite significant differences between the QLEAR Q-50 and the Cessna Citation III. Most of these changes can be attributed to the fact that the Q-50 is a much newer aircraft. Moreover, the Q-50 is slightly heavier and therefore has larger wings. This is the main reason that the ratios are smaller for the Q-50 compared to the Cessna Citation.

14.3 Landing Gear

First the general functions of the landing gear will be described, followed by the requirements and constraints, and the possible landing gear configurations and their advantages and disadvantages. After this, a trade-off is performed resulting in the final choice for the landing gear configuration. After the configuration is chosen,

the landing gear height, wheel base and track and the loads on each of the gears is computed. Finally a compliance matrix is created to check whether or not the design complies with the requirements. For the design of the landing gear and its systems a process is set-up, which can be seen in Figure 14.10.

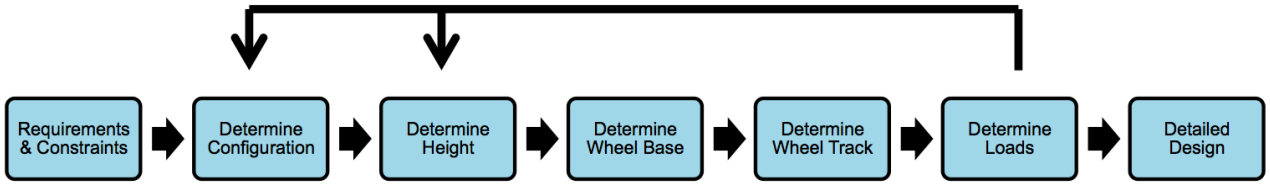

Figure 14.10: Flowchart with different steps in designing the landing gear

14.3.1 Landing Gear Configuration

Different landing gear configurations will be analyzed. The most common options are shown in Figure 14.11 [51].

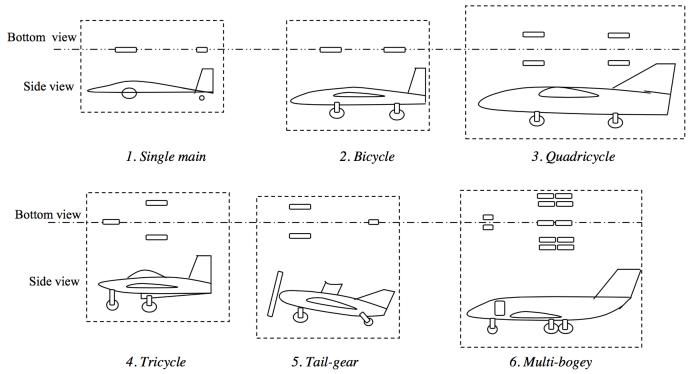

Figure 14.11: Possible landing gear configurations

Since both the *single main* and *bicycle* are configurations that are used only for small aircraft and are inherently unstable, these are eliminated immediately. The final configuration will be chosen by performing a trade-off for the remaining four configurations.
The first step in performing the trade-off is to determine the different criteria that the possible configurations will be graded on, including their weights. The criteria and their corresponding weights are shown in Table 14.22. As a method to determine the weights, the Analytical Hierarchy Process (AHP) [4] is used. The next step is to set up the grading approach. The configurations will be graded from 1 to 4, where 1 is the worst performing and 4 is the best performing. Finally, the grades are multiplied by the weights of each criterion, after which the weighted grades are summed, resulting in the final grade of the configuration. The trade-off matrix can be seen in Table 14.22.

Table 14.22: Trade-off matrix for landing gear configuration

Parameter	Quadricycle	Tricycle	Tail-gear	Multi-bogey
Weight (17.85%)	2	3	3	1
Cost (12.95%)	2	3	3	1
Manoeuvrability (36.69%)	2	4	1	3
Clearance (25.04%)	2	2	1	2
Complexity (7.47%)	2	3	3	1
TOTAL	2.0	**3.1**	1.8	2.0

As can be seen in Table 14.22, the tricycle configuration performs best. The main reason for this is the high performance in manoeuvrability and the relatively low complexity, weight and cost. Furthermore, a retractable landing gear will be used, which reduces overall drag and increases efficiency.

[4] `http://www.es.mdh.se/pdf_publications/1918.pdf`, cited 19/05/2015

14.3.2 Assumptions on Landing Gear Sizing

Table 14.23 summarizes the assumptions that were previously made on the landing gear in Section 7.3.1 where the aircraft c.g. was computed and the loading diagram was constructed. All locations are given with respect to the aircraft nose. Also, other parameters which will be used in this chapter are included in Table 14.23. These values will serve as a starting point for the sizing of the landing gear, and should adjustments be necessary, their impact on all other aircraft systems will be analyzed.

Table 14.23: Assumptions on landing gear sizing

Item	Value
Main landing gear location [m]	13.0
Nose landing gear location [m]	3.4
Most fwd c.g. [m]	12.2
Most aft c.g. [m]	12.7
OEW c.g. [m]	12.5
MTOW c.g. [m]	12.4
Fuselage length [m]	25
Tail cone length [m]	7.4
MTOW [kg]	17425
a/c deceleration [m/s^2]	4.905 [55]
a/c ground speed [m/s]	12.9 [17]
radius of turn [m]	22.86 [17]
Lateral area (A_s) [m^2]	61.85
Density (ρ) [kg/m^3]	1.225
a/c side drag coef. (C_{D_s}) [-]	0.6 [51]
Wind velocity (V_w) [m/s]	20 [56]

14.3.3 Landing Gear Height

The height of the landing gear must ensure that during the take-off rotation (or landing with a high angle of attack), the rear fuselage does not strike the ground. According to CS-25 regulations, the minimum clearance at take-off is 30 cm [50]. This situation is illustrated in Figure 14.12 [51].

The take-off angle α_{TO} was set to 10°, based on the stall angle for the entire wing which was determined in Chapter 9. Analyzing Figure 14.13 [51], the clearance angle α_C, the angle between ground and the line passing from the main gear contact with ground, should be larger than α_{TO}. The clearance angle was set to 14° in the fuselage sizing section (Chapter 14), which is indeed larger than the take-off angle.

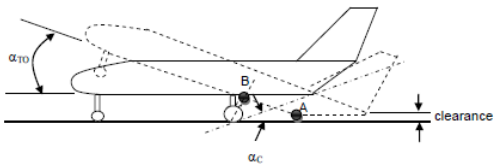

Figure 14.12: Take-off rotation and rear fuselage clearance

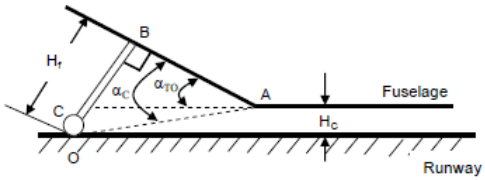

Figure 14.13: Schematic overview of take-off rotation and rear fuselage clearance

Following from trigonometry, the height of the landing gear should be equal to $AB \cdot tan(\alpha_C)$, where AB is the distance between the distance between the main gear and the beginning of the up-sweep angle of the fuselage. Analyzing the fuselage design, AB is equal to 4.1 m. Thus, an initial estimate for the landing gear height is 1.03 m. If at a later stage this value turns up not to meet all the requirements imposed on the landing gear, a small iteration process will be carried out.

14.3.4 Landing Gear Loads

In this section the loads on the landing gears will be determined. This is an essential step such that an appropriate tire can be selected. Furthermore, the load on the nose landing gear has a significant influence on the breaking efficiency and the control and stability of the aircraft during ground operations. In order to size for the most restrictive case, various positions for the center of gravity will be considered. Using the loading diagram shown in Figure 7.4 (explained in Section 14.2) and applying a safety factor of 2% for

in-flight variations [18], the most forward c.g. position is found to be at 12.0 m and the most aft one at 12.9 m with respect to the aircraft nose. Using Figure 14.14 which shows the forces acting on the aircraft and taking the sum of moments around the point where the main landing gear is mounted, one can obtain the load acting on the nose and main landing gears with Equations 14.26 and 14.27. The results are summarized in Table 14.24 and all input values can be determined using Table 14.23. With these values, the wheel base will be determined in Section 14.3.5 and a tire will be selected in Section 14.3.8.

$$F_n = \frac{B_m}{B} W \qquad (14.26)$$

$$F_m = \frac{B_n}{B} W \qquad (14.27)$$

Table 14.24: Landing gear loads

Item	Value [N]	% of MTOW
$F_{n_{min}}$	8496	5.0
F_n	20391	11.9
$F_{n_{max}}$	23790	13.9
$F_{m_{min}}$	147836	86.1
F_m	151235	88.1
$F_{m_{max}}$	163130	95.0

14.3.5 Wheel Base and Wheel Track of the Landing Gear

With the landing gear loads determined, one can estimate the percentage of the MTOW that each gear has to withstand. The results are summarized in Table 14.24

According to Roskam in [55], the load on the nose landing gear should not be lower than 5% of the MTOW. This is required such that the aircraft can be controlled during taxi and ensure that it is sufficiently stable for ground operations. Additionally, the load on the nose gear should not exceed 15% of the MTOW, case in which the brakes would no longer be efficient in bringing the aircraft to a stop. As can be seen from the results in Table 14.24 the position of the landing gears assumed in Table 14.23 yield values within these boundaries. Thus, at this stage no modifications are necessary and the wheel base remains 10.1 m. The next step is to determine the wheel track of the main landing gear, which is the distance between the most left and the most right gears (when looking at the front-view), as seen in Figure 14.15 [51]. In this figure, the overturn angle is represented by ϕ_{ot} and Y_{ot} represents the distance between the center-line and one of the main landing gears. For the determination of the wheel track, two situations will be considered: controllability and stability. However, before moving to the wheel track, the height of the c.g. needs to be estimated, since this values will be used in the following paragraphs.

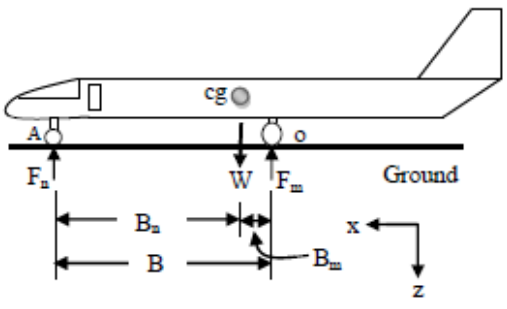

Figure 14.14: Examination of rear fuselage clearance during take-off rotation

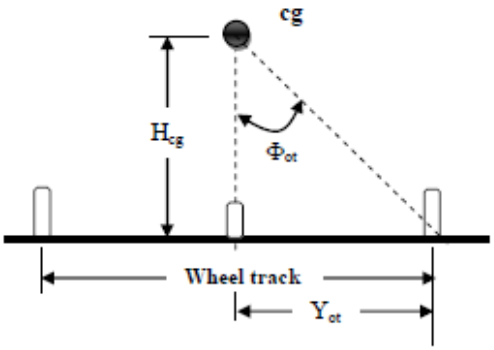

Figure 14.15: Front view of wheel track

Height of the c.g.

The weight of the main aircraft components was estimated in Section 7.3, where the location of the c.g. was determined with respect to the nose. However, for the landing gear sizing, it is also important to know the height of the c.g. A similar approach will be used in this case, the height of the c.g. being calculated with

Equation 14.28. The input values and the final results can be found in Table 14.25. The blueprints of the CRJ-200 [17] and the previously determined landing gear height of 1.03 m were used in order to estimated the height of the components considered for the analysis.

$$H_{cg} = \frac{\Sigma W_i \cdot h_i}{\Sigma W_i} \tag{14.28}$$

Table 14.25: Determination of c.g. height

Item	Weight [kg]	Height [m]
Fuselage	1972	1.32
Wing	730	0.6
Fuel	2665	0.6
Engine + Nacelle	851	2.3
Vertical Tail	110	3.9
Horizontal Tail	194	5.1
c.g. height		1.23

Ground Controllability

The wheel track should be large enough to ensure that the aircraft does not roll over while it performs a ground turn. Thus, the centrifugal force ($F_C = m\frac{V^2}{R}$) plays an important role in this case. According to [51], the minimum wheel track for ground controllability can be computed with Equation 14.29

$$Y_{ot} > \frac{F_C \cdot H_{c.g.}}{MTOW} \tag{14.29}$$

Using the input parameters given in Table 14.23 and the previously determined c.g. height, the minimum wheel track for ground controllability is found to be equal to 0.9 m and the overturn angle 36.6°.

14.3.6 Ground Stability

The wind is one of the atmospheric phenomena that is mostly affecting ground stability, the most noticeable wind on an aircraft being the cross wind. Because it acts perpendicular to the aircraft ground path, it creates a force that generates a moment which could overturn the aircraft. Thus, it is important to find the wheel track distance that prevents the aircraft to roll over when on the ground. According to [51], the minimum wheel track for ground stability can be computed with Equation 14.30, where F_W represents the cross-wind force and is calculated with Equation 14.31. H_C represents the height from the fuselage belly where the wind force acts and was determined to be 1.9 m considering the method explained in [51].

$$Y_{ot} > \frac{F_W \cdot H_C}{MTOW} \tag{14.30}$$

$$F_W = \frac{1}{2}\rho V_W^2 A_s \cdot C_{D_s} \tag{14.31}$$

Using the input parameters given in Table 14.23, the minimum wheel track for ground stability is found to be equal to 0.2 m. Since this value is smaller than that required for controllability, the final wheel track is determined to be 1.1 m, after assuming a 20% safety margin. However, based on the structural sizing of the wing box done in Chapter 11, this value can be increased, if necessary.

14.3.7 Checking for Tip-back

It is not desirable for the aircraft to tip back during any stage of the ground operations. Thus, checking whether tip-back occurs with the design choices made so far for the landing gear is an important step. The tip-back angle is defined as the maximum nose-up attitude with the tail touching the ground and the strut fully extended. Usually $\alpha_{tb} > \alpha_{TO} + 5°$. Using the take-off angle of 10° previously assumed and considering Figure 14.16, Equation 14.32 can be used to determine the minimum distance behind the most aft c.g. for the main landing gear:

$$\Delta x_{c.g.} = (l_f - x_{c.g.aft}) \cdot (1 - cos(\alpha_{tb})) \tag{14.32}$$

Using the input values from Table 14.23 and the previous equation, the main landing gear has to be at least 13.0 m from the aircraft nose, which corresponds to the assumed value in Table 14.23. Therefore, the aircraft will not tip-back in any stage of the group operations for the chosen landing gear positions.

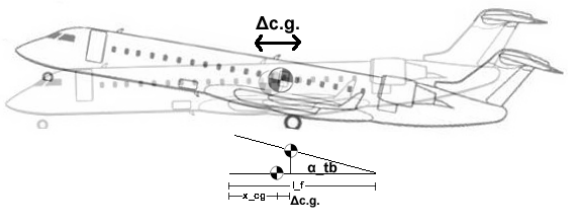

Figure 14.16: Shift in c.g. due to tip-back

14.3.8 Selecting Tire Type and Model

Now that the position of the landing gears meets the stability and controllability requirements, the next step is to choose an appropriate tire. Twin wheels will be used for the nose and each strut of the main gear. Thus, to determine the load on each tire, the loads per landing gear calculated earlier in the chapter need to be divided by two (for the nose gear) and four (for the main gear). According to Roskam a dynamic load needs to be added to the previously calculated load, according to Equation 14.33, where a_x is the deceleration rate of the aircraft and can be assumed to be 0.45g. All other parameters are defined in Figure 14.14 [51].

$$F_{n_{dynamic}} = MTOW \frac{B_M + \frac{a_x}{g} \cdot H_{cg}}{2 \cdot (B_m + B_n)} \tag{14.33}$$

After accounting for the dynamic loading, the final loading on each tire is summarized in Table 14.26. The next step is to determine the maximum tire operating speed. This value is found by assuming the maximum between $1.2 \cdot V_{S_L}$ and $1.1 \cdot V_{S_{TO}}$ [55], where the stall speeds for landing and take-off were established in the mid-term report and are equal to $V_{S_L} = 70$ and $V_{S_{TO}} = 65$ m/s. Thus, each tire should withstand a maximum speed of 84 m/s or 160 mph.

Table 14.26: Estimated tire loads

Item	Load [kg]	Load [lbs]
Main Landing Gear Tire	3854	8497
Nose Landing Gear Tire	1516	3341

With these values, a tire can now be selected. For this, the Goodrich tire catalogue was consulted [5]. Tires from the "rib" category were considered since they can perform in a wide range of operating conditions and are ideal for many runway types which is desirable for a regional aircraft. Table 14.27 illustrates a few available options. For the nose landing gear, the final tire is that corresponding to Option 3. The first and fifth options were excluded because of the high inflation pressure; the second one offered a too low maximum load and the fourth one could not accommodate for the required tire speed. A similar table with various tire options was created for the main landing gear. The final option for the main landing gear tire is shown in Table 14.28.

Table 14.27: Specifications of possible nose landing gear tires

No. [-]	Size [in]	Ply Rating [-]	Load Rating [lbs]	Infl. Pres. [psi]	Spd. Rating [mph]	Outer Diam. [in]	Width [in]	Inner Diam. [in]
1	18 x 4.4	10	3550	185	200	17.9	4.45	10
2	12.5 x 4.5	10	1800	75	120	12.85	4.85	4.5
3	18 x 5.5	10	4000	110	190	17.9	5.7	8
4	20 x 5.5	16	8750	270	185	20.15	5.7	4.25
5	24 x 5.5	12	8070	230	200	24.15	5.7	14

In order to avoid gear induced surface damages, ICAO introduced the LCN (Load Classification Number) for runway classification. Landing gears must be designed in such a way that runway LCN from which the airliner is intended to operate is higher than the design LCN of the landing gear. For a landing gear with multiple wheels per strut, the Equivalent Single Wheel Load (ESWL) is equal to $ESWL = \frac{F_n}{1.33} + \frac{F_m}{1.33}$ [55]. For the previously selected tires, the following ESWL - inflation pressure design point is shown in Figure 14.17 [55]. As can be seen in this figure, this point is within boundaries, which validates the combination of tire and inflation pressure.

[5] http://www.goodyearaviation.com/cfmx/web/aviattiresel/details.cfm?sortorder=70 cited 06-06-2015

Table 14.28: Specifications of selected main landing gear tire

Size [in]	Ply Rating	Load Rating [lbs]	Infl. Pres.[psi]	Spd. Rating [mph]	Outer Diam. [in]	Width [in]	Inner Diam. [in]
24 x 7.7	12	8750	110	200	24.15	7.65	10

14.3.9 Sizing the Shock Absorbers

An oleo-pneumatic shock strut, similar to the one outlined in Figure 14.18 [55], will be used for the landing gears. This shock absorber consists of two components: a compressed gaseous chamber that acts as a spring, absorbing the shock of the aircraft's vertical movement and the damper that acts by forcing hydraulic fluid through small orifices, causing friction and thus, slowing the oil. A telescopic oleo strut arrangement will be used because it saves space. In this case, the shock absorber is housed within the main vertical strut of the landing gear and the wheel deflects in the same line of action as the shock absorber.

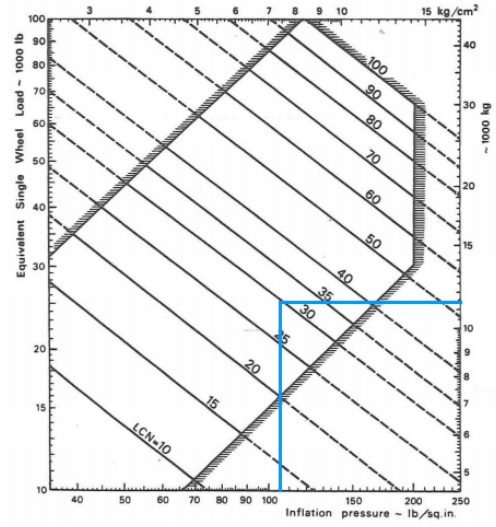

Figure 14.17: Acceptable ESWL - Inflation pressure range

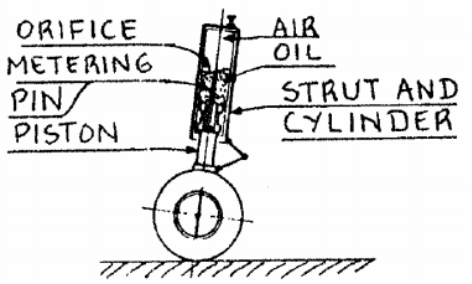

Figure 14.18: Telescopic strut

Using Equation 14.34 from Roskam, an estimate on the length of the shock absorber can be made. In this equation, v_z represents the vertical touch down rate and following from [50] it was fixed at 3.66 m/s. N_g is the landing gear load factor and was taken to be equal to 3 and η_s to 0.8 (shock absorber efficiency) [55].

$$s_{shockabs.} = \frac{v_z^2}{2 \cdot g \cdot N_g \cdot \eta_s} \tag{14.34}$$

With the previously mentioned parameters and Equation 14.34, the shock absorber length is found to be 0.28 m. A final sanity check is carried out by summing the outer diameter of the tire and the shock absorber length. Also a tire clearance of 10% is added (according to [55]). The minimum height of the fuselage from ground is 0.98 m, which is less than the previously assumed value of 1.03 m for take-off clearance, validating the feasibility of the landing gear design.

Aircraft Performance

A driving requirement for the design of the regional airliner is to lower the emissions. If the amount of fuel is reduced, the aircraft weight decreases as well. Less weight means less drag, which results in less fuel needed. When less fuel is burned, less CO_2 and NO_x is emitted. Therefore, the performance is an important aspect to look at. In this chapter, the performance of the aircraft during, climb, cruise and descend will be analyzed and the cruise performance will be optimized. The emphasis will be on the cruise phase, because this flight segment is the most fuel intensive. Furthermore, the performance during take-off and landing are analyzed and it will be checked if the requirement (Appendix D) on the take-off and landing distance are met.

15.1 Cruise Performance

After some iterations the weight and the surface area of the aircraft have changed (Section 6.2), which had an effect on the performance. In this section a brief explanation is given on how the performance during cruise is analyzed and improved. Furthermore, the results of the optimization will be given and the effect on the flight performance will be shown.

15.1.1 Performance Analysis

When considering cruise flight, the forces on the aircraft are assumed to be in equilibrium. Furthermore, it is assumed that the the thrust line acts along the same line as the flight path. The thrust and the drag force act along the same line, but in opposite directions. So, in case of equilibrium: $T = D$. The drag, and therefore the required thrust, can be computed by Equation 15.1 [57]. The input values of these equations can be found in table 15.1. The C_{D_0} is the value computed for the whole aircraft.

$$D = \frac{1}{2}\rho V^2 S C_D \tag{15.1}$$

$$C_D = C_{D_0} + \frac{C_L^2}{\pi A e} \tag{15.2}$$

$$D = C_{D_0}\frac{1}{2}\rho V^2 S + \frac{C_L^2}{\pi A e}\rho V^2 S \tag{15.3}$$

For equilibrium, $L = W$. $C_L = \frac{W}{\frac{1}{2}\rho V^2 S}$ Combining these equations leads to:

$$T = D = C_{D0}\frac{1}{2}\rho V^2 S + \frac{W^2}{\pi A e \frac{1}{2}\rho V^2 S} = D_0 + D_i \tag{15.4}$$

Power required is the thrust required multiplied by the airspeed. The thrust available is determined by the

Table 15.1: Input values for thrust required calculations

C_{D_0} $[-]$	0.015
C_D $[-]$	0.02
ρ $[kg/m^3]$	0.4
A $[-]$	8.5
e $[-]$	0.80
W $[kN]$	162.3
S $[m^2]$	43.0

engines. It is a function of the throttle setting and the altitude. For a turbofan engine, the thrust available can be assumed constant with the airspeed. $P_a = T_a V$. The thrust required and thrust available and the power available and power required are plotted at different airspeeds at the initial cruise altitude of $h =$ 11278 m (Figure 15.1).

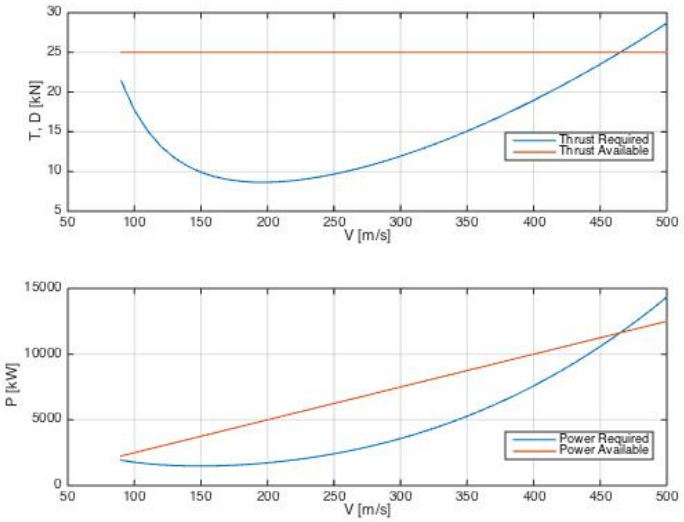

Figure 15.1: Thrust and Power required at $h = 11278$ m

15.1.2 Performance Optimization

In order to fly as efficient as possible, the performance needs to be optimized. The aim is to find the optimum speed to fly at which the least amount of fuel is used for the given range. The fuel consumption per unit time is given by Equation 15.5 as where the fuel consumption itself is given by Equation 15.6 [57]. Where c_T is the specific fuel consumption, which is assumed to be constant. The aircraft range is compute by Equation 15.7

$$F = -\frac{dW}{dt} \quad (15.5) \qquad F = c_T T \quad (15.6) \qquad R = \int_{t_i}^{t_f} V dt = \int_{W_i}^{W_f} -\frac{V}{F} dW = \int_{W_f}^{W_i} \frac{V}{F} dW \quad (15.7)$$

The subscripts i and f refer to "initial" and "final". In this case the initial and final weights of the cruise phase. $\frac{V}{F}$ is the specific range in $[\frac{m}{kg}]$. In order to maximize the range, the specific range needs to be maximized. For the Q-50, it is not of great interest to maximize the range. However, if the specific range is maximized while keeping the range constant, the required fuel in is minimized. The aim is to maximize $\frac{V}{F}$, so: $(\frac{V}{F})_{max} = (\frac{V}{c_T T})_{max} = (\frac{V}{D})_{max} = (\frac{D}{V})_{min}$. The required airspeed in order to fly at minimum $\frac{D}{V}$ is given by Equation 15.8. This airspeed is called the optimum airspeed.

$$V_{opt} = \sqrt{\frac{W}{S}\frac{2}{\rho}\frac{1}{C_{L_{opt}}}}, \quad C_{L_{opt}} = \sqrt{\frac{1}{3}C_{D0}\pi A e} \quad (15.8)$$

Using Equation 15.8 the optimum airspeed is computed. A speed of $V_{opt} = 258$ m/s is found which corresponds to a Mach number of $M = 0.88$. In order to fly at this Mach number, the aircraft should be resized. The structure should be made heavier in order to account for higher loads, and the wings and airfoil need to be reshaped in order to prevent shock wave drag. A better solution is to lower the cruise altitude by 1 kilometer. This results in an optimum airspeed of $V_{opt} = 241$ m/s and a Mach number of $M = 0.81$. Another benefit of flying at this altitude is the fact that the aircraft needs to climb less to its cruise altitude. This saves fuel, costs and lowers the emissions. In Figure 15.2, the performance diagram is given. The dashed black line drawn from the origin, which is tangent to the thrust required curve, is the line for which $\left(\frac{D}{V}\right)$ is minimum. The line touches the curve in one point, which is the point of optimum speed. The final results for the performance parameter are given in Table 15.2.

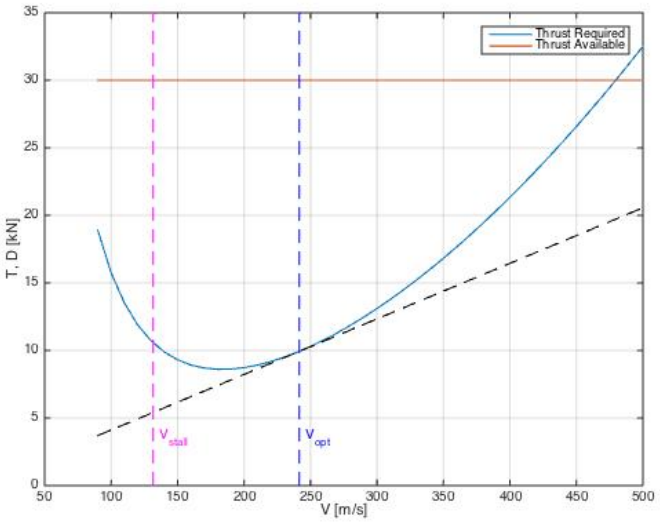

Figure 15.2: Performance diagram at $h = 10278$ m

Table 15.2: Optimized performance parameters

$V_{opt}\ [m/s]$	241.5
$M_{opt}\ [-]$	0.81
$T_r\ [kN]$	10
$P_r\ [MW]$	2398
$(L/D)_{cruise}$	17.3

15.2 Climb and Descent Performance

After analyzing and optimizing the cruise performance, take-off and landing, will be investigated. Optimization of both phases goes beyond the scope of this project. First the climbing phase need to be considered. The rate of climb, RC, is the vertical speed the aircraft has during climb and can be computed by Equation 15.9.

$$RC = \frac{P_a - P_r}{W} \tag{15.9}$$

As can be seen from Equation 15.9, the rate of climb is determined by the difference between power available, P_a and Power required, P_r. This is called the excess power. The higher the excess power, the higher the rate of climb. It is desired to have a high rate of climb in order to reduce the time to reach cruise altitude. The optimum rate of climb is reached at the airspeed where the excess power is the largest. Both power available and power required are dependent on the altitude. Therefore, the rate of climb changes during the climb. Furthermore, the weight changes during climb due to the fuel consumption, which will influence the rate of climb. When analyzing the climb, a few assumptions are made:

- The pilot performs the climb at constant indicated airspeed. The indicated airspeed is almost the same as the equivalent airspeed. However, the equivalent airspeed is not the true airspeed. The true airspeed is increasing when increasing in altitude, so the climb is unsteady.
- The climb is performed at constant throttle setting.
- The climb is a quasi-rectilinear, $\frac{d\gamma}{dV} \approx 0$
- Air Traffic Control rules and commands during climb are not taken into account.

The time to climb is computed using the energy height concept. The energy height is computed by Equation 15.10.

$$H_e = H + \frac{V^2}{2g} \tag{15.10}$$

The time to climb than can be calculated by Equation 15.11.

$$t = \int_{H_e1}^{H_e2} \frac{dH_e}{RC} \tag{15.11}$$

Ideally, it would be desired to take small step in energy height and for each height look at the most optimum rate of climb. For this analysis the height is divided in ten equal parts of 1000 m each. The airspeed at liftoff is taken as $V_{LOF} = 74$ m/s and is assumed to increase linearly to $V_{cruise} = 241$ m/s at cruise altitude. The

weight decreases linearly as well. The power available is assumed to decrease linearly from $Ta = 55$ kN at take off to $Ta = 30$ kN at cruise altitude. The thrust or power required is computed at all the ten parts. For every part the energy height is computed. Using Equation 15.11 the time to climb between two energy heights is computed. The times are summed and the final time to climb is obtained (Table 15.3). The climb angle can be computed by Equation 15.12. The average thrust available and thrust required during the climb are taken. A high climb angle results in less aircraft noise perceived on the ground.

$$sin\gamma = \frac{T_a - T_r}{W} \tag{15.12}$$

The descent phase takes place in steps. The ATC gives clearance to the pilots in order to descent to a lower flight level. For this analysis, a continuous descent is assumed. For commercial aircraft, an angle of descent of 3° is used. This corresponds to a slope of 5%. During the descent the aircraft speed is assumed to decrease gradually form, V_{cruise} to an approach speed of, $V_{app} = 70.7$ m/s. The rate of descent, ROD will be $ROD = 5\% \cdot 0.5(V_{cruise} + V_{app}) = 7.8$ m/s. The aircraft needs to descent from 10278 m to an altitude around sea level. With this rate of descent it takes the aircraft 21 minutes.

Table 15.3: Climb and descent performance

γ_{climb} [°]	11
ROC [m/s]	30
Climb Gradient [%]	19
Time to climb [minutes]	7.3
$\gamma_{descent}$ [°]	3
time to descent [minutes]	21

15.3 Take-off Performance

The performance during take-off is investigated. It needs to be checked if the take-off field length requirement is met (Appendix D). The take-off manoeuvre consist of two parts: the ground part and the airborne part. These two parts are analyzed separately.
As can be seen in Figure 15.3 [58], certain speeds are defined during take-off. Some of these speeds are specified by the FAR 25 regulations. The speeds indicate the following.

- V_1, the decision speed. In case of an engine failure, the pilot takes this speed as a reference. If the aircraft its speed is lower than V_1, the pilot stops the take off by hitting the brakes. In case of a higher speed than V_1, the pilot continuous the take off.
- V_R, the rotation speed. At this speed the pilot initiates upward rotation of the airplane.
- V_{LOF}, the liftoff speed. This speed should be 10% above the stall speed, V_{stall}
- V_2, safety speed. This is the speed to maintain in case of an engine failure at screen height, h_s. This speed should be 20% higher than V_{stall} The screen height is the minimum vertical distance that should be cleared at the end of the runaway.

The ground run is consist of the pre-rotation phase and the rotation phase. During this phase the aircraft accelerates from standstill to the rotation speed ,V_R at which the pilot initiates upward rotation of the airplane, and from V_R to the liftoff speed, V_{LOF}. To compute the distance covered during the ground run, Equation 15.13 is used.

$$s_{ground} = \frac{W_{to}V_{LOF}^2}{2g(T - D - D_g)}, \quad D_g = D_{gm} + D_{gn} = \mu_r(N_m + N_n) \tag{15.13}$$

In Equation 15.13, D_g is the drag acting on the aircraft's tires. For a concrete or asphalted runway, $\mu_r = 0.02$ is taken. The liftoff speed, V_{LOF} is taken as $1.15V_{stall}$. The thrust required during take-off is known and the drag can be easily computed.
The airborne distance is the distance covered from the moment the V_{LOF} is reached, till the airplane flies at the screen height, h_{scr}. The screen height is the minimum height of an obstacle at the end of the runway, which is $h_{scr} = 15.2$ m

$$s_a = \frac{\frac{1}{2g}V_{scr}^2 - \frac{1}{2g}V_{LOF}^2 + h_{scr}}{sin\gamma_s} \tag{15.14}$$

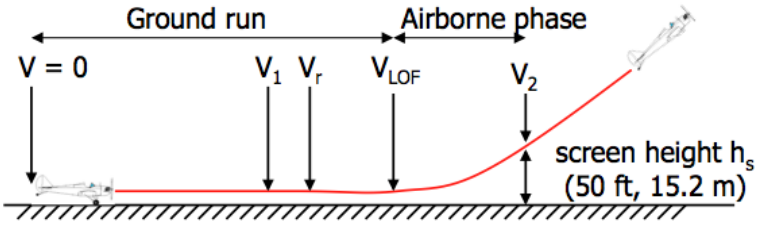

Figure 15.3: Take-off manoeuvre

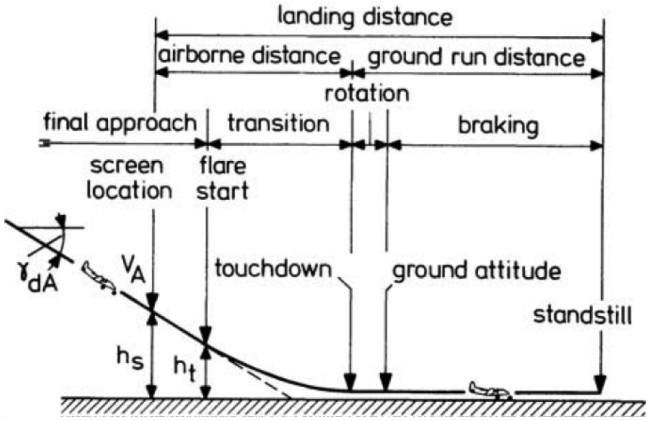

Figure 15.4: Landing manoeuvre

In Table 15.5, the results are shown. At take-off, $(L/D) = 14$.

Table 15.4: Speeds during take off manoeuvre in m/s

V_{stall}	62
V_R	68
V_{LOF}	71.2
V_2	74.2

Table 15.5: Take-off distances

$s_{ground-run}$ $[m]$	1119
$s_{airborne}$ $[m]$	152
$s_{take-off}$ $[m]$	**1271**

15.4 Landing Performance

The distance an aircraft needs in order to land is important to know for the operator. Similar to the take-off distance, the landing distance consists of two parts: the airborne part and the ground run. Both parts will be analyzed. It will be checked if the landing requirement will be met. In Figure 15.4 [57], the landing maneuver is shown. Some important parameters for these maneuver are defined:

- V_A, the approach speed. This speed is generally 1.3 times the minimum stall speed, V_{stall_l} during landing.
- V_T, touch down speed. The touchdown speed is 1.15 times V_{stall_l}.
- γ_{dA}, the slope of the descent path. This angle is about 3°.

In Table 15.6 the values of the landing speeds are shown.
The airborne distance is the length between the screen location and the point of touchdown. The aircraft should be able to fly at V_A over a 15 m obstacle at the runway threshold. The airborne distance can be computed by Equation 15.15.

$$s_a = \frac{\frac{V_A^2}{2g} - \frac{V_T^2}{2g} + h_{scr}}{\frac{1}{2}[sin\gamma_{dA} + [\frac{C_D}{C_L}]_T]} \tag{15.15}$$

The ground run is the distance from touchdown till full stop. The ground run was determined when sizing the spoilers, see Section 14.1.5. The spoilers were sized in order to be able to land within a distance of 400 meters.The landing distance is the airborne distance and ground run: $s_{landing} = s_a + s_g$. The required field length is the landing distance multiplied by a safety factor of $10/6$. Furthermore, for a wet runway the

required landing distance needs to multiplied by a factor of 1.15 also [1]. In Table 15.7 the landing distances are presented. At landing, $(L/D) = 8.12$.

Table 15.6: Landing speeds in m/s

V_{stall}	54.4
V_A	70.7
V_T	62.6

Table 15.7: Landing distances in meters

$s_{airborne}$	360
s_{ground}	400
$s_{landing}$	760
$s_{required}$ dry runway	1267
$s_{required}$ wet runway	1456

15.5 Verification and Validation

The performance is analyzed and optimized using a MATLAB script. The calculations in MATLAB were verified by hand. Furthermore, it was checked if certain changes in some parameters resulted in the effect which was expected from theory. For example, by increasing the weight, the thrust required should increase [57]. This can be seen from the performance diagram in Figure 15.5. Increasing the aspect ratio would also result in lower thrust required (Figure 15.6). The results are validated by looking at figures of different

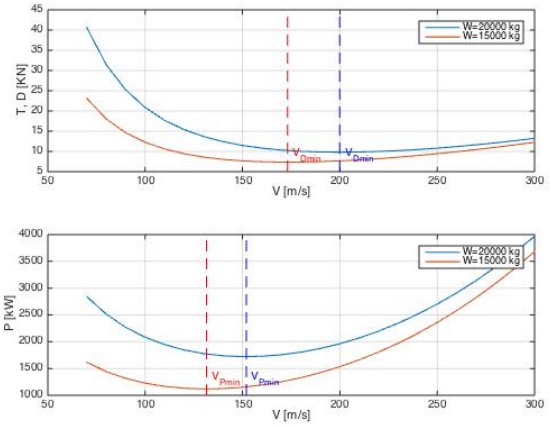

Figure 15.5: Performance diagram for two different take off weights

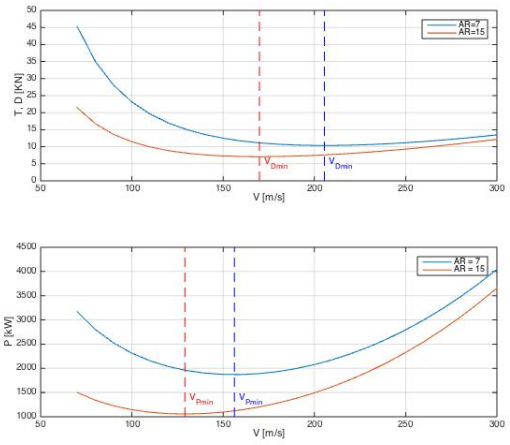

Figure 15.6: Performance diagram for two different aspect ratios

aircraft. What is noticeable is the short time to climb of the aircraft, when comparing it to other planes. A few reasons for this difference are given. First of all, the computation of the time to climb is simplified. Turns during climb and ATC commands and regulations are not taken into account. Secondly, the aircraft is 20% lighter compared to the current flying planes. This results in less power required. However, the engines deliver an amount of thrust which is comparable to other aircraft as the CRJ-200 and the ERJ-145. Therefore, the aircraft has a bigger excess power, so a higher rate of climb and therefore a shorter time to climb.

15.6 Conclusion

In order to reduce the emissions, performance is an important aspect to look at. To use as minimum fuel as possible during cruise, the aircraft should fly at $M = 0.81$ at an altitude of $h = 10278$ m. The aircraft is able to take off at a distance of 1271 m. Therefore, it meets the take-off requirement. The maximum landing distance needed is 1456 m. Therefore, it meets the requirement of a maximum landing distance of 1500 meters. It is recommended to investigate the use of speed breakers. Thrust reversers is also an option, but does at significant weight to the engines. The performance optimization during cruise can be done more detailed in the future, if the change in aircraft weight during this flight phase is taken into account. The performance during climb and descent should also be optimized in order to fly as efficient as possible.

[1] http://flightsafety.org/files/alar_bn8-3-distances.pdf

Aircraft Subsystems

Now that all main systems of the aircraft have been designed, sized and positioned, the next step is to go into slightly more detail by designing some subsystems. The most important subsystems are treated in this chapter. Starting with the fuel system in Section 16.1 and the hydraulics in Section 16.2. This is followed by the communication in Section 16.3, navigation in Section 16.4 and the cockpit systems in Section 16.5. Finally, the electrical system, including a power budget estimate is part of Section 16.6.

16.1 Fuel System

The fuel system of an aircraft is one of the most important subsystems. A proper fuel systems will provide fuel to the designated places in the aircraft, such as the engines and the APU. Furthermore, the aircraft should be able to re- and defuel in an easy and fast manner. Fuel should be transported in between tanks to enhance stability. Also, in case of emergency, the fuel should be dumped in a fast and safe manner. Sensors should give the right indications for the crew, and on their turn, valves and other control actuators should be easily controllable from the flight-deck. Lastly, the structure should withstand all the loads and vibrations which can occur during flight. The structure should be damage and fire proof. Redundancy should be kept in mind for all the above mentioned tasks.

16.1.1 Components

A fuel system can be divided into five main fuel subsystems, namely; storage, vent, distribution, feed and indicating. The main components of a fuel system are; fuel tanks, fuel lines, fittings, pipes, tubes, pumps, valves, vents, strainers, filters, fuel in- and outlets, a drain and several gauges.

Fuel Pumps

Two main different sorts of pumps are known in the fuel system of an aircraft, namely transfer and booster pumps [59]. The pumps should be able to provide fuel at any condition during flight. Booster pumps are used to feed the engines. A schematic layout can be seen in Figure 16.1 [59]. Booster pumps, however, do need feed the engines directly. Booster pumps should be able to provide the entire fuel flow rate that can be requested by the engine with the right inlet pressure. Then are so-called displacement pumps, which feed the engines [59].

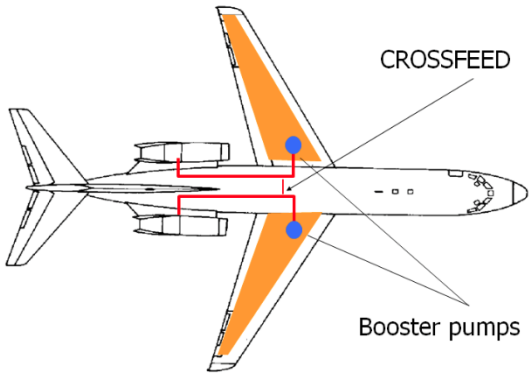

Figure 16.1: Crossfeed lines and booster pumps

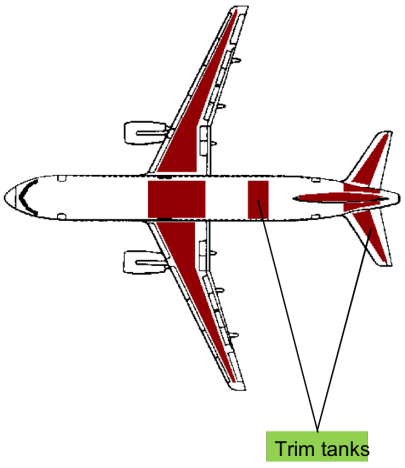

Figure 16.2: Example of trim tanks

Transfer pumps are used to transfer fuel from one tank to another. The transfer of fuel is mainly done to control the balance of the aircraft. Since the fuel is a significant weight, the alteration of it can drastically change the center of gravity. The pilot should be able to balance fuel load to reduce the banking moment by feeding the engine(s) from different fuel tanks. To balance the aircraft in a longitudinal way, sometimes trim tanks are installed in the tail section. A schematic view of trim tanks can be seen in Figure 16.2 [59]. The system should be able to jettison a large quantity of the fuel in case of an emergency.

In addition to the fuel pumps: pressurization and venting systems are installed to guarantee fuel flow at any flight condition and temperature. Vapour lock in hot weather conditions should be prevented, so that

the fuel pump operation is not disrupted and fuel injection system can work normally. In the final layout, as can be seen in Figure 16.4, both booster (red) and transfer (green/blue) pumps are used.

Fuel Lines

Fuel lines are used to basically transport the fuel from the tanks to each other and to the engines. They need to be able to withstand loads caused by manoeuvres and such and withstand the fuel pressure, so firm tubes and pipes are necessary. In Figure 16.4, the different fuel lines can be seen.

Fuel Valves

There are many kind of valves in a fuel system. Most of them can be divided into four categories, namely, hand-operated valves, manually-operated valves, motor- operated valves and solenoid-operated valves [60, 61].

For the hand-operated valves, there are cone valves and popper valves. They both are used as fuel selector valves which enable fuel to flow from a selected source to the engine. Sometimes, a gate valve, which is normally motor operated as an shutoff valve, is used as a hand-operated valve. An example is for instance the fire control valve which shuts off the fuel flow when the emergency fire handle is pulled without using electrical power.

Valves that can control the fuel flow by an off and on switch are manually-operated gate valves. Gate valves have a sealed gate that slides into the path of fuel blocking the fuel flow. To prevent a temperature increase caused by the pressure build-up when the gate is closed, a thermal relief bypass valve is used.

Motor-operated valves are used in larger aircraft. These types of valves are driven by electrical motors. The two most common are the gate valve and the plug-type valve. The plug-type valve consists of a plug or drum that is rotated to close or open.

Other valves are driven by electric solenoids, for instance the poppet-type valve that can be opened by an magnetic pull developed when an opening solenoid is energized. Solenoid-operated valves can open and close very quickly. All valves will be used on the final fuel system, as can be seen in Figure 16.4. The different valves are installed on different places. For example, the hand-operated valves are placed on the bottom of the wing to be able to manually refuel the aircraft.

Fuel Tanks

There are three types of fuel tanks, namely; rigid removable external, flexible bladder and integral fuel tanks.

To ensure the safety of the crew and the passengers, fuel tanks must be isolated by a fume- and fuel-proof surrounding that is vented and drained to the exterior of the aircraft. The fuel tank should be able to withstand the vibration, inertia, fluid and structural loads that may occur during operation. The fuel tank should be protected against impacts such as birds. Also, the crash worthiness of tanks and pipes should be ensured by the structure, to reduce the risk of leakage during impacts (armours and self-sealing tanks). To further reduce the fatality rate during accidents, modification of the chemical properties of fuels is done, to reduce the risk of ignition outside the combustion chamber (e.g. inert gas and inert foam-filled tanks). Some tanks are equipped with multiple layers of rubber, for example one vulcanized and one untreated rubber layer [59] When those type of tanks get punctured, the fuel in the tank will cause a swelling in inner layer which absorbs the fuel and expands. This swelling then seals the hole in the 'self-sealing tank'. Other self-sealing tanks have some type of sealant between two layers of material which remains dormant until the tank gets punctured, then it fills the hole, hardens and seals the tank. The open cell foam of an inert foam filled tank divides the gas space above the remaining fuel into thousands of small spaces, none of which contain sufficient vapour to support combustion. Furthermore, a firewall must be installed between the fuel tank and the engine(s) and some distance must remain between the wall and the tank in the case of wing-mounted engines. Fuel tanks must also be protected against direct lightning strikes, swept lightning strokes, and more electric discharges.

Most fuel tanks contain anti-slosh baffles to stop the fuel from shifting (sloshing) during manoeuvres. Sloshing can cause fluctuations of the centre of gravity and errors in quantity measurement. To avoid the fuel from transferring from the root to the tip of the wing during a manoeuvre, some ribs are used as separations creating multiple smaller fuel tanks. The rib lightening holes are closed with flap check valves or baffle check valves which only allow fuel to move to the inboard sections of the tank ensuring that the booster pumps located at the bottom of the tank, just above the sumps, always have fuel to pump. (A sump is a low area in a fuel tank equipped with a drain valve to remove impurities such as contaminants and water.) Multiple fuel tanks are bring several advantages, because the fuel can be transferred and so distributed over the tanks. This can be used to balance, pitch, roll and trim the aircraft as mentioned earlier, but also for instance to generate a bending relief by transferring the fuel to the tip during cruise.

There must also be a fuel strainer for the fuel tank outlet (or for the booster pump) to stop an object and prevent it from damaging the fuel system. In addition to the strainer(s) a filter is used near the fuel tank outlet to ensure that the fuel system is not affected when fuel is contaminated.

Gauges and Measuring

The fuel level must be measured accurately also the density is measured to calculate the quantity of fuel left. To be able to measure fuel levels during different loads, at different locations on the tanks, sensors should be placed.
Water condensation even as the fuel itself solidifying at low temperatures should be avoided. Therefore proper thermometers and vapor gauges should be installed to measure temperature and fuel pressure.
The pilots need to be able to see all fuel parameters in the cockpit on their instrument panel. They should be able to control all valves via control actuators.

16.1.2 Fuel Tank Volume Estimation

The fuel tank can be sized since the wing planform is known. It is determined that the front spar is located at 25% of the chord as where the back spar is located at 65%. This is visualised in Figure 16.3 [59]. On the left, a part of the wing is shown with the spars and on the right a more detailed sketch is shown with dimension parameters. The tanks extend till about 85% of the wing span, being the tip area at higher risk of (lightening) strikes [59].

Figure 16.3: Fuel tank estimation

By using Equation 16.1, the fuel tank volume can be estimated. The area's (S) can be determined by Equation 16.2. In the case of the 07-411 airfoil, it was chosen that the box is going to be a squared box for an easier structural approach, hence h_1 and h_2 will be the same.

$$V = \frac{L}{3}\left(S_1 + S_2 + \sqrt{S_1 S_2}\right) \tag{16.1}$$

$$S_i = \frac{1}{2}\left(h_{i_1} + h_{i_2}\right) w_i \tag{16.2}$$

The calculated tank volume turned out to be: **4133 l**. The structural elements of the fuel tank will take in some space. Because of that, a correction factor of 96% is applied to the calculated volume. Furthermore, the opportunity for the fuel to expand should be available, hence another correction factor of 95% is applied to account for this. After the two correction factors, the available volume for the fuel is: **3762 l**. As can be seen in Section 7.3, the required fuel weight is 2670 kg. Assuming a density of 0.81 kg/m^3 [59], the required tank volume is 3407 l. This means that the available tank volume will be sufficient for the required amount of fuel.

Fuel System Layout

The schematic view of the fuel system can be seen in Figure 16.4. The red lines indicate booster lines. The blue lines, fueling lines. The green lines, represent crossfeed lines and finally the orange ones, show the reserve fuel lines.

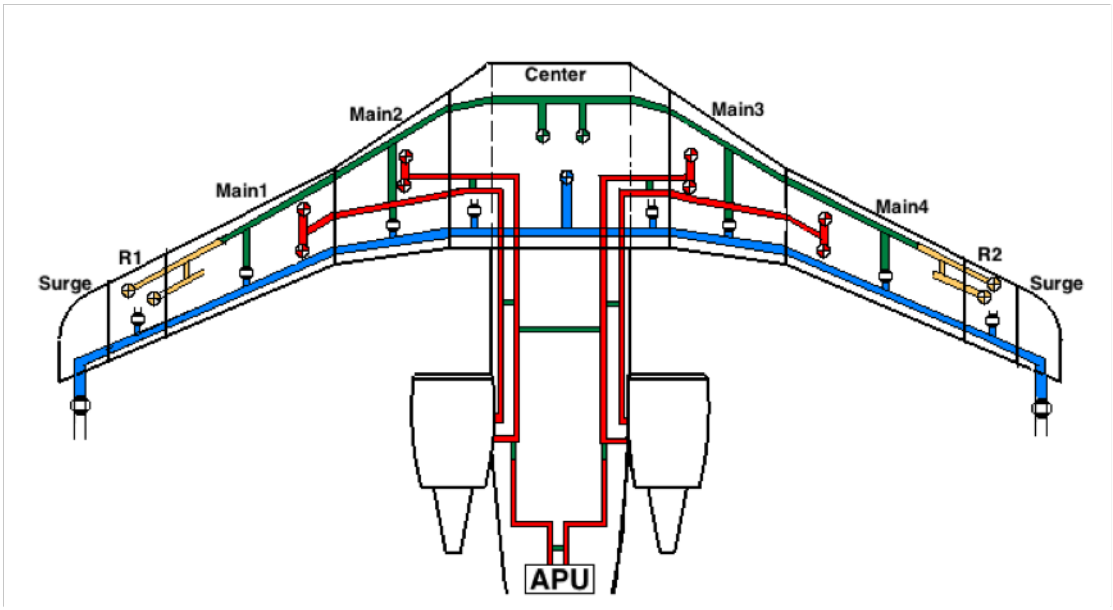

Figure 16.4: The layout of the fuel system

As can be seen in the figure, the fuel system is very redundant. This is necessary to ensure fuel flow at any instant. If one line or pump fails, other pumps can still transfer the fuel via different lines to the designated place.

16.2 Hydraulics

The hydraulic system is used for the control surfaces, landing gear retraction mechanisms, and utilities such as doors, brakes and steering. The power for the hydraulics often comes from the engine or the auxiliary power unit. This chapter will describe the hydraulic system sizing for the control actuation and landing gear. As well as the energy source and required parts for the actuation.

16.2.1 Control Actuation

In this section an actuation system for the control system will be selected. First a brief overview is given of the possible actuation systems. After this the selected actuation system is presented in the text together with the decisions which lead to that system.

16.2.2 Types of Actuation systems

There are several actuation systems available. This section will only look at viable option for this aircraft. There are 3 main types of actuators used for the ailerons:

- Hydraulic
- Electric mechanical
- Electrohydrostatic Actuation

Hydraulic System & Electromechanical

For hydraulic actuation there are several options. An example for a mechanical and hydraulic combination can be seen in Figure 16.5 [62]. As the pilot feeds a mechanical input to the flight control actuator, the summing link will rotate about the bottom pivot, applying an input to the servo valve [62].

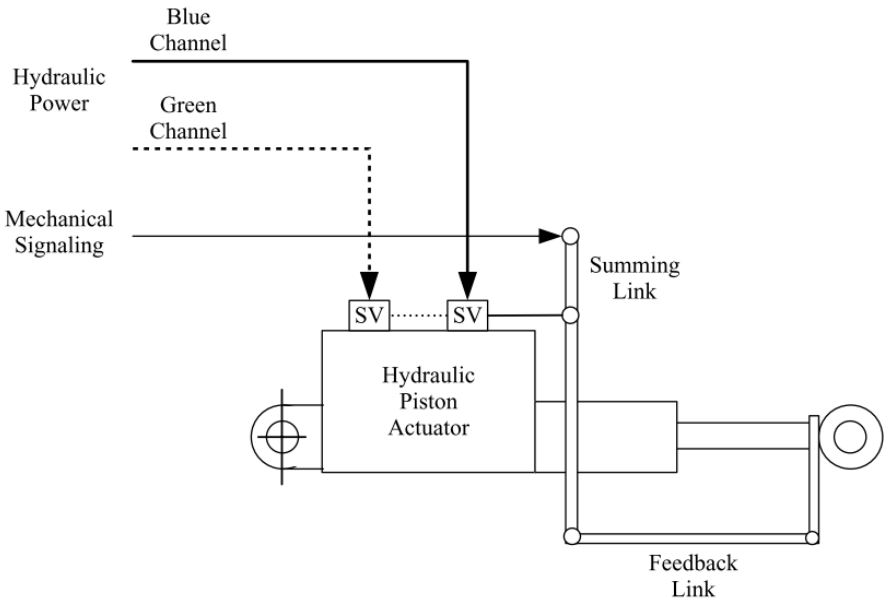

Figure 16.5: Conventional linear actuator

Although this system is very straightforward it requires very high pressures in the hydraulic actuator. For example a mechanical actuator used in the BAE 146 needs a pressure of $20.7\frac{MN}{m^2}$ or $207bar$ [62]. This requires very strong pumps and constructions for the actuator which makes them heavy. Furthermore it needs links from the input to the servos, which is extra weight.

An electromechanical actuation uses mechanical gearing to couple an electric motor to a flight control surface, such as an aileron. It does so by using a rotary gearbox, and depending on the output movement it can include a rotary-to-linear conversion gearbox. The EMA is susceptible to certain single-point failures that can lead to a mechanical jam. This is not desirable for reliability and it can lead to a problem in certification on certain control surfaces. [63, 64] Furthermore gearboxes to convert the electric motor motion to control surface motion are heavy.

Electro-Hydrostatic Actuation (EHA)

Unlike the EMA, the EHA uses a hydraulic system with electrical motor input to move the control surface. The hydraulic fluid provides a medium of transmitting the power from the motor to the actuator. The major advantage of such a method is that the actuator can be managed like a conventional hydraulic actuator. Therefore already existing semi-hydraulic systems can be easily altered to this system. And since it look so much like old systems which proven reliability the EHA system can be used for primary flight control surfaces. Another advantage is the fact that the EHA system unlike traditional hydraulic actuator systems doesn't have the inconvenience of hydraulic disconnection from aircraft supplies and the complications of bleeding the system during re-installation or maintenance [63, 64]. The electric motor control can also be easily incorporated with the fly by wire system.

16.2.3 Choice of Actuation System

For the final design an electro-hydrostatic system is chosen. Currently the system is in early stages of development, however since the aircraft is set for entry in 2035 the technology will have matured. The reason for the electro-hydrostatic systems is its benefits over traditional hydraulic systems. The EHA acts as a load path for an electric motor. This removes the need for high pressure pumps and tubing, reducing weight and the complexity of the design. The electrical power can be bundled together with the fly-by-wire cables, meaning redundancy can be easily achieved by have two sets of wires. It is also more energy-efficient over the duration of a flight in relation to hydraulic systems [65]. Because electric power is used to power the actuators no engine bleed is required. And the system can be fully operated on its own, so in case of engine failure the actuators have a separate system. Figure 16.6

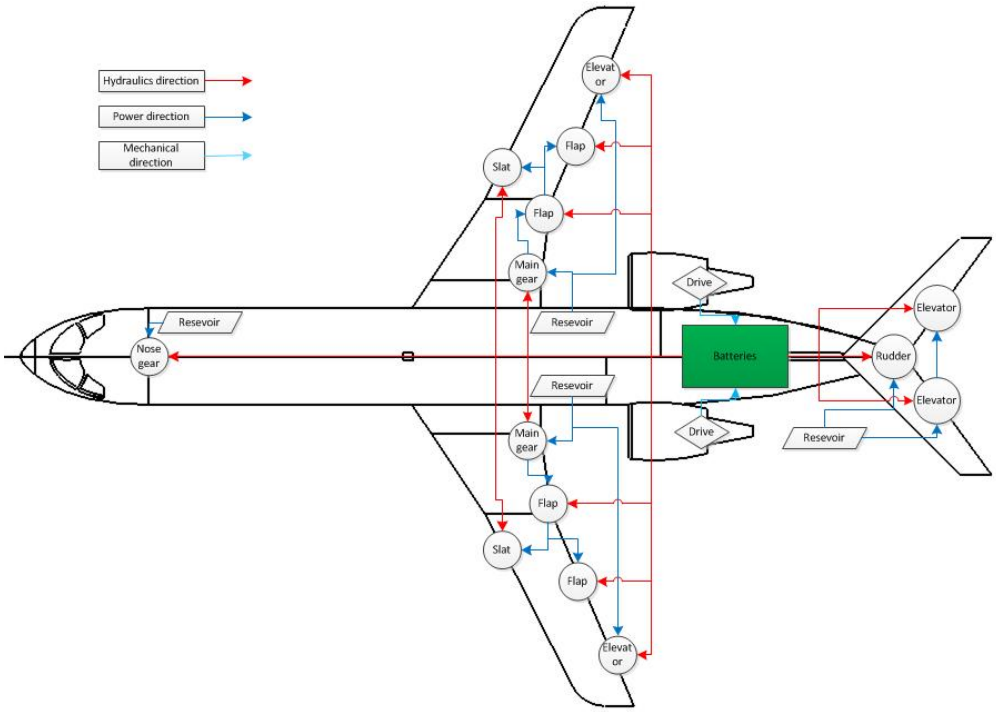

Figure 16.6: Schemactic drawing of control actuation layout

16.2.4 Landing Gear

The landing gear uses the same type of electro-hydrostatic actuators as the control surfaces however the system has some small changes. For example during the case of failure of the hydraulics the gear has to go into extended position for an emergency landing, it is not required for the gear to retract again. Contrary to the landing gear the control surfaces have to always be fully functional [62].

Not only the retraction system is powered by hydraulics but the braking system as well. All these systems will be powered by EHA systems. With the lower weight of the aircraft and the relatively low approach speed the brakes and therefore actuators can be smaller. The brakes should have their own system in case of failure of the main system.

16.2.5 Required Additional Components

Actuators alone are not enough for the complete system. In order to complete the system the following are needed: Power supply, fluid reservoir, filter, redundancy system, cooling, and lastly pipes. These components can already be seen in Figure 16.5.

Power Supply

The power for the hydraulics is provided by the engines, and otherwise by the APU. The power is generated by an accessory drive fitted to the turbine of engine. This means a loss in the turbine power and because the accessory drive has an efficiency loss the total power lost from the turbine will be larger than required power. This will decrease to the efficiency of the engine.

Hydraulic Working Fluid

The hydraulic fluid is the working medium for transmitting the power. The fluid is often a thicker than water fluid in order to allow for better performance when under pressure. A fluid compresses much less than air. The fluid in the system is kept at high pressures in order to keep weight down [62]. This high pressure means that the temperature of the working fluid increases. Because of these high temperatures the fluid must be not disintegrate in these high temperatures. The piping and pumps themselves must also be able to deal with larger temperatures. Because the temperature of the fluid is so important cooling systems are used to keep the fluid it the right operating temperature.

The fluid is stored in a reservoir which is used for fluid expansion. When the temperature increases the fluid expands and if there is no space in the system the pressure might increase too much with failure as result. Furthermore if there are small leaks in the system if there is no back-up fluid the system could empty and stop working.

Pipe Lines

Because an EHA system is used no more pipe lines from the engine to the actuators are needed which reduces the weight significantly. However there are still pipe lines from the reservoir to various actuators. These pipes must comply with the regulations and have to able to deal with the design pressures.

16.3 Communication

Almost a century ago, a rapid wing wave or a tail deflection was enough for the pilot to acknowledge visual instructions given by a person on the ground. With an increasing number of aircraft in the sky and the need to ensure safe operations, electronic communication became the norm. In this section, the essential elements of the communication system will be identified and briefly described. Also, future technologies that might be available by 2035 will be considered.

16.3.1 Required Communication Systems

Some required communication systems for the Q-50 are a VHF communication system which will enable the airplane to communicate with the ground and other airplanes.A HF communications system will provide long range communications between the aircraft and the ground or other airplanes. Communication Radio Panels (CRP) will enable the tuning of the communication systems. Audio Control Panels (ACP) will be used for communication between crew members and to make passenger announcements. A flight interphone system will be installed in the cockpit and also at the flight purser's seat.

16.3.2 Future Communication Systems

As weight reduction continues to be one of the most important factors towards more environmentally friendly aircraft it is desired for aircraft to carry less systems on board. Reducing the amount of systems will also reduce the power consumption and the amount of cables required in the aircraft. The system reduction can be achieved by integrating the different in-aircraft domains to securely share data links. These domains are aircraft control, airline information services and passenger information & information services. One other way to optimize the aircraft systems is to increase the use of wireless communications on board for critical applications. An example of such a system is the so called fly-by-wireless, which aims at an airplane without wires. The back and forth communication between critical systems goes through a wireless Bluetooth network. With these new developments in aircraft communications extra attention should also be paid on the safety and security of the wireless networks. Extra measures should be taken to guard the entire system as they become more vulnerable to cyber crime. Further development of the wireless network technologies should also contribute to a redundancy system in which aircraft would still be able to remain wireless in the future. With future introduction of the projects like the Single European Sky and NextGEN, future air to ground communication services will be merged to achieve one single data exchange link. An example of such a project is the Seamless Aeronautical Networking through integration of Data-Links, Radios and Antennas (SANDRA). This development will lead to less communication subsystems on board, which will also save weight.

16.4 Navigation

Navigation is the determination of the position and velocity of a moving vehicle, calculated on-board the aircraft. There are two main types of aircraft navigation systems [66]. Firstly, there are positioning systems such as celestial, mapping and radio navigation systems that require external systems. Secondly, there are dead reckoning systems that do not use external beacons to determine position, velocity and orientation. The main reason why navigation is a critical part of an aircraft, is to be able to safely guide the aircraft from A to B. Navigation and its accuracy and integrity are becoming increasingly important due to the steep growth of air traffic density, which increases the risk of collision. Since both position and velocity are three dimensional vectors, there is a total of six degrees of freedom which need to be covered by the navigation system. In order to cover these six degrees of freedom, multiple systems are required that can either be used alone or that are used in conjunction with others to obtain the required integrity and accuracy.

16.4.1 Required Navigation Systems

Firstly, for the measurement of the speed of the aircraft, pitot tubes are used, which make use of the pressure differences. Secondly, the altitude needs to be determined which is done by altimeters, which is based on the

mathematical model using the International Standard Atmosphere. Another option is to use radar altimeters, which uses the time between two pulses to calculate the altitude, which is often more accurate than the option of using theoretical models.

The next step is to determine the aircraft's lateral and longitudinal position. This can be done using both ground beacons such as the radial VHF Omnidirectional Radio beacon (θ system, done by phase comparison) as well as a constant Distance Measuring Equipment beacon (ρ system, based on the time difference between the pulse transmitted by the aircraft and the reception of that pulse sent back.). Using θ and ρ systems in combination provides a 2-D position fix [1]. Besides the ground beacons, there are also long range systems such as Global Positioning System (GPS) and Inertial Navigation System (INS) that uses motion and rotational sensors to continuously calculate the position, velocity and orientation of the aircraft for which no external beacons are required.

16.4.2 Future Navigation Systems

The current navigation systems used have some shortcomings. The CNS systems are not capable of giving real-time information on the present position. For navigation over land and coastal areas, ground based source navigation aids are used, for example: VOR. In order to navigate and communicate, the airplane needs to fly along these ground stations. Therefore, the aircraft cannot fly the most optimum path. This results in more emissions and more costs. Furthermore, the current systems are not able to expand in order to meet the future air traffic growth. In 1983, the International Civil Aviation Organisation, ICAO, established a committee on Future Air Navigation Systems, FANS. This committee investigated the new technologies available for navigation systems. A goal of the committee was 'to have a single navigation system providing adequate navigation for all phases of flight under all meteorological conditions all over the world for all airspace users'. A proposed system in order to meet this goal is the use of the Global Navigation Satellite System, GNSS, applied with the RNAV/RNP concept.

GNSS is expected to become a sole means navigation system. A sole means system is a navigation system that for a given phase of flight must allow the aircraft to meet all four navigation requirements: accuracy, integrity, availability and continuity of service. Using this concept, the aircraft will be able to fly through a predetermined four dimensional tunnel from start to landing (Figure 16.9). GNSS is currently used for civil and military navigation. In different parts of the worlds, different satellite systems are used. For example, Europe uses the Galileo system. Area Navigation (RNAV) enables the aircraft to fly along a desired path, instead of being restricted to an airway. An even more accurate navigation system is Required Navigation Performance (RNP) allows even greater navigation and precision accuracy and reduces step down and circling approaches and reduces missed approaches [67]. Therefore, a lot of fuel can be saved using this system. The system can only be implemented and used in the aircraft if the system is used on the ground globally as well. There are different type of RNP systems: RNP1, RNP4, RNP12.4 and RNP20. The number describes the accuracy of the system on a 2 σ probability basis. The most accurate system available is chosen.

It is expected that by 2035, this systems will be used globally. Aircraft will fly the most optimum path from A to B. Furthermore, the navigation system will be constantly connected to the ground. Aircraft will become more efficient and safer with the use of these systems. On the low emission airliner, these new systems will be implemented.

16.5 Cockpit

Instrument systems can either be direct-sensing or remote-sensing. The direct-sensing systems are the familiar dials and gauges that are present in the cockpit of older aircraft where the part that senses the situation and the part that displays it often take place in a single unit. Remote-sensing requires the information to be sensed or captured somewhere along the aircraft and then sent to the cockpit where it turns up on a display. The latter are often present as the so-called glass cockpit. These are usually easier to maintain and read. The biggest downside of remote-sensing instrument systems is that they are dependent of electricity. That is why we will opt for a glass cockpit with remote-sensing instrument systems and keep the 4 indicators of the traditional T-configuration (Figure 16.7) as redundancies placed in a less dominant location.

The instrumentation in the cockpit can be classified under three basic types which are flight instruments, engine instruments and navigation instruments although there also are some other that fall under none of the previous categories such as the instrumentation for cabin environmental systems (pressurization, air-conditioning,...), electrical power and the auxiliary power unit (APU). In general these can be regarded as position/condition instruments since they usually report the position of a certain movable component on the aircraft, or the condition of various aircraft components or systems not included in the basic types. In case

[1] https://www.faa.gov/regulations_policies/handbooks_manuals/aircraft/amt_airframe_handbook/media/ama_Ch11.pdf, cited 10/06/2015

of a glass cockpit all of these are integrated in the computer and the pilot has a default view of the flight instruments and can let other indicators appear with the press of a button.

16.5.1 Flight Instruments

Basically there are 3 flight instruments that are always present in every aircraft that is certified to fly. These are the altimeter, the airspeed indicator and the magnetic direction indicator. Most aircraft also contain an artificial horizon, turn coordinator and a vertical speed indicator. Years of flying resulted in a typical T-configuration for these indicators, as can be seen in Figure 16.7, present in most aircraft with analog flight instruments.

Figure 16.7: T-configuration of analog flight instruments

In the top centre position is the artificial horizon which is also the default view of glass cockpits. On the top left is the airspeed indicator, the top right shows the altimeter and the bottom centre contains the magnetic direction indicator, all of which are usually represented on the default screen in a glass cockpit as well.

16.5.2 Engine Instruments

Turbine engines have certain parameters that need to be looked after. For multi-engine aircraft each parameter has one gauge with each engine having a specific pointer. To limit the amount of dials and gauges the engine instruments are often placed in the centre of the cockpit so they are easily visible for the pilot and copilot. For a glass cockpit this is not of any concern since the engine parameters can be shown on the side of the screen if requested. The parameters that are most important in turbofan engines are

- Oil Pressure
- Exhaust Gas Temperature
- Turbine Inlet Temperature
- Engine Pressure Ratio
- Fuel quantity
- Fuel flow
- Tachometer (RPM gauge)
- N_1 and N_2 compressor speeds

16.5.3 Future Applications

Keeping in mind that our aircraft will take to the skies in 2035 there still is a lot of time for technical improvements. The chances of the cockpit of the future looking the same as it does today is practically zero. There are quite some technologies that haven't matured quite yet but might be perfectly applicable by 2035.

Heads Up Display (HUD)

These can be used to project useful information on the windows or on a transparent plate that can be moved in the pilots field of view. Basically all the information that is shown on the traditional Heads Down Display (HDD) can be projected here in a clear way if designed properly. HUDs have been used in military aircraft for decades and are finally finding their way into commercial aviation (and in the automotive industry). Most HUDs now are monochrome but they are also available in full colour.

Synthetic Vision

This technology can be used to combat the inability to fly in poor weather conditions where visibility is reduced significantly. Synthetic Vision uses GPS location and detailed terrain information (height differences, obstacles, runways, etcetera) from a database to generate a visual representation of what would be visible from that position. The dynamic image can be shown on the HDD or projected on the HUD in such a way that it matches what the pilot would see in clear weather. A good balance in image transparency is key in the latter situation.

Highway In The Sky (HITS) [68]

This is simply an extension of the Synthetic Vision technology where a series of rectangles are added to the screen to depict the flight path. The pilot maneuvers the aircraft through these rectangles to achieve the desired flight. For Synthetic Vision as well as for HITS a lot of information can be displayed on the same screen at the same time without cluttering it.

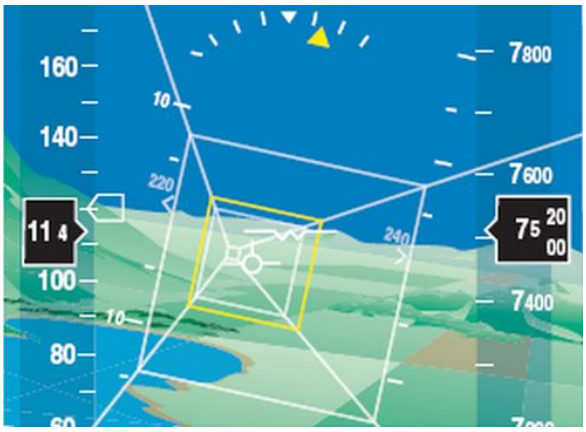

Figure 16.8: An example of synthetic vision with HITS

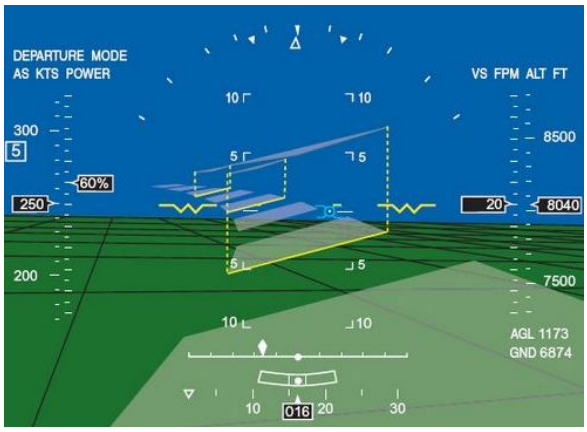

Figure 16.9: An example of HITS with extensive flight information

Touchscreen

Using a touchscreen that shows the essential buttons as a default and gives you access to all other buttons through menus could make the cockpit a whole lot easier to use and would require less parts. Although the screen might use extra electricity the reduction in maintenance will be substantial.

16.6 Electrical Systems

In this section, an outline of the design of the electrical system is described. Two main aspects are discussed, the power budget and the layout of the main wiring routes.

16.6.1 General Layout

In order to get an overview of which major components are part of the aircraft electrical system, a general layout is made which is presented in 16.10. With the main systems contributing to the electrical system, an estimation of the power budget is made.

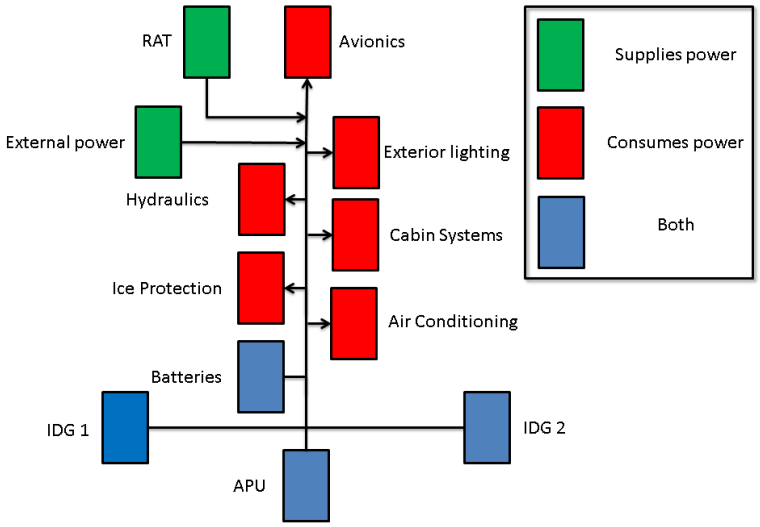

Figure 16.10: Electrical system layout

16.6.2 Power Budget

The main contributions to the power budget are identified in the layout. An rough estimating of the power consumptions of these systems is made and the outcome is presented below. In case of lacking data, Roskam [69] is used to make a rough estimation. It should be noted that the power budget is determined for cruise because data from this mission phase is more easily obtained. From [69] it known that the power used in the cruise phase suffices as a rough estimate of the maximum power needed. The power requirement derived in the following sections is the power requirement per generator. Each of the three main generators is designed to provide the power requirement independently. The three generators consist of an integrated drive generator (IDG) in each engine. These IDG provide a constant voltage and frequency regardless of input rpm. The third generator is the auxiliary power unit (APU), a small gas turbine. This setup provides double redundancy for the power generation. Redundancy of power generation is required since IDGs are failure prone due to their complex nature. In case of failure of one of the IDGs, the APU is restarted to reestablish the double redundancy. In case of complete failure of all three main generators, the ram air turbine (RAT) is deployed. This small outboard wind driven generator is designed to provide enough power for essential flight systems to allow for immediate emergency landing. The battery provide a short term backup during the transition between power supply modes. Battery packs are also used for power system initialization, including APU start, in case external (ground) power is unavailable.

Anti-Icing System

A master thesis approved by the Delft faculty of Aerospace was used as a reference for estimating the power necessary to power the anti-icing system [70]. In this thesis it was shown that this anti-icing system needs less power than when bleed-air is used, therefore reducing the fuel needed and reducing also the emissions. On the other hand it showed a snow-ball effect leading to an increase in MTOW. What effect this exactly would have for this aircraft design is beyond the scope of this exercise and it will therefore not be investigated. From this thesis, the typical value for the power required by the anti-icing system (using bleedless Glare system) was given to be 13 kW/m, in this case leading to: $P_{req_{anti\_ice}} = 13 \cdot 8 = 104kW$.

Cabin Systems

The cabin systems that are considered here are the OLED entertainment screens to compensate the lack of windows for passenger comfort, wi-fi on board, power ports to be used by passengers, the cabin lighting and the environmental control system. In Section 5.1.1 the power consumed by the entertainment system was investigated and estimated to be 1.8 kW. Another 1 kW is added to power supporting systems, such as image processors and cameras.The power consumption of the lighting system in the cabin was estimated with the help of August Kuipers, a LED-light specialist who has been investigating LED applications for over 8 years. For reference aircraft the current power budget for purely cabin lighting would be 3.11 kW, assuming 50 halogen reading spots, 2 fluorescent tubes for each row and 10 other halogen spots (cockpit, galley, etc). Of course from the sustainability (and cost) perspective the Q-50 will be equipped with only LED lighting, which will cause a reduction in power consumption of 2.85 kW, resulting in only 0.26 kW for the cabin lighting. Wi-fi on board of the airplane is provided by the router, which consumes about 20 kW,

if most power consuming router is considered [2]. As for the power ports, the most power intensive case is assumed, being every passenger adapting their laptop at the same time. For a laptop charger the power consumption is on average 90 Watt so the total will come down to 4.5 kW. For the lavatories, the following estimation is made: since the DC10 lavatory system consumes 6100 Watt and comprises 8 lavatories in a typical configuration. The Q-50 is equipped with one lavatory and therefore it is estimated that the power consumed will be 678 Watt. Last, the power consumed by the air conditioning system is estimated to be 1 kW per passenger, leading up to 50 kW for the entire aircraft [3]. Therefore the cabin systems will in total consume 78.24 kW

Avionics

For the Douglas DC10, the power consumed by the avionics system is 7.25 kW. This is a 380 seat aircraft and therefore not directly comparable to the Q50. However, the systems in the cockpit that are needed will not decrease for smaller aircraft and therefore it could be assumed that the power consumed is comparable. However all electrical products have become more efficient, on the other hand current airplanes use glass cockpits which contain a lot of screens and other modern electrical systems which would increase the power consumption. The assumption is made that these two factors cancel each other out and the power budget stays the same.

Hydraulics

The power consumed by the hydraulics system is assumed to be negligible during cruise, because the corrections that have to be made to the control surfaces are negligible.

Exterior Lighting

The power consumption of the DC10 is stated to be 200 Watt in cruise. Though the size difference is not likely to be relevant for the power consumption of the exterior lighting, the age difference is. Modern LED units provide an equal light intensity at a fraction of the power. At least half the power is assumed to be saved by transition to LED lighting. This sets the exterior lighting power estimation at 100 Watt.

16.6.3 Conclusion

To conclude, the rough power budget estimation in the cruise phase is presented in Table 16.1.

Table 16.1: Power consumption during cruise

System	Power consumed (kW)
Ice protection	104
Cabin systems	78.24
Hydraulics	0
Avionics	7.25
Exterior lighting	0.01
Total	189.5

[2] http://www.satcom1.com/cabin-cockpit-solutions/router-management/
[3] https://dspace.lib.cranfield.ac.uk/bitstream/1826/7422/1/Rolando_Vega_Diaz_Thesis_2011.pdf, page 93

Allocation of Resources and Budget Breakdown

The cost of an aircraft is generally driven by the technical resources. These resources tend to grow during the aircraft design process, which also makes the cost of the aircraft grow. To be able to manage this issue a resource allocation is performed where the technical resources that drive the design of the Q-50 are defined. The resource allocation process first allocates the technical resources, where after a maximum value is set for the resources. Consequently, a contingency plan is set up to define the steps that are taken in case the maximum resource value is exceeded. This chapter gives an overview of the technical resources that are relevant for the Q-50 which are mass, drag and power and their corresponding budget breakdowns.

17.1 Drag

The drag budget is estimated using the methods defined in reference [51]. The total drag is the total of the drag per subsystem. Figure 17.1 shows the budget drag coefficient contribution in percentages. Figure 17.2 shows the budget for the absolute drag during cruise in percentages. C_{D_0} is computed for the entire aircraft and is equal to 0.015.

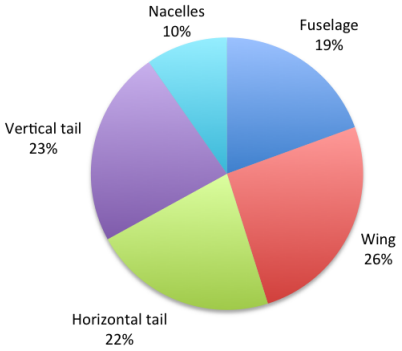

Figure 17.1: Drag coefficient budget for the sub systems of the Q-50

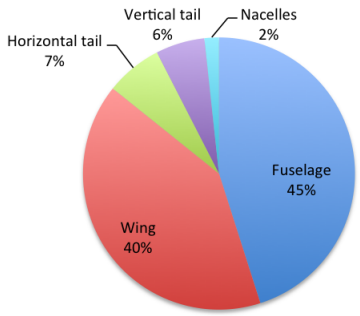

Figure 17.2: Drag budget during cruise for the sub systems of the Q-50

17.2 Mass

The mass budget is determined from the Class II weight estimation as stated in Table 7.5. Figure 17.3 shows the mass per sub-system as percentages of the total operational empty weight. Figure 17.4 shows the mass budget of the sub-sub-systems of the Q-50.

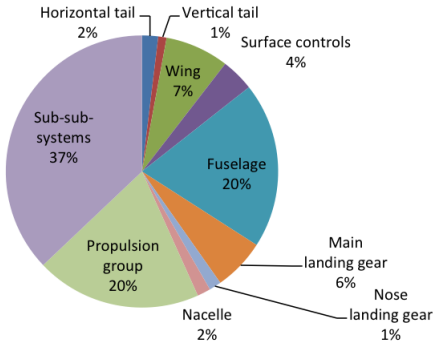

Figure 17.3: Mass budget for the sub-system groups of the Q-50

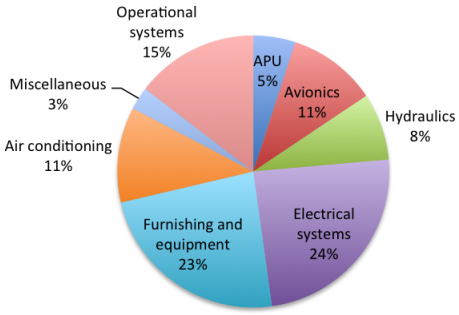

Figure 17.4: Mass budget for the sub-sub-systems of the Q-50

17.3 Power

The power budget is determined by looking at the power consumption of the subsystems of the Q-50. Figure 17.5 shows the power consumption for different sub-systems as a fraction of the total electrical power available as stated in Table 16.1.

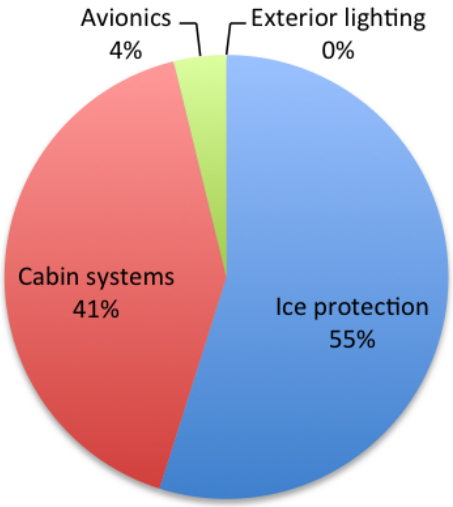

Figure 17.5: Power budget during cruise for the Q-50

17.4 Contingencies

As a maximum budget for the technical resources a small margin of 5% is taken for the actual values. The 5% value is heuristically determined taking into account that further performance improvement and weight reduction will be achieved. The maximum values for the aerodynamic drag during cruise is determined to be 27806 N. The maximum electrical power consumed on the Q-50 is 189.5 kW and the maximum operational empty weight is set to 10243 kg.

If the technical resource budget is exceeded in the design process, measures should be taken to bring the exceeded value back within the set limit. For example, in case the maximum operational empty weight is exceeded the amount and type of sub-systems of the Q-50 should be reconsidered.

Sensitivity Analysis

This chapter shows the results for the sensitivity analysis performed for the Q-50. As a way to manage contingencies in aircraft design a sensitivity analysis for the OEW and the MTOW is performed. Furthermore, as mentioned in the market analysis, the Q-50 will be extended to a family of aircraft complying with the different requirements set by the operators. The sensitivity analysis analyses the sensitivity of the design for a change in major system parameters. It is used to establish a degree of feasibility for the final design whilst sticking to the initial design point in Class 1. The analysis is performed using the Class II iterations, with the same procedure as that shown in Chapter 6. The aerodynamic and structural effects of these changes are not taken into account. The parameters of interest are the fuselage length, cruise speed, engine weight and maximum range.

Figure 18.1 shows the weight sensitivity for the change in fuselage length. It can be noted from the figure that the growth rate increases significantly after passing a 20% growth in fuselage length. The weight increase at 20% fuselage length increase is also 20%. Figure 18.1 also shows the sensitivity of the wing surface area for the change in fuselage length. A 20% increase in fuselage length leads to a 14% change in wing surface area.

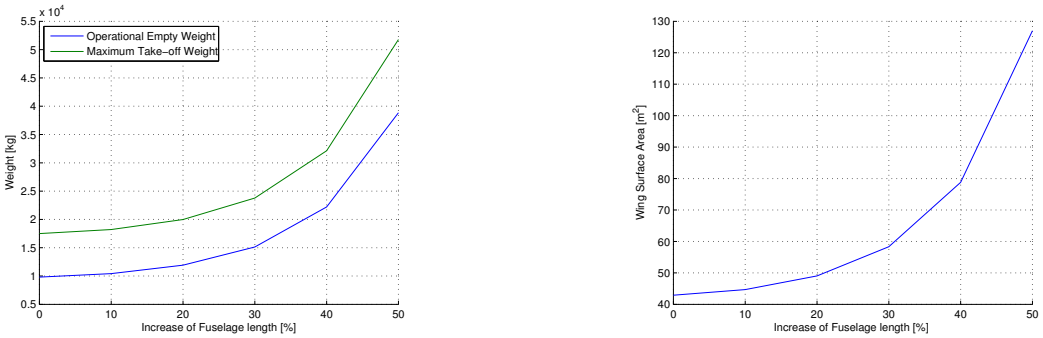

Figure 18.1: Sensitivity analysis for the aircraft weight and wing surface as a function of the fuselage length

Figure 18.2 shows the weight sensitivity for the change in cruise speed. From the figure it can be noted that a 10% increase in cruise speed leads to a weight increase of 11%. The figure also shows the sensitivity of the wing surface area for the change in cruise speed. A 10% increase in cruise speed leads to a 0.01% increase in wing surface area. An increase of more than 10% for the cruise speed is not feasible for the configuration of the Q-50 as the cruise speed is already at M = 0.81. Figure 18.3 shows the sensitivity for the weight if the cruise speed is decreased. A 20% decrease in cruise speed shows a 7% decrease in aircraft weight. A 20% decrease in cruise speed shows a 4% decrease in wing surface area.

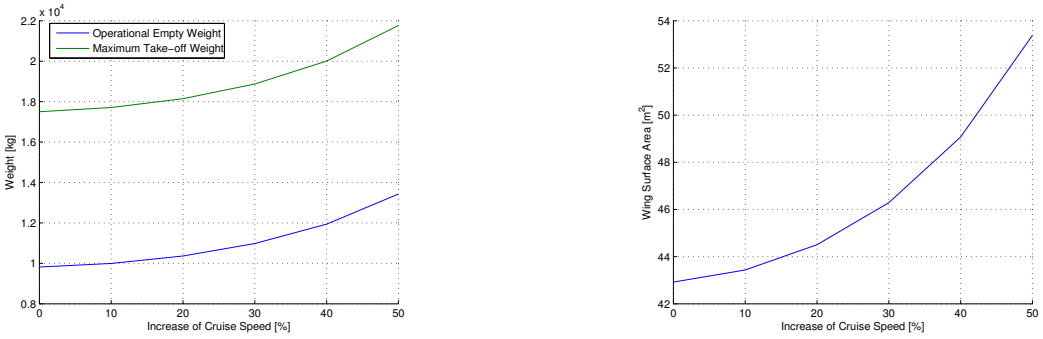

Figure 18.2: Sensitivity analysis for the aircraft weight and wing surface as a function of the increase in cruise speed

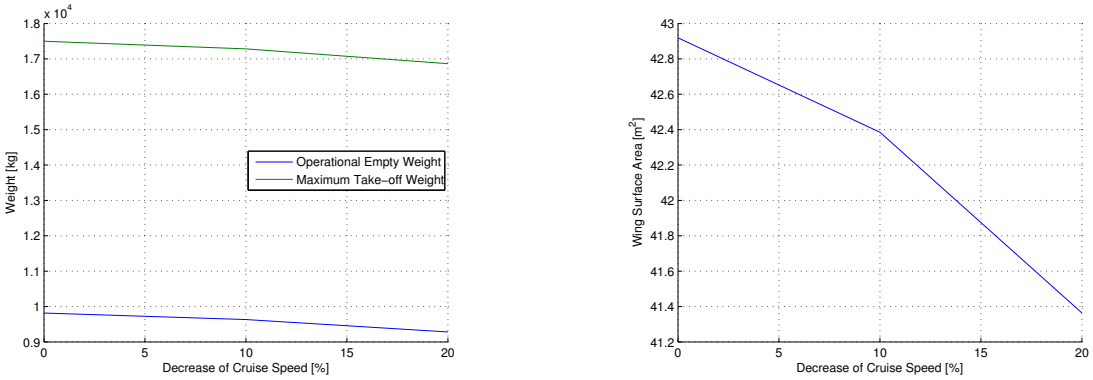

Figure 18.3: Sensitivity analysis for the aircraft weight and wing surface as a function of the decrease in cruise speed

Figure 18.4 shows the weight sensitivity for the change in engine weight. It can be noted from the figure that the growth rate increases significantly after passing a 30% growth in engine weight. The aircraft weight increase at 30% engine weight increase is 20%. Figure 18.4 also shows the sensitivity of the wing surface area for the change in engine weight. A 30% increase in fuselage length leads to a 14% change in wing surface area.

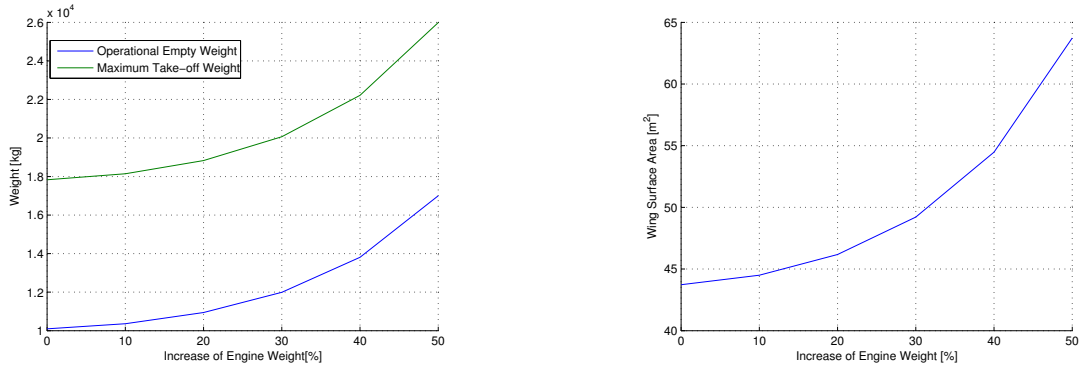

Figure 18.4: Sensitivity analysis for the aircraft weight and wing surface as a function of the engine weight

Figure 18.5 shows the weight sensitivity for the change in maximum payload weight. It can be noted from the figure that the growth rate increases significantly after passing a 42% growth in maximum payload weight. The aircraft weight increase at 42% maximum payload weight increase is 20%. The figure also shows the sensitivity of the wing surface area for the change in maximum payload weight. A 42% increase in maximum payload weight leads to a 63% change in wing surface area, which is not feasible for the same aircraft configuration. A more feasible increase in wing surface area is a 16% increase to 50 m^2. A 22% increase in maximum payload weight leads to a 16% increase in wing surface area. Parts of the aircraft payload are amount of passenger and amount of fuel. The design of the aircraft is as sensitive for an increase in amount of passengers or maximum range as it is for the increase in payload weight. The maximum range is driven by the amount of fuel, consequently also by the payload weight.

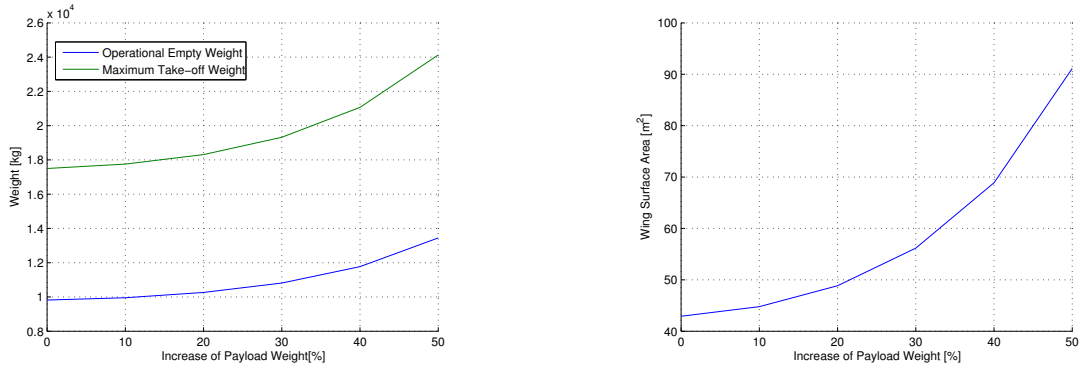

Figure 18.5: Sensitivity analysis for the aircraft weight and wing surface as a function of the maximum payload weight

Operations and Maintenance

Now that the design of the Q-50 has been finalized, it is important to take a look at the logistics and operations of the aircraft in order to analyse the different steps and phases during operations (including maintenance) of the aircraft. This is important since operations is by far the largest part of the aircraft's life, and therefore sufficient knowledge on the different phases of operations during the design and development phases of the process can lead to an increase in sustainability and a decrease in emissions and cost for the operational life of the aircraft. Section 19.1 covers the basics on operational side. This is followed by the analysis of the availability in Section 19.2 and maintenance in Section 19.3.

19.1 Operations

This section will cover the functional flow block diagrams at multiple levels, followed by the ground handling in terms of a turnaround chart and finally the air traffic management systems of the future, which will all contribute to a more sustainable aviation industry.

19.1.1 Functional Flow Block Diagram

In order to analyse and improve the operations of the QLEAR Q-50, first the functional flow during operations on multiple levels needs to be set up. The FFBD of level 1,2 and 3 can be seen in Figures 19.1 until 19.3.

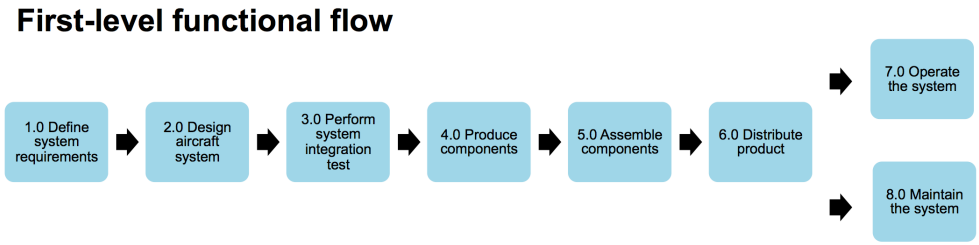

Figure 19.1: Functional Flow Block Diagram first level

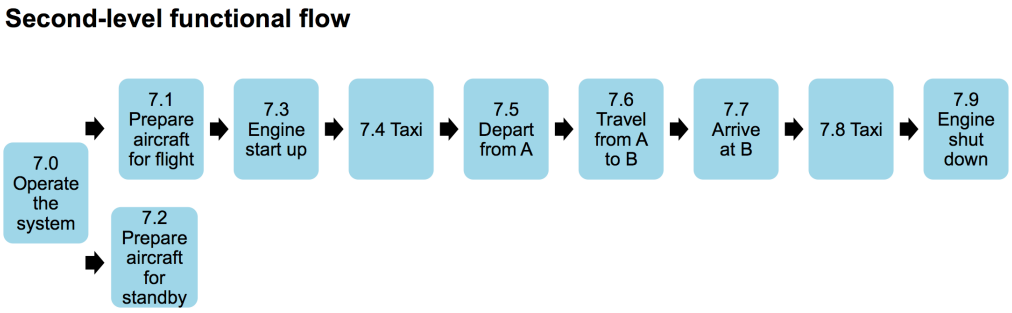

Figure 19.2: Functional Flow Block Diagram second level

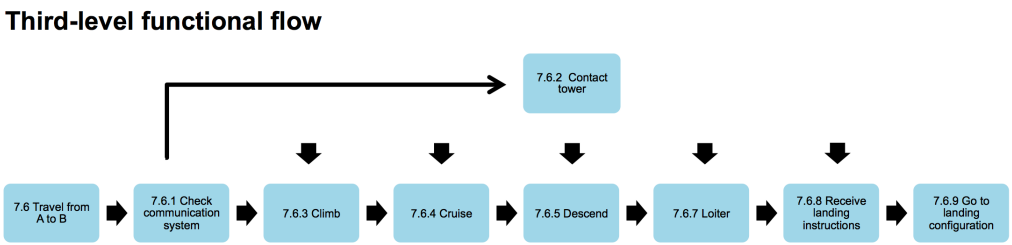

Figure 19.3: Functional Flow Block Diagram third level

19.1.2 Ground Handling

The next step is to go into more detail for the operations of the aircraft. This can be done on both the operational level as well as the maintenance level (Section 19.3). The turnaround chart in Figure 19.4 includes all tasks to be performed in between arrival and departure at the gate and the time for each tasks. The process times are based on both Boeing [1] and Linköping University, Airport Logistics [2].

QLEAR Q-50		Time since parking																				
Ground Activity	Duration [min]	1	2	3	4	5	6	7	8	9	10	11	12	13	14	15	16	17	18	19	20	21	22
Place pylons	1	1																					
Attach stairs/bridge	1	1																					
Unload luggage	7							7															
Load luggage	5										5												
Deboard	5					5																	
Maintenance handling	10										10												
Water	8								8														
Fuel	8													8									
Cleaning	6													6									
Catering	5														5								
Security & Cabin check	4																	4					
Board	5																			5			
Remove stairs/bridge	1																						1
Remove Pylons	1																						1

First critial path	
Second critical path	
Third critcal path	

Figure 19.4: Turnaround chart for the Q-50

From Figure 19.4 it can be seen that the total turnaround time for the Q-50 is 22 minutes. The first critical path depends on the bridge, de-boarding, cleaning, catering, security check and boarding. By reducing or even avoiding cleaning and catering on flights, the turnaround time can be reduced to 20 minutes. This depends on the approach the airline prefers to take, whether to go for low-cost, which means less service or legacy, which means a higher level of service.

The wingspan of 19.2 m and the fuselage length of 25 m are in compliance with requirement OP-4 from Appendix D regarding the maximum allowable parking dimensions, which should not exceed 42 by 30 m.

A big percentage of the turnaround time is taken up by maintenance checks. These are performed to make sure everything is safe in order for the aircraft to perform its next flight. A typical line maintenance flow chart including the different tasks and decisions to be made is shown in Figure 19.5 [71].

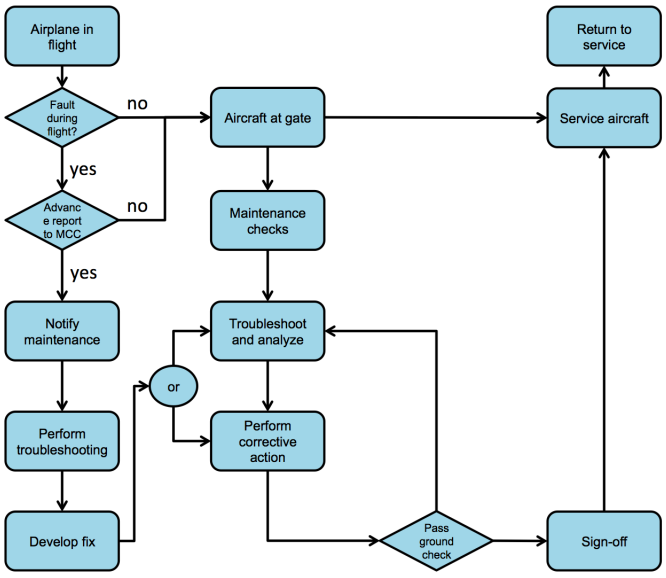

Figure 19.5: Flowchart of line maintenance operations

19.1.3 Air Traffic Management

Not only the operations at the airport play an important role in the efficiency of the aircraft, but also the operations in the air are important for the efficiency. Air Traffic Management (ATM) is the totality of all

[1] http://www.boeing.com/assets/pdf/commercial/airports/acaps/737.pdf, cited 17-06-2015
[2] http://www.diva-portal.org/smash/get/diva2:133720/FULLTEXT01.pdf, cited 17-06-2015

systems regarding the departure, flight and arrival of aircraft. The more efficient the ATM systems work, the higher the efficiency of the trip and therefore the lower the fuel consumption and thus emissions. Since the aviation industry is growing with an average of 4.1% [3], the density of aircraft in airpsace increases and therefore the safety decreases. Moreover, in 2010 there have been 19.4 billion minutes of en-route delay [4]. Both in Europe as well as in the United States, programs have been developed to increase the efficiency, safety and decrease emissions, of which the benefits will be described below.

SESAR

Single European Sky ATM Research is an initiative of the European Commission, Eurocontrol and the aerospace industry [5]. It is an approach to meet future capacity needs and reduce emissions. Moreover, by defragmentation of the airspace, the aircraft will be able to fly directly to their destination, reducing the distance and therefore the fuel consumption on each flight. SESAR promises a decrease of 10% in fuel consumption per flight [6] and thus a 10% reduction in CO_2 emissions. Besides gaseous emissions, SESAR reduces the noise emission by better flight paths and optimized climb and descent [7]. In order to obtain and provide all digital information, the System Wide Information Management (SWIM) system has been created. This will increase the accuracy of the information and will make sure that the information between different systems can be shared smoothly [8].

NextGen

NextGen is an initiative of the Federal Aviation Administration and is a national airspace system which will transition the ATM from a ground-based system to a satellite-based system. NextGen will make use of multiple systems (including SWIM):

- Automatic Dependent Surveillance-Broadcast (ADS-B): a satellite-based alternative for radar, which determines the precise aircraft location and streams flight information to the cockpit.
- Collaborative Air Traffic Management Technologies (CATMT): a decision-support and data-sharing tool, which will allow for a collaborative environment between pilots and controllers.
- Data Communications: digital instructions to supplant voice communications.
- NextGen Weather will provide tailored weather information using SWIM, to develop reliable flight plans and make better decisions during flight when necessary.

NextGen will reduce the delays by 35% in 2025. Also, using GPS will improve the accuracy during approach and departure, resulting in a smaller separation distance between aircraft and therefore an increase in capacity. Moreover, due to the higher accuracy during cruise, the aircraft can fly more direct routes, resulting in shorter flight time and thus a reduction in fuel consumption and emissions.

Continuous Descent Approach (CDA)

Continuous Descent Approach (CDA) is the landing procedure by which the aircraft uses a flight idle setting and a constant glide slope. In this way the fuel consumption and noise nuisance are reduced. CDA will become possible with both SESAR and NextGen within the coming 15 years. The CDA, together with the optimized flight path used by both SESAR and NextGen can be seen in Figure 19.6.[9]

19.2 Availability

Availability of an aircraft is defined as the degree, percent, or probability that a system will be ready or available when required for use [72]. Figure 19.7 [10] shows the breakdown structure of the time division of an aircraft during its operational life. In red, the aircraft operational unavailability can be seen. The operational availability of the aircraft cannot be precisely specified, because each airline has its own operational philosophy and therefore a custom-made maintenance schedule. For this reason this aspect of the operational life will be handed over to the customer and will not be treated further in this report.

[3] http://www.iata.org/pressroom/pr/pages/2014-10-16-01.aspx, cited 16-06-2015
[4] http://ec.europa.eu/transport/modes/air/single_european_sky/, cited 16-06-2015
[5] http://ec.europa.eu/transport/modes/air/sesar/doc/2010_06_sesar_environment_en.pdf, cited 16-06-2015
[6] http://www.sesarju.eu/sites/default/files/documents/reports/European_ATM_Master_Plan.pdf,cited 16-06-2015
[7] http://ec.europa.eu/transport/modes/air/sesar/doc/2010_06_sesar_environment_en.pdf, cited 16-06-2015
[8] https://www.faa.gov/nextgen/update/progress_and_plans/swim/, cited 16-06-2015
[9] http://ec.europa.eu/transport/modes/air/sesar/doc/2010_06_sesar_environment_en.pdf, cited 17-06-2015
[10] http://www.iata.org/whatwedo/workgroups/Documents/MCC-2013-DUB/Day2/1130-1215_Operational_Availability_AIRBUS.pdf, cited 18-06-2015

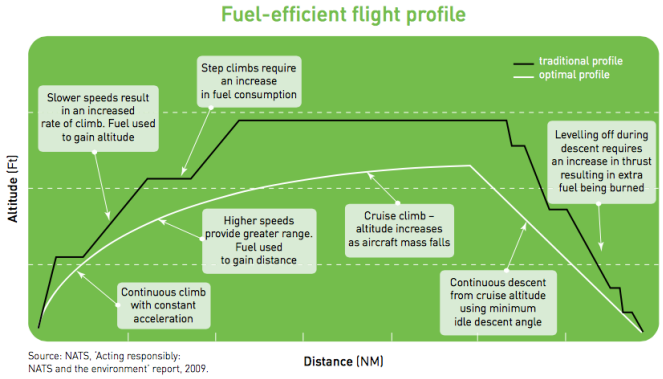

Figure 19.6: Optimized flight path of SESAR and NextGen including Continuous Descent Approach

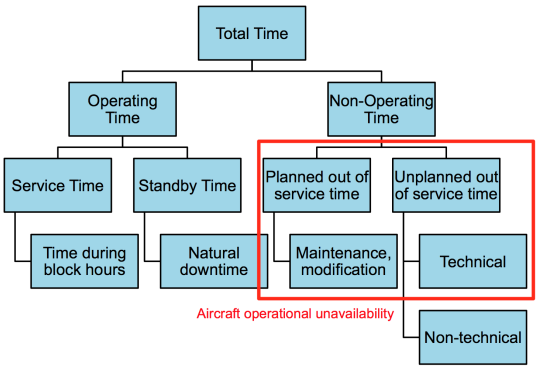

Figure 19.7: Breakdown structure of the time division for an aircraft

19.3 Maintenance

Aircraft maintenance consists of checks, repairs, inspection and modification of the aircraft to make sure that it is safe to perform the mission that it is designed for, under certain predefined operating conditions. Maintenance is important for safety, but also for the performance and operational efficiency of the aircraft.

19.3.1 Types of Maintenance

There are different types of maintenance: preventive maintenance and corrective maintenance. Preventive maintenance is done before a functional failure occurs, while corrective maintenance is performed after a functional failure. Preventive maintenance can be periodic or conditions based maintenance (Figure 19.9). There are different types of periodic checks:

- A checks. These are general inspections performed every two weeks to monthly. The interior and exterior of the aircraft are checked.
- C checks. C checks are scheduled every 12 to 18 months depending on the operator. The checks include functional and operational checks, cleaning and servicing.
- D checks. D checks are performed every 6 years. For these checks, the aircraft needs to be taken out of service for several weeks. During the D check, the aircraft is partly stripped. External components are checked extensively and some components may be changed.

Condition based maintenance is a maintenance strategy where it is decided to perform maintenance based on the state of the system [11]. The condition of the aircraft can be monitored in several ways. Examples are, noise measurements, vibration measurements, shock pulse measurement and thermography. Condition based maintenance has many advantages over periodic maintenance. It minimizes the time spent on maintenance and therefore, minimizes the cost. It improves the reliability of the equipment because the state of the aircraft is monitored continuously. However, the monitoring systems are expensive to install and are not able to withstand all operating conditions. Because there is not a planned maintenance schedule, when maintenance do needs to be performed, there is a chance that there will not be staff available.

Another maintenance aspect to look at is the replacement policy. There are two main types of policies. There is the age replacement maintenance policy where replacements occurs after a part has reached a certain age T. The other policy is called block age replacement, where replacement occurs every T units of time [73]. Both policies are illustrated in Figures 19.8, 19.9. Block replacement is a bit wasteful, because relatively new systems are replaced. However, this policy is easier when looking at the aspect of planning the maintenance checks.

19.3.2 Maintenance Strategy for the Q-50

The use of a condition based maintenance strategy will be optimal for the aircraft. There will be some cost for the acquisition of systems that monitors the condition of the aircraft. However, cost can be reduced by shortening the planned maintenance. The C and D checks still need to be performed, however the A checks can be shortened or be done less frequently. The preventive checks can be scheduled according to

[11] http://www.maintenanceassistant.com/condition-based-maintenance/

the most up to date MSG (Maintenance Steering Group) report. The Maintenance Steering Group, MSG, is a document that presents a methodology to be used on creating a schedule for maintenance. The MSG-3 is the most up to date version.

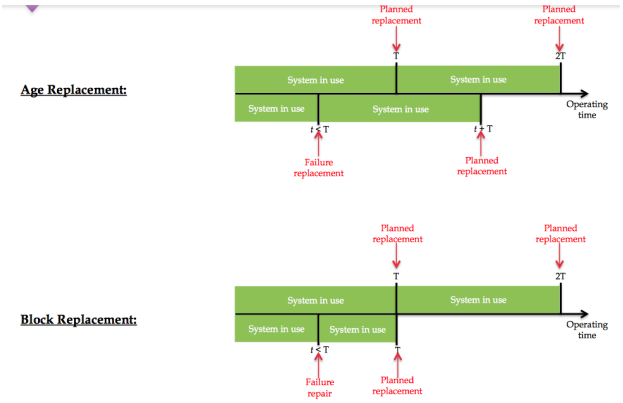

Figure 19.8: Age- and block replacement policies

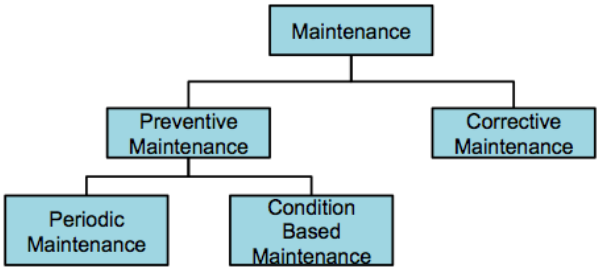

Figure 19.9: Types of maintenance

What distinguishes the Q-50 from other aircraft is the extensive use of composite materials. These materials require a different maintenance program than metals, which are widely used in current aircraft. The Federal Aviation Administration developed even a 'critical composites maintenance and repair issues' course [12]. Boeing is one of the first aircraft manufactures that developed and built a civil aircraft which uses mainly composite materials, namely the B787. The maintenance cost of the B787 are lower than the other Boeing aircraft. Composites require less scheduled maintenance than metals, due to the fact of lower risk of corrosion and fatigue [25]. Besides these benefits, there are some challenges for the maintenance of composites. Composite materials are pretty sensitive to impact damage, production failure and excessive loading. However, damages are less visible compared to damage on metals. During maintenance the aircraft needs to be checked on damage, in order to assure safe operations in the future. A technique that can be used for composite maintenance is shearography technology [74]. Shearography is a non destructive optical measurement method, which provides the user with results quickly. It can detect defects inside composite materials. A new technique which can be implemented on the Q-50 in the future is Structural Health Monitoring, SHM [13]. For SHM a system of sensors is placed on the aircraft, which can detect if there are cracks or defects in the structure by sending electrical signals through it. This technique is currently in a development phase and can be applied in the future to the Q-50 in order to monitor the state of the aircraft.

When corrective maintenance needs to be performed after a failure, it is desired that the aircraft returns into service as fast as possible. Therefore, spare aircraft parts need to be in stock. Also, when preventive maintenance is done, enough spare parts need to be available in order to replace weak and damaged parts. Another point of attention when it comes to maintenance of the Q-50 are the screens inside the aircraft. These screens provide the passengers a view outside and are important for the flight experience. Even small defects in the screens can cause inconvenience for the passenger. Therefore, it is vital that the screens are checked during the most frequent maintenance check (the A check) and that there are always enough screens in stock in order to replace a defect screen.

19.3.3 Conclusion

For the QLEAR50, the most optimal maintenance strategy is condition based maintenance. A-checks can be shortened or be done less frequently, while C and D checks remain necessary. Damage in composites are checked using shearography technology. It is recommended to do a more extensive investigation in systems that monitor the state of the aircraft. Furthermore, when it comes to replacement policy it is advised to compute if block replacement or age replacement is more cost efficient in the long term.

[12] http://www.tc.faa.gov/its/worldpac/techrpt/ar0854.pdf
[13] http://www.compositesworld.com/articles/structural-health-monitoring-composites-get-smart

Reliability and Risk Management

20.1 Risk Management

Risk management is a way to clearly determine risks and possible ways to mitigate those risks. Risk maps are used to visualise each individual risk based on probability and consequence and shows which of the two should be reduced to lower the risk. Ideally both consequence and probability will be reduced but this is not always possible.

1. **Moisture absorption**
   Composites are prone to moisture absorption which reduces the strength of the fibers that carry the tensile loads. In some cases it might even seep through the skin into compartments within the aircraft resulting in trapped dead weight and offsetting the balance of the aircraft. The probability of composite parts of the Q-50 absorbing moisture is quite high since ambient air is humid by nature (although it can vary greatly). If the aircraft is subjected to humid air for a long enough time the strength of the fibres will decline substantially resulting in potential structural failure. Structural failure is obviously not acceptable so mitigation in this case is very important. Ways to reduce the probability are a protective coating and/or layer of protective paint. Scratches would still be a way for moisture to enter the structure even though scratches would be detected during maintenance. The thickness of parts were increased by about 25% to compensate for this (together with a skin thickness increase to compensate for barely visible impact damage and material scatter adding up to an increase of 140%). This would result in a reduction of the consequence. The evolution of this risk can be seen in Figure 20.1 as the blue dots.

2. **Undetected damage**
   Maintenance is performed with regular intervals to inspect for damage but impact damage is not always visible on composite parts due to its low ductility. Inner delamination could be happening without it showing on the surface which results in a weakening of the structure without the maintenance crew even knowing. This could end up to structural failure which is unacceptable. The Q-50 will have aluminium leading edges on its wings, stabilizers and engine inlet to minimize the probability of damage being undetected since these have a higher chance of impact. We will also implement a smart sensing system that detects damage in the structure and forwards this to the maintenance crew on the ground to reduce probability even more. The thickness of the parts have been increased as well to reduce the consequence in the unlikely event that any of the CFRP parts are damaged without anyone knowing. The evolution of this risk can be seen in Figure 20.1 as the red dots.

3. **Electrical failure**
   Power is provided to all systems by the IDGs or the APU in case one or both of the IDGs fail. IDGs are notoriously unreliable (for aviation standards) which is not necessarily a big problem since the APU can compensate for the drop in power supply. Failure of the electrical wiring is also a possibility which could happen when lightning strikes or when some parts suddenly draw a lot of power due to malfunction. When all power suppliers fail or the wiring fails, all control over the aircraft will be lost with fatal results. Surge protectors and circuit breakers are introduced to reduce the chance of wiring burning through and redundant wiring is installed to compensate for the event that the primary wiring fails. A mesh comparable to the one of the smart sensing system is introduced in the skin to guide lightning through the skin without it short-circuiting the entire electrical system. It also helps making the aircraft visible on radar. Suppose both the primary and secondary wiring system fail or the entire power supply fails, the installed Ram Air Turbine (RAT) will deploy and provide the minimum required energy for simple controllability. The evolution of this risk can be seen in Figure 20.1 as the green dots.

4. **Hydraulic failure**
   Hydraulic systems are required to move the control surfaces and are thus very important for the controllability of the aircraft. Fluids are under pressure contained within airtight tubes and casings and driven by pistons. The pressure will diminish or even disappear as soon as the piston does not fit neatly in its casing or there is a leak in the tubing. If this is the case controlling the aircraft is (nearly) impossible. The Q-50 will be outfitted with EHA (Chapter 16) which will drastically reduce the chances of this happening. The evolution of this risk can be seen in Figure 20.1 as the cyan dots.

5. **Tire blowout**
   Wear and tear and runway debris are the main causes of tire blowout. If this happens the aircraft will skid over the runway with increased drag and decreased controllability and in a worst case scenario will end up off the runway. To reduce the consequence of a blowout each landing gear will be outfitted with 2 tires where each tire is able to carry the entire load on the gear if this is required. This way a blowout does

not result in an uncontrollable aircraft. The evolution of this risk can be seen in Figure 20.1 as the yellow dots.

6. **Hostile passenger**
   If one of the passengers has ill intentions for any reason whatsoever he could be able to take over control of the aircraft and do with it what that person desires. Post 9/11 regulations have toughened security regulations to restrict access to the cockpit. We will comply to regulations by introducing a thick and sturdy wall attached to one of the frames right behind the cockpit. This way the pilots cannot be overpowered and are able to land the plane so the hostile passenger can be apprehended. The evolution of this risk can be seen in Figure 20.1 as the magenta dots.

7. **0 visibility landing**
   Weather conditions play a huge role in the possibility of landing the plane. If there is very thick fog for example, the landing strip cannot be seen from a safe distance so approaching safely is hard to do. Often airplanes will be redirected to nearby airports where weather conditions are more favourable. When using the synthetic vision (see Section 16.5.3) a virtual representation of the surrounding area is projected on the screen making redirection obsolete. The evolution of this risk can be seen in Figure 20.1 as the white dots.

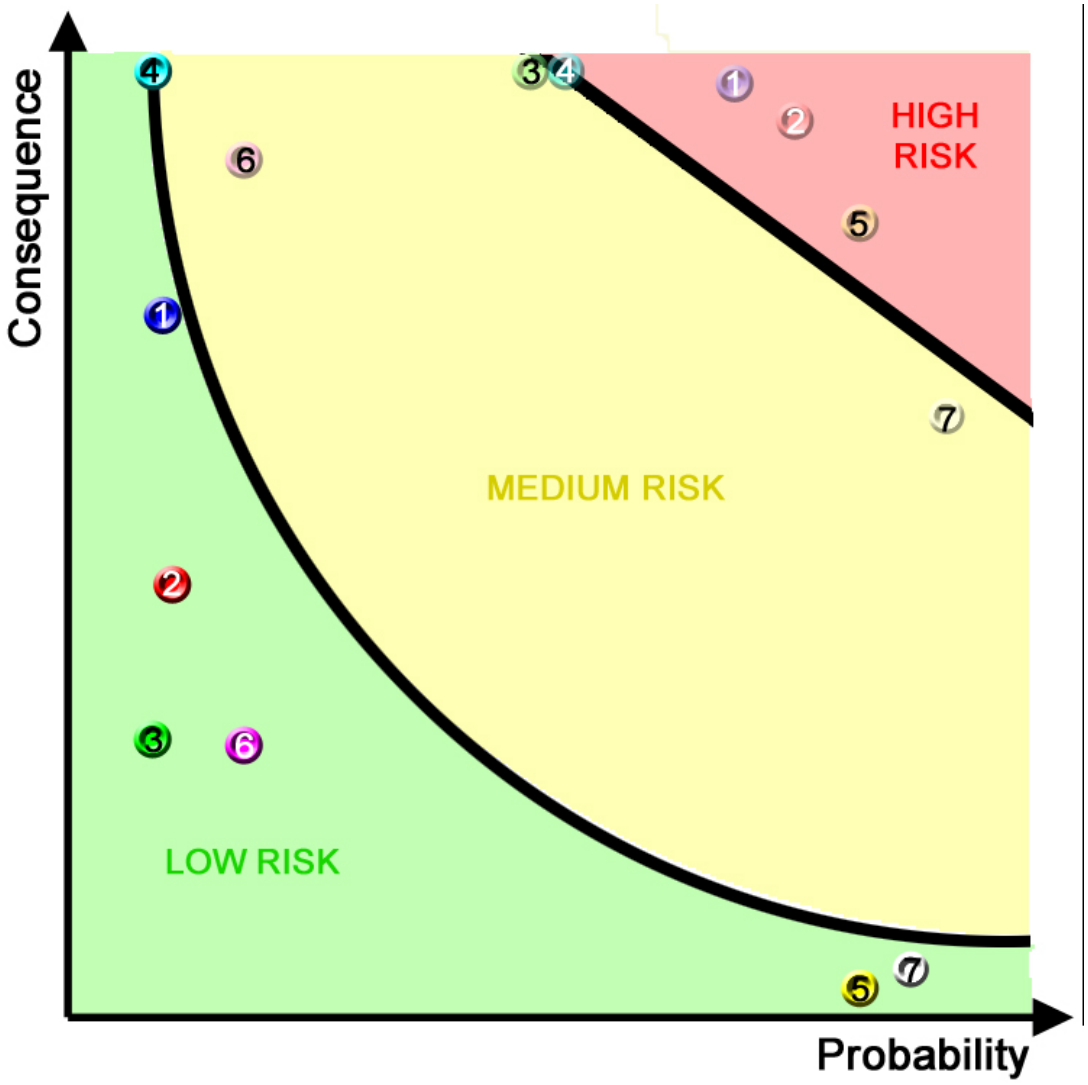

Figure 20.1: The risk map of the previously mentioned risks

20.2 Reliability

Reliability is the probability that a system will perform in a satisfactory manner for a given period of time when used under specified operating conditions [18]. In this section a qualitative analysis of the reliability of

some aircraft subsystems will be made. A fault tree analysis will be made and a reliability block diagram will be made in order to get more insight in the reliability of the system.

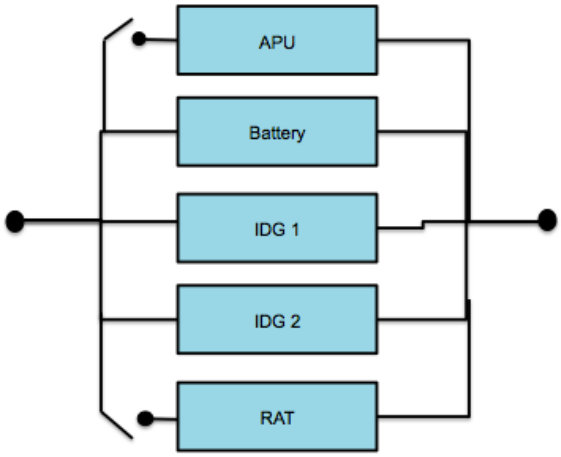

Figure 20.2: Reliability block diagram for the electrical system

20.2.1 Electrical System

The electrical system of the aircraft is crucial in order to keep flying safely. A complete failure of the system, can result in the aircraft being uncontrollable and will lead to a crash. Therefore it is important to have large redundancy in the system. When one part of the system failed, there should be some back up. For the electrical system a reliability block diagram is constructed (figure 20.2). This diagram gives an indication of the redundancy of the system. If the blocks in the diagram are connected in series, it means that if one part of the system fails, the whole system will fail. In figure 20.2 the blocks (which represents part of the electrical system) are connected parallel. A failure in one of the block, does not result in a failure of the entire system. The parts that are connected in the system with a switch (RAT and APU), represent standby (or passive) redundant system. During flight these systems are switched off. However, if one of the active systems fails, these systems can be switched on [1].

20.2.2 Aircraft Structure

The aircraft structure is the core of the aircraft. There are different types of structural failures. Some structural failures have minor consequences. The aircraft is still able to continue to fly and land safely. Structural failures can also be catastrophic. A fault tree analysis is made of a catastrophic structural failure, as can be seen in Figure 20.3.

20.2.3 Propulsion

The propulsion system of the aircraft keeps the aircraft flying. A complete failure of the system would mean that the aircraft should make an emergency landing immediately. Failure of the fuel system and a direct engine failure can lead to a propulsion failure. However, a direct engine failure can be more catastrophic. A fault tree analysis is made of the event of an engine failure (figure 20.4).

[1] www.sars.org.uk/old-site-archive/.../p3c30.pdf

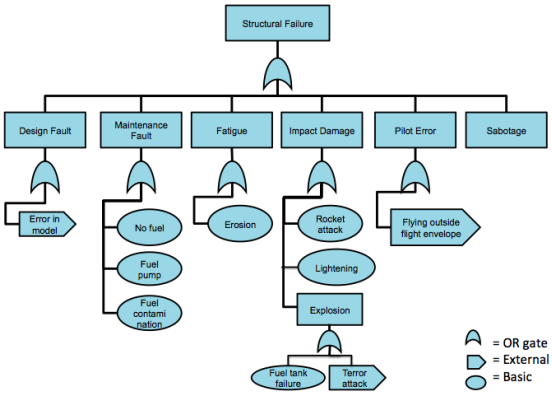

Figure 20.3: Reliability block diagram for the structural system

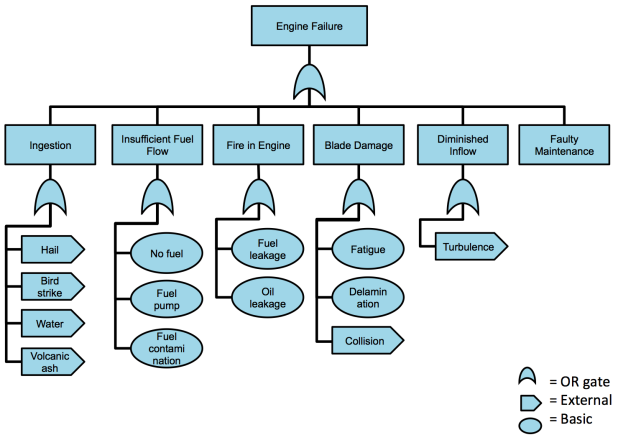

Figure 20.4: Fault Tree Analysis of an engine failure

Production Plan

This section gives an overview of the production process. The layout of the production facility is presented, as well as the logistics and planning.

21.1 Production Philosophy

The design philosophy of the production process revolves around "Lean Manufacturing" as described in the midterm report [1]. Multiple aspects of lean production are applied in the production of this aircraft. An analysis of the production process describes the aspects application to each specific production process. The production process is depicted in 21.1.

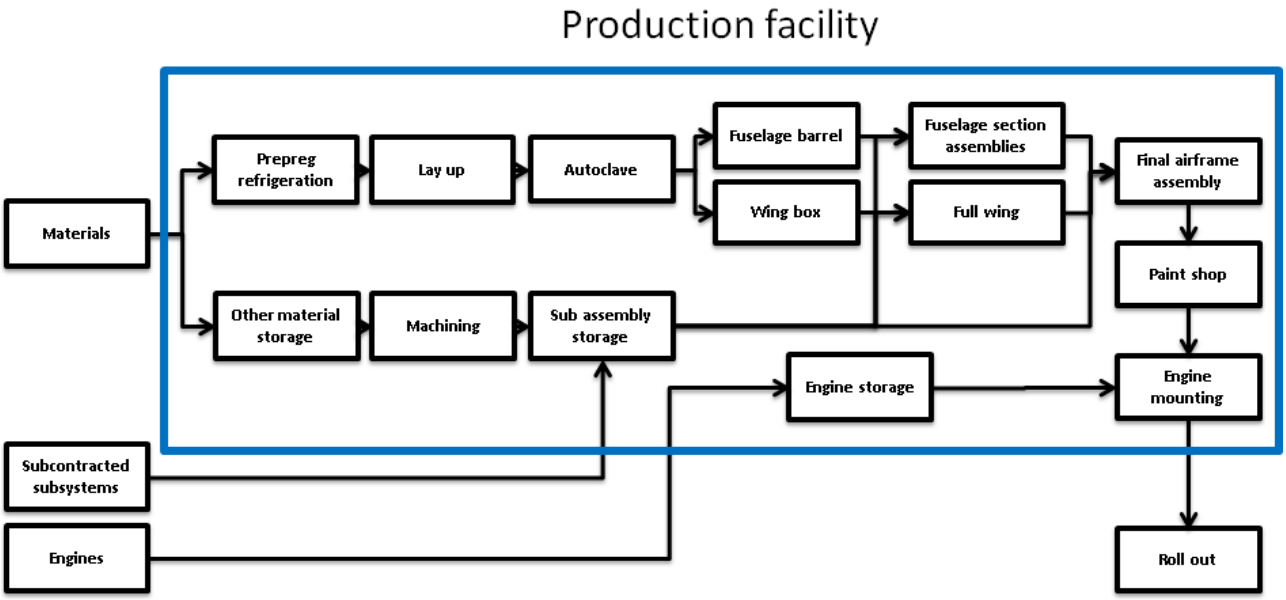

Figure 21.1: Production process overview

21.2 Production Facility

The production of the airframe including final assembly takes place in a centralized facility, as illustrated by the blue rectangle in 21.1. This poses a major increase in sustainability as opposed to a production set-up of the likes of Airbus or Boeing. Outsourcing of sub-assemblies to manufactures around the globe requires (air)transportation to the final assembly line. Transportation could suffer delays and thereby frustrate the production process. The stockpiles required to compensate for delays are wasteful to both space and capital. These problems are mitigated by centralizing production into a single facility where possible.

21.3 Storage and Stockpiling

Storage is essential to the production process as it compensates for any delayed deliveries. However, stockpiling requires storage space, which is considered wasteful as storing an item does not add value to the aircraft. The capital required to purchase these items far in advance is trapped capital. An important example of this trapped capital is engine storage, as the engines are the most capital intensive components of an aircraft. The time between purchase and sale of a certain item is minimized in order to reduce the amount of trapped capital. This corresponds to the "Just in Time" principle. Most parts and subsystems do not have a shelf life that pose an influence on the production process. However, the usage of prepreg composite material has a finite shelf life at room temperature. The delivery interval could be reduced to allow for immediate use of the prepreg strips. This would require frequent, polluting transport. Also, any unforeseen delays in the production process would cause this valuable material to go to waste. The prepreg strips are therefore refrigerated.

21.4 Quality Assurance

Quality assurance is a continuous process during production. It starts with determining whether the materials and subsystems that are delivered to the production facility meet the required standards. At every manufacturing and assembly stages, non-destructive tests are performed. Defects require complete rejection of the affected composite part. This rejection is very costly though unavoidable. The discarded sections can be recycled for use in other applications, see Section 5.2 Small allowances are required for the sections to fit when they are joined during assembly. The jigs used during the manufacturing process also require frequent calibration.

21.5 Layup

The main airframe structures, such as wing sections and fuselage sections, are made of carbon fiber reinforced plastics, supplied as prepreg strips. The process of positioning the prepreg strips is a very delicate one. Most of this layup process consist of repetitive tasks and great surfaces. This allows for automation using an automatic fiber laying machine. This approach reduces human errors and increases the accuracy required for an aerospace application such as this aircraft. The amount of skilled workers is greatly reduced by the use of automation. The narrow shape of the prepreg strips reduces the material waste caused by trimming of the edges of larger sheets.

21.6 Autoclave

The autoclave is one of the largest pieces of machinery of the production line as half of the wing span should fit lengthwise and the full fuselage cross section widthwise. The autoclave is also one of the greatest power consuming appliances since the curing process is performed at elevated temperatures and pressures. The efficiency should be a large consideration for the selection of an autoclave.

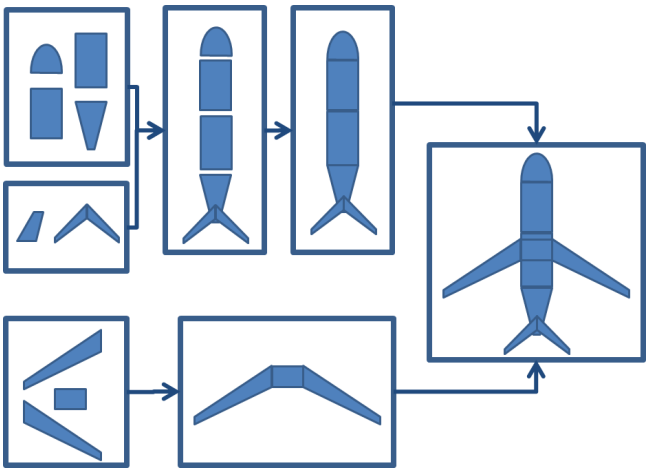

Figure 21.2: Schematic overview of assembly line

21.7 Subsection Assembly

After curing, the wings, stabilizers and fuselages are assembled along separate paths as can be seen in Figure 21.2. This ensures the continuous production of wings even when the fuselage is delayed, and vice versa. Another advantage of this disjoint approach is the increase accessibility of the individual sections. Jigs can allow for the individual sections to change orientation without interference from the other section. Several subsystems are installed at this stage. For the wing, high lift devices, anti-icing systems and control surfaces are installed. The stabilizers are installed on the aft fuselage section. The front section has the flight deck and avionics installed. The fuselage is joined to allow for the installation of wiring and interior. The wing is joined as well to have the full span assembled.

21.8 Final Airframe Assembly

The final stage of airframe assembly is where wing and fuselage meet. The two are joined structurally, electrical wiring installed and lines for both hydraulics and fuel are connected. After installation of the remaining subsystems such as landing gear, the first subsystems are ready for testing.

21.9 Paint Shop

After the complete assembly of the airframe, the bare fuselage and wing surfaces are not protected to the environment and require a coating of paint to prevent water from entering the composite and damaging the fibers. The paint coating allows for outside storage while waiting for engine mounting.

21.10 Engine mounting

The engines are often the last component of the aircraft to be mounted. The great cost of turbofans limits the amount of engines in storage. Installing the engine at the final stages of assembly prevents damage and capital expenses.

21.11 Roll out

Roll out marks the start of ground and flight testing, which is the last step before customer flight proving and delivery. At roll out, the aircraft production is considered complete.

Cost Analysis

All technical and operational aspects of the design of Q-50 have been addressed so far. In this chapter it is time to look at the financial side of the design, based on those aspects, as it should be possible to sell the aircraft at a reasonable price with reasonable operating costs for the potential buyer. In predicting costs, a lot of uncertainties present themselves because the data on which cost estimations are based are kept secret, as aviation is a commercial and competitive business. In this chapter an approach is made to estimate the costs as accurately as possible, and the uncertainties that come with it are examined. At the end of this chapter also a method to predict the return on investment is presented. Before going into detail about the specifics of the calculations, it is recommended to take a look at the cost break-down structures of airplane price and operating costs. They can be found in Appendix E in Figures E.1 and E.2 respectively, each accompanied by a list of abbreviations. The structure is based on the approach presented by Roskam [69], and all further methods and parameters in this chapter (if not noted otherwise) originate from this book. It should also be noted that all costs are on 2014 level, as the requirement was expressed for this level as well. Certain values originate from before 2014 and are corrected with an inflation factor [75].

22.1 Aircraft Unit Price Estimation

The main elements that influence the price of the Q-50, are determined based on statistic relations and therefore some uncertainties present themselves. In a sensitivity analysis, combinations of specific inputs are examined to identify these uncertainties.

As a first estimation, the input values shown in Table 22.1 are used. It must be noted that not all inputs are shown in this table, for example the number of passengers or the labor rates, as these are given facts. The outcome of this combination of input parameters yields a value of almost 24 million dollars unit price per aircraft, which is comparable to values found on the internet for the CRJ-200: 20-25 million (the values are heuristically determined)[1] [2]. The unit cost constraint in this case is 35 million, such that novelties to reduce emissions can be included. Therefore, during the sensitivity analysis it is also examined if these novelties were maybe not taken into account by the method used. In the third column of Table 22.1 the uncertainty level is given and the fourth column explains the source.

Table 22.1: Input values first aircraft price iteration

Input parameter	**Value**	**Uncertainty level**	**Source**
Engine price [mln USD]	4	High	20% of the reference aircraft price of 20 million [76]
MTOW [lbs]	38404	Low	Design outcome
Cruise speed [knots]	470	Low	Design outcome
Material difficulty factor	3	High	Roskam [69]
Prod. rate per month	6	High	CRJ-200 reference [3]
Direct operating cost [USD/nm]	7.7	High	Iterations 22.2
Number of test airplanes	5	Zero	Roskam [69]
CAD experience factor	0.8	Zero	Roskam [69]
Avionics system price [USD]	500 0000	High	Garmin glass cockpit [4]

The take-off weight is assumed to be certain, since it has already undergone multiple iterations. The cruise speed might still change however the change will be small (see Chapter 15). The material factor is a correction factor which depends on the type of materials used in the construction of the airplane and it is used to calculate the cost of the materials. The highest correction factor is 3 and is used for carbon-composite airframes. However the data used in this book often originate from 1970 and therefore the chance is high that the cost of materials is overestimated, since carbon composites used to be very expensive but have become cheaper with time. The production rate during the production phase depends on the market demand and it influences the return on investment. The main goal is that the required return on investment is met. The direct operating cost is also subject to change as it is an iterative process as well, as described in the next section. The number of test airplanes and the Computer Aided Design (CAD) experience factor are assumed fixed, since the testing program has to be sufficient but not more than that and the CAD experience factor

[1] http://www.flightrun.com/bombardier-crj200/price
[2] http://www.aircraftcompare.com/helicopter-airplane/Bombardier-CRJ-200/92

is assumed to be as low as possible which reduces the manhours needed, as CAD experience is a standard these days.

Sensitivity Analysis of the Aircraft Price Estimation

To detect the influence of the uncertainties described above on the total price of the aircraft a sensitivity analysis is performed. The parameters for which the likelihood to change is medium or high, are changed by a factor appropriate to the parameter. The results are shown in Table 22.2.

Table 22.2: Sensitivity analysis of aircraft price

Iteration number	**1**	**2**	**3**	**4**	**5**	**6**	**7**
Engine price [mln USD]	4	2	6	4	4	4	4
Material difficulty factor	3	3	3	1	3	3	3
Prod. rate per month	6	6	6	6	10	6	6
Direct operating cost [USD/nm]	7.7	7.7	7.7	7.7	7.7	4	7.7
Avionics system price [USD]	500,000	500,000	500,000	500,000	500,000	500,000	400,000
Total aircraft price [mln USD]	23.98	18.78	29.17	20.42	24.01	23.90	23.85

It can be concluded that the engine price and the material factor have the biggest influence, after which production rate, avionics system price, and DOC follow. For the material factor, more research can be done to easily estimate a reasonable value. In the materials chapter 10, it is determined to use CFRP composite material which is estimated to have a value of 100 dollar per kg, according to Ir. Fernandez-Villegas. With OEW = 9755 kg, the material cost would approximately be 1 million dollars. Using $F_{mat} = 3$, the method of Roskam estimates the material cost to be 4 million dollars, which seems to be overestimated. When $F_{mat} = 1$ is used, the cost is 1.35 million which is closer to the rough estimation. Therefore it is decided that the material factor should be 1. It is chosen not to downscale the material factor to come to a materials cost of approximately 1 million dollars because it is not totally clear what is included in the material cost predicted by Roskam. For example it could include adhesives and materials such as bolts, which are not taken into account in the rough estimation of 100 dollar per kilogram. The price of the avionics system has an almost direct influence on the aircraft price. The production rate has only a small influence and should be determined on the basis of the return on investment requirement. The same holds for the DOC, as it is very important on its own but it does not influence the unit cost in such a way that a small increase or decrease would cause major issues.

22.2 Operating Cost

The same approach as for the aircraft price is used, where the main inputs are identified and subjected to a sensitivity study to determine their influence and uncertainty. As shown in the break-down structure, the total direct operating cost is divided into the direct operating cost and the indirect operating cost. In this section the direct operating cost will be discussed and examined elaborately, however the indirect operating cost is estimated as a certain percentage of the direct operating cost.

Direct Operating Cost

In Table 22.3 the list of input values for the first estimation is given. The outcome is DOC = 7.26 USD p/nm, or 3,000 USD/p.hr. This means that for one trip with the Q-50 over a range of 1080 nautical miles (= 2000 km) the operational costs yield 7,840 USD. To validate that this is a reasonable outcome, it was compared to a direct operating cost analysis of the CRJ-200 and the ERJ-145 [6], a program supported by many operators. The study shows that the hourly cost for the owner to operate a CRJ-200 is 3,759 dollars and 3,931 for the ERJ-145. It must be noted that this includes indirect operating costs as well. The conclusion that can be taken from this is that the indirect operating cost should not be more than 25% of the total operating cost. If this is achievable is explained in section 22.2. To examine the sensitivity of the DOC with respect to the input values, six iterations are performed. The results are shown in Table 22.4. The sensitivity analysis shows that the aircraft and engine price have high influence on the direct operating cost (because of their depreciation cost), the avionics system price shows only small influence. It can also be seen that a reduction

[6] https://www.aircraftcostcalculator.com/

Table 22.3: Input values first DOC iteration

Input parameter	Value	Uncertainty level	Source
Aircraft price [mln USD]	23.98	High	Iteration 22.1
Engine price [mln USD]	4	High	See Table 22.1
Avionics system price [USD]	500,000	High	See Table 22.1
MTOW [lbs]	38404	Low	Design outcome
Block speed [knots]	413	Low	Design outcome
Block time [hrs]	2.6	Low	Design outcome
Fuel cost [USD/gallon]	1.79	Low	IATA[5]
Fuel weight [lbs]	5886	Low	Design outcome
Maintenance cost [USD/nm]	2.09	Medium	CRJ-200 [77]

Table 22.4: Sensitivity analysis of direct operating costs

Iteration number	1	2	3	4	5	6
Aircraft price [mln USD]	23.98	18.78	35	23.98	23.98	23.98
Engine price [mln USD]	4	4	4	6	4	4
Avionics system price	500,000	500,000	500,000	500,000	400,000	500,000
Maintenance cost [USD/nm]	2.09	2.09	2.09	2.09	2.09	1.5
Direct operating cost [USD/nm]	7.26	6.85	8.12	7.66	7.25	6.66

in the maintenance cost causes a direct reduction in the operational costs. The maintenance cost is likely to change because of the large use of composite material, which is cheaper in maintenance 19.3.

Indirect Operating Cost

It is estimated that DOC = 0.564 TOC and IOC = 0.436 TOC yielding IOC = 5.6 USD/nm, see Figure E.3 in Appendixt E [72]. This is an average estimation, and therefore is subject to change. For example the passenger service could be limited if low-budget is the marketing strategy, which will reduce the IOC. It can be concluded from this that with the initial found direct operating cost, the total operating cost will be more that its competitors. In future design phases therefore, the direct operating cost calculation method should be revised and reduced.

22.3 Return on Investment for QLEAR Company

As was determined in Chapter 4, QLEAR wants to bring 805 Q-50 aircraft on the market. The question is, from the research phase onwards, how long does it take for QLEAR to get a return on the investment? The return on investment is computed by:

$$RoI = \frac{N_{mnth} N_{r_m} AEP - Investment}{Investment} \cdot 100\% \tag{22.1}$$

Where in this case the time span in which these parameters are evaluated is 5 years, since the requirement states that the return on investment should be 5% after 5 year. The aircraft price is assumed independent of the number of years that have passed. N_{mnth} indicates the number of months that have gone by, in this case $5 \cdot 12$ is 60 months, and N_{r_m} is the manufacturing production rate per month as mentioned in the sensitivity analysis of the aircraft price estimation. The production rate assumed in the first iteration of the aircraft price, was estimated to be 6 per month. The investment is calculated as follows:

$$Investment = C_{RDTE_{non-profit}} + N_{mnth} N_{r_m} \frac{C_{MAN}}{N_m} \tag{22.2}$$

Where the first iteration for the aircraft price yields $C_{RDTE_{non-profit}}$ = 0.863 billion dollars and C_{MAN} = 16.67 billion dollars, for the entire program. N_m is the number of aircraft produced in the manufacturing phase, which is 805. With these values the first iteration for the return on investment would be 3.74%, which means that it does not meet the requirement. As stated before there are lots of uncertainties present in the cost calculation and therefore the return on investment calculation is highly uncertain. Assuming that the initial values are good estimates, the return on investment requirement can be met by increasing the production rate. After some iterations it is found that at least 410 aircraft should have been produced and sold after 5 years, leading to a required production rate of 6.9 aircraft a month and a return of investment of 5.05%.

Table 22.5: Recommended final input values for aircraft price

Input parameter	Value
Engine price [mln USD]	7
Material difficulty factor	1
Prod. rate per month	6.17
Direct operating cost [USD/nm]	7.53
Avionics system price [USD]	500,000

Table 22.6: Recommended input values for operating cost

Input parameter	Value
Aircraft price [mln USD]	28.19
Engine price [mln USD]	7
Avionics system price [USD]	500,000
Maintenance cost [USD/nm]	1.5
Indirect operating cost fraction	0.37

22.4 Recommended Inputs

The conclusion that can be drawn from this chapter is that the cost estimation process is a complex process, dealing with a lot of uncertainties and many interacting components as for example the aircraft price depends on the direct operating cost, and the direct operating cost on the aircraft price. Based on the discussion of the most influential input parameters, sets of input values for the aircraft price and operating cost estimations are recommended and shown in Tables 22.5 and 22.6 respectively. Unfortunately, it is still a given fact that these estimations are not highly accurate and changes will present themselves in future design phases. The engine price is recommended to be estimated at 7 million dollars, as the previously estimated aircraft price is far below the requirement and this discrepancy could be used for the development of highly efficient, innovative engines. As discussed before, the material price according to the Roskam method was over estimated and therefore the material factor is recommended to be set to 1. To meet the return on investment requirement, the production rate should be 6.17. The direct operating cost is 7.53 USD/nm because of the increase in aircraft and engine price and a reduction in maintenance cost, see Table 22.6. The avionics system price is recommended to stay 500,000 dollars as there are no clear indications whether this will decrease or increase for the Q-50 design. Therefore, the aircraft price is estimated at 28.19 million dollars. The maintenance cost is recommended to be estimated a fraction of 30% lower than for the CRJ-200, because the Q-50 is mainly made out of composite material. The indirect operating cost is recommended to be 37%, assuming a budget airline, to decrease the total operating costs because they are reasonably high. This yields a direct operating cost of 7.53 USD/nm, an indirect operating cost of 5 USD/nm and a total operating cost of 13.35 USD/nm.

Lastly, it is recommended to extend the research extensively for the main input parameters to decrease the uncertainties. Especially the operating cost needs more attention as the outcome is high when compared to competitors. As a way to decrease uncertainties, one could think of the possibility to for example contact an avionics systems business to make an offer.

Noise and Emissions

23.1 Noise

There are three main contributors to aircraft noise, engine, landing gears, and high lift devices. It is however complicated to fully predict the noise for each of these subsystems. There are several noise countering measures taken in this design all with a given noise decrease, however this decrease in dB cannot be accumulated. Because dB are a logarithmic scale they can't be added and it is important from what baseline they are taken. Therefore the values given in this chapter of not a definitive number, but they give an indication of the possible savings.

23.1.1 Landing Gear Noise

When the landing gear is extended, they are not only a large source of drag but it also contributes to the noise. The struts and the wheels have a wake which produces noise. But the the smaller exposed parts are also prone to noise production.[78] To predict the noise of all the separate components with the current models is prone to uncertainties. In aircraft with fixed gears the wheels and struts are often covered with profiles. These kind of landing gear fairings will also be used on this design. The wheels will not be covered but the struts and main axle housing will have a low drag fairing. This will cover all pipes and linkages. The shape is not yet determined but will most likely have a airfoil shape to reduce the drag a much as possible, and reduce vortices to a minimum. Is has been shown that in the mid frequency range a solid fairing for the landing gear can save up to 4.5 dB in noise.[79] Furthermore, when the landing gear is deployed and the doors are kept open, there is a 2 dB higher sound pressure compared to closed landing gear doors with extended gears. This requires a slightly more complex design, and is especially challenging in this design because of the relatively small landing gear compared to wing mounted aircraft.

23.1.2 Engine Noise

The gasses that are expelled from a jet engine have a high temperature compared to the surrounding air. This creates vortices and turbulent air. This turbulent air contains more energy which emits in noise [80]. This engine will use a larger fan with vanes behind the fan to counter vortices and therefore noise. Another feature for this engine are the chevrons [81]. The chevrons promote better hot and cold gas mixing which means less turbulent flow. It does have the downside of a slight loss in thrust. However the thrust loss is around 1% and the decrease in noise is 3dB, and therefore very promising [82]. To determine the engine noise from the jet stream, or core section, the jet velocity has to be known as well as the cross sectional area and temperature. However the calculations are not accurate. It does give an indication on the savings. Experiments have shown that halving the jet velocity yields a 24dB saving [80]. This is however very large and the experiment is already quite old. Beside the sound pressure the sound frequency is influential on the perceived noise levels. Determining the frequencies for the flow is a lengthy calculation and a study on its own, however vibrations in turbomachinery is something that can be combated.

The turbomachinery noise follows from the part not moving fully frictionless. Jet engines have very little moving parts compared to piston engines and the parts that move only have little friction surfaces and therefore the part noise is very little compared to the turbulent air noise for example. Using high-end bearings and better lubrication. Equally improved production methods allow for smaller tolerances which reduces the vibrations in the system.

Lastly the combustion noise of the engine. This noise is harder to get rid off. Although for most cases it is not the primary source of the noise [83, 80]. During low jet velocities the core noise is however the main contributor [80]. In order to damp the sound from the combustors a sound absorbing material. Most likely it will be a honeycomb-like structures covered with a porous cover in form of perforated metal plates or wire meshes [82]. No material is known yet, because the operating conditions are not fully known, and therefore, the choice of a specific material is postponed.

23.1.3 High Lift Devices

Flaps are a major contributor to noise. The configuration on this aircraft is not beneficial for noise. Slats are often a source of noise and this design uses full span wise slats. However it is not possible to go without them because of the required maximum lift coefficient. The main source for slat noise originates from the cove behind the slat. This cove creates vortices and thereby noise. Covers are implemented to create a smoother surface and transition from slat to main wing. These covers offers a sound pressure reduction of 2-4 dB and a change in frequency [84]. Equally on the trailing edge the double slotted flaps are a source of noise. The

flow coming of the trailing edge is the unsteady flow coming of the flaps [80]. It is also believed that the edge of the flaps creates vortexes which interact with the flow of the wing without the flaps and creates a lot of noise [78].

23.2 Emissions

The emissions requirement is met at two stages, the aircraft emissions but also the emissions in the production facilities of the aircraft.

23.2.1 Engine Emissions

Using the GSP 11 gas turbine software two engine models have been examined. One with the intended intercooler and one without (Chapter 12). The program shows that the intercooler gives a 25% reduction in NOx emissions. A desired reduction in CO and unburned hydrocarbons is achieved by better compressors with higher pressure ratios and a larger bypass ratio. This all to keep the fuel consumption low. This low fuel consumption is also made possible by the low weight and low drag. Because of the low weight and drag, little thrust is needed during cruise which reduces fuel consumption. The fuel consumption can be reduced by 49% compared to the ERJ-145 because of the improved pressure ratios.

The engines will use a blend of biofuels combined with normal kerosene. The biofuels are CO_2 neutral since they are made of organics which consume CO_2 during their lifetime. This will result in another reduction in emissions. Quantification is difficult because most of the fuel compositions are classified and therefore it is difficult to determine the reaction products when burned, though tests have shown improvements [85].

23.2.2 Facility Emissions

Not only the aircraft improves environment friendliness, the production facilities and offices make improvements as well. First of all the larger surfaces will be fitted with solar panels to cover the first part of electrical needs. Furthermore all exhausts where fossil fuels are burned, like the heating or ovens, will be fitted with a catalyst to filter the exhaust fumes and further reduce emissions.

Combining all the above mentioned actions, the required reductions in emissions and noise are to be met. Although definitive values are missing the given reductions of the individual improvements are a good indication of the possible end result.

Requirements Compliance Matrix & Feasibility Analysis

After the aircraft is completely designed, it is time to check if all the requirements set in the beginning of the process are met. If they are not met, also the reason has to be know, to be able to understand the impact of the failure. The requirements compliance matrix is a table containing all requirements and indicates with a tick mark, if the requirement is met or not. In the next row, the actual value is shown, after which the section is shown, where this requirement value is expressed. The rationale why the design does not meet the requirement, or which modifications would be required in order to meet the requirement is explained in the second section (Feasibility Analysis).

24.1 Compliance Matrix

As explained, the compliance matrix contains the list of requirements, which has to be met by the design. The compliance matrix can be seen in Table 24.1. The full requirement list can be found in Appendix D. In the table, the labels shown in the first column, represent certain requirement as can be found in the full requirements list. Note that the certification requirements are not shown in the table, since this is a extended list, where during the initial design less attention is payed to.

Table 24.1: Compliance matrix

Requirement	Achieved	Value [unit]	Section
AeP-1: $C_{L_{max}}$			
AeP-1.a: $cruise$	√	1.7	9.2
AeP-1.b: $take-off$	√	1.9	14.1.1
AeP-1.c: $landing$	√	2.5	14.1.1
AeP-2: C_D	√	0.021	15.1.1
AeP-2.a: C_{D_0}	√	0.015	15.1.1
AeP-2.b: Oswald factor (e)			
AeP-2.b.1: $cruise$	√	0.83	App A
AeP-2.b.2: $landing$	√	0.80	App A
AeP-3: L/D			
AeP-3.1: $cruise$	**X**	17.3	15.1.2
AeP-3.2: $take-off$	√	14.0	15.3
AeP-3.3: $landing$	√	8.1	15.4
AFP-2: Range	√	2000 km	not in report
AFP-3: Mach number	√	M 0.81	15.1.1
AFP-4: Altitude	√	10278 m	15.1.1
AFP-5: Landing distance	√	1456 m	15.4
AFP-6: Take-off distance	√	1267 m	15.3
AFP-7: Long. stability	√	-	13.2
AFP-8: Lat. stability	√	-	13.3
AFP-9: Rate Of Climb	√	13 m/s	15.2
AFP-10: Climb Gradient	√	19 %	15.2
PS-1: Max. thrust	√	55 kN	6.4
PS-2: SFC	√	0.34	12.3
PS-3: $Noise_{to}$	?	?	-
PS-4: $Noise_{la}$	?	?	-
PS-5: $Noise_{sl}$	?	?	-
PS-6: $Emission_{CO_2}$	√	50%	23.2
PS-7: $Emission_{NO_x}$	√	25%	23.2
WP-1: MTOW	√	17,425 kg	7.3
WP-1.1: OEW	√	9755 kg	7.3
WP-1.2: PW	√	5000 kg	7.3
WP-1.3: FW	√	2670 kg	7.3
WP-2: MLW	√	-	-

Continued on next page

Continued from previous page

Requirement	Achieved	Value [unit]	Section
Siz-1: PAX	√	50	8.2
Siz-2: Seat pitch	√	31 ¨	8.2
Siz-3: Cabin height	√	1.85 m	8.2
Siz-4: Cargo	√	800 kg	8.2
Siz-5: Aisle width	√	0.41 m	8.2
Op-1: Service	√	2022	Chp 25
Op-2: Cost	√	USD 28.19 million	22.4
Op-3: ROI	√	5.03 %	22.3
Op-4: Parking area	√	30x25	19.1.2
Op-5: Radar	√	-	20.1

Almost all requirements are met, as can be seen in the matrix. For the one which are not met or available, an explanation is given in the next section.

24.2 Feasibility Analysis

As can be seen in the compliance matrix, the L/D requirement during cruise is not achieved. However, the difference is small and the value is still sensitive to changes, since the detailed sizing is still in a preliminary state. So, it is likely that the requirement will be achieved in a later stage. Changes with respect to wing design can result in this achievement. Unfortunately, the acoustic emissions are unquantified at this stage, since it is very hard to determine the right values at this stage of the design. More additional research and testing should be conducted to be able to come up with real and reliable values for the noise reduction. It can be assumed, that a reduction of 10 dB is a reasonable value. All the other requirements are met and have realistic values, which confirms the right heading during the design.

Future of QLEAR Q-50

As soon as the design phase of the aircraft is done, QLEAR Q-50 needs to be produced. This chapter provides an outline on the tasks that need to be carried out before the aircraft is able to enter into service. The Gantt chart in Figures 25.1 - 25.2 covers the period immediately after the end of the DSE and up to the aircraft delivery to the airlines. Also, a Work Flow Diagram is shown in Figure 25.3.

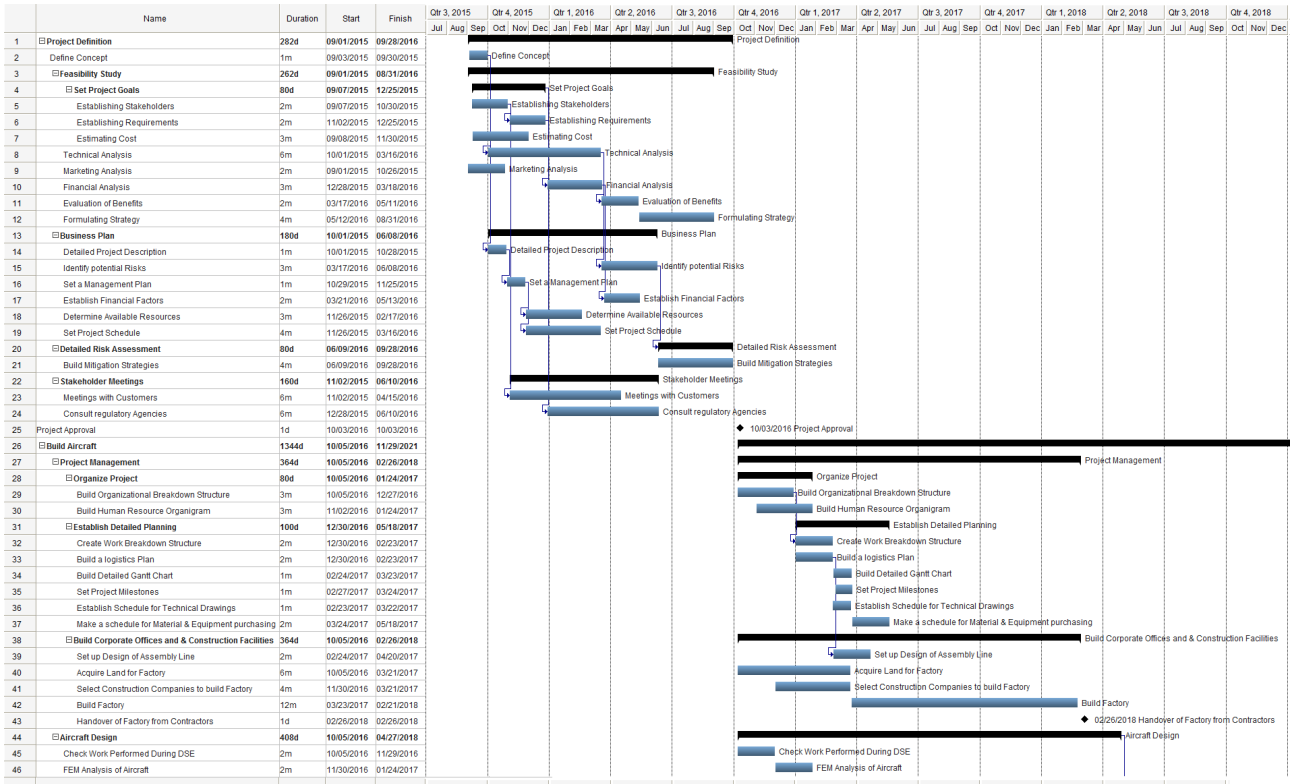

	Name	Duration	Start	Finish
1	**Project Definition**	**282d**	**09/01/2015**	**09/28/2016**
2	Define Concept	1m	09/03/2015	09/30/2015
3	**Feasibility Study**	**262d**	**09/01/2015**	**08/31/2016**
4	**Set Project Goals**	**80d**	**09/07/2015**	**12/25/2015**
5	Establishing Stakeholders	2m	09/07/2015	10/30/2015
6	Establishing Requirements	2m	11/02/2015	12/25/2015
7	Estimating Cost	3m	09/08/2015	11/30/2015
8	Technical Analysis	6m	10/01/2015	03/16/2016
9	Marketing Analysis	2m	09/01/2015	10/26/2015
10	Financial Analysis	3m	12/28/2015	03/18/2016
11	Evaluation of Benefits	2m	03/17/2016	05/11/2016
12	Formulating Strategy	4m	05/12/2016	08/31/2016
13	**Business Plan**	**180d**	**10/01/2015**	**06/08/2016**
14	Detailed Project Description	1m	10/01/2015	10/28/2015
15	Identify potential Risks	3m	03/17/2016	06/08/2016
16	Set a Management Plan	1m	10/29/2015	11/25/2015
17	Establish Financial Factors	2m	03/21/2016	05/13/2016
18	Determine Available Resources	3m	11/26/2015	02/17/2016
19	Set Project Schedule	4m	11/26/2015	03/16/2016
20	**Detailed Risk Assessment**	**80d**	**06/09/2016**	**09/28/2016**
21	Build Mitigation Strategies	4m	06/09/2016	09/28/2016
22	**Stakeholder Meetings**	**160d**	**11/02/2015**	**06/10/2016**
23	Meetings with Customers	6m	11/02/2015	04/15/2016
24	Consult regulatory Agencies	6m	12/28/2015	06/10/2016
25	Project Approval	1d	10/03/2016	10/03/2016
26	**Build Aircraft**	**1344d**	**10/05/2016**	**11/29/2021**
27	**Project Management**	**364d**	**10/05/2016**	**02/26/2018**
28	**Organize Project**	**80d**	**10/05/2016**	**01/24/2017**
29	Build Organizational Breakdown Structure	3m	10/05/2016	12/27/2016
30	Build Human Resource Organigram	3m	11/02/2016	01/24/2017
31	**Establish Detailed Planning**	**100d**	**12/30/2016**	**05/18/2017**
32	Create Work Breakdown Structure	2m	12/30/2016	02/23/2017
33	Build a logistics Plan	2m	12/30/2016	02/23/2017
34	Build Detailed Gantt Chart	1m	02/24/2017	03/23/2017
35	Set Project Milestones	1m	02/27/2017	03/24/2017
36	Establish Schedule for Technical Drawings	1m	02/23/2017	03/22/2017
37	Make a schedule for Material & Equipment purchasing	2m	03/24/2017	05/18/2017
38	**Build Corporate Offices and & Construction Facilities**	**364d**	**10/05/2016**	**02/26/2018**
39	Set up Design of Assembly Line	2m	02/24/2017	04/20/2017
40	Acquire Land for Factory	6m	10/05/2016	03/21/2017
41	Select Construction Companies to build Factory	4m	11/30/2016	03/21/2017
42	Build Factory	12m	03/23/2017	02/21/2018
43	Handover of Factory from Contractors	1d	02/26/2018	02/26/2018
44	**Aircraft Design**	**408d**	**10/05/2016**	**04/27/2018**
45	Check Work Performed During DSE	2m	10/05/2016	11/29/2016
46	FEM Analysis of Aircraft	2m	11/30/2016	01/24/2017

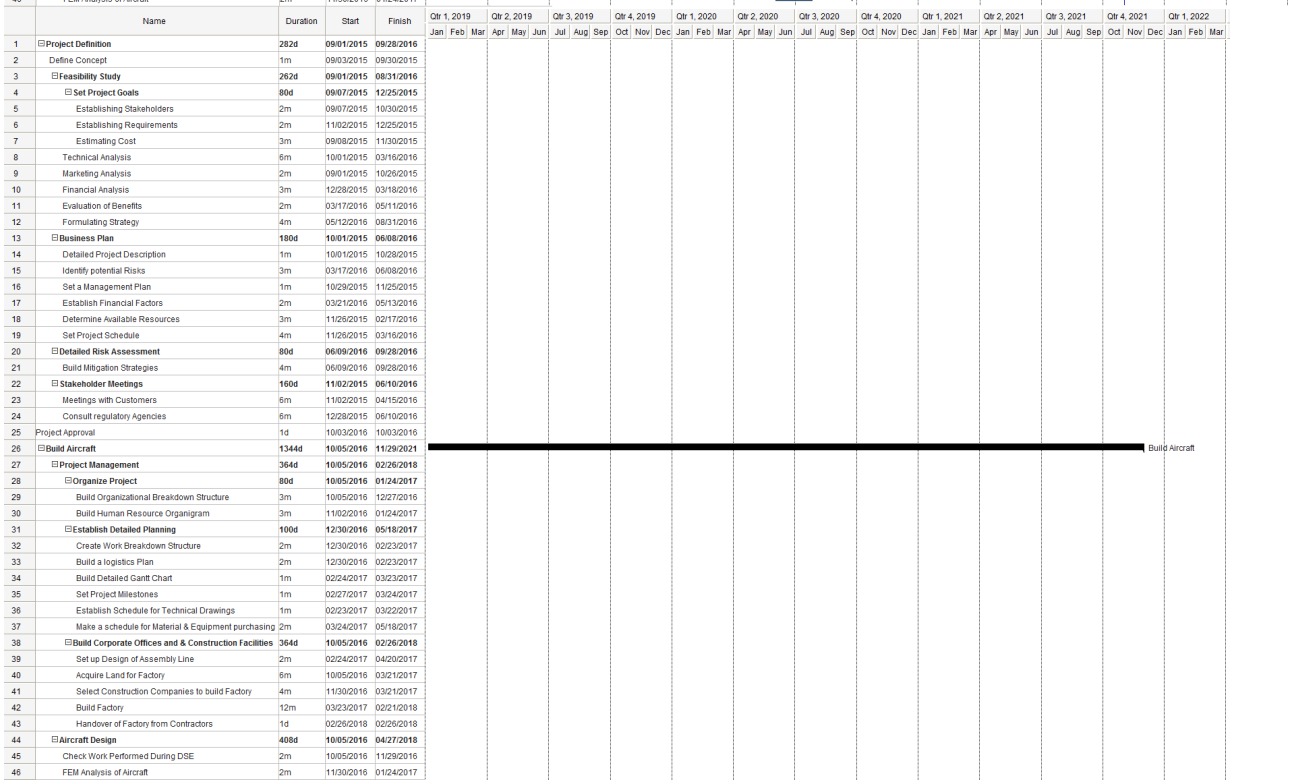

	Name	Duration	Start	Finish
1	**Project Definition**	**282d**	**09/01/2015**	**09/28/2016**
2	Define Concept	1m	09/03/2015	09/30/2015
3	**Feasibility Study**	**262d**	**09/01/2015**	**08/31/2016**
4	**Set Project Goals**	**80d**	**09/07/2015**	**12/25/2015**
5	Establishing Stakeholders	2m	09/07/2015	10/30/2015
6	Establishing Requirements	2m	11/02/2015	12/25/2015
7	Estimating Cost	3m	09/08/2015	11/30/2015
8	Technical Analysis	6m	10/01/2015	03/16/2016
9	Marketing Analysis	2m	09/01/2015	10/26/2015
10	Financial Analysis	3m	12/28/2015	03/18/2016
11	Evaluation of Benefits	2m	03/17/2016	05/11/2016
12	Formulating Strategy	4m	05/12/2016	08/31/2016
13	**Business Plan**	**180d**	**10/01/2015**	**06/08/2016**
14	Detailed Project Description	1m	10/01/2015	10/28/2015
15	Identify potential Risks	3m	03/17/2016	06/08/2016
16	Set a Management Plan	1m	10/29/2015	11/25/2015
17	Establish Financial Factors	2m	03/21/2016	05/13/2016
18	Determine Available Resources	3m	11/26/2015	02/17/2016
19	Set Project Schedule	4m	11/26/2015	03/16/2016
20	**Detailed Risk Assessment**	**80d**	**06/09/2016**	**09/28/2016**
21	Build Mitigation Strategies	4m	06/09/2016	09/28/2016
22	**Stakeholder Meetings**	**160d**	**11/02/2015**	**06/10/2016**
23	Meetings with Customers	6m	11/02/2015	04/15/2016
24	Consult regulatory Agencies	6m	12/28/2015	06/10/2016
25	Project Approval	1d	10/03/2016	10/03/2016
26	**Build Aircraft**	**1344d**	**10/05/2016**	**11/29/2021**
27	**Project Management**	**364d**	**10/05/2016**	**02/26/2018**
28	**Organize Project**	**80d**	**10/05/2016**	**01/24/2017**
29	Build Organizational Breakdown Structure	3m	10/05/2016	12/27/2016
30	Build Human Resource Organigram	3m	11/02/2016	01/24/2017
31	**Establish Detailed Planning**	**100d**	**12/30/2016**	**05/18/2017**
32	Create Work Breakdown Structure	2m	12/30/2016	02/23/2017
33	Build a logistics Plan	2m	12/30/2016	02/23/2017
34	Build Detailed Gantt Chart	1m	02/24/2017	03/23/2017
35	Set Project Milestones	1m	02/27/2017	03/24/2017
36	Establish Schedule for Technical Drawings	1m	02/23/2017	03/22/2017
37	Make a schedule for Material & Equipment purchasing	2m	03/24/2017	05/18/2017
38	**Build Corporate Offices and & Construction Facilities**	**364d**	**10/05/2016**	**02/26/2018**
39	Set up Design of Assembly Line	2m	02/24/2017	04/20/2017
40	Acquire Land for Factory	6m	10/05/2016	03/21/2017
41	Select Construction Companies to build Factory	4m	11/30/2016	03/21/2017
42	Build Factory	12m	03/23/2017	02/21/2018
43	Handover of Factory from Contractors	1d	02/26/2018	02/26/2018
44	**Aircraft Design**	**408d**	**10/05/2016**	**04/27/2018**
45	Check Work Performed During DSE	2m	10/05/2016	11/29/2016
46	FEM Analysis of Aircraft	2m	11/30/2016	01/24/2017

Figure 25.1: Gantt Chart (1/2) for the period after the DSE ending

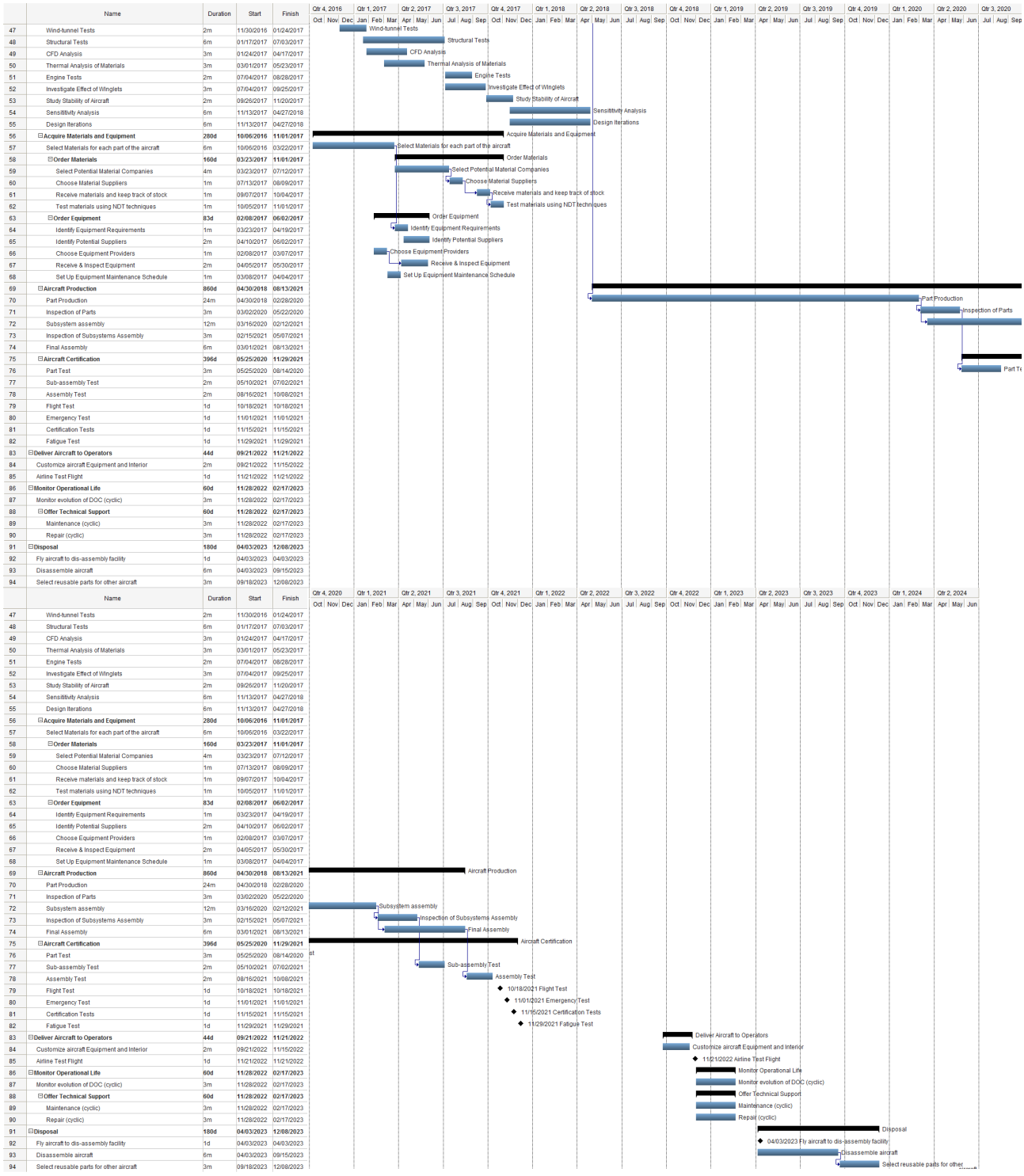

Figure 25.2: Gantt Chart (2/2) for the period after the DSE ending

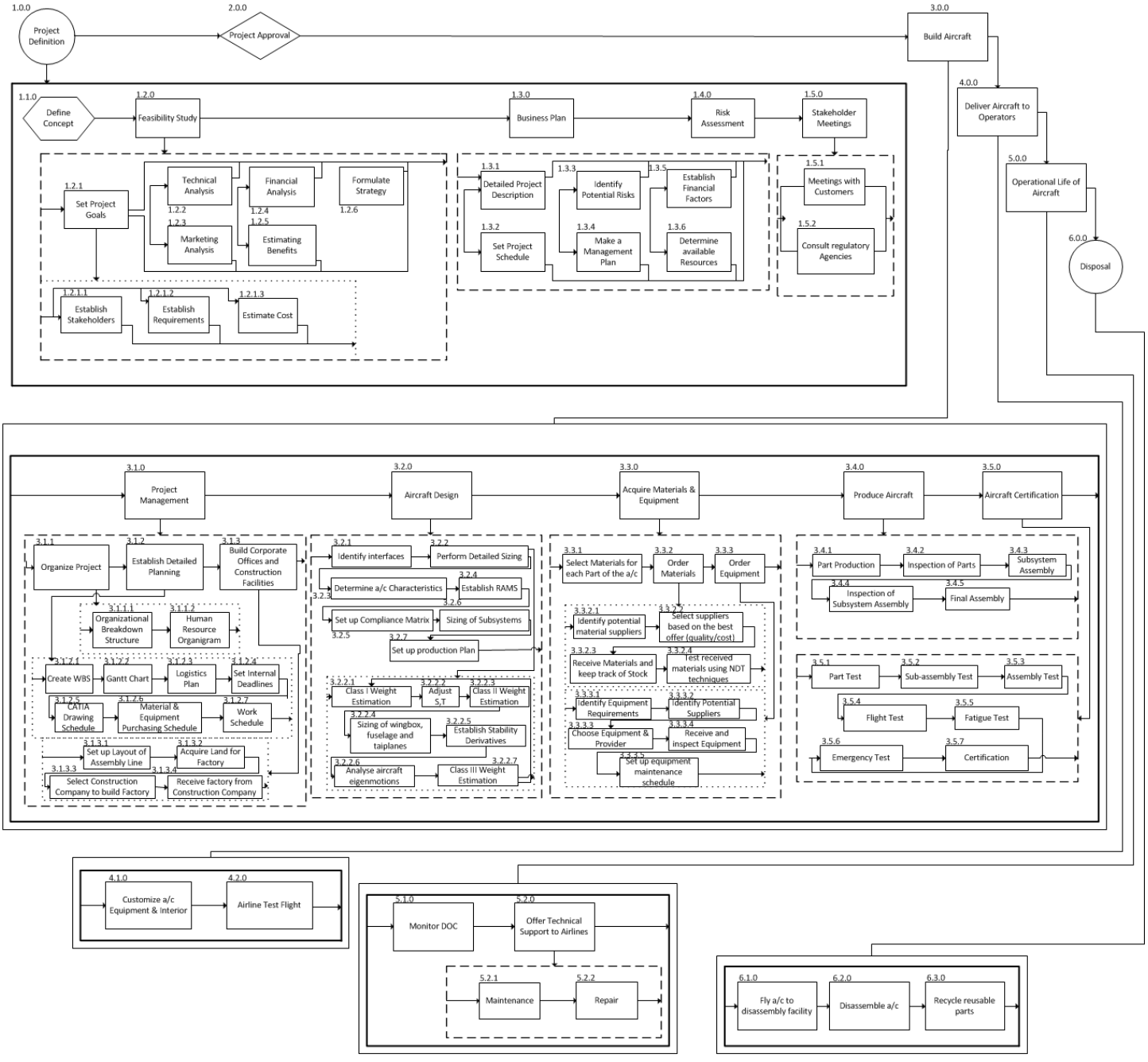

Figure 25.3: Work Flow Diagram for future development of Q-50

Conclusion and Recommendations

26.1 Conclusion

The Design Synthesis Exercise had very clear and fixed requirements regarding emissions which were not to be altered. The design of the aircraft started based on these and other, more flexible requirements. For things to run smoothly everyone in the team was assigned to a specific technical and organizational task and guiding tools were used, such as a Gantt and N2 chart, as a means to provide an overview.

The 50-seater market is diminishing, while the 70-seater is emerging. With the Q-50, QLEAR has the aim to revive the 50-seater market. A market analysis was performed to get acquainted with the competition and compare our flexible requirements with their specifications and alter where deemed fit. For example the ceiling and cruise speed have been raised and the range has been shortened. Following these requirements one design out of 16 different concepts was elected after going through several trade-offs and weight estimations. This final design has been designed in as much detail as possible and has been presented in this report as the QLEAR Q-50.

With an increase in air transportation the next years, strict requirements on CO_2, NO_x and acoustic emission where set. The Q-50 boasts a lot of technologies to achieve these reductions such as massive use of CFRPs, detailed custom designed engines for increased efficiency, an optimized airfoil suited to the cruise phase and a high climb rate to be able to reach cruise altitude in a relatively short time. Using these technologies, a reduction of 50% CO_2 and 25% NO_x emission is achieved, which is compliant with the set requirements. An reduction of 10dB in noise is expected, by using chevrons, landing gear fairings and slat cove covers. However, at this stage it is not possible to exactly quantify this noise reduction without performing actual tests.

The Q-50 has a conventional design which facilitates certification but uses a windowless fuselage to decrease weight and construction time and costs. OLED screens on the interior show a live stream of the surroundings as an alternative. They will also be used to show flight information, points of interest and advertisements if so desired by the operator. The use of composites reduces the aircraft weight. Although like metals, composites do not show fatigue and corrosion, they require an extensive maintenance program. Maintenance cost are saved by using a condition based maintenance policy.

Black metal design offers a preliminary design of the structures, which may lead to an over design of the fuselage structure. Further optimization of the carbon fiber lay ups will lead to a better design. The carbon fiber weave direction is strongly dependent on the shape of the structure, its purpose and the loads it has to withstand. Furthermore, modelling the wingbox and the tailbox as a tapered rectangular box gives a a good design for the structures. However, in reality the wing- and tailbox will show better performance as because of the camber of the top and bottom cover of the boxes.

Having parking dimensions of 30 by 25 meters, the Q-50 it able to park at nearly all regional airports. The compact size enables easy loading of passengers and luggage resulting in a quick turn-around time of only 22 minutes which can be reduced to 20 depending on the level of service offered.

QLEAR cares about how the Q-50 is produced and how it will be handled at the end of its life. That is why the facilities will be coated with titanium dioxide (TiO_2) to render oxides of nitrogen harmless and we will be using zeolites impregnated with polyethylenimine (PEI) to capture CO_2 from our smokestacks. The production line will also be applying the lean manufacturing system to maximize sustainability. Furthermore is the Q-50 fully recyclable assuming research for recycling techniques does not grind to a halt.

This exceptionally sustainable aircraft will be available in 2035 for the price of USD 28.2 million, far below the imposed maximum of USD 35 million.

26.2 Recommendations

Now that the project is finished it is time to reflect on what has been done the past 11 weeks, what has been achieved and most importantly what has been learned. Considering the team consisting of 9 BSc students and time was limited, there were things that were not covered due to time constraints or due to lack of knowledge. Throughout the entire project assumptions and simplifications were made as to be able to get everything done in the limited amount of time. In this section the some recommendations for further analyses are discussed.

Aerodynamics

- Use Computational Fluid Dynamics (CFD) for better airflow simulation.
- Design a new airfoil for the Q-50.

- Investigate the options of noise prevention regarding the High Lift Devices.
- Flight tests to determine the final performance of the winglets.

Materials & Structures

- Test material samples to determine the exact properties in non-laboratory environments.
- Determine detailed weight savings by going windowless.
- Determine specific fibre orientation instead of using the Black Metal Approach (possible 20% weight reduction)
- Implement Carbon NanoTube Metal Matrix Composites (CNT-MMC).
- Design the ribs in detail.
- Design the frames in detail.
- Design the floor beams and supports.
- Design the interior.
- Investigate and design for wingbox - fuselage interaction.
- Investigate and design for sensing skin - lightning mesh interaction.

Propulsion

- Fan design for optimal performance and noise.
- Design the combuster, in order to optimize for the combustion temperature.
- Further investigation into engine noise.

Performance

- Flight tests to determine the eigenmotions in real life.
- Investigate the option of a cruise-climb profile.
- Perform a performance optimization of the climb and descent phase in order to save fuel.
- Investigate the option of using thrust reversers and speed brakes during landing.

Operations and Maintenance

- Make an more detailed maintenance plan.
- Further investigation on using Structural Health Monitoring techniques.

Table 26.1: Values and properties of the Q-50

Crew	2 +1
Seating Capacity	50
Length	26.5 m
Wing Span	19.2 m
Height	6.25 m
Wing Area	43 m^2
Fuselage Diameter	2.6 m
Turn Radius	22.8 m
Take-off Thrust	55 kN
Max. Payload Weight	5000 kg
Operational Empty Weight	9755 kg
Maximum Take-off Weight	17425 kg
Range	2000 km
Cruise speed	867 km/h
Cruise altitude	10278 m

Bibliography

[1] DSE group 16. Low-emission regional airliner mid-term report. Technical report, Delft University of Technology, May 2015.

[2] DSE group 16. Low-emission regional airliner design report. Technical report, Delft University of Technology, April 2015.

[3] E. Torenbeek. *Synthesis of Subsonic Airplane Design*. Delft University Press, 1^{st} edition, 9 1996.

[4] DSE group 16. Low-emission regional airliner project plan. Technical report, Delft University of Technology, April 2015.

[5] Embraer Commercial Aviation. Market forecast 2014-2033. `http://www.embraercommercialaviation.com/MarketInfo/VPC_MktOutlook_2014.pdf`, 2014. [Accessed on 1-5-2015].

[6] Bombardier. Market forecast 2014-2033. `http://www.bombardier.com/content/dam/Websites/bombardiercom/supporting-documents/BA/Bombardier-Aerospace-20140717-Commercial-Aircraft-Market-Forecast_2014-33.pdf`, 2014. [Accessed on 1-5-2015].

[7] B. Young. Continued advances in oled technologies and materials accelerate the emergence of new high performance displays and lighting products. Technical report, OLED Association, March 2010.

[8] Tse-Hao Ko, Juu-Jiuh Jaw, and Ying-Chie Chen. The effect of pyrolysis on the properties of stabilized pan fabric reinforced phenolic resins for 2d carbon composites. *Polymer Composites*.

[9] V. McConnell. The making of carbon fibre. `http://www.compositesworld.com/articles/the-making-of-carbon-fiber`, 2008. [Accessed on 17/06/15].

[10] K. Wood. Carbon fiber reclamation: Going commercial. `http://www.compositesworld.com/articles/carbon-fiber-reclamation-going-commercial`, 2010. [Accessed on 21-05-2015].

[11] J. Pieper. Carbon fiber from lignin, supercomputing simulates production with a promising wood derivative. `https://www.nics.tennessee.edu/carbon-fiber`, 2014. [Accessed on 20/06/2015].

[12] X. Xu, C. Song, J.M. Andresen, B.G. Miller, and A.W. Scaroni. Novel polyethylenimine-modified mesoporous molecular sieve of mcm-41 type as high-capacity adsorbent for co_2 capture. *Energy & Fuels*, 16(6):1463 – 1469.

[13] M.M. Ballari and H.J.H. Brouwers. Full scale demonstration of air-purifying pavement.

[14] Dr.J.Roskam. *Airplane Design, preliminary sizing of airplanes*. Roskam Aviation and Engineering Corporation, Kansas: The University of Kansas, 1985.

[15] Civil Aviation Safety Authority. Standard passenger and baggage weights. *Civil Aviation Advisory Publication, No 235-1(1)*, 1990.

[16] J. Hale. Aeromagazine - boeing 787 from the ground up. `http://www.boeing.com/commercial/aeromagazine/articles/qtr_4_06/`, 2006.

[17] Bombardier. Bombardier crj200. `http://www2.bombardier.com/Used_Aircraft/pdf/CRJ200_EN.pdf`, June 2006.

[18] E. Gill, G. LaRocca, and W. Verhagen. Lectures of systems engineering & aerospace design. `blackboard.tudelft.nl`, 2013.

[19] I.H. Abbott and A.E. Von Doenhoff. *Theory of Wing Sections*. Dover Publications, 1st edition, 1959.

[20] D. Raymer. *Aircraft Design: A Conceptual Approach*. American Institute of Aeronautics and Astronautics, Inc,, 4^{th} edition edition, 2006.

[21] M. Nila and D. Scholz. From preliminary aircraft cabin design to cabin optimization. *Deutscher Luft- und Raumfahrtkongress*, 2010.

[22] J.D. Anderson. *Fundemantals of Aerodynamics*. Mc Graw Hill, 2011.

[23] M. Sadraey. *Aircraft Performance Analysis*. VDM Verlag Dr. Müller, 2009.

[24] J. Ostrower. 787 design highlights: systems and materials. http://www.flightglobal.com/news/articles/787-design-highlights-systems-and-materials-362157/, 2011. [Accessed on 13/06/2015].

[25] J. Hale. Boeing 787 from the ground up. http://www.boeing.com/commercial/aeromagazine/articles/qtr_4_06/, 2006. [Accessed on 14/06/2015].

[26] L. B. Ilcewicz, T. H. Walker, K. S. Willden, G. D. Swanson, G. Truslove, S. L. Metschan, and C. L. Pfahl. Application of a design-build-team approach to low cost and weight composite fuselage structure. NASA Contractor Report NAS1-18889, NASA, December 1991.

[27] M. Kaminski and C. Kassapoglou. Failure of composite laminates under cyclic loads.

[28] T.S. Coope, D.F Duncan, R.S. Trask, and I.P. Bond. Metal triflates as catalytic curing agents in self-healing fibre reinforced polymer composite materials. *Macromolecular Materials and Engineering*, 299(2):208–218, 2014.

[29] Z. Kleinman. Self-healing aeroplane wings 'to fix tiny cracks'. http://www.bbc.com/news/technology-33047859, 2015. [Accessed on 27-06-2015].

[30] C. Red. Composites in commercial aircraft engines, 2014-2023. http://www.compositesworld.com/articles/composites-in-commercial-aircraft-engines-2014-2023, 2015. [Accessed on 14/06/2015].

[31] S. Trimble. Lockheed martin reveals f-35 to feature nanocomposite structures. http://www.flightglobal.com/news/articles/lockheed-martin-reveals-f-35-to-feature-nanocomposite-357223/, 2011. [Accessed on 14/06/2015].

[32] Zyvex performance materials launch line of nano-enhanced adhesives that add strength, cut costs. http://web.archive.org/web/20121016170430/http://www.zyvextech.com/www/dcms/files/data-sheets/epovex-adhesive-pr.pdf, 2009. [Accessed on 14/06/2015].

[33] O. Schrenk. A simple approximation method for obtaining the spanwise lift distribution. Technical report, NACA, April 1940.

[34] T. Megson. *Aircraft Structures for Engineering Students*. Elsevier, 4^{th} edition, 2007.

[35] M.C.Y. Niu. *Composite Airframe Structures*. Hong Kong Conmilit Press LTD., 2^{nd} edition, 1996.

[36] D. Howe. *Aircraft Loading and Structural Layout*. Aerospace series.

[37] H. Cohen, G.F.C. Rogers, and H.I.H. Saravanamuttoo. *Gas Turbine Theory*. Longman Group Limited, 4^{th} edition, 1996.

[38] P.P. Walsh and P. Fletcher. *Gas Turbine Performance*. Blackwell Science, 2^{nd} edition, 2004.

[39] J.P van Buijtenen, W.P.J. Visser, T. Tinga, S. Shakariyants, and F. Montella. *Gas Turbines*. TU Delft, 3^{rd} edition, September 2007.

[40] GSP Development Team. *GSP 11 user Manual*. NLR, 11.4.4.0 edition, November 2014.

[41] N. Cumpsty. *Jet Propulsion*. Cambridge University Press, 2^{nd} edition, 2003.

[42] H. Canie're, A. Willockx, E. Dick, and M. De Paepe. Raising cycle efficiency by intercooling in air-cooled gas turbines. *Applied Thermal Engineering*, 29(16):1780–1787, 2006.

[43] J.P. Bédécarrats and F. Strub. Gas turbine performance increase using an air cooler with a phase change energy storage. *Applied Thermal Engineering*, 29(5-6):1166–1172, 2009.

[44] S. Boggia and K. Rüd. Intercooled recuperated gas turbine engine concept. *AIAA*, 41st Joint Propulsion Conference(AIAA 2005-4192), 2005.

[45] L. Jenkinson, P. Simpkin, and D. Rhodes. *Civil Jet Aircraft Design*. Butterworth-Heinemann, 2001.

[46] Dr.J.Roskam. *Determination of Stability, Control and Performance Characteristics: FAR and Military Requirements*. Roskam Aviation and Engineering Corporation, Kansas: The University of Kansas, 1986.

[47] et. al. J.A. Mulder. Flight dynamics lecture notes. Delft Univeristy of Technology.

[48] S. Gudmundsson. *General Aviation Aircraft Design: Applied Methods and Procedures*. Butterworth and Heinemann, 1st edition, 2014.

[49] M. Sadraey. Spoiler design. `http://faculty.dwc.edu/sadraey/Spoiler%20design.pdf`. [Accessed on 15/06/15].

[50] EASA. *Certification Specifications for Large Aeroplanes CS-25*. EASA, September 2007. Amendment 3.

[51] M. Sadraey. *Aircraft Design:A Systems Engineering Approach*, volume I. Wiley, 1^{th} edition, October 2012.

[52] Dr.J.Roskam. *Preliminary Calculation of Aerodynamic, Thrust and Power Characteristics*. Roskam Aviation and Engineering Corporation, Kansas: The University of Kansas, 1987.

[53] R. Vos. Lectures of advanced aircraft design i. `blackboard.tudelft.nl`, 2012.

[54] Dr.J.Roskam. *Airplane Design, preliminary configuration design and integration of the propulsion sytem*. Roskam Aviation and Engineering Corporation, Kansas: The University of Kansas, 1985.

[55] Dr.J.Roskam. *Layout of Landing Gear and Systems*. Roskam Aviation and Engineering Corporation, Kansas: The University of Kansas, 1986.

[56] Airbus. Flight operations briefing notes - landing techniques, March 2008.

[57] G.J.J. Ruijgrok. *Elements of Airplane Performance*. VSSD, 2nd edition, 2009.

[58] M. Voskuijl. Lectures of flight and orbital mechanics. `blackboard.tudelft.nl`, 2012.

[59] D. Steenhuizen. Lectures of aerospace design & systems engineering elements 2. `blackboard.tudelft.nl`, 2013.

[60] Civil Aviation Safety Authority. Aviation maintenance technician handbook-airframe (chp.14). 2012.

[61] H. Gavel. On aircraft fuel systems, conceptual design and modeling. 2007.

[62] I. Moir and A. Seabridge. *Aircraft Systems*. John Wiley & Sons. Ltd, Chichester: West Sussex, 2008.

[63] S.L. Botten, C.R. Whitley, and A.D. King. Flight control actuation technology for next-generation all-electric aircraft. *Technology Review Journal*, Millennium Issue(Fall/Winter), 2000.

[64] M. Fanliang. Actuation systems design with electrically powered actuators. Msc by research thesis, Cranfield University: school of Engineering, 2011.

[65] S. Frischemeier. Electrohydrostatic actuators for aircraft primary flight control - type, modelling and evaluation. Technical report, Hamburg: TU Hamburg, Section Aircraft Systems Engineering, 2006.

[66] C. Bos. Lectures of avionics and operations. `blackboard.tudelft.nl`, 2014.

[67] Universal Avionics. Understanding required navigation performance and area navigation operations. White Paper WHTP-2013-16-10, Universal Avionics systems corporation, October 2013.

[68] Federal Aviation Administration. *Instrument Procedures Handbook*. U.S. Department of Transportation, faa-h-8083-16 edition, 2014.

[69] Dr.J.Roskam. *Component Weight Estimation*. Roskam Aviation and Engineering Corporation, Kansas: The University of Kansas, 1985.

[70] L. van Veen. Assessment of heated glare for wing ice protection. Technical report, Delft University of Technology, October 2013.

[71] W. Verhagen. Airline maintenance & operations. `blackboard.tudelft.nl`, 2014.

[72] G. Williams. Lectures of air transport. `recil.grupolusofona.pt/bitstream/handle/.../1831.pdf`, 2005.

[73] Shey-Huei Sheu. A generalized age and block replacement of a system subject to shocks. *"Department of Industrial Management, National Taiwan Institute of Technology"*, 108(2):345–362, 1996.

[74] J. Collrep and E. Moser. Maintenance inspection of composite materials with shearography. *ECNDT*, pages 1–4, 2006.

[75] Aircraft Commerce. Consumer price index (cpi) conversion factors for years 1774 to estimated 2025 to convert to dollars of 2014. `http://liberalarts.orgegonstate.edu/sites/liberalarts.oregonstate.edu/files/polisci/faculty-research/sahr/inflation-conversion/pdf/cv2014.pdf`, 2014. [Accessed on 15/06/2015].

[76] S.O.L. Zijp. Development of a life cycle cost model for conventional and unconventional aircraft. Technical report, Delft University of Technology, June 2014.

[77] Aircraft Commerce. Owners and operators guide: Crj family. `www.team.aero/.../owners_n_operators_guide_crj.pdf`, 2009. [Accessed on 15/06/2015].

[78] W. Xunnian L. Yong and Z. Dejiu. Control strategies for aircraft airframe noise reduction. *Chinese Journal of Aeronautics*, 26(2):249 – 260, 2013.

[79] K. Boorsma, X. Zhang, and N. Molin. Landing gear noise control using perforated fairings. *Acta Mechanica Sinica*, 26(2):159–174, 2010.

[80] H.H. Hubbard. *Aeroacoustics of Flight Vehicles: Theory and Practice*, volume 1: Noise Sources. NASA, August 1991.

[81] K.B.M.Q. Zaman, J.E. Bridges, and D.L.Huff. Evolution from 'tabs' to 'chevron technology' - a review. *13th Asian Congress of Fluid Mechanics*, 2010.

[82] G. Müller and M. Möser. *Handbook of Engineering Acoustics*. 2^{nd} edition.

[83] Oakland International Airport. Master plan - sound and noise. Technical report, Port of Oakland, March 2006.

[84] M.R. Khorrami and D.P. Lockard. Effects of geometrical details on slat noise generation and propagation. *AIAA*, 27th AIAA Aeroacoustics Conference(AIAA-2006-2664), 2006.

[85] IATA. Report on alternative fuels. Technical report, IATA, March 2009.

[86] Embraer. Erj145 performance. `http://www.embraercommercialaviation.com/AircraftPDF/E145_Performance.pdf`, June 2013.

[87] ICAO. *Enviromental Technical Manual: Procedures for the Noise Certification of Aircraft*, volume I. ICAO, 1^{th} edition, July 2012.

[88] ICAO. *Enviromental Technical Manual: Aircraft Engine Emissions*, volume II. ICAO, 1^{th} edition, July 2008.

[89] Embraer. Erj145 cabin. `http://www.embraercommercialaviation.com/AircraftPDF/E145_Cabin.pdf`, June 2013.

Detailed Aerodynamic Analysis

This appendix is provided to give detailed insight into the method of the aerodynamic analysis of the main wing. For more details on the method used to generate the lift polar, see Reference [18]. The input values used in this method are presented in Table A.1.

Table A.1: Input parameters used to determine the lift curve

Input parameter	**Value [unit]**	**Source**
Cruise Mach number, M_{cruise}	0.81 [-]	Performance requirement
Aspect ratio, A	8.5 [-]	Design outcome
Airfoil efficiency, η	0.95 [-]	Approximation, [18]
Sweep angle at 50% of the chord, $\Lambda_{0.5c}$	21.6 [degrees]	Design outcome
Sweep angle at 25% of the chord, $\Lambda_{0.25c}$	25.3 [degrees]	Design outcome
Maximum lift coefficient of the airfoil, $C_{l,max}$	1.47 [-]	Javafoil analysis
Angle of attack at zero lift of airfoil, $\alpha_{C_l=0}$	-4.45 [degrees]	Javafoil analysis
Taper ratio, λ	0.27 [-]	Design outcome
Sweep angle at leading edge, Λ_{LE}	25 [degrees]	Design outcome
Stall factor, $\Delta\alpha_{C_L,max}$	2.5 [degrees]	Follows from $C_{L,max}$ and $\frac{dC_L}{}$

As mentioned in Chapter 9, the following relation was used to make the $C_L - C_D$ curve for the main wing:

$$C_{D,w} = C_{D_{0,w}} + \frac{C_{L,w}^2}{\pi A e} \tag{A.1}$$

Where $C_{D_{0,w}}$ was computed using the relations presented in Reference [23]. For the exact method it is referred to Chapter 3 of this book. The input values can be found in Table A.2.

Table A.2: Input parameters used to determine $C_L - C_D$ curve

Input parameter	**Value [unit]**	**Source**
Lift coefficient of the main wing, $C_{L,w}$	-	Obtained lift curve
Aspect ratio, A	8.5 [-]	Design outcome
Oswald factor, e	0.83 [-]	Matlab function, Shevell method [1]
Oswald factor during landing, $e_{landing}$	0.80 [-]	Matlab function, Shevell method [1]
Mean aerodynamic chord, MAC	2.013 [m]	Design outcome
Maximum thickness to chord ratio t/c_{max}	0.11 [-]	Airfoil characteristic
Cruise Mach number, M_{cruise}	0.81 [-]	Performance requirement
Wing span, b	19.2 [m]	Design outcome
Wing surface area, S	43.0 [m^2]	Design outcome
Minimum drag coefficient of the wing, $C_{D_{min,w}}$	0.00603 [-]	Javafoil analysis

Flight Schedule Of The Competition

This appendix shows the flight schedule of a couple of CRJ200 and ERJ145 operated by Delta and US Airways. From these tables the average daily flight time is deduced. Note that all links placed show the flight schedule for that particular aircraft from the last couple of days with respect to the time of visiting the page.

Delta - N981EV [a]	STD	STA	Flighttime
29 May	0:40	1:54	1:14
29 May	2:58	3:39	0:41
29 May	12:12	13:04	0:52
29 May	13:51	15:13	1:22
29 May	15:38	16:59	1:21
29 May	19:30	20:38	1:08
29 May	21:04	22:12	1:08
29 May	22:55	0:42	1:47
30 May	12:33	14:14	1:41
30 May	14:50	15:42	0:52
30 May	16:07	17:04	0:57
30 May	17:45	18:36	0:51
30 May	19:02	19:59	0:57
30 May	21:15	22:21	1:06
31 May	13:41	14:42	1:01
31 May	15:23	17:15	1:52
31 May	17:45	19:29	1:44
31 May	20:10	21:33	1:23
31 May	21:58	23:31	1:33
01 June	0:54	1:57	1:03
01 June	9:45	10:50	1:05
01 June	13:10	14:31	1:21
01 June	14:57	16:25	1:28
01 June	17:05	18:42	1:37
01 June	19:07	20:46	1:39
01 June	21:26	22:20	0:54
01 June	22:45	23:46	1:01
02 June	2:58	3:39	0:41
02 June	13:20	14:12	0:52
02 June	13:56	15:07	1:11
02 June	15:32	16:38	1:06
02 June	18:00	19:14	1:14
02 June	19:39	20:50	1:11
02 June	21:30	22:22	0:52
02 June	22:48	23:44	0:56
Average daily flighttime			8:20
Average missiontime			1:11
Average number of flights per day			7

[a] http://www.flightradar24.com/data/airplanes/n981ev/

US Airways - N223JS [a]	STD	STA	Flighttime
29 May	2:30	3:51	1:21
29 May	9:15	10:31	1:16
29 May	11:25	12:49	1:24
29 May	13:15	14:45	1:30
29 May	15:05	16:11	1:06
29 May	16:40	17:57	1:17
30 May	15:10	16:23	1:13
30 May	16:52	18:07	1:15
30 May	18:50	19:32	0:42
30 May	20:10	21:06	0:56
30 May	21:54	23:21	1:27
30 May	23:55	1:26	1:31
31 May	2:40	4:24	1:44
31 May	11:00	12:35	1:35
31 May	13:35	15:25	1:50
31 May	16:00	17:39	1:39
31 May	18:20	19:40	1:20
31 May	20:05	21:24	1:19
31 May	22:05	23:04	0:59
31 May	23:50	0:54	1:04
1 June	2:25	3:33	1:08
1 June	9:25	10:25	1:00
1 June	11:30	12:50	1:20
1 June	13:25	14:53	1:28
1 June	15:45	17:47	2:02
1 June	18:45	20:43	1:58
1 June	21:32	23:22	1:50
1 June	23:55	1:36	1:41
Average daily flighttime			9:43
Average missiontime			1:23
Average number of flights per day			7

[a] http://www.flightradar24.com/data/airplanes/n223js/

Stability and Control Derivatives

The stability and control derivatives are shown in Table C.1. The formulae used for their derivations is also shown in this table. They are based on Roskam [46] and the Flight Dynamics Reader [47].

Table C.1: Stability and control derivatives

Derivative	Sign	Formula	Value
C_{X_0}		$-\frac{W sin\gamma_0}{\frac{1}{2}\rho V^2}$	0
C_{X_u}	>0	$-C_{D_u}$ - $2C_D$	-0.122599062
C_{X_α}		C_L - C_{D_α}	0.103183898
$C_{X_{\dot{\alpha}}}$		neglected	0
C_{X_q}		neglected	0
$C_{X_{\delta_e}}$		neglected	0
C_{Z_0}		$-\frac{W cos\gamma_0}{\frac{1}{2}\rho V^2}$	-0.35198636
C_{Z_u}		$-C_{L_u}$ - $2C_D$	-0.453002286
C_{Z_α}	<0	-$C_{L_{alpha}}$ - C_D	-6.134259205
$C_{Z_{\dot{\alpha}}}$		-$C_{N_{h_\alpha}} \left(\frac{V_h}{V}\right)^2 \frac{d\epsilon}{d\alpha} \frac{S_h l_h}{S\bar{c}}$	-2.051475385
C_{Z_q}	<0	-$2C_{N_{h_\alpha}} \left(\frac{V_h}{V}\right)^2 \frac{S_h l_h}{S\bar{c}}$	-8.205901542
$C_{Z_{\delta_e}}$	<0	-$C_{N_{\delta_e}} \left(\frac{V_h}{V}\right)^2 \frac{S_h}{S}$	-0.719881363
C_{m_u}		neglected	0
C_{m_α}	<0	$C_{N_{w_\alpha}} \frac{x_{c.g.}-x_w}{\bar{c}}$-$C_{N_{h_\alpha}}(1-\frac{d\epsilon}{d\alpha})\left(\frac{V_h}{V}\right)^2 \frac{S_h l_h^2}{S\bar{c}}$	-0.59473098
$C_{m_{\dot{\alpha}}}$	<0	-$C_{N_{h_\alpha}} \left(\frac{V_h}{V}\right)^2 \frac{d\epsilon}{d\alpha} \frac{S_h l_h^2}{S\bar{c}^2}$	-0.4618845
C_{m_q}	<0	-1.1$C_{N_{h_\alpha}} \left(\frac{V_h}{V}\right)^2 \frac{S_h l_h^2}{S\bar{c}}$	-20.62379526
$C_{m_{\delta_e}}$	<0	$-C_{L_{\alpha_h}} \alpha_{\delta_e} \eta_h V_h$	-3.613025199
$C_{m_{TC}}$		neglected	0
C_{Y_β}	<0	$C_{Y_{\beta_w}} + C_{Y_{\beta_f}} + C_{Y_{\beta_v}}$	-2.644385437
$C_{Y_{\dot{\beta}}}$		$C_{L_{\alpha_v}}(\frac{d\sigma}{d\beta}\frac{S_v}{S}(l_p cos(\alpha_f) + z_p sin(\alpha_f)))/b$	0.004782323
C_{Y_p}	<0	$2C_{Y_{\beta_v}}(z_v cos(\alpha) - l_v sin(\alpha))/b$	0.002129582
C_{Y_r}	>0	$-2C_{Y_{\beta_v}}(l_v cos(\alpha) + z_v sin(\alpha))/b$	0.016575791
$C_{Y_{\delta_a}}$		neglected	0
$C_{Y_{\delta_r}}$		$\left(C_{l_{\alpha_v}}\right)(k' K_b) cl\delta (S_v/S)$	0.188163312
C_{l_β}	<0	$C_{l_{\beta_{wf}}} + C_{l_{\beta_h}} + C_{l_{\beta_v}}$	-0.066385839
$C_{l_{\dot{\beta}}}$		$C_{Y_{\dot{\beta}}}(z_p cos(\alpha_f) - l_p sin(\alpha_f))/b$	-0.001600418
C_{l_p}	<0	$C_{l_{p_w}} + C_{l_{p_h}} + C_{l_{p_v}}$	-0.945029972
C_{l_r}	>0	$C_{l_{r_w}} + C_{l_{r_v}}$	0.198142165
$C_{l_{\delta_a}}$	>0	$\left(\alpha_{\delta_a}\right)\left(k/\beta\right)\left(\beta C'_{l_\delta}\right)$	0.05243378
$C_{l_{\delta_r}}$	>0	$((z_v cos(a) - l_v sin(a))/b) C_{Y_{\delta_r}}$	0.014302251
C_{n_β}	>0	$C_{n_{\beta_w}} + C_{n_{\beta_f}} + C_{l_{\beta_v}}$	0.04275171
$C_{n_{\dot{\beta}}}$		$C_{Y_{\dot{\beta}}}(l_p cos(\alpha_f) + z_p sin(\alpha_f))/b$	0.002182035
C_{n_p}	<0	$C_{n_{p_w}} + C_{n_{p_v}}$	-0.085062945
C_{n_r}	<0	$C_{n_{r_w}} + C_{n_{r_v}}$	-0.298099112
$C_{n_{\delta_a}}$	<0	$k_a C_{L_w} C_{l_{\delta_a}}$	-0.0064110783
$C_{n_{\delta_r}}$		$-C_{Y_{\delta_r}}((l_v cos(a) + z_v sin(a))/b)$	0.118276779

Full Requirement List

The list of requirements is based on the needs of the stakeholders and on the certification specification for large aircraft, i.e. CS-25 of the European Aviation Safety Agency.[50] For the conceptual design the requirements are chosen up to the sub-system level. The lower level systems will be treated in a later phase of the project. The detailed requirements are subject to change during the project due to the evolution in design of the aircraft.

The requirements are split up in different categories all with their own code to identify them by.

Aerodynamic Performance

AeP-1 The complete aircraft lift coefficient, C_Lmax, in -
- **AeP-1.a** Cruise, $C_{L_{max}}$, shall be between 1.5 - 1.9 [14]
- **AeP-1.b** Take-off, $C_{L_{max_{TO}}}$, shall be between 1.7 - 2.1 [14]
- **AeP-1.c** Landing, $C_{L_{max_L}}$, shall be between 1.9 - 3.3 [14]

AeP-2 The full aircraft drag coefficient, C_D, in cruise shall be no larger than 0.030
- **AeP-2.a** The zero lift drag coefficient, C_{D_0}, shall be no larger than 0.020. [3]
- **AeP-2.b** The wing lift distribution, Oswald factor e, at -
  - **AeP-2.b.1** At cruise shall at least be 0.8 [3]
  - **AeP-2.b.2** At landing shall at least be 0.7 [3]

AeP-3 The lift over drag, $\frac{C_L}{C_D}$, during -
- **AeP-3.1** Cruise, $\left(\frac{C_L}{C_D}\right)_{cruise}$, shall be at least 17.5 [3, 14]
- **AeP-3.2** Take-off, $\left(\frac{C_L}{C_D}\right)_{TO}$, shall be at least 11.6 [3, 14]
- **AeP-3.3** Landing, $\left(\frac{C_L}{C_D}\right)_{L}$, shall be at least 7.8 [3, 14]

Aircraft Flight Performance

AFP-1 Minimum performance of the aircraft shall be achieved at altitudes ranging from sea-level to 3048 m, and temperatures ranging from ISA standard, $288K$, $\pm 30°$.

AFP-2 The aircraft shall have a maximum range of 2000 km.

AFP-3 The aircraft shall have a basic cruise speed of -
- **AeP-3.a** Mach 0.75 for jet aircraft.
- **AeP-3.b** Mach 0.55 for propeller aircraft.

AFP-4 The aircraft shall have a service ceiling of -
- **AeP-4.a** 11,278 m (37,000 ft) for jet aircraft.
- **AeP-4.b** 7,925 m (26,000 ft) for propeller aircraft.

AFP-5 The maximum landing length shall be no more than 1500 m.[86]

AFP-6 The take of field length shall be no more than 1800 m. [86]

AFP-7 The aircraft shall be longitudinally stable.

AFP-8 The aircraft shall be lateral stable.

AFP-9 The Rate of climb shall be at least 6.8 m/s

AFP-10 The climb gradient shall be at least 2.4% [3, 50]

Propulsion System

PS-1 The maximum total thrust shall be 64 kN [follows from F=ma using take off distance and MTOW]

PS-2 The single engine specific fuel consumption shall be no more than 0.35 during take-off

PS-3 The effective perceived noise level at take-off shall be no larger than 74.1 dB. [87]

PS-4 The effective perceived noise level at landing shall be no larger than 86.5 dB. [87]

PS-5 The effective perceived noise level at the sideline shall be no larger than 79 dB. [87]

PS-6 The mass of emitted gaseous pollutant of CO_2 shall be reduced by at least 50 % [88]

PS-7 The mass of emitted gaseous pollutant of NOx shall be reduced by at least 25 % [88]

Weight Performance

WP-1 The maximum take off weight [MTOW] will be no larger than 23,000 kg
- **WP-1.1** The operational empty weight shall be no more than 11000 kg
- **WP-1.2** The maximum payload shall be no more than 5500
- **WP-1.3** The maximum fuel capacity shall be no more 4500

WP-2 The maximum landing weight shall be no larger than 22,500 kg. [14]

Sizing

Siz-1 The aircraft shall have a capacity of 50 passengers, and crew of 2 pilots + 1 flight attendants.
Siz-2 The seat pitch for the fuselage shall be at least 26 in, or 0.66 m. [caa]
Siz-3 The cabin height shall be no smaller than 1.85 m in the aisle.[89]
Siz-4 The capacity of the cargo bay shall be no more than 1060 kg. [20 kg per pax + crew]
Siz-5 The width of the aisle shall be at least 0.41 m to accommodate refreshment trolley's.[50]

Operation

Op-1 The first aircraft shall go into service in 2035.
Op-2 Unit cost shall not exceed $ 35 million. (2014 level)
Op-3 The return on investment shall be at least 5% after 5 years.
Op-4 The parking area shall not exceed 42 m x 30 m,in compliance with current airport gate dimensions. [London city airport]
Op-5 The aircraft material shall ensure that the existing radar technology is able to detect the aircraft for safe air traffic control operations.

Certification With the given baseline parameters for weight and performance the aircraft will fall under CS-25 certification. All the certification requirements given below follow from the cs-25 regulations which can be found in [50]

Ce-1 The maximum load factor for manoeuvre shall be no more than 2.5
Ce-2 The reference stall speed is determined by $V_{sr} = \frac{V_{CL_{max}}}{\sqrt{n_{zw}}}$; $V_{CL_{max}} = \frac{n_{zw}W}{qS}$; n_{zw} = Load factor to the flight path at Vclmax
Ce-3 The take off speeds shall follow -
- **Ce-3.a** Vef (calibrated airspeed at which the critical engine is assumed to fail) must be selected for the airplane, but must not be less than 1.05 Vmc
- **Ce-3.b** V1 must not be less than Vef plus the speed gained with the critical engine inoperative during the time interval between the instant at which the critical engine is failed and the instant at which the pilot recognises and reacts to the engine failure
- **Ce-3.c** Vef must not be less than Vmcg (minimum control speed on the ground)
- **Ce-3.d** V2min may not be less than 1.08Vsr and 1.1Vmc[CS25.107 (b)]
- **Ce-3.e** V2 must not be less than V2min and Vr plust the speed increment attained before reaching a height of 11m above the take-off surface.
- **Ce-3.f** Vr may not be less than V1; 105% of Vmc; the speed taht allow reaching V2 before reaching a height of 11m above take-off surface

Ce-4 Each part of the structure shall be –
- **Ce-4.a** Suitably protected against deterioration or loss of strength in service due to any cause, including weathering, corrosion and abrasion.
- **Ce-4.b** Have adequate provisions for ventilation and drainage.

Ce-5 Passenger doors shall not be located with respect to any propeller disc or any other potential hazard so as to endanger persons using that door.
Ce-6 Each emergency exit shall have a size of at least 48 by 51 cm.
Ce-7 For each emergency exit that is not less than 1.8 metres from the ground, an assisting means shall be provided.
Ce-8 The maximum loads on the main wheel tyre shall corresponding to the most critical combination of airplane weight (up to the maximum weight) and centre of gravity position
Ce-9 For airplanes having only one passenger aisle, no more than 3 seats abreast shall be placed on each side of the aisle in any one row.

Ce-10 The airplane must be able to maintain a cabin pressure altitude of not more than 4572 m in the event of any failure of the pressurisation system.

Ce-11 Each dispensing equipment shall supply protective oxygen of 15 minutes duration at a pressure altitude of 2438 m with a respiratory minute volume of 30 litres per minute

Ce-12 The maximum operating limit speed (VMO/MMO, airspeed or Mach number, whichever is critical at a particular altitude) is a speed that shall not be deliberately exceeded in any regime of flight (climb, cruise, or descent).

Ce-13 No uncontrolled increase in cell temperature of the battery shall result when the battery is recharged (after previous complete discharge)

- **Ce-13.a** At maximum regulated voltage or power
- **Ce-13.b** During a flight of maximum duration
- **Ce-13.c** Under the most adverse cooling condition likely to occur in service

Ce-14 Engines shall be located in such a way that failure or malfunction of any engine will not prevent continued safe operation of the remaining engines or require immediate action by any crew member.

Ce-15 Engines must be able to restart in flight regardless regardless of whether windmilling provides enough electrical power.

Ce-16 Propeller blade failure shall not damage critical systems or structures.

Ce-17 Propeller clearances may not be less than -

- **Ce-17.a** Ground clearance. There must be 18 cm (7 inches) (nose wheel landing gear) or 23 cm (9 inches) (tail-wheel landing gear) between each propeller and the ground.
- **Ce-17.b** Structural clearance. There must be –
  - **Ce-17.b.1** At least 25 mm (1 · 0 inch) radial clearance between the blade tips and the airplane structure, plus any additional radial clearance necessary to prevent harmful vibration;
  - **Ce-17.b.2** At least 13 mm (0 · 5 inches) longitudinal clearance between propeller blades or cuffs and stationary parts of the airplane; and
  - **Ce-17.b.3** Positive clearance between other rotating parts of the propeller or spinner and stationary parts of the airplane.

Ce-18 Fuel tanks shall be installed in such a way that no fuel is released near the fuselage/engines:

- **Ce-18.a** The effects of crushing and scraping actions with the ground should not cause the spillage of enough fuel, or generate temperatures that would constitute a fire hazard.
- **Ce-18.b** Fuel tank installations must be such that the tanks will not rupture as a result of an engine pylon or engine mount or landing gear, tearing away.

Cost abbreviations

This appendix provides the reader with the cost break-down structures mentioned in Chapter 22, each accompanied by list of abbreviations and their explanation. It should be noted that all costs are in USD/nm, except the aircraft estimated price which will be in USD.

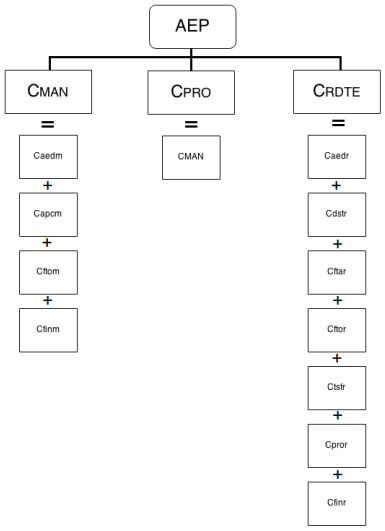

Figure E.1: Aircraft estimated price break-down structure

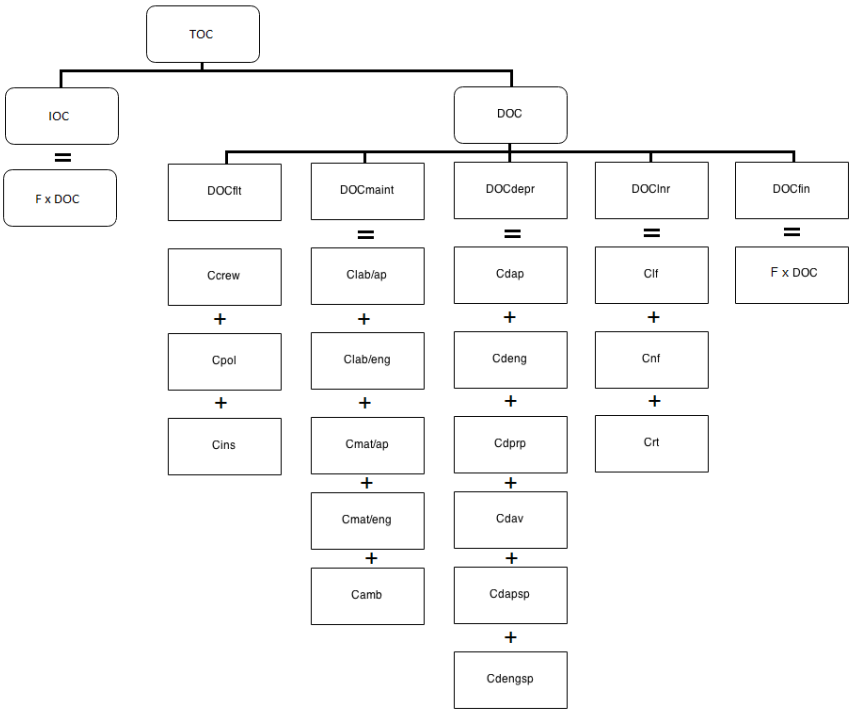

Figure E.2: Direct operating cost break-down structure

Table E.1: Aircraft price abbreviations

Abbrev.	Explanation
AEP	Aircraft estimated price
C_{MAN}	Manufacturing cost
C_{PRO}	Manufacturer's profit
C_{RDTE}	Research, development, testing and evaluation cost
C_{aed_m}	Airframe engineering and design cost, during manufacturing phase
C_{apc_m}	Airplane production cost, during manufacturing phase
C_{fto_m}	Flight test operations cost. during manufacturing phase
C_{fin_m}	Financing cost, during manufacturing phase
C_{aed_r}	Airframe engineering and design cost, during manufacturing phase
C_{dst_r}	Development support and test cost, during research phase
C_{fta_r}	Cost for flight test airplanes, during research phase
C_{fto_r}	Flight test operations cost, during research phase
C_{tsf_r}	Cost for test and simulation facilities, during research phase
C_{pro_r}	Manufacturing profit, during research phase
C_{fin_r}	Financing cost, during research phase

Table E.2: Direct operating cost abbreviations

Abbrev.	Explanation
DOC	Direct operating cost
DOC_{flt}	DOC of flying
DOC_{maint}	DOC of maintenance
DOC_{depr}	DOC of depreciation
DOC_{lnr}	DOC of landing, navigation & registration fees
DOC_{fin}	DOC of financing
C_{crew}	Crew cost
C_{pol}	Fuel and oil cost
C_{ins}	Insurance cost
$C_{lab/ap}$	Labor cost of airframe and systems maintenance
$C_{lab/eng}$	Labor cost of engine maintenance
$C_{mat/ap}$	Material cost of airframe and systems maintenance
$C_{mat/eng}$	Material cost of engine maintenance
C_{amb}	Applied maintenance burden
C_{dap}	Depreciation cost of airframe and systems
C_{deng}	Depreciation cost of engines
C_{dprp}	Depreciation cost of propellers
C_{dav}	Depreciation cost of avionics
C_{dapsp}	Depreciation of airframe and systems spare parts
C_{dengsp}	Depreciation of engine spare parts
C_{lf}	Landing fees
C_{nf}	Navigation fees
C_{rt}	Registration taxes

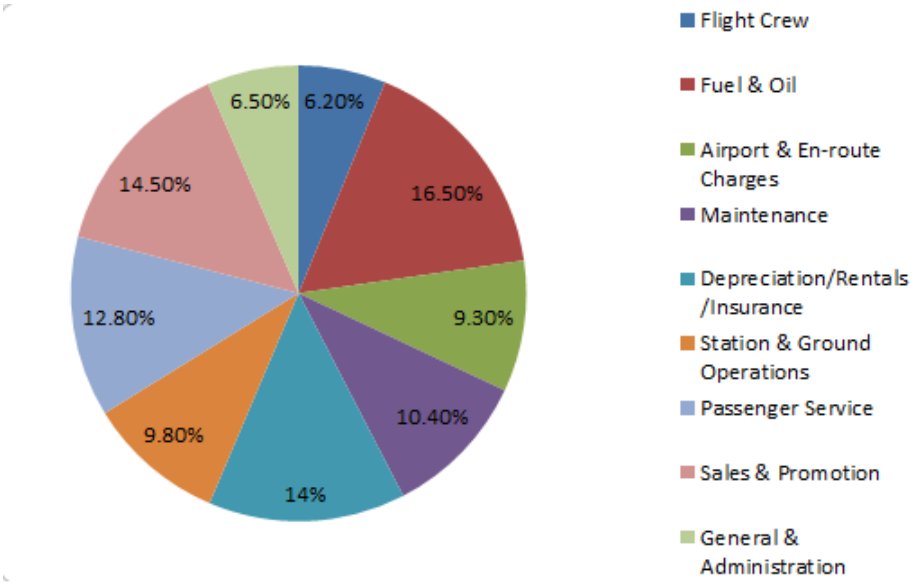

Figure E.3: Operating cost allocation [72]

Governing Equations for Structural Analysis

Wing Dimensions
In order the calculate the dimensions of the wing, the following equations are used:

- **Local Chord Length** For $z \leq L_1$:
$$c(z) = c_r \tag{F.1}$$
For $z > L_1$:
$$c(z) = c_r - \frac{c_r - c_t}{L_2} z \tag{F.2}$$
- **Local Height of the Wing Box**
$$h(z) = 0.10 \cdot c(z) \tag{F.3}$$
- **Local Width of the Wing Box**
$$w(z) = 0.40 \cdot c(z) \tag{F.4}$$
- **Local Thickness**
$$t_i(z) : t_{element} \cdot c(z) \tag{F.5}$$
- **Cross-sectional Areas**
The area of the top and bottom plate is given by:
$$A_i = w(z) \cdot t_i \tag{F.6}$$
The area of the side plates is given by:
$$A_i = h(z) \cdot t_i \tag{F.7}$$

From the wing dimensions and the wing geometry, the forces and corresponding stresses can be calculated using the following equations:

- **Lift**
For the ellipse and the linear distribution, two variables are defined, namely the major and the minor axis. $major = \frac{b}{2}$ and $minor = \frac{2 \cdot Lift}{\pi \cdot major}$. Where the term $Lift$ is equal to the amount of lift of the load case. The term in the square root, is the elliptical distribution and the second term is the lienar distribution.
$$l(z) = \frac{\sqrt{minor^2 - \frac{minor^2}{major^2} \cdot z} - \frac{Lift}{major^2} \cdot z + \frac{Lift}{major}}{2} \tag{F.8}$$
- **Fuel Weight**
$$W_f(z) = \theta(z) \cdot c^2(z) \tag{F.9}$$
- **Moment or Torsion**
$$M_j / T_j = F_i \cdot d = \int_0^a f_i(x) \cdot d(x) \, \mathrm{d}x \tag{F.10}$$
- **Bending Stress**
$$\sigma_z = \frac{I_{xx} M_y - I_{xy} M_x}{I_{xx} I_{yy} - {I_{xy}}^2} x + \frac{I_{yy} M_x - I_{xy} M_y}{I_{xx} I_{yy} - {I_{xy}}^2} y \tag{F.11}$$
- **Open section Shear flow**
$$q_b = -\frac{I_{xx} S_x - I_{xy} S_y}{I_{xx} I_{yy} - {I_{xy}}^2} \int_0^s tx \, \mathrm{d}s - \frac{I_{yy} S_y - I_{xy} S_x}{I_{xx} I_{yy} - {I_{xy}}^2} \int_0^s ty \, \mathrm{d}s \tag{F.12}$$
- **Constant Shear flow (closed section)**
$$q_0 = \frac{\int_s p q_b \, \mathrm{d}s}{2A} \tag{F.13}$$
- **Torsion Shear flow**
$$q_T = \frac{T}{2A} \tag{F.14}$$
- **Total Shear flow**
$$q = q_b + q_0 + q_T \tag{F.15}$$
- **Shear Stress**
$$\tau = \frac{q}{t} \tag{F.16}$$

Material Tables

Table G.1: CFRP prepreg properties from two major suppliers

	Longitudinal (0°) tensile			Longitudinal (0°) Compression			Transverse (90°) tensile			FLEXURAL(0°)				
Prepreg	Strength^t [MPa]	Knockdown^t [MPa]	Modulus^t (GPa)	Strength^c [MPa]	Knockdown^c [MPa]	Modulus^c (GPa)	Strength [MPa]	Modulus [MPa]	ILSS [MPa]	Strength^f [MPa]	Modulus^f [MPa]	Density [kg/m^3]	Specific strength^t [Nm/kg]	Specific strength^c [Nm/kg]
Hexcel 8551-7	2758	1147	158	1620	673,92	148	76	8343	-	-	-	1500	0,765	0,449
Hexcel 8552-AS4	2207	918	141	1531	636,896	128	81	10000	128	-	-	1580	0,581	0,403
Hexcel 8552-IM7	2724	1133	164	1690	703,04	150	64	12000	137	-	-	1570	0,722	0,448
Hexcel 913	2280	948	134	1540	640,64	123	-	-	-	-	-	1610	0,589	0,398
Hexcel M21	3050	1269	178	1500	624	146	-	-	97	-	-	1580	0,803	0,395
Hexcel M76	2447	1018	154	1579	656,864	-	-	-	121	1627	144	1300	0,783	0,505
Hexcel M91	3520	1464	176	1880	782,08	-	-	-	105	-	-	1616	0,906	0,484
Toray M30S	2990	1244	175	1370	569,92	-	51	7800	88	1520	145	1530	0,813	0,372
Toray M35J	2450	1019	205	1270	528,32	-	49	7500	88	1520	180	1540	0,662	0,343
Toray M40J	2450	1019	230	1270	528,32	-	53	7700	88	1520	195	1550	0,658	0,341
Toray M46J	2210	919	265	1080	449,28	-	47	7100	78	1420	220	1590	0,578	0,283
Toray M50J	2010	836	295	980	407,68	-	40	6900	78	1270	240	1610	0,519	0,253
Toray T1000G	3040	1265	165	1570	653,12	-	60	7500	88	1570	145	1570	0,806	0,416
Toray T400H	2250	936	145	1570	653,12	-	65	8700	98	-	-	1570	0,596	0,416
Toray T700S	2550	1061	135	1470	611,52	-	69	8500	88	1670	120	1570	0,676	0,390
Toray T800H	2650	1102	170	1570	653,12	-	63	8500	98	1620	150	1570	0,702	0,416

Table G.2: Metal alloy properties

Alloy	Ultimate strength [MPa]	Yield strength [MPa]	Modulus [GPa]	Shear strength [MPa]	Shear modulus [GPa]	Machinability [%]	Elongation at break [%]	Density [kg/m³]	Thermal expansion [µm/mK]	Strength per kilogram [kNm/kg]	Price [$/kg]
Al 2014-T4	430	280	73,0	260	28	-	17	2800	22,7	100,0	2,22
Al 2014-T6	490	430	73,0	290	28	70	9	2800	22,7	153,6	2,22
Al 2017-T4	400	240	73,0	260	27	70	15	2790	24	86,0	2,22
Al 2124-T851	460	430	71,0	285	27	70	20	2780	21,9	154,7	2,22
Al 5052-H38	310	250	70,0	165	26	50	5	2680	23,8	93,3	2,22
Al 5052-O	190	80	70,0	125	26	30	25	2680	23,8	29,9	2,22
Al 5083-H32	340	250	71,0	210	27	30	13	2660	23,9	94,0	2,22
Al 5083-O	310	150	71,0	172	27	30	17	2660	23,9	56,4	2,22
Al 5086-O	280	110	71,0	160	27	30	20	2660	23,8	41,4	2,22
Al 6061-T6	310	270	69,0	207	26	50	15	2700	23,6	100,0	2,22
Al 6064-T4	241	145	69,0	165	26	50	22	2700	23,6	53,7	2,22
Al 6064-T6	310	276	69,0	207	26	50	12	2700	23,6	102,2	2,22
Al 7075-O	240	120	72,0	152	27	-	13	2800	23	42,9	2,22
Al 7075-T6	580	510	72,0	331	27	70	10	2800	23,2	182,1	2,22
Al 7178-O	300	103	72,0	150	27	-	12	2830	23,4	36,4	2,22
FeC-17-7	1379	1275	196,5	-	-	-	14	7806	12	163,3	2,00
FeC-300M	2055	1731	205,0	80	-	-	11	7840	12	220,8	3,00
FeC-A656	621	552	200,0	-	-	-	12	7850	12	70,3	0,70
FeC-D6AC	1930	1724	163,0	-	-	50	7	7860	12	219,3	5,00
FeC-HY-TUF	1517	1276	-	-	-	-	5	7770	12	164,2	2,00
Ni-718 @ 760°C	855	750	152,0	-	-	-	10,2	8230	13	91,1	15,00
Ni-718 @ room	1395	1175	200,0	-	-	-	22,3	8230	13	142,8	15,00
Ti-6Al-4V	970	970	114,0	550	44	-	14	4430	8,6	219,0	17,00
Ti-8Al-1Mo-1V	937	937	120,0	-	46	-	19	4370	8,6	214,4	17,00